CRANFIELD UNIVERSITY

C. A. FERREIRA DE SOUSA

VERTEBRATE SOMITE DEVELOPMENT AND NEURAL PATTERNING

SCHOOL OF HEALTH

PhD THESIS

2013

Supervisor: D. Tannahill; C. Toro

CRANFIELD UNIVERSITY

SCHOOL OF HEALTH

PhD THESIS

C A FERREIRA DE SOUSA

Vertebrate somite development and neural patterning

Supervisor: D Tannahill; C Toro

September 2013

This thesis is submitted for the degree of

Doctor of Philosophy

ABSTRACT

The segmentation of the axial skeleton and peripheral nervous system involves a complex integration of multiple patterning molecules. For the latter, axon-repelling molecules in the posterior half-sclerotome are particularly important. This study built on a previously performed mouse microarray screen for novel candidate genes in the posterior half-sclerotome. Multiple candidates were selected for whole-mount *in situ* hybridization in chick. Two were expressed in the posterior half-sclerotome: *thrombin receptor (F2R)* and *fibronectin leucine rich transmembrane protein-2* (*Flrt2*). Flrt2 was selected for siRNA-mediated knockdown and a new *in ovo* transfection technique for somites successfully developed. Scrambled siRNA-transfection did not affect morphogenesis, somite patterning or axon guidance. However, *Flrt2* siRNA-transfection resulted in defects in notochord, dermomyotome and neural tube morphogenesis, and in the de-fasciculation and mis-targeting of spinal axons into the posterior half-sclerotome and dermomyotome. Hence, Flrt2 may be a chemorepellent for spinal axons.

An unidentified peanut agglutinin (PNA)-binding glycoprotein in the posterior half-sclerotome was previously shown to repel spinal axons. In this project, the expression of a family of mucin-type O-glycosylation enzymes (which could glycosylate the PNA-binding protein) was investigated by whole-mount *in situ* hybridization in chick, but none was differentially expressed in the posterior half-sclerotome. One candidate for the PNA-binding glycoprotein, Presenilin1, was investigated because of previously published loss of spinal nerve segmentation in *Presenilin1* mutants. However, analysis of *Presenilin1*-hypomorphic mutant mouse embryos showed this was not the PNA-binding molecule. Live-immunostaining for a second candidate, prolyl 4-hydroxylase, beta polypeptide (P4HB), showed its expression coincided with PNA-binding at the surface of posterior half-sclerotome cells. *P4HB* siRNA-transfection into somites reduced PNA binding and disrupted spinal axon segmentation and expression of a posterior sclerotome marker, *Uncx4.1*. Overall, these results suggest that P4HB is a strong candidate to be the key PNA-binding glycoprotein in the posterior half-sclerotome that repels spinal axons.

For those that inspired me;

TABLE OF CONTENTS

LIST OF FIGURES

LIST OF TABLES

LIST OF ABBREVIATIONS

AP	Anteroposterior
BLAST	Basic Local Alignment Search Tool
CNS	Central nervous system
DRG	Dorsal root ganglia
dsRNA	Double -stranded RNA
ECM	Extracellular matrix
EMT	Epithelial-to-mesenchymal transition
esiRNA	Endonuclease-digested duplexes
FGF	Fibroblast growth factor
FNIII	Type III fibronectin-domain
HH	Hamburger and Hamilton
LRR	Leucine rich repeats
NICD	Notch intracellular domain
PBST	PBS with 0.1% Triton-X100
PEG	Polyethylene glycol
PEI	Polyethylenimine
PNA	Peanut agglutinin
PNS	Peripheral nervous system
PSM	Pre-somitic mesoderm
RALDH2	Retinaldehyde dehydrogenase type 2
RGCs	Retinal ganglion cells
RISC	RNA-induced silencing complex
shRNA	Short-hairpin RNA
siRNA	Short interfering RNA
SVZ	Subventricular zone
WMISH	Whole-mount *in situ* hybridization

CHAPTER 1- INTRODUCTION

1.1- Vertebrate segmentation

During embryogenesis, elaboration of the main body axis starts by sequential subdivisions, from head to tail. Segmentation underlies the body-plan of both protostome and deuterostome animals and defines one of the traits of the vertebrate subphylum, namely, the segmented vertebrae of the axial skeleton (Richmond and Oates, 2012).

The basic tissue organization underlying all vertebrate and many invertebrate embryos is called metamerism that consists of a repeated sequence of segments. This segmental organization offers two major advantages. First, it provides the articulation of the skeletal elements, providing flexibility to the otherwise rigid and immotile skeleton. Secondly, it offers a degree of modularity and semi-autonomy differentiation within the segments (Maroto and Whittock, 2009).

1.1.1- Segmentation of the adult vertebrate

Many tissues in the vertebrate body are segmented. One of the most well-known examples is the axial skeleton with its display of vertebrae and intervertebral discs. The segmentation provides flexibility-with-rigidity to the structure, and also protection for the nervous system within the vertebral foramen. In addition, the musculature of the thorax is another segmented structure. This close relationship provides the motility to the vertebrate trunk (Christ *et al*., 2000).

The vertebrate skeleton has an exo- and endoskeletons. The endoskeleton is mainly the notochord and axial skeleton and is divided into vertebral column, cranium and the pectoral and pelvic girdles and during development remains cartilaginous or ossifies later during development. By contrast, the exoskeleton consists of various mineralized structures, such as dermal bones, plates and scales.

Vertebrate bone is a vascular tissue composed of osteocytes embedded in an extracellular matrix (ECM) and type I collagen. Cartilage, on the other hand, is an

avascular tissue composed of chondrocytes, and the ECM contains type II collagen (Pourquié, 2009).

Superimposed on the segmental structure of the axial skeleton is the segmentation of the peripheral nervous system (PNS) of the trunk. Spinal nerves have two components, motor and sensory axons, that emerges from the spinal cord in pairs on each side of the midline of the vertebral body and leave by the intervertebral foramen (Fig.1.1) (Hughes *et al.*, 2009). The axons of motor neurons exit the ventral spinal cord, while the axons of sensory neurons collected in the segmentally arranged dorsal root ganglia (DRG) enter the dorsal spinal cord. These axons together form the mixed spinal nerve that will innervate specific myotomes and dermatomes (Hughes *et al*., 2009).

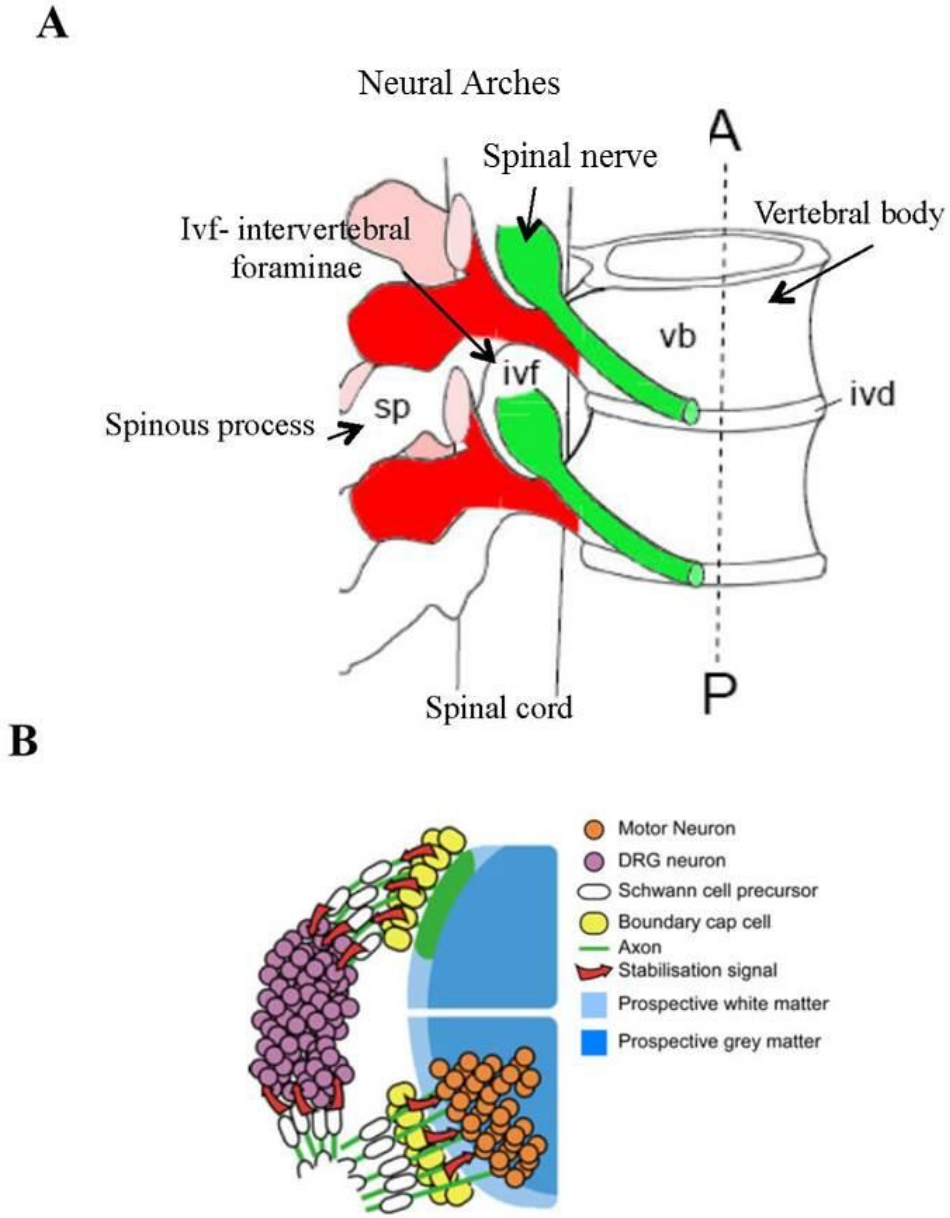

Figure 1.1- Diagram showing the segmental arrangement of vertebrae with the imposition of the nervous system. (A) Spinal nerves exit through the intervertebral foraminae (ivf) localised dorsal to the vertebral body, and vertebral bodies are separated by intervertebal discs (ivd). Schematic adapted from Hughes *et al.* (2009). (B) Diagram of a transverse section of the spinal cord. Motor axons exit the spinal cord ventrally and sensory axons from neurons in the dorsal root ganglia (DRG) enter the spinal cord dorsally. Boundary cap cells are localised at both entry and exit zones. Schematic from Vermeren *et al*. (2003).

1.1.2- Embryonic segmentation

Somitogenesis occurs dynamically as new tissue is being formed. It is this process that offers the basic pattern of the musculoskeletal system; blood vessels and the peripheral nervous system (Maroto and Whittock, 2008). Somitogenesis is the most important example of vertebrate segmentation. It represents the most segmented structure of the body plan, that gives rise to both segmental (e.g. axial skeleton) and metameric (dermis and skeletal muscle) elements. Somites also play a key role in controlling different aspects of the central and peripheral nervous system organization (Sharpe and Mason, 2008).

Somites develop from the segmental plate mesoderm (pre-somitic mesoderm) in an anterior-posterior sequence on either side of the notochord; and they are sequentially added to the growing embryo elongating its axis and organizing vertebral skeleton, muscles, nerves and blood vessels. The dorsal portion of the somite remains epithelial and forms the dermomyotome, which differentiates into muscle and dermis, while the ventral portion undergoes an epithelio-mesenchymal transition, leading to the formation of the sclerotome. The sclerotome will later give rise to the vertebrae, ribs, intervertebral discs and tendons (Pourquié, 2009).

There are many processes by which segments can be formed within embryos, but morphologically they can be categorised into one or two processes. One involves simultaneously the specification of segments with the division of pre-existing domains into smaller segments. The other process by which segments may form involves the sequential addition of segments to one end of a domain, resulting in a progressive elongation of segmenting domains until they bud off.

1.2- Formation of the pre-somitic mesoderm during gastrulation

The mesoderm arises during the process of gastrulation, which generates the three germ layers – mesoderm, endoderm, and ectoderm. The mesoderm forms the somites and yields the largest pool of cells in the vertebrate body that will later give rise to cartilage, bone, skeletal muscle and tendon (Maroto and Whittock, 2008: Wolpert *et*

al., 2007). The endoderm forms the gut and associated organs, while the ectoderm will develop into the skin and nervous system (Wolpert *et al.*, 2007).

In amniotes, the primitive streak is the site of gastrulation. The primitive streak is formed due to collective ingression of epiblast cells towards the primitive streak promoted by the fibroblast growth factor (FGF)-regulated transcription factor Snail. These cells are stem-like progenitor cells (Maroto *et al*., 2012) and different regions of epiblast cells around the primitive streak give rise to specific tissues (Fig. 1.2). At the tip of the primitive streak there is Hensen's node that plays a role in the induction of the nervous system and acts as an organizer of cell movement during late gastrulation (Vasiev *et al.*, 2010).

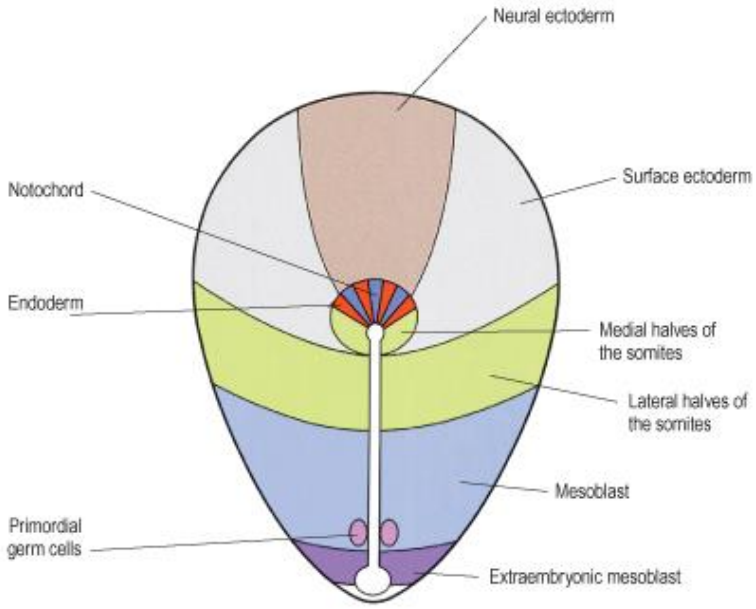

Figure 1.2- Fate-map of the epiblast regions that will give rise to specific tissues. Figure from Standring (2005).

Epiblast cell ingression is a continuous process that starts anteriorly and goes on until the primitive streak retreats caudally. Definitive endoderm is generated from cells of lateral epiblast origin that move towards the primitive streak and ingress through it (Lawson and Schoenwolf, 2003) (Fig. 1.3). At stage 3+ in the chicken embryo (Hamburger & Hamilton, 1951), presumptive dorsal foregut cells ingress from the primitive streak into the lower layer, while presumptive ventral foregut cells ingress into

the middle layer and then move laterally; they only enter the lower layer when they reach the lateral border of the middle layer (Kimura *et al.*, 2006) (Fig. 1.3). As Hensen's node regresses, the notochord (axial mesoderm) is laid down in the midline from progenitors ingressing through the node (anterior streak). More lateral regions of mesoderm (paraxial, intermediate, lateral plate) arise from progenitors ingressing from progressively more posterior regions of the streak (Fig. 1.3 and Fig. 1.4).

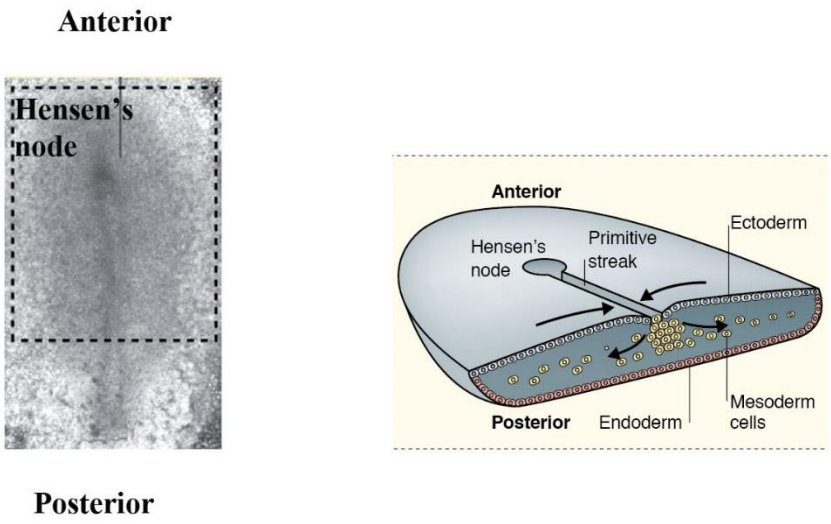

Figure 1.3- Epiblast cells ingress through the primitive streak to form the endoderm and mesoderm. On the left is a photograph of a Hamburger-Hamilton (HH) stage 3+ chicken embryo in dorsal view, showing the location of Hensen's node at the tip of the primitive streak. On the right is a diagram showing cell migration through the primitive streak. Figure from Maroto *et al.* (2012).

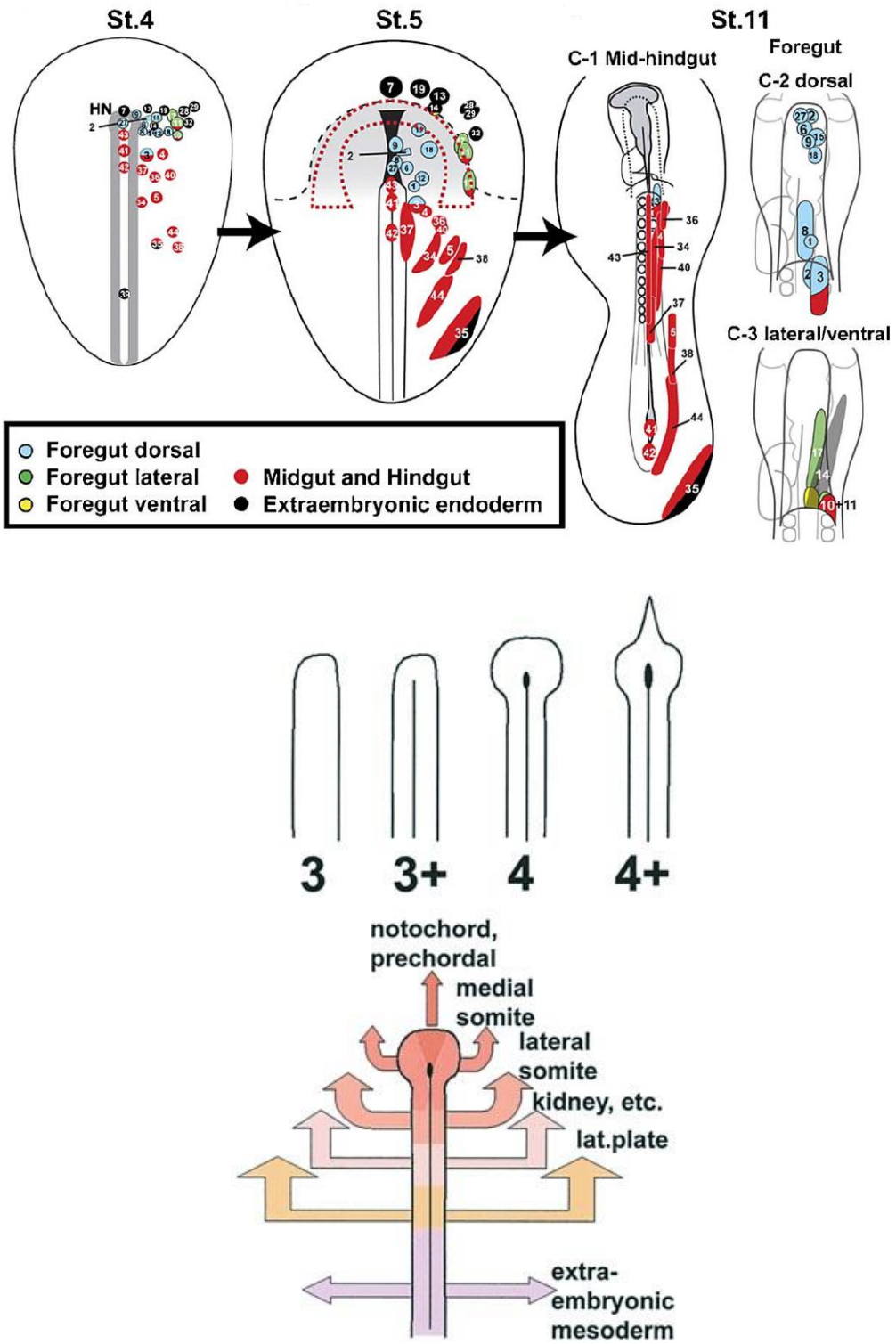

Figure 1.4- Cells ingressing at progressively more posterior regions of the primitive streak form progressively more lateral regions. Top schematic (endoderm) from Kimura (2006). Bottom schematic (mesoderm) from Stern (2004).

1.3- Somitogenesis

The somites bud from the anterior pre-somitic mesoderm (PSM). PSM cells are not committed to a somitic fate, their differentiation is controlled by inductive external signals (Pourquié, 2001; Maroto *et al.*, 2012). Somites are formed in pairs from the paraxial mesoderm on either side of the notochord. During segmentation, the length of the segmental plate remains fairly constant comprising the material for 12 prospective somites, which means that the rate of somite formation must be somehow linked to proliferation. Morphologically, somite differentiation involves the formation of defined boundaries by an epithelial-to-mesenchymal transition (EMT) in the ventral half of the somite that divides the somite into epithelial dermomyotome dorsally and mesenchymal sclerotome ventrally. The newly formed somite is an epithelial ball with a central cavity called a somitocoele containing mesenchymal cells (Kuan *et al*., 2004). The number of somitocoeles corresponds to the number of prospective somites that are contained within the segmental plate. The borders between individual somitocoeles are not well delineated and they do not represent compartments before somites are formed The first step in the EMT is the loss of the cell-cell cohesion between individual cells in the epithelium, primarily by downregulation of cadherins, this step is known as "activation". E-cadherin downregulation contributes to the accumulation of free β-catenin in the cell, important for transducing Wnt signals. This step is followed by the stimulation of cell motility "migration" in order for the mesenchymal cells to disperse (Maroto and Whittock 2008).

The newly formed somites are already pre-patterned along the anteroposterior (AP) axis into anterior and posterior divisions (Takahashi *et al.*, 2010) (see section 1.4). As new somite formation involves budding off from the PSM, and then morphological changes can be observed in the anterior portion, where the cells increase in number and become denser and are arranged in a simple epithelium at the periphery of the paraxial mesoderm (Stern and Keynes, 1987). Once somites are formed from the more posterior PSM, the more anterior somites become mature. Consequently, the somites are most easily identified in terms of their position relative to the PSM; the youngest somite (immediately anterior to the PSM) is termed somite I (Christ *et al*., 2007) (Fig. 1.5). During somite formation, they undergo morphogenesis in the paraxial region: the

somites decrease in length as they expand laterally. When a younger somite (II in Fig. 1.5, section A) is compared to a mature somite (VII from Fig. 1.5, section B), the width decreases by a factor of two, while the length increases by half. From this perspective, it can also be seen that the somite height also increases progressively (compare Fig. 1.5 sections A and B).

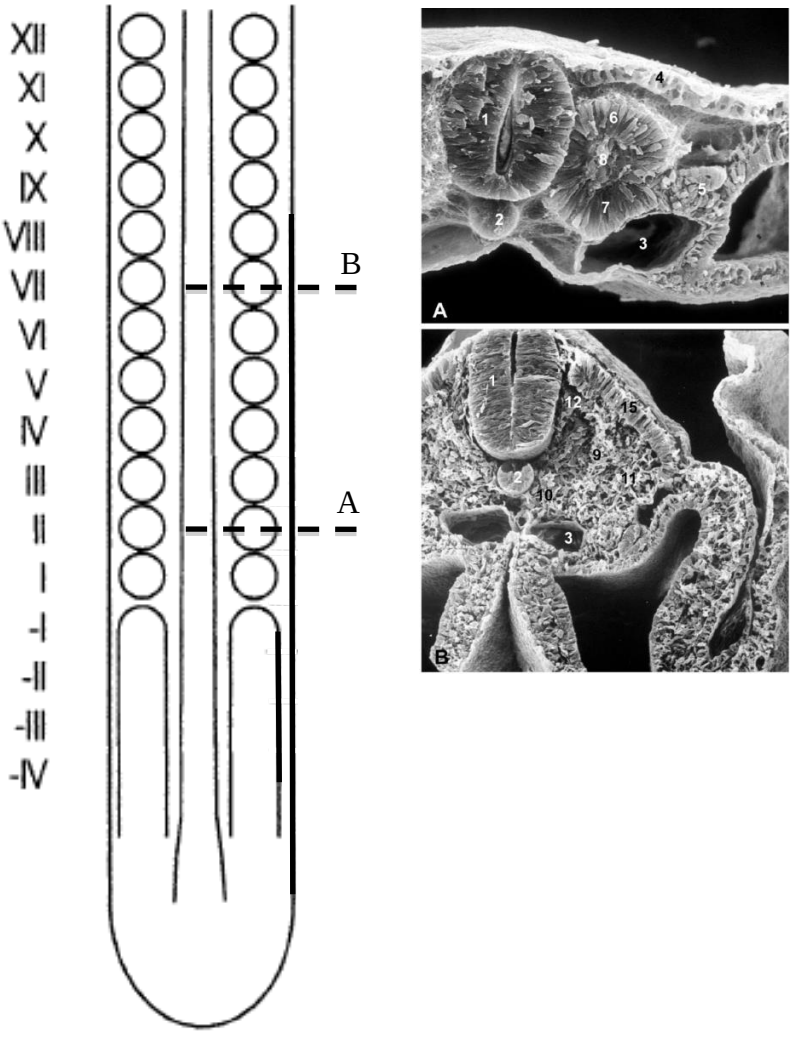

Figure 1.5- Somite maturation. Left: Schematic illustration of somite organization in the vertebrate body plan (adapted from Maroto and Whittock, 2008). Dotted lines show the level of the sections shown in A and B. Right: (A) Transverse section of a young epithelial somite. (B) Transverse section of a mature somite with an epithelial dermomyotome dorsally and mesenchymal sclerotome ventrally. Figure from Christ *et al.* (2007).

Somites are sequentially formed in an anterior-posterior direction, making the anterior somites older than the posterior ones, therefore in Fig. 1.5, somite XII is the oldest formed somite. Each 90 minutes a chick somite is formed and in chick there are 50 somites, in mice there are 65 somites and 500 in snake (Gomez *et al*., 2008). The process by which somites are formed involves a periodic molecular mechanism (Fig. 1.6) and a cell movement described in Fig. 1.7 and in more detail in section 1.4.

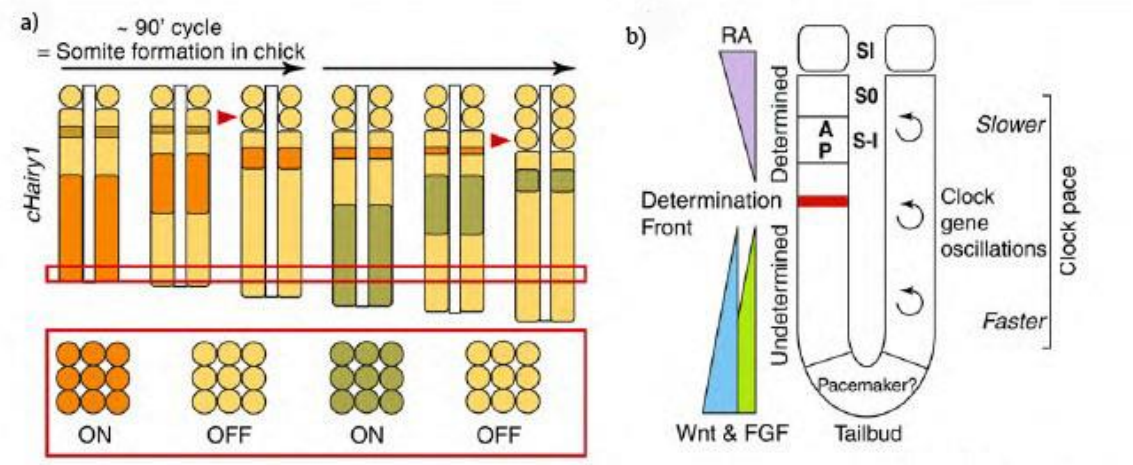

Figure 1.6- Dynamic gene expression in the PSM during somitogenesis. (a) Periodic waves of gene expression present during chick development across the PSM, with a 90-minute periodicity. (b) The intersection of various extracellular signalling gradients (left hand side of diagram) determines the location within the PSM of the "determination front", anterior to which cells become segmentally determined, and clock oscillations slow down (right hand side of diagram). Figure from Gomez *et al*. (2008).

Time-lapse experiments have revealed cell movements involved in formation of new somite boundaries within the anterior PSM (Kulesa and Fraser, 2002). There are a small number of cells in the anterior-medial region of the segmental plate (Fig. 1.7A, white dot) next to the neural tube and anterior to the presumptive somite boundary (white arrow) that come together and form a distinct subgroup and separate slightly from the PSM (Fig. 1.7B). This subgroup movement appears like a sleeve of about one cell thick and extends about five cell diameters anterior to the PSM between S0 and the

segmental plate (white arrow). About the same time a different set of cells within the segmental plate come together (Fig.1.7A,B; near black dot), and initiate tissue separation. This group of cells extend about four cell diameters posterior to the PSM border between s0 and the segmental plate (white arrow).

After tissue separation, epithelialisation seems to first occur at the anterior and medial border of the somite s0, then it starts to orchestrate cell exchanges, where the group of cells within the s0 (white dot) move towards the posterior direction while the second group of cells within the segmental plate (black dot) move in the anterior direction. These opposing movements create a gap on the medial side of the segmental plate (Fig. 1.7B-D), leading to the formation of the somitic border. In order for s0 to separate from the segmental plate, the cells of the somite and the segmental plate propagate in the medial-to-lateral direction (Fig. 1.7B-F, white arrow) conferring sI status to somite s0. It now has an appearance of an epithelial structure, resembling a ball elongated in the radial direction (Fig. 1.7E,F) (Kulesa and Fraser, 2002).

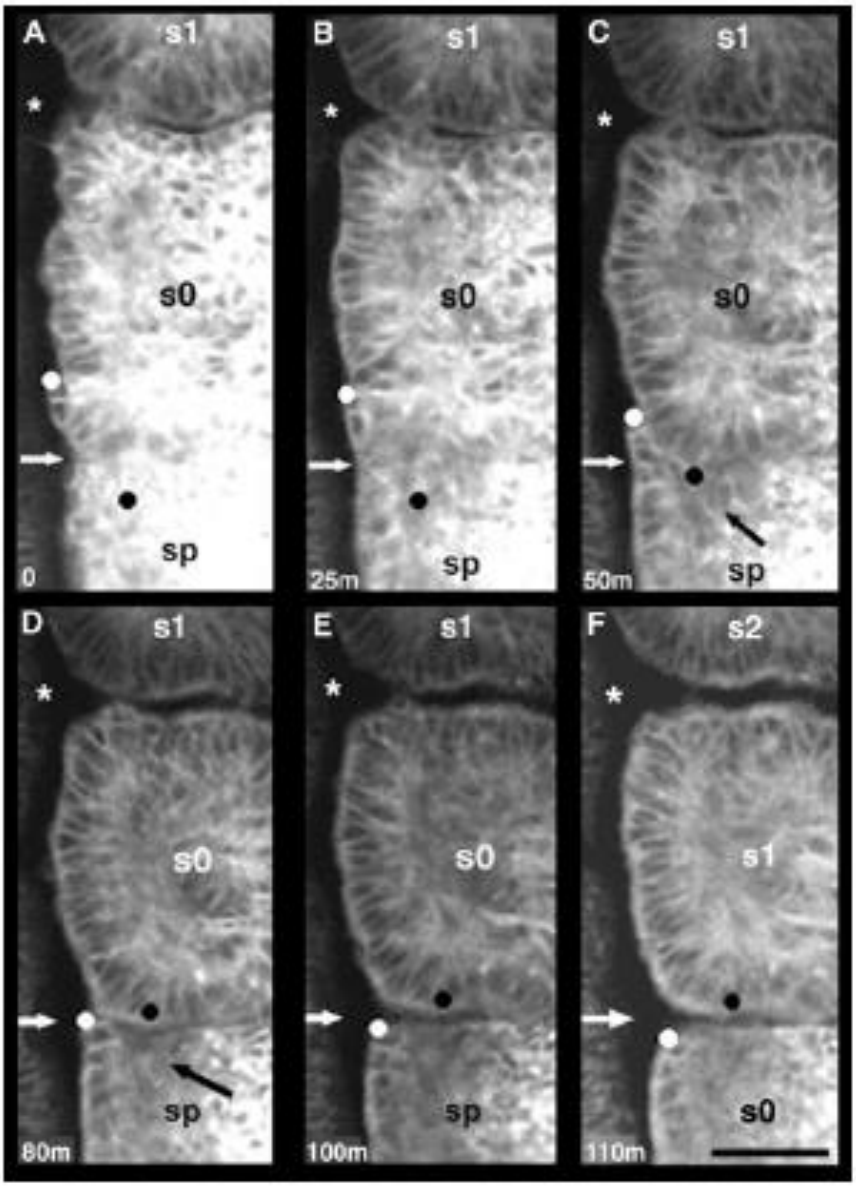

Figure 1.7- Confocal time-lapse imaging series of somite boundary formation. (A) Initiation of somite s0 separation from the segmental plate is marked by the separation of a sleeve of cells (white dot). At the same time, a second subgroup of cells in the segmental plate (black dot) coalesce. The presumptive somite boundary (white arrow) and anterior border of s0 (asterisk) are labeled. (B) The sleeve of cells (white dot) moves in the posterior direction, and the second subgroup of cells (black dot) begins to move in the anterior direction. (C) The anterior movement of the second subgroup of cells (black dot) leaves a gap in the tissue in the anterior portion of the segmental plate (black arrow). (D) The sleeve of cells (white dot) folds into the gap in the segmental plate while the second subgroup of cells (black dot) becomes integrated into s0. (E) The sleeve of cells (white dot) becomes part of the anterior border of the segmental plate, and the cells from the segmental plate (black dot) form part of the posterior border of s0. (F) Completion of the posterior border transforms s0 into s1. Scale bar, 50 μm; elapsed time is in minutes. Figure from Kulesa and Fraser (2002).

1.4- Anteroposterior Polarization of the Presomitic Mesoderm

The anterior-posterior polarization of the PSM and hence the patterning of the peripheral nervous system in the trunk depend upon the set-up of the anterior-posterior axis of the embryo. One aspect is the large scale arrangement of the vertebrate body by the *Hox* code (Wolpert *et a*l., 2007). *Hox* genes affect not only AP body axis formation but also the patterning of different body segments (Gilbert, 2006). First found in *Drosophila*, they turned out to be highly conserved during evolution. The *Hox* genes encode homeodomain-containing transcription factors and in vertebrates, *Hox* genes are organised in four clusters (A, B, C and D) (Fig.1.8). *Hox* gene expression is initiated during the formation of the primitive streak, and after gastrulation their initial patterning function is complete (Maroto and Whittock, 2008). The expression of different *Hox* genes in different regions of the body (Fig. 1.8) (Gilbert, 2006) forms a '*Hox* code' that imparts regional differences along the body axis e.g. different vertebral identities (e.g. lumbar vs thoracic) are imparted by different combinations of *Hox* genes.

Despite the ancestral relation between mouse and chicken, they differ in the number of vertebrae, which is reflected in changes in *Hox* gene expression. Mice (like all mammals) have only seven cervical vertebrae (Fig. 1.9). These are followed by 13 thoracic vertebrae, 6 lumbar vertebrae, 4 sacral vertebrae and a variable number of caudal vertebrae. In the chicken, there are 14 cervical vertebrae, 7 thoracic vertebrae, 12-13 lumbosacral vertebrae and 9 sacral vertebrae (Fig. 1.9) (Gilbert, 2006). Fig. 1.9 shows the somites contributing to the different vertebrae and the corresponding *Hox* gene expression patterns in the chicken versus mouse.

How somite polarization along the anteroposterior axis first arises has been intensively investigated. Somite polarization in the pre-somitic mesoderm (PSM) is governed by a molecular oscillator termed the segmentation clock. It was first postulated by Cooke and Zeeman (1976) (cited in Kulesa *et al.,* 2007), and has now been confirmed by the expression of several genes showing cyclic patterns in the PSM (Gridley, 2006). The oscillations observed within cells at the posterior end of the PSM are synchronized through the intercellular interaction between neighbouring cells (Koichiro *et al*., 2009). These boundary-forming cells have an instructive effect on the

cells anterior to them and cause them to epithelialize and separate (Kulesa and Fraser, 2002). Two important molecules have been identified which mediate the property of boundary induction: Notch and Lunatic fringe (Wolpert *et al*., 2007).

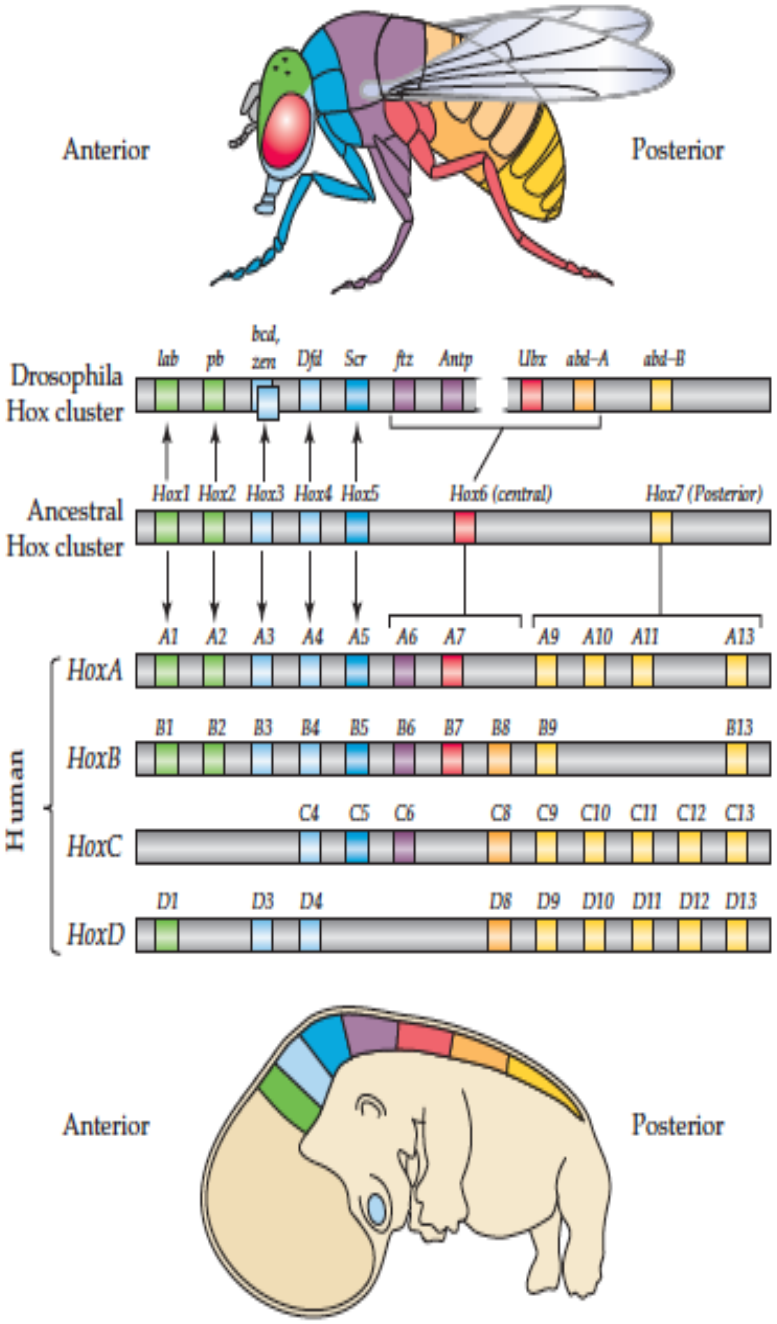

Figure 1.8- Parallels between *Drosophila* and human *Hox* genes. The different pattern of *Hox* gene found in both species in each particular body region. Figure from Gilbert (2006).

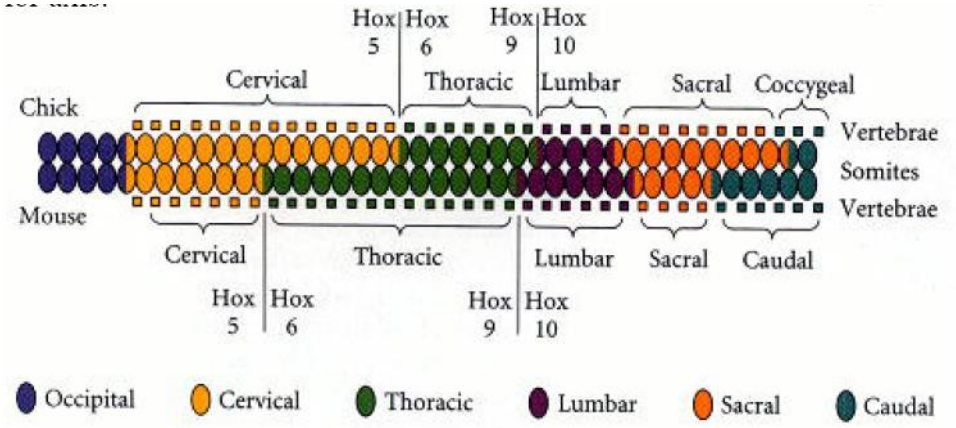

Figure 1.9- Similarity between mouse and chick in the *Hox* patterning and somite fate. Figure from Gilbert (2006).

Notch, a transmembrane protein, acts as a receptor for the transmembrane ligands Delta and Serrate: their binding to Notch results in its proteolytic cleavage, releasing the Notch intracellular domain (NICD), which enters the nucleus where it interacts with DNA-binding proteins and activates target gene expression (Fig.1.10). Notch target genes include the *Hes/Hey* genes, which encode basic helix-loop-helix transcriptional repressors. Lunatic fringe, a glycosyl transferase, is encoded by a Notch target gene and at the same time negatively modulates Notch activity.

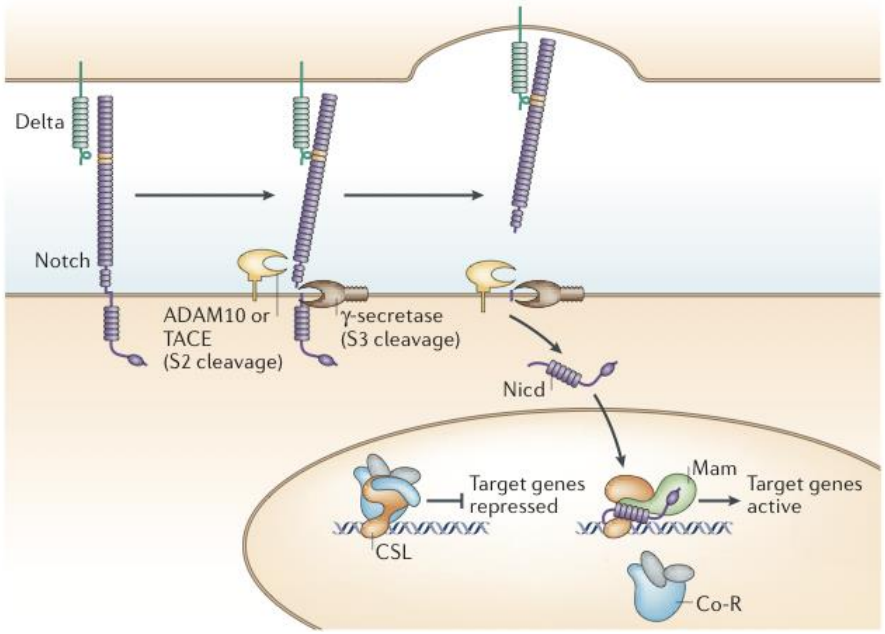

Figure 1.10- The core Notch pathway. **Figure from Bray (2006).**

Somite polarity starts to be predetermined in the PSM triggered by a genetic cascade initiated by Notch/Tbx6-dependent activation of the transcription factor Mesp2 just anterior to the determination front in the PSM (Fig. 1.6; Fig. 1.11) (Maroto *et al*., 2012). Mesp2 is subsequently downregulated in the posterior half of the prospective somite but remains active in the anterior half; Mesp2 induces Eph-ephrin signalling leading to somite boundary formation (Fig. 1.11) (Maroto *et al*., 2012).

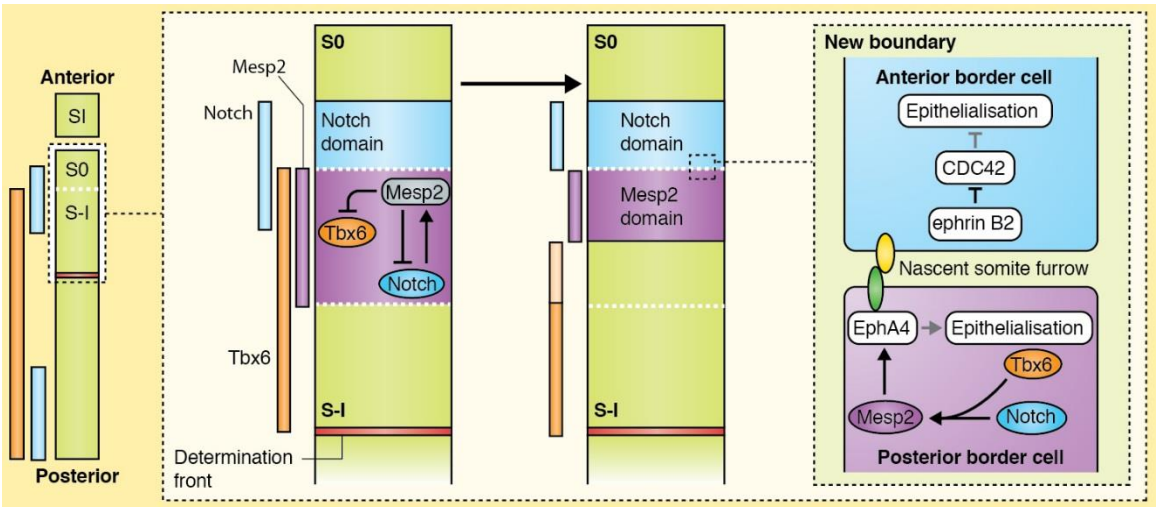

Figure 1.11- Somite boundary formation and anterior-posterior patterning. A genetic cascade initiated by Notch/Tbx6-dependent activation of the transcription factor Mesp2 just anterior to the determination front leads to activation of Eph/ephrin signalling and the formation of a new somite boundary. Downregulation of Mesp2 in the posterior half of the presumptive somite and its maintenance in the anterior half is critical for the specification of anterior and posterior somite compartments. Figure from Maroto *et al*. (2012).

Notch and its ligands, Delta-like1 (Dll1) and Delta-like3 (Dll3) have a key role in somitogenesis. Mouse *Notch-1* is expressed in the whole presomitic mesoderm, with a peak of expression in the next-to-be-formed somite. Dll1 and Dll3-mediated Notch signalling and Mesp2 keep the stripe segmentation on the PSM. Feedback loops of *Dll1* and *Mesp2*, in which Dll1-Notch signalling induces *Dll1* and *Mesp2* expression and Mesp2 suppresses *Dll1* expression, are essential for anterior-posterior polarity, while *Dll3* is necessary for localization and integration of expression and *Dll1* and *Mesp2* (Fig. 1.11 and Fig. 1.12) (Maroto and Whittock, 2008). Its disruption leads to a delay in

somitogenesis and defects in somite development characterized by irregular border formation (Conlon *et al*., 1995) and cause development defects. Dll3-null mice have a shortened trunk and a small tail and a disorganised axial skeleton and a similar phenotype is present in embryos that lack any of the genes involved in the pre-patterning of the PSM.

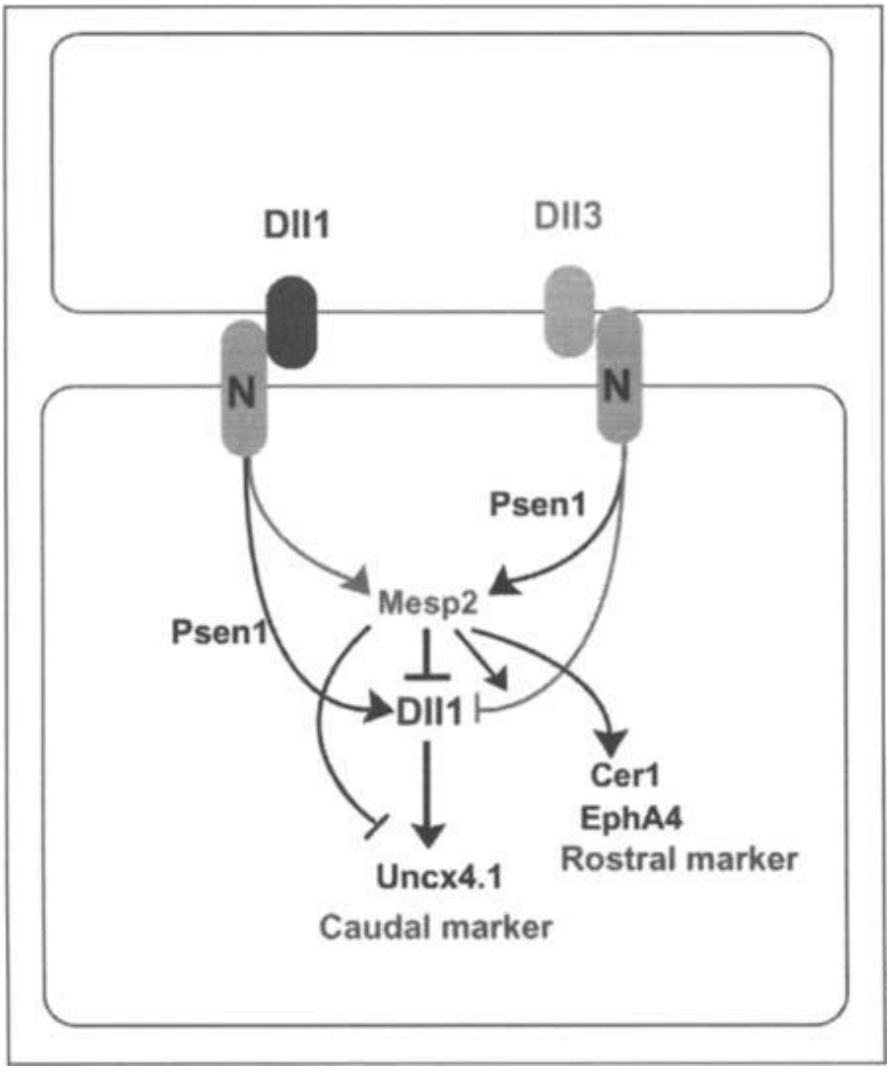

Figure 1.12- Genetic interactions in the PSM that are important for establishing anterior-posterior patterning. Figure from Maroto and Whittock (2008).

Notch is a large transmembrane receptor that recognizes two other transmembrane proteins, Delta and Serrate. Fig. 1.12 and Fig. 1.14 shows a model of somitogenesis involving Notch and its ligands, Delta-like1 (Dll1) and Delta-like3 (Dll3), and the γ-secretase complex component Presenilin 1 (Ps1), leading to a periodic arrangement of signalling and receiving cells in the presomitic mesoderm and establishment of somite boundaries. The transmembrane protein Notch binds to its transmembrane ligands on adjacent cells; first the ∂-secretase complex and then the gamma-secretase complex (which includes Presenilin1) cleave the Notch receptor and the Notch intracellular domain (NICD) translocates to the nucleus (see Fig. 1.10) (Koizumi *et al.*, 2001, Johnson *et al.*, 2009). Presenilin is one of the markers of somitogenesis and it is required for segmentation of the presomitic mesoderm into somites (Donoviel *et al.*, 1999). In mammals presenilin has two isoforms 1-2: presenilin is a multi-pass transmembrane protein that together with nicastrin, Aph-1 and PEN-2 forms the gamma-secretase complex that cleaves Notch at S3 and S4 (Fiúza and Martinez Arias, 2007). This complex releases the Notch intracellular domain (NICD) from the membrane to the nucleus where it is enrolled in a correct somite boundary formation via segmentation clock, also inhibits muscle cell differentiation via Wnt suppression (Fiúza and Martinez Arias, 2007).

1.4.1- Molecular oscillation clock within somitogenesis

The segmentation of the PSM involves a dynamic and periodic mRNA expression of different genes, called ‘clock’ genes. The existence of this molecular clock within the segmental plate in the cells destined for somite formation involves the Notch target genes *Hairy1* and *Hairy2* in chick and *Hes1* and *Hes*7 in mouse across the PSM (Koichiro *et al*., 2009). All of these genes appear to be regulated by the Delta-Notch pathway (Andrade *et al*., 2007), Wnt and Fgf signalling (Pourquié, 2001), and essential for segmentation of the segmental plate (Stockdale *et al*., 2000). This cyclic gene pattern can be thought of as a “travelling wave” movement that is present in a synchronized periodic fashion across the PSM until the anterior limit of the PSM where then a somite pair buds off and a new wave is initiated from the posterior PSM in a new cyclic fashion.

A number of other genes in the PSM have been identified that include components of the Notch, Wnt and Fgf pathways that are connected (Fig. 1.13; Fig. 1.14). Components of these pathways are cyclically present in the PSM suggesting their dynamic involvement in the wavefront. As previously described, Notch signalling is required to keep negative-feedback loops encoded by Hes7 and Lunatic fringe (Lfng). The downregulation of Wnt signalling arrests oscillation in the anterior PSM ensuring that the oscillations occur with the correct periodicity. Cells posterior to the determination front are maintained in a non-determined state due to FGF activity, and changes in FGF signalling are reflected in somite size (Maroto *et al.*, 2012).

This cyclic gene pattern can be thought of as a "travelling wave" movement; the area of high expression moves from a posterior to anterior direction where it is arrested by Mesp2, nevertheless, it is the Notch-dependent cell-cell interactions that are responsible for synchronization of the clock genes (Andrade *et al.*, 2007). It is important to have an insight into this pathway, as small changes can have large effect on embryonic development.

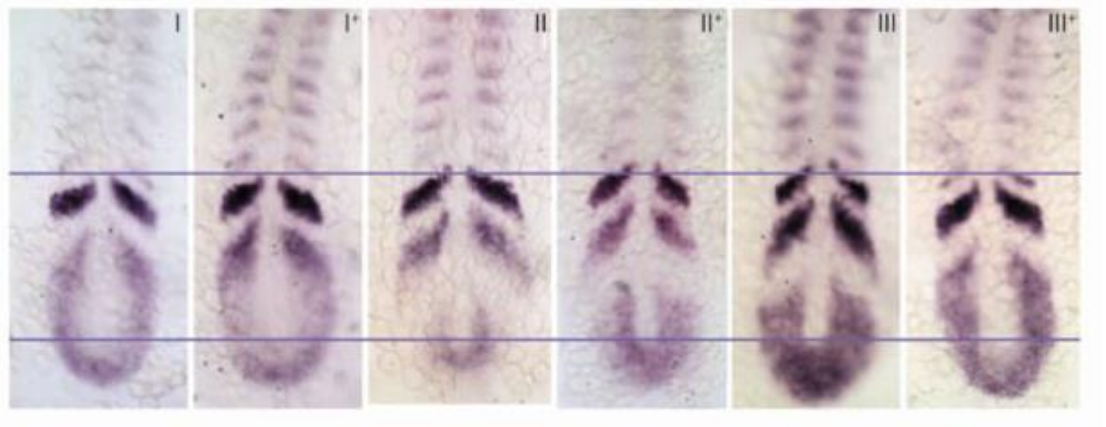

Figure 1.13- Different patterns of expression of the Notch ligand gene *deltaC* in the PSM in the zebrafish. Phases are designated from I to III+ to match the terminology for the *c-hairy1* cycle in the chick. Figure from Jiang *et al.* (2000).

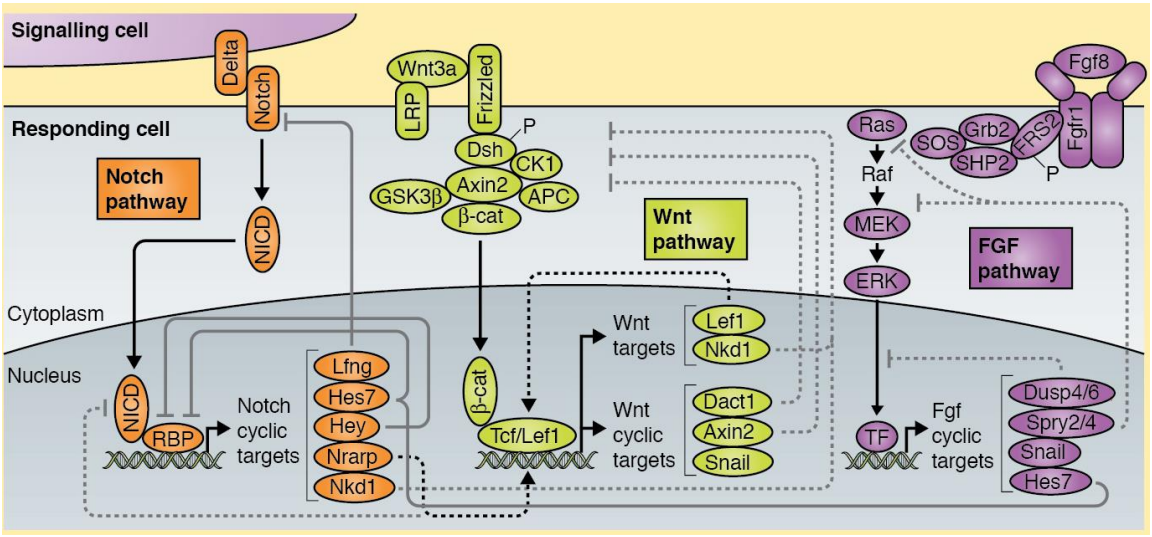

Figure 1.14- Segmentation clock during somitogenesis, regulation of Notch, Fgf and Wnt pathways. Notch and Fgf-regulated genes oscillate asynchronously to cycling genes of the Wnt pathway. Figure from Maroto *et al.* (2012).

1.4.2- Other signalling pathways important for somite formation

A key component for symmetric somite formation (i.e. the co-ordination of left and right somites) is retinoic acid. Retinoic acid regulates somite boundaries through signalling. This is a gradient signal that runs in the opposite direction of an anterior gradient of fibroblast growth factor (FGF) 8 and Wnt3A (Figure 1.15) (Gridley, 2006). Retinoic acid biosynthetic enzyme retinaldehyde dehydrogenase type 2 (RALDH2), also acts upon the somite synchronization across the left-right axis.

Dynamic *FGF8* expression occurs in the posterior part of the PSM. As the axis elongates, the wavefront of *FGF8* moves in a posterior direction so that signalling levels remain constant to the PSM moving. Cells move up through the PSM as development proceeds so that cells are initially part of the region where FGF signalling prevails but levels start to get lower as the gradient becomes less. *FGF8* perturbations result in the formation of abnormally small somites and in one abnormally large somite meaning *FGF8* is important for control somite size formation (Baker *et al*., 2006).

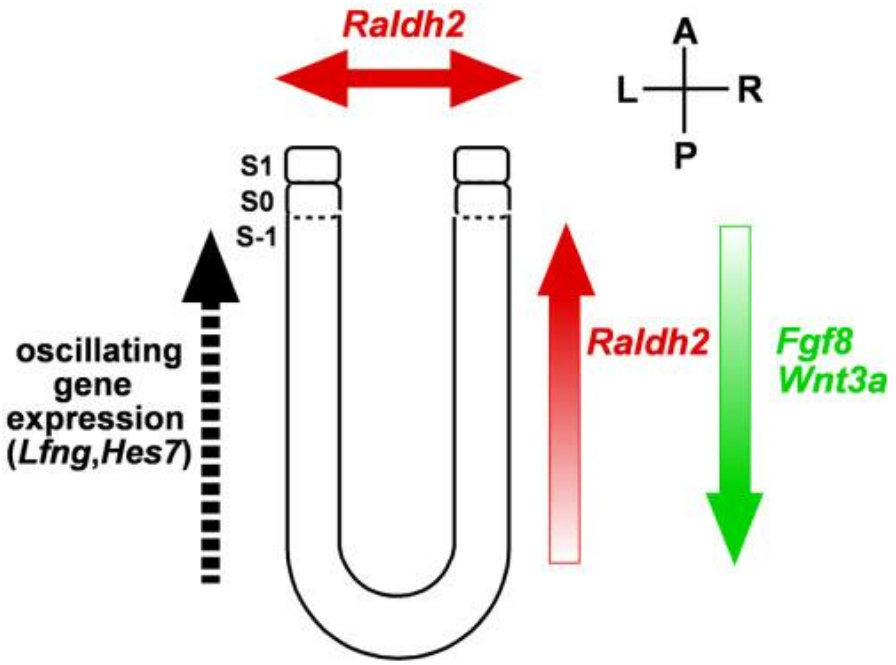

Figure 1.15- Major signalling pathways besides Notch regulating somitogenesis. Molecular oscillator and the segmentation clock in somite formation. Genes comprising this clock have a cyclic expression pattern in the presomitic mesoderm progressing from posterior to anterior direction (dotted black arrow). The periodic signal is converted into a repeated array of regularly spaced somite boundaries by a mechanism that involves decreasing posterior-anterior gradient of Fgf8 and Wnt3a expression (green arrow). The function of these two genes is controlled by a gradient of retinoic acid signalling, the decreasing expression of *Raldh2* that runs in the opposite direction (red arrow) and also on the left-right axis (double red arrow). S1, most recently formed somite; S0, somite in the process of forming the posterior somite boundary; S-1, region of the presomitic mesoderm that will form the next somite. Figure from Gridley (2006).

1.5- Somite fate

Different regions of a somite have different fates. The older somites start to differentiate earlier than recently formed somites, and start to acquire morphological differences that allow distinction between different types of tissue. The dorsal half of the somite keeps its epithelial character, differentiating into the dermomyotome. The dermomyotome later subdivides into a superficial dermatome and a deeper myotome. The dermatome will give rise to the dermis while the myotome develops into epaxial muscles (vertebral column muscles) from its dorsal component and hypaxial muscles (limb and body wall muscles) from its lateral part (Pourquié *et al.*, 1995). The rest of the

somite will become sclerotome by an EMT. This polarization of the somite therefore leads to two somitic compartments, the dermomyotome and the sclerotome (Fig. 1.16 (Christ *et al*., 2007)**.** In addition, there is a sclerotomal fissure, von Ebner's fissure, that divides the sclerotome into anterior (A-half) and posterior (P-half) halves. This morphological marker reflects the site of resegmentation of the sclerotome into the vertebral bodies at a later stage of development (Maroto and Whittock, 2008) (see section 1.5.2).

Somites are ultimately responsible for the arrangement of the different segmental structures, the vertebrae and the intervertebral discs, the ribs, muscles, tendons, ligaments, dorsal root ganglia, peripheral spinal nerves, and blood vessels of the adult vertebrate trunk.

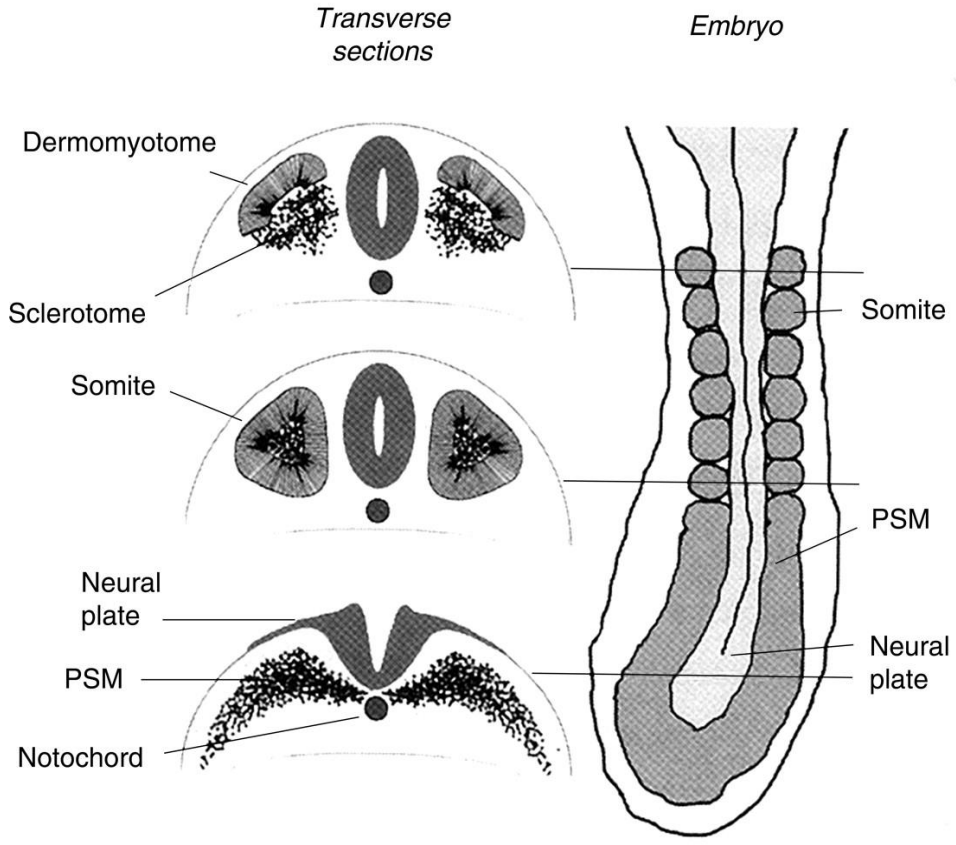

Figure 1.16- Somite cross sections at different levels during development, showing how somite differentiation differs from anterior to posterior. The anterior somites have already differentiated into sclerotome and dermomyotome while the pre-somitic mesoderm (PSM) is still forming more somites. Figure from Wills and Dormans (2006).

1.5.1- Formation of the dermomyotome and myotome

The dermomyotome is formed as an epithelium overlying the sclerotome (Figs. 1.16 and 1.17). This sheet expands, becoming rectangular, and eventually it becomes separated by the inter-somitic blood vessels. This epithelial region later undergoes EMT to form the dermatome which will give rise to the connective tissue, endothelium and dermis of the back (Gilbert, 2006).

Cells at the lips of the dermomyotome undergo local de-epithelialisation and migrate under the dermomyotome or central dermomyotome that span the anteroposterior length of the somite, and together form the myotome that will later give rise to the epaxial muscles. These muscles are formed from a region closest to the neural tube and will give rise to the intercostal musculature between the ribs as well as the deep muscles of the back. There are also myoblasts formed in the region further from the neural tube producing the epaxial muscles of the body wall, limbs, and tongue (Gilbert, 2006). Dermomyotomal fate is determined and maintained by dorsalizing signals from adjacent structures (e.g. neural tube and ectoderm) (Figs. 1.16 and 1.17) (Christ *et al*., 2007).

Neurotrophin-3 from the neural tube specifies the dermatome, the precursor of dermis tissue (Maroto *et al.,* 2012). The removal of the neural tube leads to cell death and degeneration in the medial dermomyotome (Fleming *et al*., 2001). Consequently, the dorsal dermis and the epaxial muscles, both derived from the dermomyotome, are absent or deformed. Subsequently, if the neural tube is replaced by the induction of Wnt-1 expressing cells, some but not all of the dermomyotome tissues are recovered. Therefore, Wnt-1 appears to be responsible for the formation of the dermis but not of the epaxial muscles, suggesting the importance of other signals originating from the ectoderm, and also demonstrating the cooperation of both structures in dermomyotome differentiation and fate.

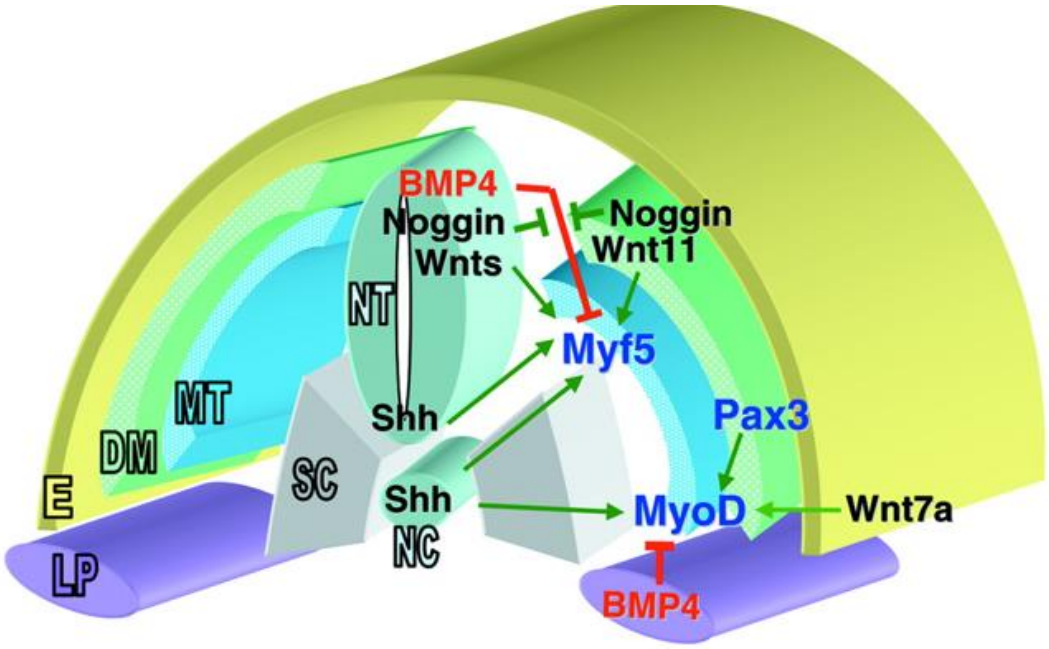

Figure 1.17- Signalling pathways and transcription factors involved in myotome formation. Somite cells receive signals from surrounding tissues including Wnts, Sonic hedgehog, Noggin and BMP4, inducing expression of the myogenic transcription factor genes *Myf5* and *MyoD* and commitment to the myogenic lineage. Committed myoblasts migrate laterally to form the myotome (MT), which eventually forms the skeletal musculature. *Pax3* promotes myogenesis in the lateral myotome. E, ectoderm; DM, dermomyotome, LP, lateral plate mesoderm; SC, sclerotome; NC, notochord; NT, neural tube. Adapted from Chargé and Rudnicki (2004).

1.5.2- Sclerotome fate

Sclerotome formation is characterized by an epithelio-mesenchymal transition (EMT) of the ventral half of the somite and the migration of mesenchymal cells under the notochord to form the peri-notochordal tissue (Christ *et al*., 2007). The sclerotome is separated into anterior and posterior halves by a morphological feature called von Ebner's fissure. The halves have different areas (central, dorsal, lateral, ventral) and markers (Fig. 1.18) and each one of them participates in the formation of the axial skeleton by forming different structures (Fig. 1.18).

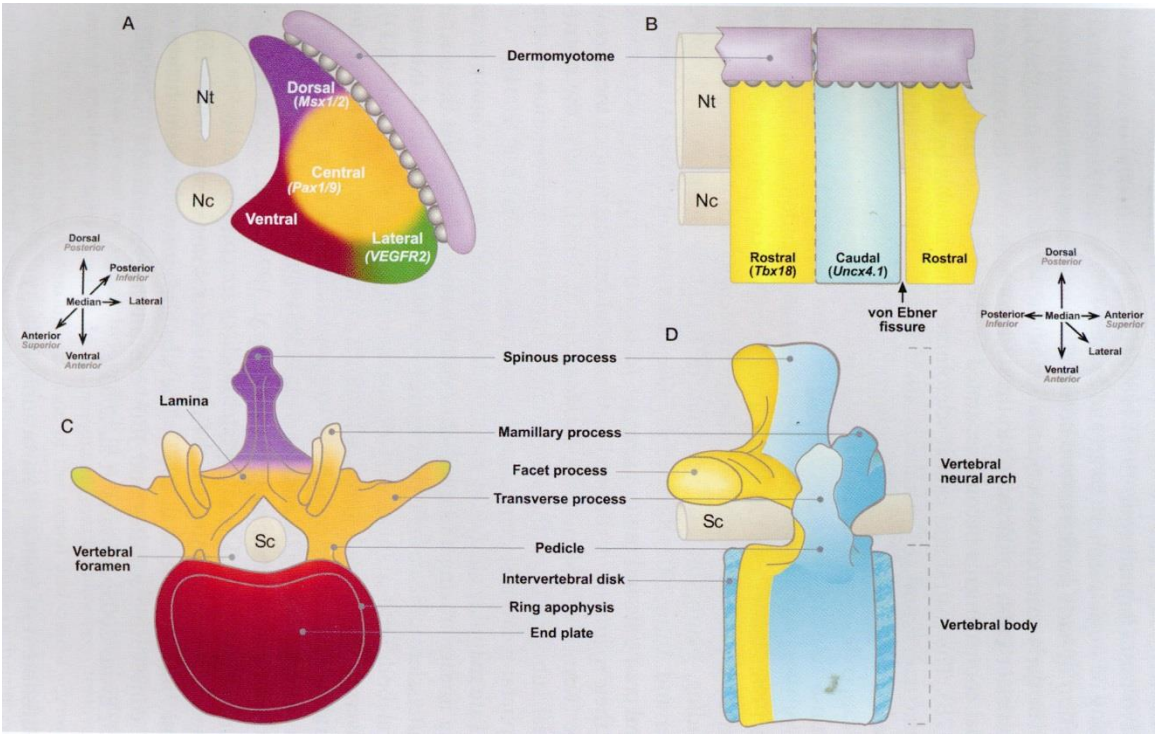

Figure 1.18- Sclerotome divisions according to molecular markers and the fate map of their contribution to vertebrae. (Nt) neural tube, (Nc) notochord, (Sc) spinal cord. Figure from Pourquié (2009).

Sclerotome subdomains receive signals from the surrounding structures, as described in section 1.5.1, to differentiate into their final structures. These genes are expressed under the influence of signals from the midline notochord and floorplate (Kuan *et al*, 2004). It is the anterior-central half-sclerotome that is ultimately responsible for ensuring that the spinal nerves exit the spinal cord and are not trapped by bone. The trajectory of spinal nerves is controlled by surrounding tissues induced by the notochord. Somite grafting has shown that a single somite generates a single muscle segment but it contributes to two adjacent vertebrae; where a single vertebra derives from a recombination of the anterior half of one somite with the posterior half of the next-anterior somite in the series is a process called resegmentation (Saga and Takeda, 2001) (Fig. 1.19). The resegmentation hypothesis stipulates that the region of the somite that forms the vertebrae is the sclerotome, and that its polarization into anterior and posterior halves is critical in positioning the early elements of the nervous system correctly into the developing vertebral column (Kuan *et al*., 2004). Somite cell lineage

studies, involving surgical grafting of half-somites from quail into chick embryos, confirmed that vertebral bodies arise from cells of adjacent somites (Aoyama and Asamoto, 2000). It is this arrangement that allows for a flexible and strong vertebral column.

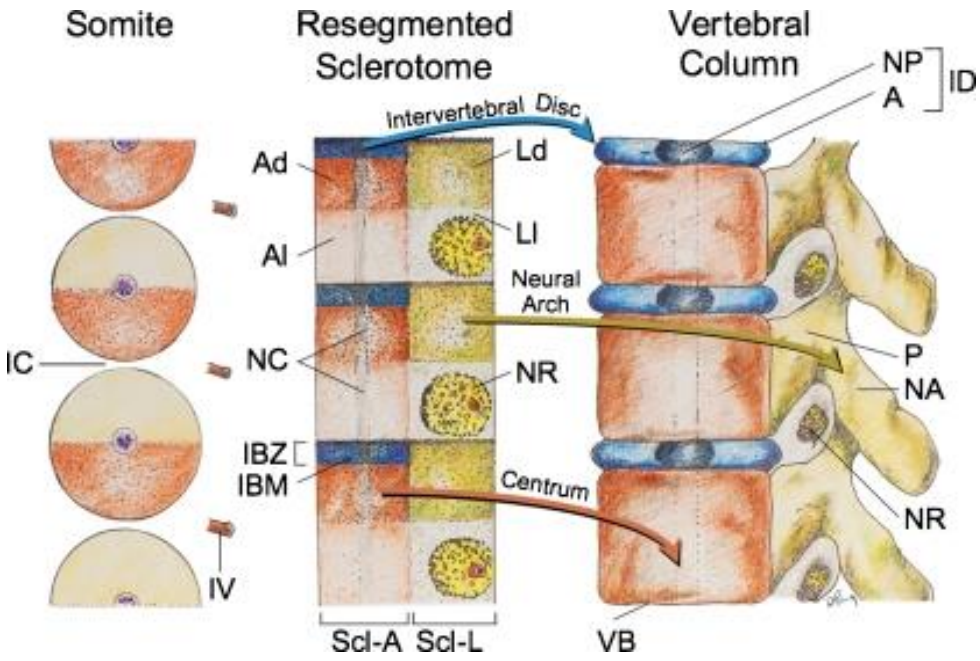

Figure 1.19- Segmentation and resegmentation in amniotes to form the mature vertebral column. "During resegmentation, the sclerotome is formed from the caudal and rostral halves of two adjacent somites, such that the middle of the resegmented sclerotome lines up with the intersomitic cleft (*IC*). Both the axial sclerotome (*Scl-A*) and lateral sclerotome (*Scl-L*) develop dense and loose zones. The dense zone of the lateral sclerotome (*Ld*) becomes the neural arch (*NA*) and pedicle (*P*), which is attached to the rostral part of the vertebral body (*VB*) formed from chondrification of the loose (*Al*) and part of the dense zones (*Ad*) of the axial sclerotome. The rostral layer of the dense zone of the axial sclerotome soon forms the intervertebral boundary zone (*IBZ*) containing intervertebral boundary mesenchyme (*IBM*), which ultimately forms the annulus (*A*) and, together with notochord remnants (*NC*), the nucleus pulposus (*NP*) of the intervertebral disc (*ID*). The loose zone of the lateral sclerotome (*Ll*) does not form bone but promotes emergence of the nerve roots (*NR*). Thus, the neural arch is derived from a single somite but the vertebral body receives contributions from two adjacent somites. *IV* intersomitic vessel. *Arrows* indicate developmental fates of the sclerotomes". Figure and legend from Pang and Thompson (2011).

Parallel to resegmentation, the notochord also undergoes a differentiation process, as a result of the orchestration of signals such as Noggin, Fgf and Shh together with activity of the transcription factor Sox9, that leads to the formation of the

intervertebral discs and the annulus fibrosus, where the continuous notochordal cells become incorporated into the intervertebral discs (Fig. 1.20) (McCann *et al.*, 2012).

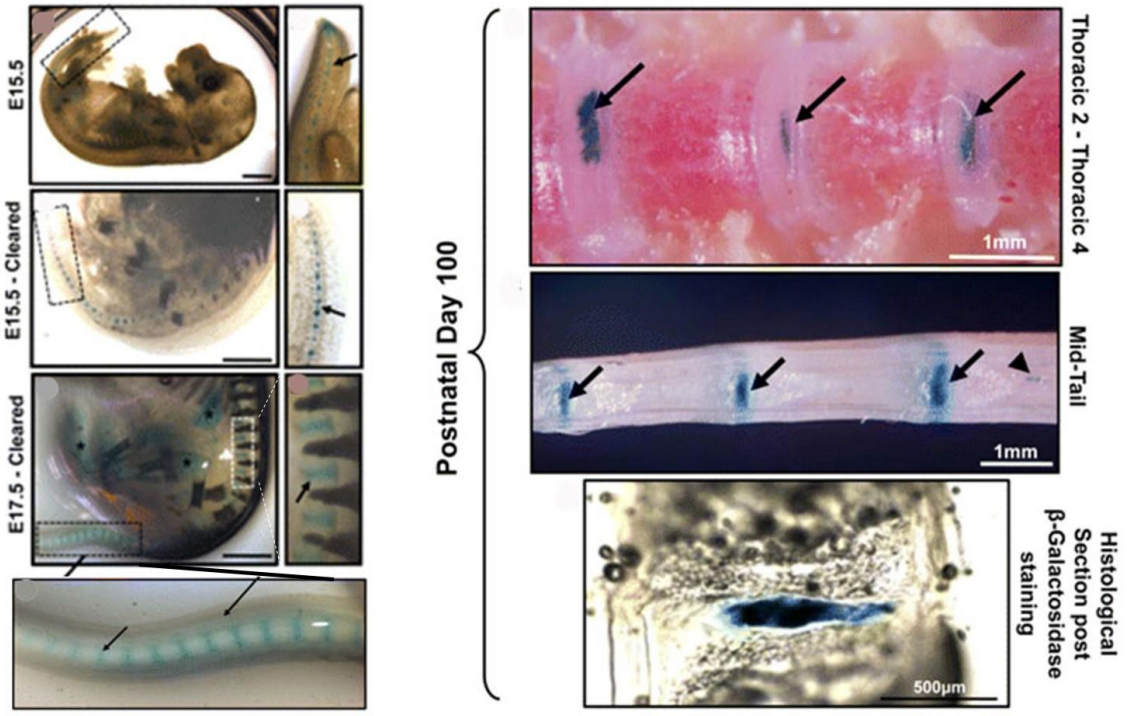

Figure 1.20- The notochord forms the intervertebral discs. Cell lineage studies using embryos from a notochord-specific Cre driver line crossed with a ubiquitous β-galactosidase reporter line (Notocre/+;R26R/+). Staining pattern of β-galactosidase, demonstrating the localization of notochord-derived cells through development (stages indicated) showing expression within the intervertebral discs from the tail to the upper thoracic spine. Figure from McCann *et al.* (2012).

1.6- Sclerotome and Peripheral Nervous System development

As has been described in earlier sections, the sclerotome is divided into anterior- (A-half) and posterior-halves (P-half), with distinct molecular, cellular and functional characteristics. It is the difference between these two halves that is responsible for the segmentation of the peripheral nervous system (PNS). The restriction of peripheral

nerves to the anterior-half sclerotome was initially described by Remak in 1855, and later by Thus Tellu in 1923, but it was suggested that motor axons first grow towards the myotome and then become confined to the posterior half (as referenced in Maroto and Whittock, 2008). It was only in 1984 that Keynes and Stern discovered that axons only cross over the anterior sclerotome (Keynes and Stern, 1984). Since then many studies have been carried out to try to explain the mechanism behind this finding but it is still poorly understood. However, what is known is that the structures responsible for this mechanism are the somites which guide axons after they exit the spinal cord: this was determined in the following manner.

Rotation experiments were carried out in neural tube and in segmental plate mesoderm (Fig. 1.21) (Keynes and Stern, 1984). First, a portion of neural tube opposite 2 or 3 somites was rotated 180º around the anteroposterior axis prior to axon outgrowth, so that the previous anterior half-somite came now to lie in the opposite half. After two days of recovery it was possible that the rotation of the neural tube did not have any effect on the orientation of the axons, since they had still grown out through the anterior halves (Fig. 1.21-a). Second, a portion of segmental plate mesoderm, 2-4 presumptive somites long, was rotated 180º around the anteroposterior axis; this time, however, the rotation had an impact on the axons, which traversed the posterior (original anterior) halves of the somite (Fig. 1.21b). This last rotation led to a new milestone in research into patterning of the peripheral nervous system in the trunk, by proving that the somites are solely responsible for the guidance of motor axons (Keynes and Stern, 1986).

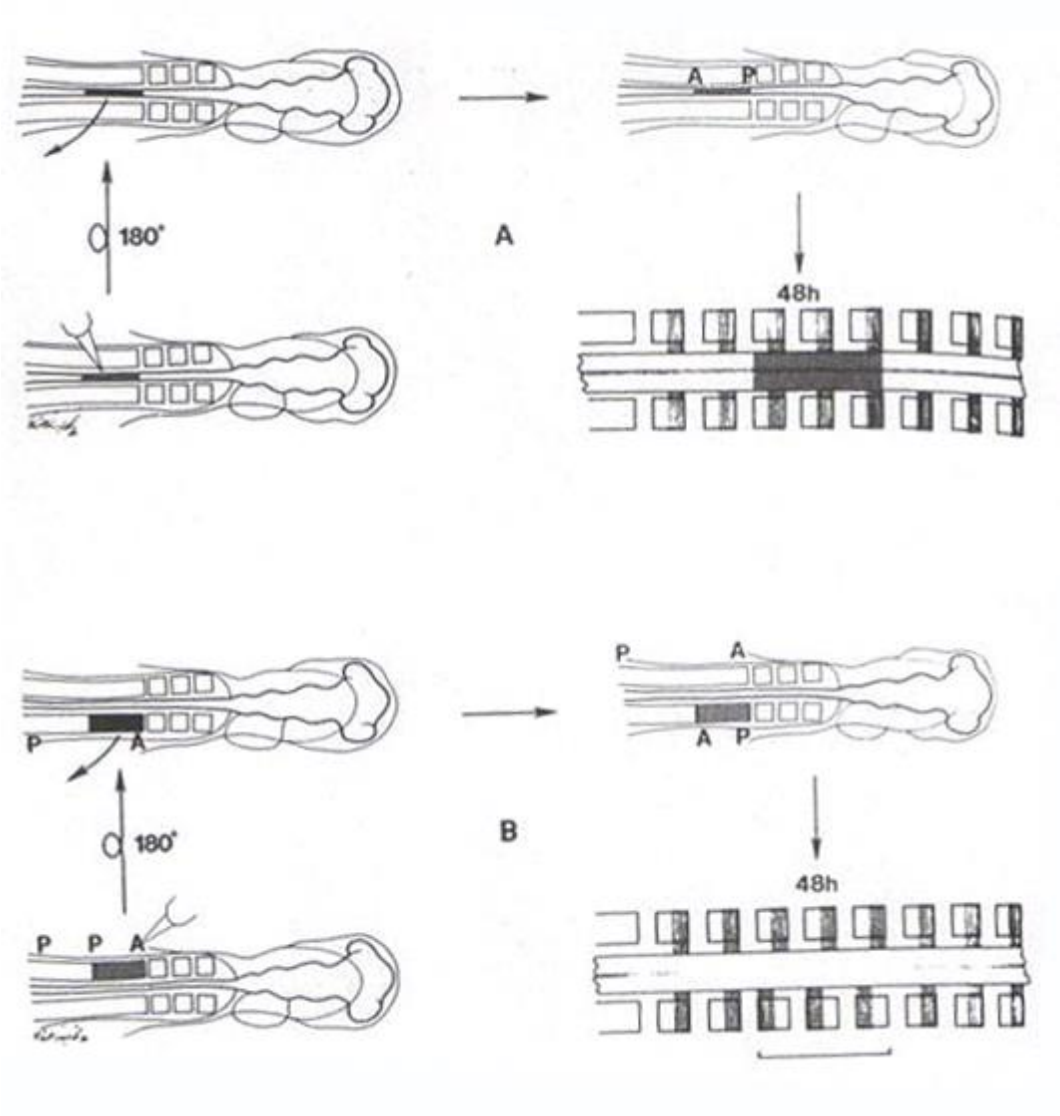

Figure 1.21- Diagram showing neural tube (A) and segmental plate (B) rotation experiments. A- 180º rotation of the neural tube did not have any impact on axonal patterning. B- 180º rotation of the PSM demonstrated the importance of the somites for axonal patterning. Figure from Keynes and Stern (1986).

To try to further understand how each somite half contributes to axon patterning a new grafting assay was done, this time anterior or posterior half-somites were grafted into the place of a whole somite of the host chick embryo (Fig. 1.22) (Stern and Keynes, 1986). Grafting an anterior half-somite gave rise to a sclerotome with an unusually wide anterior portion containing wide spinal nerves (Fig. 1.22a). As expected, the grafting of posterior half-somites gave rise to a sclerotome with an unusually wide posterior

portion with the spinal nerves more distantly spaced than usual (Fig. 1.22b) (Stern and Keynes, 1986). The same experiments also showed that the somitic environment was responsible for confining migrating trunk neural crest cells - which give rise to the sensory dorsal root ganglia that differentiate in the anterior half-sclerotome (see section 1.7) - to the anterior half-sclerotome (Stern and Keynes, 1986). The molecular control of the patterning of trunk neural crest cell migration through the anterior half-sclerotome has been intensively studied since this discovery (see section 1.7).

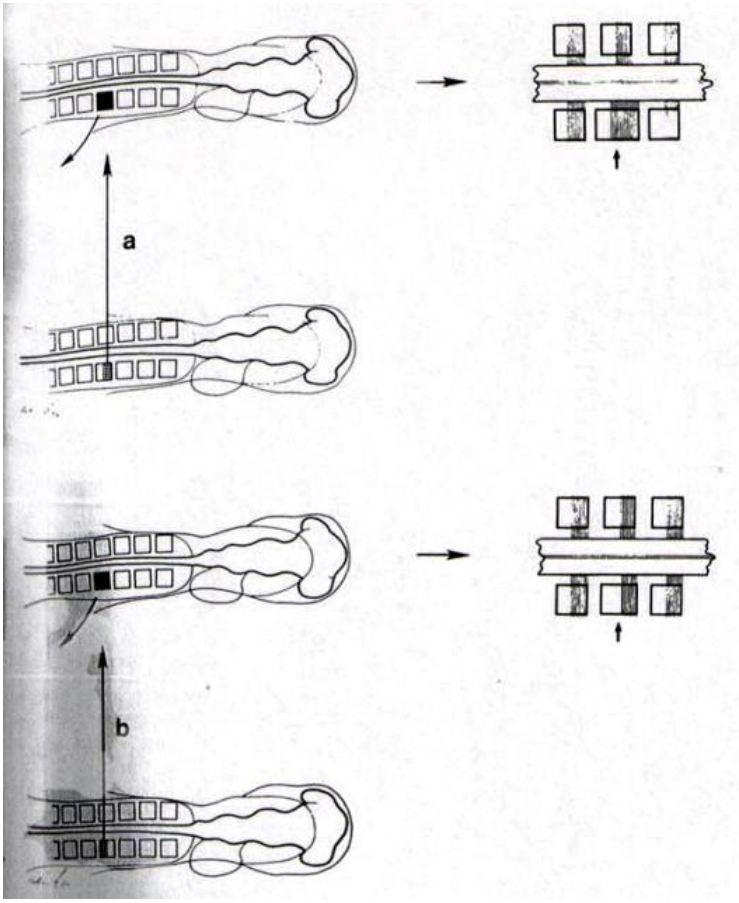

Figure 1.22- Diagram showing the procedures for constructing compound somites. (A) Compound anterior somites. (B) Compound posterior somites, produced in the corresponding way. Compound anterior somites give rise to a longer segment through which passes an abnormally wide spinal nerve. Compound posterior somites give rise to a longer segment whose caudal portion is abnormally wide and without nerves. Figure from Stern and Keynes (1986).

These experiments suggested that it is due to the permissive environment in the anterior-half that the developing PNS axons grow and migrate through it, while the posterior-half has repulsive barriers not allowing PNS axon passage, imposing the segmental arrangement of the spinal nerves. The differences between the two somite-halves are responsible for the arrangement of bones and nerves, in the trunk which defines the structure of the vertebral column and allows a flexible spinal cord while maintaining protection of the delicate spinal cord. This arrangement is orchestrated to allow the correct neural connection between the spinal cord and periphery.

These assays allowed a clear understanding of the fundamental differences between both halves: the anterior-half sclerotome forms a permissive environment in which neural crest cells can differentiate to form the dorsal root ganglia (see next section), as well as for motor and primary sensory axons. Several studies have investigated how the antero-posterior patterns of the PNS is established, but despite many breakthroughs the mechanisms are still not completely understood. However, many molecular differences have been found in an attempt to explain this segmentation. As described in section 1.4, antero-posterior polarity in the somite is linked to the segmentation process by the molecular clock that regulates mesodermal segmentation, and to Notch-Delta signalling associated with it (Kuan *et al*., 2004). The transcription factor *Mesp2* not only participates in regulating interactions with the *Notch1* pathway to arrest the segmentation clock, but also plays an important role in the subdivision of the somite. The creation of a *Mesp2*-null mice led to interesting results where the mutant not only displayed altered expression of the posterior-half-somite markers *meox1* and *dll1*, but also lacked the anterior-half-somite marker *Notch2*, suggesting that *Mesp2* functions in the control of anterior- and posterior-half-somite specification (AP-polarity). Furthermore, *Mesp2* mutants did not have an anteroposterior polarization and almost all somites had posterior-half characteristics, giving rise to mice with fused vertebral columns and with trapped dorsal root ganglia (Fig. 1.23) (Saga *et al*., 1997).

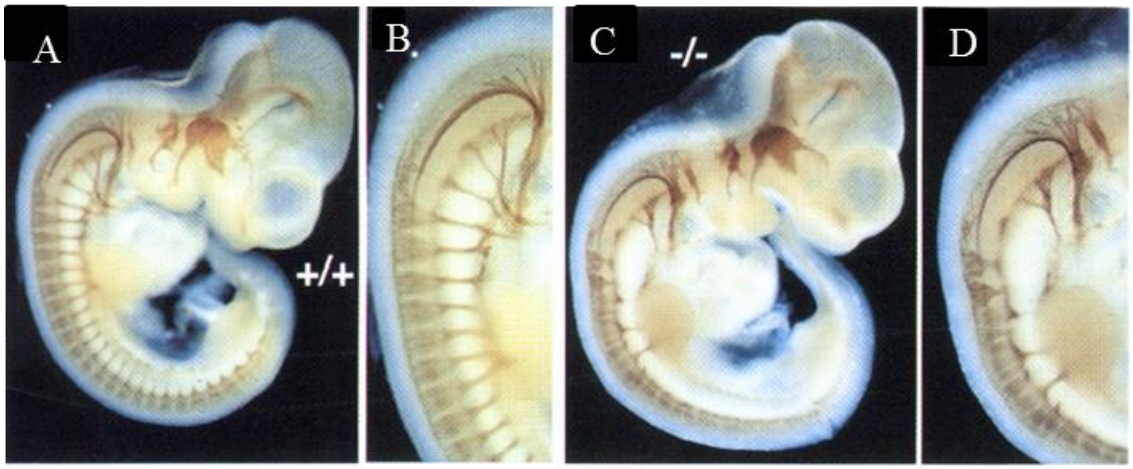

Figure 1.23- Neurofilament immunostaining in wild-type mouse and *Mesp2*-null mouse embryos at 10.5 d.p.c. reveals defects in spinal nerve patterning. (A,B) Axonal segmentation can be seen in the wild-type embryos, with the spinal nerves exiting through the anterior somite towards the ventral area of the embryo. (C,D) In the *Mesp2*-null mutant, cervical nerves so not exit through the centre of the sclerotome, while thoracolumbar spinal nerves do not exit through the sclerotome at all except to innervate the limbs. The dorsal root ganglia are also disrupted. (The cranial nerves and ganglia are unaffected.) Figure from Saga *et al.* (1997).

In the same way that *Mesp2* expression is restricted to the anterior half of the sclerotome, there are a number of other genes that have been shown to have restricted expression within the sclerotome (Figure 1.24) (Kuan *et al*., 2004). The role of many of these genes remains to be determined.

Figure 1.24- (On next page) Summary of molecules showing differential expression in the anterior versus posterior half of somites. The molecules are subdivided into four main groups. At the top is shown a schematic diagram of somite formation from the presomitic mesoderm (segmental plate, blue). The anterior/posterior somite polarity is indicated by the division of each somite into anterior (green) and posterior (red) halves, and the expression patterns of individual molecules are shown in blue (presomitic mesoderm), green (anterior half- somite) and red (posterior half-somite). Molecules with temporally dynamic expression patterns in the presomitic mesoderm are indicated by diagonal hatching. Figure from Kuan *et al*. (2004).

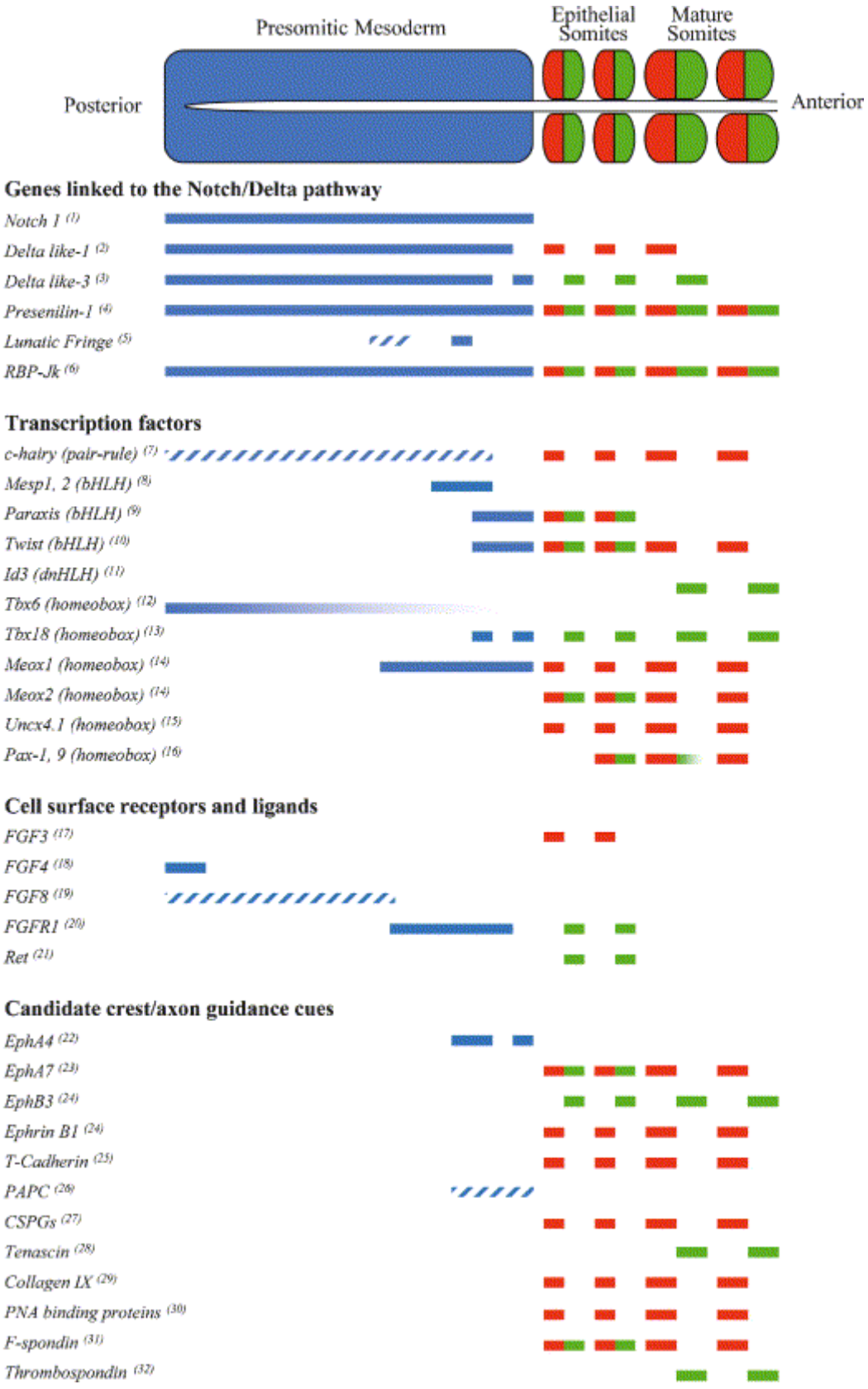

Figure 1.24- **On previous page**

The interaction of *Mesp2* with *Dll1*- and *Dll3*- mediated *Notch* signalling has an impact on the anterior- and posterior- somite-half divisions reinforcing anteroposterior identities, and the further elaboration of anterior- and posterior-half-somite fate, via the reciprocal activation and suppression of anterior- and posterior-half-somite markers such as *Cer1* and *Uncx4.1* (Maroto and Whittock, 2008). In addition, the different molecular expression patterns within the anterior versus posterior halves of somites are responsible for the formation of a set of different tissues.

As described earlier, somites can be subdivided into anterior and posterior halves, which exhibit different characteristics. The establishment of somite borders and anterior and posterior somite-halves has received considerable attention. In 1987, Stern and Keynes demonstrated that cells from the same sclerotome half could mix between themselves, whereas those of opposite halves remained separate when juxtaposed (Stern and Keynes, 1987). Consequently, the anterior and posterior somite-halves form distinct cellular boundaries. From further analysis, it was concluded that this is responsible for the formation of segmental borders while the determination of anterior and posterior compartments in the somite occurs at the level of the pre-somitic mesoderm.

Additional insight into the relationship between somite anteroposterior polarisation and border formation derives from the analysis of *EphA4* and *ephrinB2*. Ephrins and Ephs are cell-surface molecules that have been implicated in the formation and maintenance of somite boundary, and that are selectively expressed in prospective anterior or posterior compartments in the anterior PSM. The expression of these molecules has been conserved among vertebrates, and in mouse and chick PSM, both *EpHA4* and *EphrinB2* are expressed in similar domains but have different functions (Pourquié, 2001). In zebrafish, *EphA* signal blockage results in complete lack of somites. Conversely, ectopic *EphA4* can induce ectopic boundaries in the zebrafish mutant fused somites. The Eph-related family also play an important role in axon guidance and cell migration. Development of the peripheral nervous system (PNS) spinal nerves is influenced by the somite, in particular, the ventromedial somite derivative, the sclerotome. As mentioned, it is within the sclerotome that the anteroposterior polarisation/division of the somite is maintained during somite maturation. It is within the anterior-half region of the sclerotome that the PNS

components – not just motor axons, but also neural crest-derived sensory dorsal root ganglia (DRG) (see section 1.7) - are found.

Neuronal connections are made by axons that migrate to a specific target by a growth cone, which detects molecular guidance cues in the surrounding environment. Studies have come up with explanations for such guidance. It seems that axons respond to four possible guidance forces: attractive and repulsive cues, which can either be short-range or long-range (Kolodkin and Tessier-Lavigne, 2011). Most work on trunk PNS patterning has concentrated on the repulsive nature of posterior half-somites and that is why today it is known that a set of genes is differentially expressed on both sclerotomal halves (Fig. 1.24).

Several classes of molecules have been found in the somites consistent with the axonal guidance function; these include peanut agglutinin (PNA)-binding molecules, chondroitin sulphate proteoglycans, T-cadherin, Semaphorin3A, neuropilins (Roffers-Agarwal and Gammill, 2009) and ephrins (Hughes *et al.*, 2009). Some of the molecules are already well characterised and their role in axonal guidance was found to be important but not vital, suggesting the involvement of alternative pathways and additional molecules. However, double knock-out of Sema3F/Neuropilin2 and Sema3A/Neuropilin1 signalling had an impressive effect on the organization of the peripheral nervous system, as motor axons sprout in an apparently unsegmented pattern along the spinal cord and dorsal root ganglia are fused, although sympathetic ganglion segmentation was unaffected (Fig. 1.25) (Roffers-Agarwal and Gammill, 2009). Nevertheless, motor axons still keep together in fasciculated bundles in the double mutant embryos, rather than exploring the surrounding tissues, suggesting that another repellent molecule is present in the sclerotome.

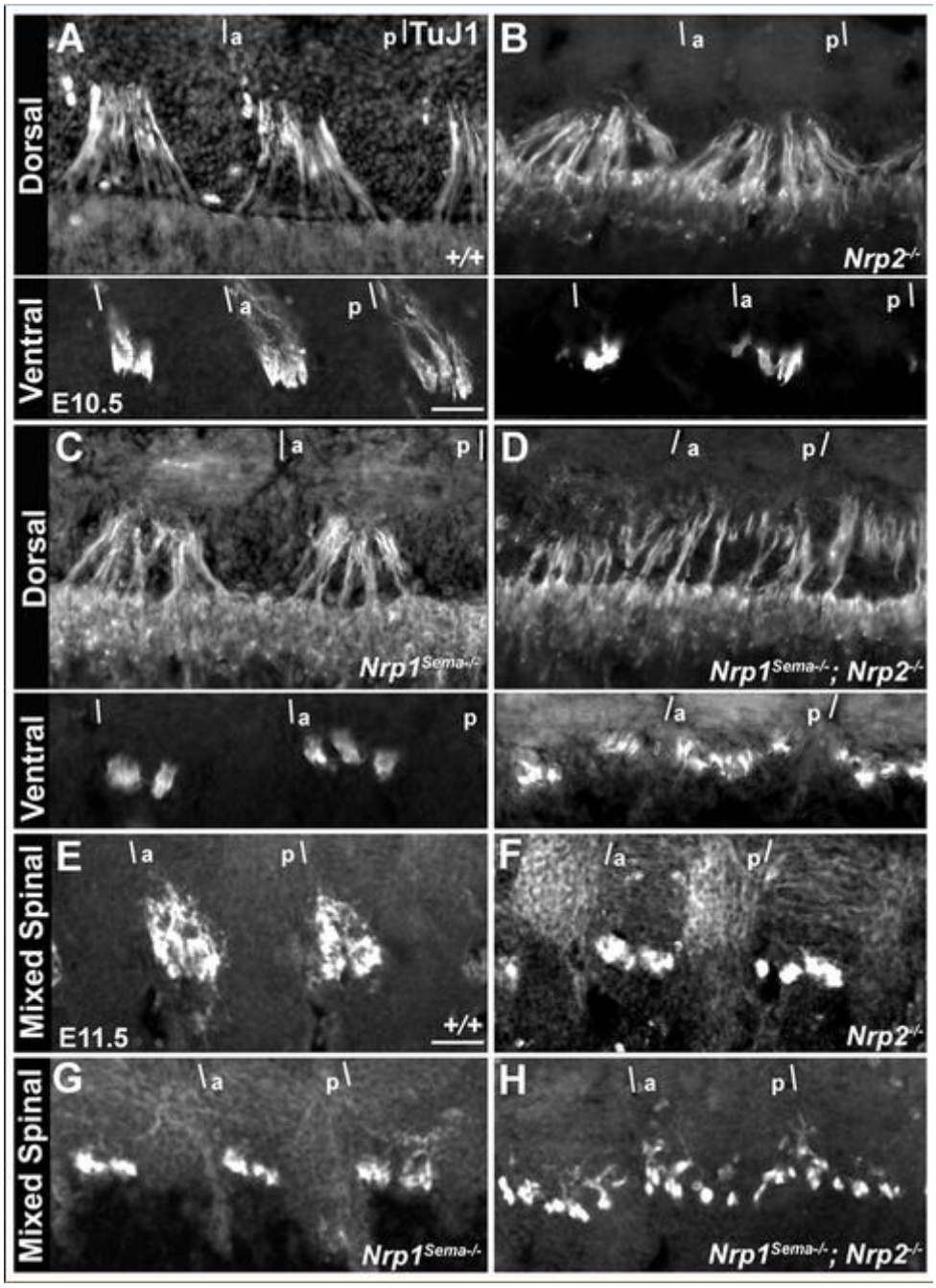

Figure 1.25- Nrp1 and Nrp2 are required for segmentation of motor axons and dorsal root ganglia. (A-D) E10.5 embryos show initial motor axon projections from the spinal cord in dorsal sections, whereas the bottom panels show the fasciculation of the same projections in more ventral sections of the same embryos. (A) Wild-type embryo, motor axons project only into the anterior sclerotome, fasciculating into a single ventral root in each segment. (B) *Nrp2*$^{-/-}$ mutant, motor neuron projection is initiated along the entire length of the somite, but fasciculate into a single ventral root. (C) *Nrp1*$^{Sema-/-}$ motor axons project adjacent to the anterior somite, but ventral roots are defasciculated within the anterior sclerotome. (D) *Nrp1*$^{Sema-/-}$;*Nrp2*$^{-/-}$ motor neurons initiate projections all along the spinal cord and these projections are defasciculated throughout the somite. (E-H) Ventral section through E11.5 embryos. (E) Spinal nerves

are organized in a single bundle in the anterior sclerotome of wild-type embryos. The plane of section captured a length of the nerve. (F) *Nrp2* mutant embryos exhibit a single bundle of spinal nerves in the anterior somite. (G) *Nrp1*$^{Sema-/-}$ spinal nerves fasciculate into multiple bundles within the anterior sclerotome. (H) Double mutant embryos contain multiple spinal nerve bundles distributed throughout the length of each segment. a, anterior; p, posterior. Anterior is to the left. Scale bars: in A, 50 μm in A-D; in E, 100 μm in E-H, all longitudinal sections stained with β-tubulin (TuJ). Figure from Roffers-Agarwal and Gammill (2009).

1.7- Neural crest formation and migration

During gastrulation, the neural induction process also begins, i.e., the development of the neural plate. At the border of the neural plate, the neural crest is induced. After the neural tube forms during neurulation, the neural crest separates from neuroepithelial cells by an epithelial-to-mesenchymal transition (EMT) and then neural crest cells migrate extensively through the embryo to give rise to a wide variety of derivatives including most neurons and all glia of the peripheral nervous system, many cartilages and bones of the face and skull, and pigment cells (reviewed by Theveneau and Mayor, 2012; Clay and Halloran, 2011).

Neural crest migration involves loss of cell-cell adhesion and myosin-based forces. Changes in cadherin expression are critical for NC migration, including adhesion functions together with promotion of RhoGTPases (Rho) and Rho Kinase (ROCK) signalling. It is at this point that the first oscillation of gene expression starts with the downregulation of N-cadherin protein that mediates the adhesion between cells and is anchored to the actin cytoskeleton via catenin complex. N-cadherin downregulation is achieved via BMP signalling resulting in the reduction of cell adhesion and in the cleavage of N-cadherin, releasing a cytoplasmic fragment to the nucleus that induces the transcription of pro-EMT genes such as Cadherin6B, which promotes a de-epithelialization during which premigratory neural crest cells lose polarity and start to migrate. (Fig.1.26). Another cadherin necessary for migration is Cad11, which is upregulated during neural crest migration; in the absence of Cad11 neural crest fail to form lamellipodia (Clay and Halloran, 2011).

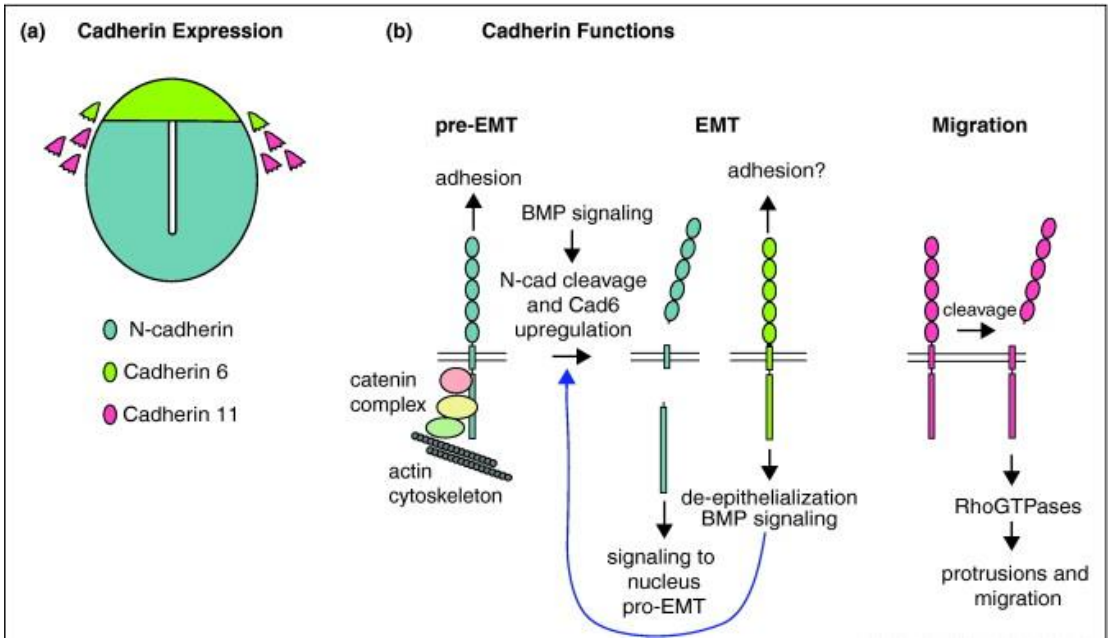

Figure 1.26- Cadherin expression and function during neural crest cell migration. (A) Transverse section of neural tube and migrating neural crest cells, showing cadherin expression patterns. (B) Cell-cell adhesion and signalling functions of different cadherins in neuroepithelial cells, before and during epithelial-mesenchymal transition (EMT) and during neural crest migration. Figure from Clay and Halloran (2011).

Different neural crest derivatives can be found along the entire neural axis (Fig. 1.27). Cephalic neural crest cells contribute to cartilages and bones of the face and neck, and form the odontoblasts (dentine-producing cells) of teeth. Neural crest cells are also important for the formation of the cardiovascular system: they form the connective tissue of the aorticopulmonary septum that separates the pulmonary and systemic circulations, as well as pericytes and smooth muscle in the carotid arteries and systemic aorta and pulmonary arteries (Le Douarin and Kalcheim, 1999). Neural crest cells form the neurons and glia of all peripheral autonomic ganglia (sympathetic, parasympathetic, enteric), and the chromaffin cells of the adrenal medulla. They also form most peripheral sensory neurons (the remainder, in specific cranial sensory ganglia, arise from cranial neurogenic placodes; Schlosser, 2006).

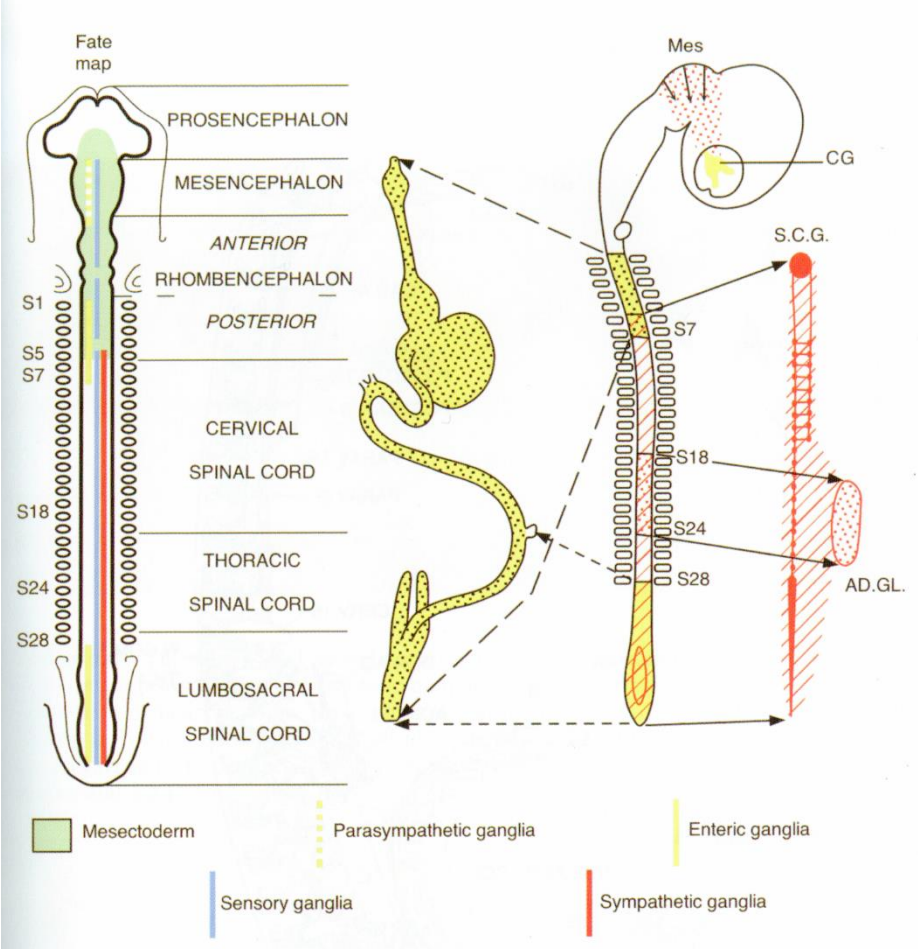

Figure 1.27- Neural crest cell derivatives can be found along the entire neural axis. Neural crest give rise to different types of ganglia at different somite levels. Figure from Le Douarin and Kalcheim (1999). AD.GL., adrenal gland; C.G., ciliary ganglion; Mes, mesencephalon; S, somite; S.C.G., superior cervical ganglion.

The sensory neurons of the peripheral nervous system (PNS) transmit information from the peripheral targets to the spinal cord and brain. These neurons are collected into ganglia: the dorsal root ganglia (DRG) organized bilaterally along the spinal cord, and the sensory ganglia of the cranial nerves in the head. Sensory neurons within these ganglia originate from the neural crest and certain cranial neurogenic placodes; all peripheral glia, including the satellite glia of sensory ganglia, arise from the neural crest. Brain-derived neurotrophic factor (BDNF) and neurotrophin-3 (NT-3) signalling from the neural tube promote the development of neural crest cells into DRG, but the development of the DRG is linked with the segmentation of the mesoderm and

only occurs once the somite is dissociated into dermomyotome and sclerotome in anterior to posterior direction and display segmented pattern through anterior somitic halves (Le Douarin and Kalcheim, 1999).

During early migration, around stage 14 HH in chick and E9.0 in mouse, neural crest migrates ventrally between the somites along intersomitic vessels (1-Fig. 1.28) and between the neural tube and somites (2-Fig. 1.28). Shortly after, around stage 15/16 HH in chick and E9.5 in mouse, neural crest starts to migrate ventrolaterally into the anterior sclerotome (3- Fig. 1.28) towards the dorsal aorta (4- Fig. 1.28). In mouse, some neural crest cells also migrate over the dermomyotome however this does not happen in chick. Around stage 20 HH in chick and E10.5 in mouse, neural crest cells in the anterior sclerotome condense into segmental dorsal root ganglia (5- Fig. 1.28) while the neural crest present in the dorsal aorta segregate into sympathetic ganglia (6- Fig. 1.28). Also at this stage, neural crest cells start to migrate dorsolaterally above the dermomyotome in chick (7- Fig. 1.28) (Gammill and Roffers-Agarwal, 2010).

In chick, mouse and rat, migrating neural crest cells are restricted to the anterior sclerotome that expresses EphA/B receptors while the posterior sclerotome, from which neural crest cells are excluded, expresses ephrin-B ligands. Furthermore, semaphorins 3A and 3F are also expressed in the posterior sclerotome (Theveneau and Mayor, 2012). (Fig. 1.28). The inhibition of either ephrin or Sema3F/Neuropilin2 (Nrp2) signalling leads to ectopic migration through the posterior sclerotome and unsegmented migration of trunk neural crest but the patterning of the ganglia is not affected (Gammill and Roffers-Agarwal, 2010). However, DRGs are no longer segmented when both Sema3F/Nrp2 and Sema3A/Nrp1 signalling are blocked, leading to the model of sequential Neuropilin signalling presented in Fig. 1.28. The migration of the neural crest along the dorsolateral pathway is controlled by endothelin and Slit/Robo signalling from the surrounding tissues (Gammill and Roffers-Agarwal, 2010). Table 1.1 summarises what is known about the molecules involved in patterning trunk neural crest cell migration (and also, where relevant, in patterning motor axon trajectories). Despite progress in identifying the function of some of these molecules, there is still much to discover. For example, application of the lectin peanut agglutinin (PNA) to chick embryo explants caused neural crest cells to migrate through the posterior as well as

anterior sclerotome, suggesting that PNA-binding glycoproteins are required for segmental trunk neural crest migration (Krull *et al.*, 1995).

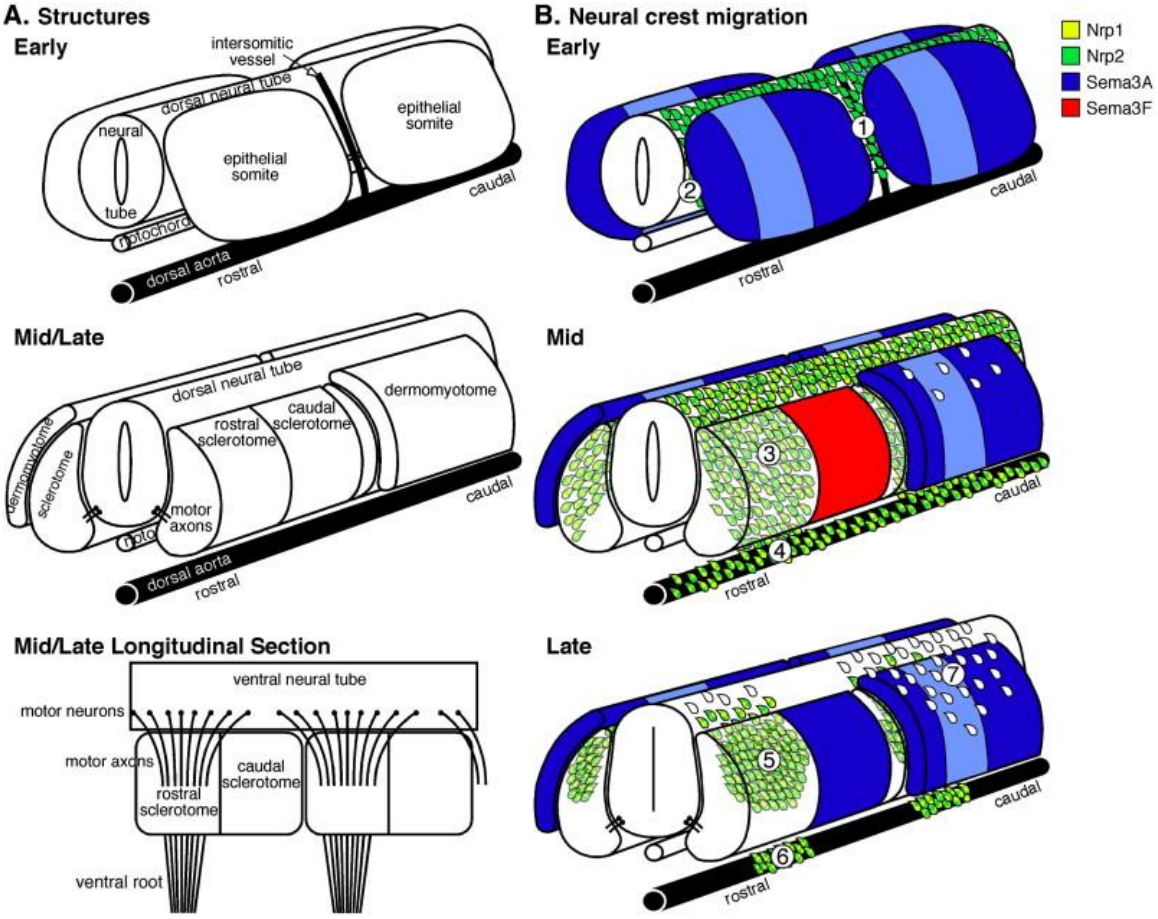

Figure 1.28- Diagram of the different pathways of neural crest migration during different stages of somite maturation, leading to neural crest cell migration through the anterior somite. Figure from Gammill and Roffers-Agarwal (2010). Early stages represent stage 14 HH in chick and E9.0 in mouse; middle stages are between 15/16 HH in chick and E9.5 in mouse; and late stages represent stage 20 HH in chick and E10/E10.5 in mouse.

Table 1.1- The phases of trunk neural crest migration and the responsible environmental guidance cues identified so far. Different proteins have different roles dependent on their position. Table adapted from Gammill and Roffers-Agarwal (2010).

Phase	Pathway	Cue	Proposed role	
All	*All*	Fibronectin, laminin		Permissive, integrin adhesive substrate for neural crest migration
Initial	*1. Intersomitic*	None known	+	Attracts neural crest cells to intersomitic vessels
	2. Over neural tube	None known	**?**	Promotes neural crest migration between the neural tube and somites
Mid	*3. Ventrolateral Somites*	Semaphorin3A in dermomyotome	–	Repels Neuropilin1-expressing neural crest cells from intersomitic space
		Semaphorin3F in caudal sclerotome	–	Restricts Neuropilin2-expressing neural crest cells and motor axons to rostral sclerotome
		Ephrins in caudal sclerotome	–	Trigger cell–cell interactions in Eph-expressing neural crest cells leading to segmental migration in chick
		CXCL12 in sclerotome	+	Attracts CXCR4-expressing migratory neural crest cells ventrally into the sclerotome
		F-spondin sclerotome	–	Integrin anti-adhesion
		Peanut agglutinin (PNA) binding glycoproteins	–	Glycan moiety is required for segmental neural crest migration, the glycosylated proteins are unknown
		T-cadherin	–	Reduces adhesion to caudal sclerotome
		Thrombospondin in myotome	+	Promotes neural crest migration and proliferation
	4. Ventrolateral Dorsal aorta	Neuregulin in mesenchyme around dorsal aorta	+	Attracts ErbB2/B3-expressing neural crest cells ventrally past the sclerotome
		CXCL12 at the	+	Attracts CXCR4-expressing migratory neural

Phase	Pathway	Cue		Proposed role
		dorsal aorta		crest cells to the dorsal aorta
		Semaphorin3A in limbs, dermomyotome and notochord	–	Restricts Neuropilin1-expressing neural crest cells near the dorsal aorta
Late	*5. Ventrolateral Somites*	Semaphorin3A in caudal sclerotome	–	Drives metameric dorsal root gangliogenesis and ventral root formation
	6. Ventrolateral Dorsal aorta	Segmental ephrinB1 expression in ventral mesenchyme	–	Sorts EphB2-expressing sympathetic precursors into segmental condensations
	7. Dorsolateral	Slit expression in dermomyotome during early/mid migration	–	Repels Robo-expressing neural crest cells from the dorsolateral path
		ephrin expression in the dermomyotome	–	Repels EphB3-expressing early/mid phase migratory neural crest cells, attracts EphB3-expressing melanoblasts
		Chick: endothelin3 in dermomyotome and ectoderm	+	Attracts EDNRB2-expressing melanoblasts
		F-spondin in dermomyotome	–	Integrin anti-adhesion
		Peanut agglutinin (PNA) binding glycoproteins	–	Transiently expressed PNA-binding glycoproteins in the dermomyotome block dorsolateral neural crest migration

1.7.1- Identification of a repulsive cue for DRG axons in the posterior half-sclerotome

Culture assays have also given information about the selectivity and preferences of DRG axons relative to surrounding tissues that help confine sensory axons to the anterior sclerotome (Fig. 1.29) (Tannahill *et al*., 2000). An interesting study involving a lectin, peanut agglutinin (PNA), demonstrated the importance of PNA-binding molecules in the segmentation of the PNS. Within the somites, this lectin only binds to cells of the posterior- but not anterior-half-sclerotome (Stern *et al.* 1986). Normally in the presence of a somite extract, the growth cones of cultured DRG neurons collapse, but when PNA is present in the somite extract, growth cone collapse is blocked (Davies *et al.,* 1990). This assay not only indicates that PNA binds to an axon-repelling molecule that could be responsible for PNS segmentation, by not allowing DRG axons to pass through the posterior half-sclerotome, but also that the molecule responsible for the segmentation is in the posterior half-sclerotome. Furthermore, as described in section 1.7 on neural crest cell migration, PNA application to chick explants also abolishes the segmental migration of neural crest cells (Krull *et al.,* 1995), suggesting that the same PNA-binding glycoprotein could block both the migration of both neural crest cells and neural crest-derived DRG axons in the posterior-half-sclerotome.

Subsequent SDS-PAGE analysis of the PNA-binding glycoprotein fraction localised two molecules of molecular weight 48kD and 55kD (Davies *et al.*, 1990). A rabbit antiserum raised against the 48 and 55 kD proteins was able to eliminate the growth cone collapse, and when chick embryo sections were stained with this antiserum, its staining was comparable to PNA staining, i.e., staining was only seen in the posterior half of the sclerotome (Davies *et al*., 1990). Due to the scientific technology of the time, the full amino acid sequence was not available, however the assay has been redone and fragments of the sequence were obtained (Keynes *et al.* unpublished). In this work, I have used siRNA knockdown to study the importance of the PNA-binding protein thus identified in patterning the PNS.

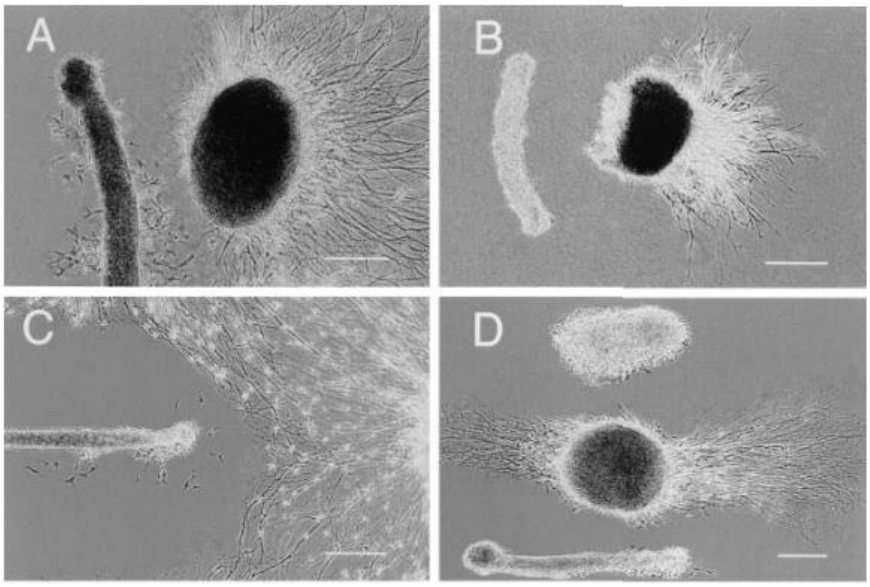

Figure 1.29- Chemorepulsion between different tissues demonstrated in a collagen gel culture of chick stage 28 dorsal root ganglia surrounded by different tissues. (A) With a piece of stage 17 notochord, residual peri-notochordal mesenchyme cells are visible. (B) Dermomyotome next to a dorsal root ganglion: the axons migrate radially from the DRG on the side opposite the dermomyotome. (C) Stage 17 HH notochord dropped in a culture of several dorsal root ganglia: all the axons avoided a radius around the notochord forming a "halo" effect. (D) Dorsal root ganglia surrounded by a notochord on the bottom and dermomyotome on the top, similar to what happens in the sclerotome. Scale bar = 200 μm. Figure from Keynes et al. (1997).

1.8- The chicken as a model system

The chicken embryo has been used as a model in embryological studies, including somitogenesis, mainly due to its easy accessibility for manipulation during most of its development as well as the more recent development of transfection techniques such as *in ovo* electroporation, which allows plasmid DNA or morpholinos to be targeted to specific tissues *in vivo*, including the neural tube and somites (Pourquié, 2001; Scaal *et al*., 2004; Stern, 2005). As previously discussed, the study of the molecular biology of somite development is important in understanding how the body plan is established. Many types of experiments can be done either *in ovo* or in culture in the chick (Pourquié, 2001; Stern, 2005).

Chicken embryos are staged according to Hamburger and Hamilton (1951), based on developing structures and days of embryonic development (Appendix A). Furthermore, the use of quail-chicken grafting techniques to label specific cell populations enabled many insights into the contribution of the somites and somite compartments to different structures, as well as into segmentation and embryological development (Christ *et al*., 2000).

The chicken has 14 cervical vertebrae that, except for the atlas and axis, are linked with highly mobile apophyseal joints, each with fibrocartilaginous intervertebral discs. There are seven rib-bearing thoracic vertebrae, where the second to fifth are fused into a bony column. The sixth thoracic vertebrae is free, and the seventh fused with the synsacrum, and the articulations within this region are saddle joints (Bellairs and Osmond, 1998). The caudal part of the vertebral column is highly specialized.

1.9- Overall Aims

As discussed above, the processes by which segmentation of the vertebral axial skeleton and peripheral nervous system develop involve the complex integration of multiple patterning molecules. Of particular note is the importance of repulsive molecules present in the posterior half-somite. Since the posterior half-somite is responsible for axonal guidance and neural crest migration, understanding the differential expression of genes within this half is of great importance.

This project is a continuation of previous work started at the Wellcome Trust Sanger Institute (Hughes *et al.*, 2009) and in collaboration with Professor Roger Keynes at the Department of Physiology, Development and Neuroscience at the University of Cambridge. The previous work carried out at the Sanger Institute consisted of a sophisticated microarray study using dissected mouse half-somites in order to identify all differentially expressed genes between anterior and posterior half–somites. Many possible candidates for genes involved in anteroposterior somite polarity and axonal repulsion were revealed (Hughes *et al.*, 2009). Antisense RNA probes were used to confirm the expression of those genes in whole mouse embryo by *in situ* hybridization.

The overall aim of my PhD project was to analyse the role in axial segmentation (peripheral axon guidance, neural crest migration and/or vertebral column formation) of a selection of the genes identified in the mouse half-somite microarray screen (Hughes *et al.*, 2009), using the chick embryo as a model system.

The original objectives were to clone chicken homologues of candidate mouse genes identified in the half-somite microarray screen of Hughes *et al.* (2009) and to localize their expression in chick embryos by whole-mount *in situ* hybridisation, then to select one gene expressed in the posterior-half sclerotome and study its function in embryonic segmentation using a loss-of-function approach. Although not anticipated in the original objectives, a new technique for transfecting chicken somites *in ovo* with short interfering RNA (siRNA) was developed as part of the project. Finally, given the importance of a previously unidentified PNA-binding glycoprotein for axon guidance in the somites, the expression was also studied of a family of glycosylation enzymes that might be needed to synthesise the PNA-binding glycoprotein, and two candidates for the PNA-binding protein itself were also investigated.

CHAPTER 2- MATERIALS AND METHODS

2.1- Incubation and staging of chicken embryos

Fertilized wild-type chicken (*Gallus gallus domesticus*) eggs were delivered weekly (Winter Egg Farm, Hertfordshire) and stored at 14ºC. Eggs were incubated with the long axis placed horizontally in a humidified incubator at 38-39ºC until the embryos reached the required embryonic stage. Embryos were staged according to Hamburger and Hamilton (1951) (HH stages) or by days of incubation (embryonic days, E).

2.2- Synthesis of antisense RNA probes from chicken cDNA using PCR

2.2.1- Total RNA isolation for cDNA synthesis

E3 and E5 chicken embryos were rinsed with cold diethylpyrocarbonate (DEPC)-treated phosphate-buffered saline (PBS) and transferred to a methanol-washed Petri dish coated with Sylgard (Dow Corning). The extra-embryonic membranes were removed with forceps pre-cleaned with RNAse Zap (Ambion). Embryos were placed into RNAlater (Ambion) and stored overnight at 4ºC. For E3 embryos, total RNA was extracted using the RNeasy kit (Qiagen) according to the manufacturer's instructions. For E5 embryos, 700 µl RLT buffer from the Qiagen RNeasy kit (with β-mercaptoethanol, according to the manufacturer's instructions) was added to the embryos, 2-3 embryos per centrifuge tube. The embryos were disrupted by vortexing for 30 seconds and using a mortar and pestle, followed by homogenisation using a sterile 19-gauge syringe needle. The lysate was spun down at 4ºC at 12100 x g for 5 minutes. The supernatant was divided into two fresh microcentrifuge tubes. 350 µl of 70% ethanol was added and mixed by pipetting. The sample, including any precipitate that formed, was placed onto an RNeasy MiniElute spin column (Qiagen) in a 2 ml collection tube. The tube was closed and centrifuged for 15 seconds at 8000 x g. The flow-through was discarded. The same RNeasy MiniElute spin column was loaded with the second supernatant sample. The column was closed and centrifuged for 15 seconds at 8000 x g. The flow-through was discarded. 700 µl of RW1 buffer (Qiagen RNeasy kit) was added to the RNeasy spin column and then re-centrifuged for 15 seconds at 8000 x g. Once the flow-through

was discarded, 500 µl of RPE buffer were added to the spin column and centrifuged for 2 minutes at 8000 x g. The flow-through was discarded. A second aliquot of 500 µl of RPE buffer was added to the spin column and re-spun for 2 minutes at 8000 x g. The flow-through was discarded, and to dry the column an additional centrifuge was carried out at full speed for 1 minute. The spin column was them transferred into a new 1.5 ml collection tube, and 30 µl DEPC-treated water was added directly into the silica-gel membrane prior to centrifugation at 25000 x g for 1 minute. A further 20 µl of DEPC-treated water was added and the column was spun down again at 25000 x g for 1 minute. The total RNA concentration and integrity was further analysed using a Picodrop spectrophotometer.

2.2.2- cDNA synthesis

For the cDNA synthesis, the iScript cDNA Synthesis Kit (Bio-Rad) was used. 7 µl of Reverse Transcription Mix (4 µl of 5X iScript reaction mix, 2 µl of Oligo dT20 primer, 1 µl of iScript Reverse Transcriptase) was added to DEPC-treated water and 1 µg of total RNA to a final reaction volume of 20 µl. The contents of the tube were mixed by pipetting and briefly spun-down in a microfuge (≤1000 x g) to settle the contents. The tube was further incubated at 42ºC in a thermal cycler for 75 minutes followed by a cycle of 85ºC for 5 minutes. The cDNA was stored at -20ºC.

2.2.3- Primer design

RNA probes were designed using the following protocol. First, transcript sequences for all selected genes were obtained via NCBI GenBank and Ensembl. Primer pairs for each transcript were designed using the Primer-Blast tool available from the National Center for Biotechnology Information (NCBI) (http://www.ncbi.nlm.nih.gov/tools/primer-blast/) (Ye *et al*., 2012). The primers were selected according to the following rules: (1) the primer length had to be between 17 to 30 base pairs, (2) their CG content had to be between 50 to 60%, (3) their melting temperature should be between 55 and 80ºC. The resulting amplification product should be no longer than 1200 base pairs and no smaller than 400 base pairs. All

potential primers were checked against the *G. gallus* (taxid:9031) genomic database using the Basic Local Alignment Search Tool (BLAST) from NCBI. The outputs from this last step were used to exclude all primers giving more than one significant region of identity (80% cut-off) against the whole chicken genome, or sharing more than 70% similarity with other genes. The selected primers were synthesised (Sigma) with the T7 primer sequence (TAATACGACTCACTATAGGGAG) appended to the 5' end of the reverse primer, so as to allow direct generation of digoxigenin-labelled antisense RNA probe by *in vitro* transcription using T7 RNA polymerase. Primers used to produce the RNA probes can be found in Appendix B.

2.2.4- Polymerase chain reaction to prepare template for riboprobe synthesis

cDNA samples (2 µl) were pipetted into a 0.2 ml thin-wall centrifuge tube and 36 µl of DEPC-treated water, 6 µl of each primer, and 50 µl of Reddy Mix PCR Master Mix (AB Gene) was added to each. The contents of the tube were briefly mixed and spun down. The tubes were placed on a heating block of a hot-lid thermal cycler pre-heated to 95ºC. Cycling commenced with an initial 2-minute denaturation step at 95ºC followed by 34 cycles of 95ºC for 25 seconds, annealing at 50ºC for 45 seconds and elongation at 72ºC for 1 minute. The cycling was finished with an extension step of 72ºC for 5 minutes. The PCR product length was then checked by agarose gel electrophoresis. The products were stored at -20ºC until needed for riboprobe synthesis.

2.2.5- Riboprobe synthesis

20 µl *in vitro* transcription reactions were prepared by adding to a 0.2 ml thin-wall PCR tube in the following order: 9 µl DEPC-treated water, 4 µl nucleoside triphosphate (NTP) mix (2.5mM ATP, 2.5mM CTP, 2.5mM GTP, 1.67mM UTP, 0.833mM digoxigenin-11-UTP), 2 µl T7 transcription buffer (Ambion), 2 µl T7 RNA polymerase, 1 µl RNase inhibitor (Invitrogen), and 2 µl PCR product (see preceding section 2.2.4). The contents of the tube were mixed by pipetting and briefly spun-

down in a microfuge (≤1000 x g) to settle the contents. The tube was further incubated at 37ºC in a thermal cycler for 2 hours, after which 1 µl DNaseI was added and the tube further incubated at 37ºC in a thermal cycler for 15 minutes. To stop the reaction, 1 µl of 0.5M EDTA was added and mixed by pipetting and the tube contents spun down. The probe was then analysed using a Picodrop spectrophotometer.

2.3- *In situ* hybridization

2.3.1- Embryo fixation and dehydration

HH stage 19-22 embryos were dissected from the egg with fine-tipped forceps and washed twice in phosphate-buffered saline (PBS). Forceps and surgical scissors were used to remove all extra-embryonic tissue prior to immediate incubation in 4% paraformaldehyde for 2 hours at room temperature or overnight at 4ºC. After fixation, embryos were rinsed in PBS on a mechanical shaker for 5 minutes, and dehydrated through a series of 10-minute washes with 25, 50, 75% methanol/PBS and 100% methanol. This was followed by one more 30-minute wash in 100% methanol. Embryos were stored in methanol at -20ºC until required.

2.3.2- Whole-mount *in situ* hybridization

The method used for whole-mount *in situ* hybridization (WMISH) is based on Wilkinson (1998). Embryos were rehydrated into PBST (PBS with 0.1% Triton-X100) through a series of 75% methanol/ultra-pure water, 50% methanol/ultra-pure water, 25% methanol/PBST. Embryos were transferred into 18-well plates (Nunc). Unless specified, all reagents were diluted in PBST and all washes were for 10 minutes in PBST on a rocking platform at room temperature. To increase permeability of the probe, embryos were incubated at room temperature in 10 µg/ml proteinase K (Roche) for the following durations: embryos up to stage 15 HH (Hamburger and Hamilton, 1951) for 5 minutes, stage 18 HH for 10 minutes and stage 24 HH for 15 minutes. Embryos were rinsed once, post-fixed for 20 minutes in 4% formaldehyde and washed twice to remove the fixative. Embryos were equilibrated with

hybridization mix [50% formamide, 5XSSC (Sigma), 2% blocking powder (Boehringer, 1096176), 0.1% Triton X-100, 0.1% CHAPS (Sigma), 1 mg/ml tRNA (Sigma), 5mM EDTA, 50 µg/ml heparin] by rinsing once in a 1:1 mixture of PBST/ hybridization mix and then twice with hybridization mix. Plates were then placed at 67ºC in a hybridization rocking oven for a minimum pre-hybridization of 2 hours up to 12 hours, after which the solution was changed to pre-warmed hybridization solution containing approximately 1 µg/ml RNA probe, and incubated for at least 12 to 72 hours. In order to avoid cross contamination, WMISH probes were never near each other when the hybridization was being done; the vials were leak-proof, and each probe was only reused three times.

After incubation, embryos were rinsed twice and washed once with pre-warmed hybridization mix, washed twice for 30 minutes with hybridization mix and twice with a 1:1 mixture of hybridization mix/PBST or MABT (100 mM maleic acid,, 150 mM NaCl, 0.1% Triton X-100 pH 7.5) for embryos stage HH 24 at 60ºC. Embryos were removed from the oven and rinsed 3 times with PBST or MABT. All traces of hybridization solution were removed by seven 30-minute washes in PBST or MABT at room temperature in a rocking shaker.

To block non-specific binding, embryos were incubated for 2 hours in a blocking solution (10% sheep serum in PBST) for 1-3 hours at room temperature. This was replaced with blocking solution containing alkaline phosphatase-conjugated anti-digoxigenin Fab fragments (Roche) at 1:2000 dilution, and embryos were incubated for a further 12-18 hours at 4ºC. The antibody was removed by rinsing the embryos 3 times in PBST with 1 mM levamisol, followed by 4 hours of washes with buffer changes every 30 minutes; in some cases, embryos were left overnight at 4ºC.

The alkaline phosphatase was detected by a mixture of 4-nitro blue tetrazolium chloride (NBT) and 5-bromo-4-chloro-3'-indolyphosphate (BCIP). Initially embryos were washed twice in NTMT (100 mM NaCl, 100 mM Tris-HCl pH 9.5, 50 mM $MgCl_2$, 0.1% Triton X-100), followed by the addition of the reaction mixture (4.5 µl/ml NBT and 3.5 µl/ml BCIP in NTMT). Developing reactions were left in the dark until a deep purple colour had developed; this could take 3 hours to 5 days, in the latter case the stain solution was replaced daily with fresh stain solution. Embryos were then washed 3 times in PBST and fixed in 4% paraformaldehyde for

12-18 hours at 4ºC. The fixative was removed by several PBS washes. Embryos were photographed under a dissecting microscope (Leica) and prepared for vibratome sectioning.

2.3.4- Clearing and photography of embryos after *in situ* hybridization

Embryos were dehydrated into methanol through a series of 10-minute washes with 25% methanol/PBS, 50% methanol/PBS, 75% methanol/deionised water and 100% methanol, then washed twice (10 minutes each) in methanol. Embryos were transferred to a 2:1 mixture of benzylbenzoate: benzyl alcohol (BABB): methanol and left in this solution until they were cleared and the background staining was reduced. The embryos were photographed under a dissecting microscope (Leica), then brought back into methanol via three 30-minute washes and stored at 4ºC.

2.4- Transfection of embryonic tissue or cultured cells

2.4.1- Preparation of siRNA or plasmid DNA with the transfection agent.

Lyophilized FITC-labelled RNA duplexes (Dharmacon Thermo Scientific) were obtained in 2' deprotected, annealed and desalted form, dissolved in PCR grade water (Roche) at 3 µg/µl and stored in aliquots at -80ºC. The final transfection solution was 1µg/µl siRNA, 10% polyethylene glycol (PEG) (Carbowax 6000, Union Carbide) and 20% Turbofect^{TM} (Thermo Fisher Scientific, Lafayette. CO; Catalog # R0541). For 2.8 µl of siRNA preparation, 1 µl of siRNA, 1.2 µl of 20% PEG stock and 0.6 µl of Turbofect^{TM} were incubated at room temperature for 30 minutes before application.

This technique was also tested using pCAβ-EGFPm5 (Bron *et al*., 2007), a kind gift from Dr. Matthieu Vermeren (Department of Physiology, Development and Neuroscience, University of Cambridge, UK). The final transfection solution contained 2 µg/µl plasmid, 10% PEG and 40% Turbofect^{TM}. For a final 5 µl of solution, 1µl of plasmid, 2 µl of 20% PEG stock and 2 µl of Turbofect^{TM} were used. This solution could only be used once.

Borosilicate glass capillaries (WPI, outside diameter 1.5 mm, inside diameter 1.12 mm) were pulled on a Narishige Puller PC-10 at 62ºC. The tips were broken to obtain a fine opening and capillaries were then attached to a rubber tube (Sigma). The siRNA solution was aspired into the capillary.

2.4.2- Preparation of chick embryos for *in ovo* transfection

After reaching the required embryonic stage, eggs were removed from the incubator and left for 1 hour at room temperature to reduce heartbeat. Eggs were cleaned with 100% methanol, and then 3-4 ml of albumin removed using a 19-gauge syringe needle. The upper side of the egg was reinforced with adhesive tape (Sellotape, 1.2 mm width), and a small window (1x1 cm) was cut using curved scissors. The embryo was then raised to the level of the window by re-pipetting albumen. In order to visualize the embryo, a small amount of 5% India ink (Pelikan fount) in PBS was injected using a 22-gauge syringe needle. A small incision (needle-size) was made in the vitelline membrane in the most posterior part of the embryo using a microscalpel Feather® (PFM Medical ref: 200300715) or a bent syringe needle tip.

2.4.3- Somite targeting *in ovo*

The glass capillary containing siRNA/plasmid transfection solution was inserted into the most posterior (newly formed) somite of stage 9-12 HH embryos and carefully pushed parallel to the neural tube until the most anterior somite was reached, or until resistance was felt from the somite, using small wave movements. Once the most anterior somite was reached, the needle was pulled back somite by somite and the solution injected into each somite for 5-10 seconds (see Fig. 2.1). It was possible to observe the somites filling up with solution and the tissue turned slightly white and sticky. When the last somite was filled, the embryo was lowered by removing 5 ml of albumin using a 19-gauge syringe needle, then a drop of albumin was dropped on top of the embryo and the window closed with sellotape. The egg was immediately moved to an incubator and left to develop for a further two days (to 22-24 HH), when

somite strips were removed from some embryos for culture (section 2.4.6), or for a further five days (to stages 26-27 HH), before fixing in 4% paraformaldehyde for 3 hours at room temperature or 12 hours at 4ºC. Embryos were then dehydrated into methanol as described in section 2.3.1 and stored at -20ºC.

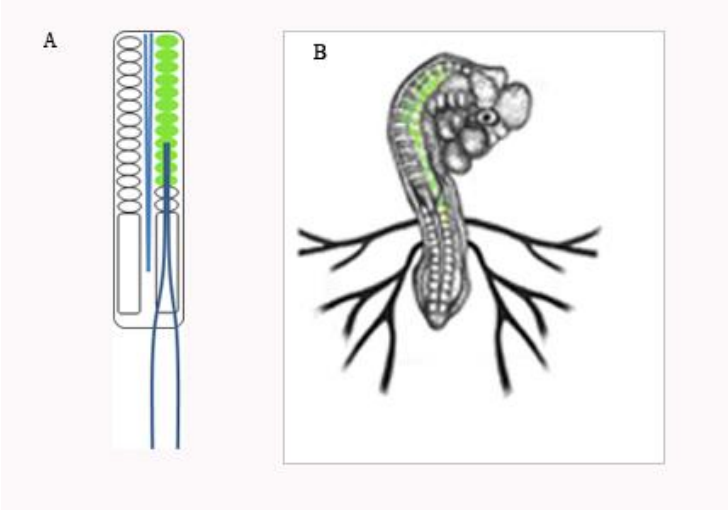

Figure 2.1. Schematic representation of somite transfection *in ovo*. A: Schematic dorsal view of the trunk region of a day-2 chick embryo, with anterior to the top. The right hand side of the embryo is the manipulated side; the green colour illustrates the injection of several somites (in green) using a pulled glass capillary. B: Representation of a transfected chick embryo at HH 19 *in ovo*.

2.4.4- Neural tube targeting using *in ovo* electroporation

The glass capillary containing siRNA/plasmid transfection solution was placed into the trunk neural tube of stage 16 HH embryos and pushed anteriorly along it until it reached the vagal area (level of somites 1-7), where the solution was slowly expelled. Once it was possible to see the neural tube walls turning white, the needle was removed and the embryo electroporated using the BTX square wave electroporator ECM 830 (Genetronics) configured to deliver four 25 millisecond pulses of 5V at 10 millisecond intervals across the embryo through a gold-plated electrode 0.5 of mm diameter and a platinum-plated electrode of 0.5 mm diameter, held 0.6 mm apart with an Adjustatrode electrode holder (Intracel). A drop of albumin

was added and the embryo lowered by removing 5 ml of albumin using a 19-gauge syringe needle. The window was covered with sellotape, and the eggs replaced in the 38ºC incubator for 24 hours.

2.4.5- Evaluation of siRNA impact after *in ovo* transfection

After transfection, embryos were incubated in a humidified incubator at 39ºC for 16 hours, and the transfection area examined under a fluorescence dissecting microscope. The impact of the knockdown was evaluated by assessing blood flow, heartbeat, and trunk deformities. Twisted and dead embryos were recorded and removed. Surviving embryos were placed in the humidified incubator and assessed again 24 hours later. Embryos were kept until stage 22-24 HH.

Embryos were sacrificed, fixed and dehydrated into methanol as described in section 2.3.1, analysed by either whole-mount *in situ* hybridization (section 2.3) or immunohistochemistry (section 2.5) and photographed.

2.4.6 Culture of *in ovo*-transfected somite strips

2.4.6.1- Preparation of in *ovo*-transfected somite strips for culture

Chick embryos in which somites had been transfected (section 2.4.3) at stages 9-12 HH were incubated until stage HH 22-24, removed from the egg and rinsed in warmed L-15 Leibovitz medium (PAA Laboratories Ltd) supplemented with 1% L-Glutamine-Penicillin-Streptomycin solution (Sigma). Embryos were positioned on their sides and pinned down using insect pins (the head and last three somites) in a Sylgard-coated culture dish. The endoderm and part of the mesoderm were removed with a micro-scalpel Feather® (PFM Medical, ref: 200300715). The neural tube plus somites were then pinned ventral-side up, the remaining mesoderm removed and somites separated from the neural tube. Somite strips were removed from both sides. Three somites at the anterior and posterior extremities were discarded. The non-transfected side was used as the control side of the embryo.

2.4.6.2- Culture of intact in *ovo*-transfected somite strips

Somite strips prepared as described in section 2.4.6.1 were collected into non-treated 4-well culture slides (BD Falcon) (both strips from the same embryo were put in the same well) with warmed L-15 Leibovitz medium (PAA Laboratories Ltd) supplemented with 1% L-Glutamine-Penicillin-Streptomycin solution (Sigma), and left to recover for 12 hours at 39ºC in a humidified box. To prevent cells from differentiating into fibroblasts, a notochord fragment was added into each well together with the strips. siRNA knockdown efficiency was evaluated by live immunostaining as described in section 2.5.2.

2.4.6.3- Culture of dissociated *in ovo*-transfected somite strips

Somite strips from 2 *in ovo*-transfected embryos were prepared as described in section 2.4.6.1 and collected into a 2-ml LoBind tube (Eppendorf) with warmed L-15 Leibovitz medium (PAA Laboratories Ltd) supplemented with 1% L-Glutamine-Penicillin-Streptomycin solution (Sigma). Strips were dissociated with a 25-gauge syringe needle, and 20 µl of cells were transferred into each well of non-treated 4-well culture slides (BD Falcon) with 490 µl of pre-warmed medium. To prevent cells from differentiating into fibroblasts, a notochord fragment was added into each well together with the strips. Slides were cultured in a humidified box at 38ºC for 16 hours. siRNA knockdown efficiency was evaluated by live immunostaining as described in section 2.5.2.

2.4.7- Transfection of retinal cells and astrocytes in culture

Chick embryos were removed from the egg at stage HH 22-24, rinsed and transferred into a Sylgard-coated culture dish containing pre-warmed L-15 Leibovitz medium (PAA Laboratories Ltd) supplemented with 1% L-Glutamine-Penicillin-Streptomycin solution (Sigma). Eyes were removed with a micro-scalpel Feather® (PFM Medical, ref: 200300715) and dissociated as described in section 2.4.6.3.

Human astrocyte cells (Neu7) were kindly provided by Dr. Elizabeth Muir (Department of Physiology, Development and Neuroscience, University of Cambridge). Cells were re-suspended in pre-warmed F12 medium with 1% L-

Glutamine-Penicillin-Streptomycin solution (Sigma), 10X B127 and 5% Nerve Growth Factor (NGF, Sigma, N2513) and transferred into 4-well glass slide culture dishes (BD Falcon).

Neu7 cells and chick retinal cells were incubated in a CO_2 incubator at 38ºC for 16 hours, after which 12.5 µg of siRNA were dissolved in 100 µl of 5% glucose and 1.5 µl of Turbofect^{TM}. 10 µl of this transfection mix were dissolved in 490 µl of DMEM (Sigma) supplemented with the B127 and NGF as for the F12 medium, and added to the cell culture. After incubation in a CO_2 incubator at 38ºC overnight, cells were washed with DMEM three times and incubated for a further three hours with B127/NGF-supplemented DMEM. Once the cells had recovered, live immunostaining was carried out as described in section 2.5.2.

2.5- Immunohistochemistry

2.5.1- Whole-mount immunohistochemistry

Dehydrated embryos in methanol were transferred to 2-ml microfuge tubes and bleached at room temperature in 6% hydrogen peroxide in methanol for 1 hour or until the embryos turned white. Embryos were rehydrated into PBST through a series of 10-minute washes in 75%, 50% and 25% methanol in PBST, incubated for 3 hours in blocking solution (10% sheep serum in PBST), then incubated for 12-18 hours at 4ºC with primary antibody diluted in blocking solution (Table 2.1). Where appropriate, fluorescein-conjugated or rhodamine-conjugated peanut agglutinin (PNA) (Vector Labs, catalogue numbers FL-1071 and RL-1072 respectively) was also added at 1:500. Embryos were then washed 4 times for 20 minutes each in PBST, before incubation with the appropriate secondary antibody (Table 2.2). After using fluorescent secondary antibodies, embryos were washed 3 times with PBST for 10 minutes each and then prepared for vibratome sectioning. When a biotinylated secondary antibody had been used, Neutravidin350 (Alexa Fluor 350 conjugate of NeutrAvidin biotin-binding protein; Invitrogen A-11236) was used at 1:1000 in PBS. Alkaline phosphatase-conjugated secondary antibodies were used for some embryos, in which case the colour reaction was performed as described in section 2.3.2. Embryos were then washed seven times for 30 minutes each in MABT and twice for

10 minutes each in PBS and then cleared in series of 25%, 50% and 70% glycerol in PBS. Embryos were photographed using a Leica dissecting scope and sectioned using a vibratome.

2.5.2- Live immunostaining of cultured tissue/cells

4-well culture slides containing siRNA-transfected somite strips (intact or dissociated; section 2.4.6) or astrocytes (section 2.4.7) were blocked by adding 10% sheep serum to the supplemented medium and incubating for 15 minutes. Rhodamine-conjugated peanut agglutinin (PNA) (Vector labs) and anti-protein disulfide isomerase (PDI) antibody (Sigma) were added to each well except one (negative control; also see section 2.5.3) for each slide at a dilution of 1:500, and incubated for 1 hour at 38ºC. The medium was removed and the cells were fixed in 4% paraformaldehyde for 30 minutes, then washed with PBS three times for 5 minutes each, and incubated with secondary antibody (for the anti-PDI antibody) for 2 hours at room temperature. Wells were removed according to the manufacturer's protocol and slides mounted with Fluoromount G (Southern Biotech). Slides were viewed using a Zeiss Axioskop fluorescence microscope.

2.5.3- Controls for anti-PDI immunohistochemistry

Controls used for PDI binding efficiency were: absence of primary antibody in one well per slide; pre-absorbed antibody with PDI at 5x molarity of the anti-PDI antibody (Sigma, P3818) in one well of each slide; use of rabbit IgG at the same concentration as the anti-PDI antibody instead of the anti-PDI primary antibody in one well of each slide. All assays were also carried out using a non-transfected strip. Each assay was repeated at least 3 times.

Table 2.1- Primary antibodies and dilutions used for immunohistochemistry.

Antigen	Antibody Type	Dilution	Source, catalog no.
EphA4 (N-terminal)	Rabbit polyclonal	1:50	AbGent, P54764
Fgfr1 (N-terminal)	Rabbit polyclonal	1:50	AbGent, P1136
Fgfr3 (C-terminal)	Rabbit polyclonal	1:50	AbGent, P22607
Fgfr2 (N-terminal)	Rabbit polyclonal	1:50	AbGent, P21802
Flrt3	Rabbit polyclonal	1:50	Santa Cruz, sc-82156
Fluorescein	Alexa488-conjugated rabbit polyclonal	1:50	Invitrogen, A-11090
Neurofilament-160 kD	Mouse IgG2a	1:250	Zymed/Invitrogen
Protein Disulfide Isomerase (PDI)	Rabbit polyclonal	1:500	Sigma, P7496

Table 2.2- Secondary antibodies and dilutions used for immunohistochemistry.

Antigen	Conjugated with	Raised in:	Dilution	Source, catalog no.
Mouse IgG	Alkaline phosphatase	Goat	1:100	Bethyl, AP90-105AP
Mouse IgG2a	Biotin	Goat	1:100	Southern Biotech, 1080-08
Rabbit IgG	Alexa Fluor 594	Goat	1:2000	Invitrogen, A-11012

2.6- Vibratome sectioning

Embryos were embedded in 10% gelatine (300 Bloom from Sigma)/PBS at 39ºC for 30 minutes. During this time, cryomoulds were prepared with gelatine and left to set at room temperature for 15 minutes. The embryos were transferred into cryomoulds and the gelatine flattened and set at 4ºC for 30 minutes. Gelatine blocks were cut and fixed with 4% PFA at 4ºC for at least 72 hours. Blocks were subjected to three 10-minute washes in PBS then trimmed and mounted onto a Leica VT1000S vibratome. Using a steel blade, sections were cut at a thickness of 70 µm, oriented onto the surface of glass slides (VWR International), and mounted with Fluoromount G (Southern Biotech). Sections were photographed with a camera attached to a Zeiss Axioskop fluorescence microscope.

2.7- Alcian blue staining

Chick embryos at stage 27 HH (E5) were collected and dehydrated as described in section 2.3.1. Embryos were transferred to 70% ethanol and left on the shaker for two hours, then transferred into acetic ethanol solution (30% glacial acetic acid in ethanol) and left for a further two hours, then transferred into Alcian blue solution [20% Alcian Blue (Sigma) in acetic ethanol] and left for 24 hours. Once stained, embryos were transferred back into acetic ethanol and left for another 24 hours. Embryos were then rehydrated through a series of 70%, 50%, 25% of ethanol diluted in deionised water for two hours each and then a further two hours in just deionised water. To remove muscle and connective tissue, embryos were transferred into 30% sodium borate for 24 hours, and then for several hours in 0.1% trypsin in 30% sodium borate. Once most of the tissue had been removed, embryos were transferred back into 30% sodium borate for one hour and graded back to deionised H_2O. For clearing, embryos were transferred into 0.5% potassium hydroxide for as long as necessary. For photographing, they were graded from 0.5% potassium hydroxide into 100% glycerol.

CHAPTER 3- GENE EXPRESSION ATLAS

3.1- Introduction

One of the aims of this project was to investigate whether the genes identified in the posterior half-somite of the mouse in a differential microarray screen (Hughes *et al.*, 2009) are also expressed in the posterior sclerotome in the chick model, and if so, to select one of these molecules and study its function in axonal guidance in the chick. The differential microarray screen in mouse was performed as shown in Fig. 3.1.

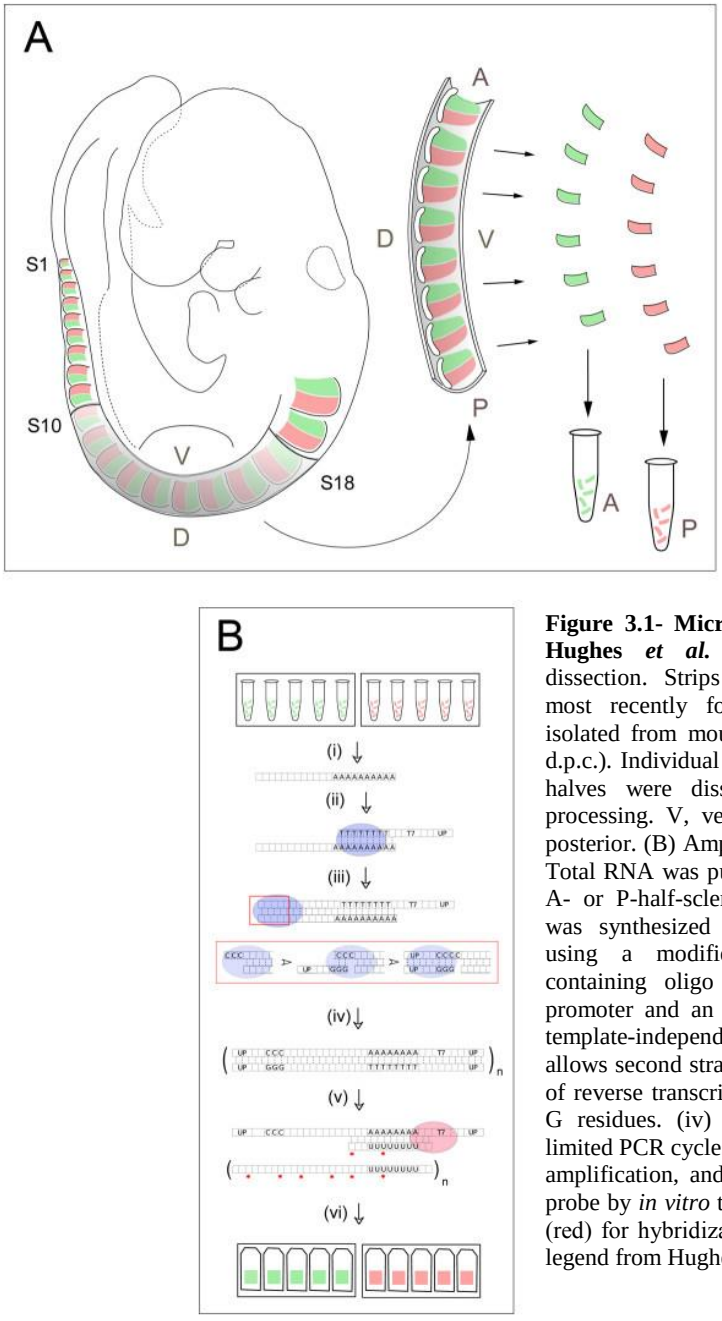

Figure 3.1- Microarray screen procedure from Hughes *et al.* (2009). "(A) Half-sclerotome dissection. Strips corresponding to the 10–18th most recently formed somites (S10-S18) were isolated from mouse embryos at TS15 (9.5–10.25 d.p.c.). Individual A- (green) or P-sclerotome (red) halves were dissected and pooled for further processing. V, ventral; D, dorsal; A, anterior; P, posterior. (B) Amplification of sclerotome RNA. (i) Total RNA was purified individually from pools of A- or P-half-sclerotomes. (ii) First strand cDNA was synthesized by reverse transcriptase (blue) using a modified Clontech SMART primer containing oligo (dT), a T7 RNA polymerase promoter and an universal primer (UP). (iii) The template-independent addition of 3' C residues allows second strand synthesis by strand- switching of reverse transcriptase using a second UP bearing G residues. (iv) Global cDNA amplification by limited PCR cycles using a UP alone. (v, vi) Further amplification, and generation of antisense-labelled probe by *in vitro* transcription using T7 polymerase (red) for hybridization to microarrays." Figure and legend from Hughes *et al.* (2009)

Two genes whose expression had previously been characterized in the chick - an anterior sclerotome marker, *Tbx18*, and a posterior sclerotome marker, *Uncx4.1* – were used as a positive control. The 12 genes selected from Hughes *et al.* (2009) whose expression patterns in chick are described in this chapter are: *glypican-6* (*Gpc6*); *hyaluronan synthase 2* (*Has2*); *phosphatase and tensin homologue* (*Pten*); *tissue inhibitor of metalloproteinase 3* (*Timp3*); *cystatin C* (*Cst3*); *coagulation factor II (thrombin) receptor* (*F2r*); *E26 avian leukemia oncogene 2, 3' domain* (*Ets2*); *fibroblast activation protein* (*Fap*); *insulin-like growth factor-binding protein 5* (*Igfbp5*); *roundabout homolog 1* (*Robo1*); *transforming growth factor beta receptor II* (*Tgfbr2*) and *fibronectin leucine rich transmembrane protein 2* (*Flrt2*). This chapter includes for each gene a brief introduction to the gene and results and discussion together describing the expression pattern and indicating whether the gene could be responsible for the repulsive role of the posterior sclerotome in axonal guidance.

3.2- Positive controls: *Tbx 18* and *Uncx4.1*

In order to validate the whole-mount *in situ* hybridization (WMISH) data, positive control *in situ* hybridization studies where carried out for molecules already known to be expressed in chicken somites: *Tbx18* and *Uncx4.1*. Tbx18 is a T-box transcription factor known to control the development of diverse tissues and organs during development (Wehn and Chapman, 2010), whose expression in somites is restricted to the anterior half-sclerotome (Haenig and Kispert, 2004). Uncx4.1 is a homeodomain transcription factor that controls the development of the vertebrate skeleton (Leitges *et al.*, 2000; Mansouri *et al.*, 2000), and which is expressed during development in the posterior half-sclerotome (Schrägle *et al.*, 2004). Images from the studies are shown in Fig. 3.2.

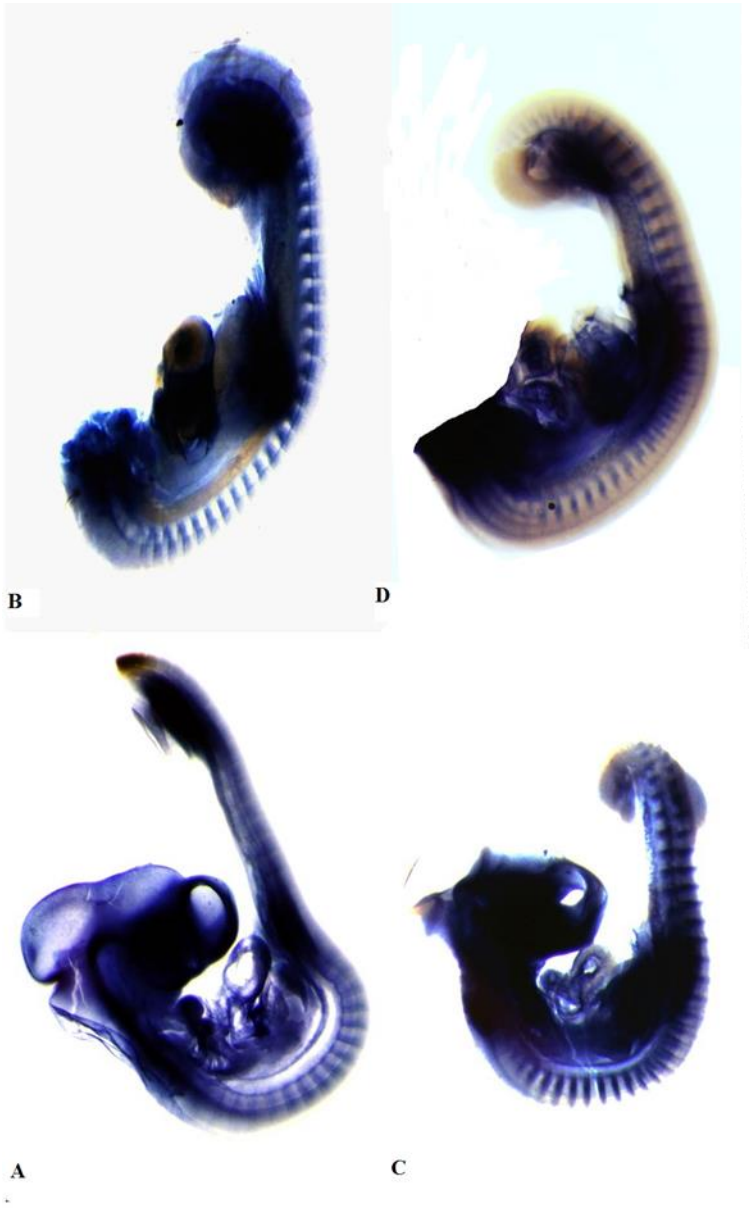

Figure 3.2- Representative WMISH images for positive control genes already known to be expressed in chicken somites. (A) *Tbx18* expression in a chick embryo at stage 18 HH. (B) *Tbx18* expression in a chick embryo at stage 26 HH. (C) *Uncx4.1* expression in a chick embryo at stage 18 HH. (D) *Uncx4.1* expression in a chick embryo at stage 26 HH.

Confirmation that the WMISH was successful was provided by positive control molecules displaying the expected complementary expression patterns, with *Tbx18* in the anterior half-sclerotome and *Uncx4.1* in the posterior half-sclerotome.

Tbx18 expression was restricted to the anterior half-somite (Fig. 3.2A,B), Expression in the heart was seen by stage 12 HH, but was not visible in the somites until stage 16 HH. By stage 19 HH, *Tbx18* expression was seen in the limbs. By stage 29 HH, *Tbx18* expression in the somites disappeared, leaving expression only in the heart and limbs, as described by Haenig and Kispert (2004).

Uncx4.1 expression was reported as restricted to the posterior half-somite from stage 16 HH to 26 HH (Mansouri *et al*., 2000) (Fig. 3.2C,D). By stage 19 HH *Uncx4.1* expression was also seen in the limb buds (Fig. 3.2D).

Both positive control genes demonstrated expression patterns as described in the literature, validating the WMISH technique.

3.3- Glypican-6 (Gpc6)

Glypican-6 (Gpc6) belongs to a family of heparan sulphate proteoglycans (HSPGs) (Song and Filmus, 2002) that are known to have a role in axonal guidance (Bloechlinger *et al.*, 2004). There are six glypicans (Gpc1 to Gpc6) (Song and Filmus, 2002; Luxardi *et al*., 2007). *Gpc6* was identified in 1999 and found to be expressed in the mesenchyme of the mandibular process, the smooth muscle cells of the dorsal aorta, the kidney and, interestingly, the intervertebral discs (Veugelers *et al.*, 1999; Song and Filmus, 2002). Hughes *et al.* (2009) showed by WMISH that *Gpc6* was present in the posterior half-sclerotome, hence *Gpc6* was selected to see whether it is also expressed in the posterior half-sclerotome of chicken. Amplification of mRNA for this gene was successful and WMISH data were obtained for HH stages 22 and 25 (Fig. 3.3).

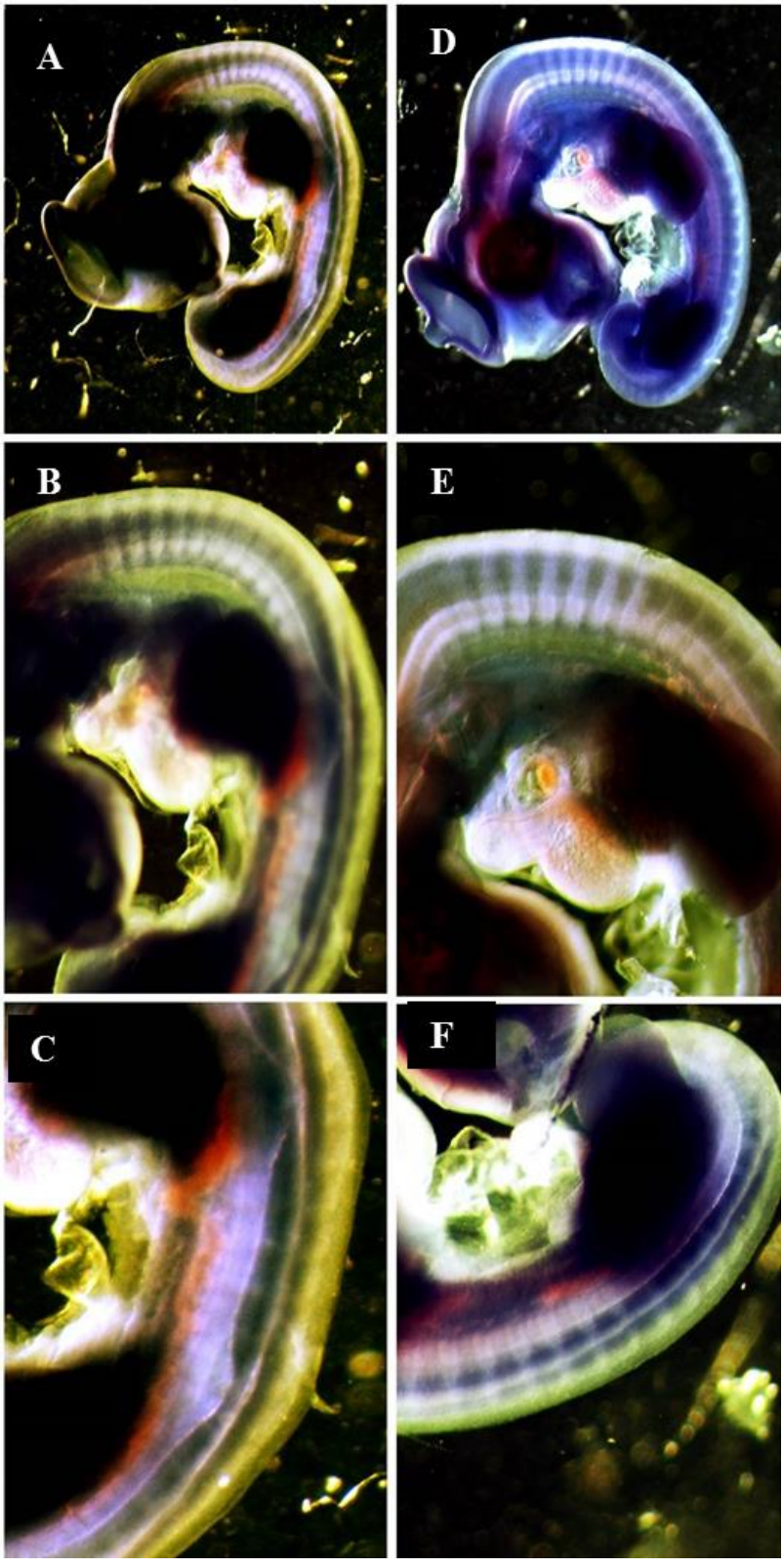

Figure 3.3- Whole-mount *in situ* hybridization for *Gpc6* for chick embryos at stages 22 HH (A-C) and 25 HH (D-F). Panels A and D show *Gpc6* expression in the whole embryo; panels B and E show expression in the vagal and trunk region; panels C-F show expression in the more posterior trunk.

According to Hughes *et al.* (2009), *Gpc6* expression was detected by the microarray and WMISH in the posterior sclerotome of mouse, however the same is not visible in the chick model. As shown in Fig. 3.3, *Gpc6* appears to be expressed in the anterior-half of the sclerotome and in the neural tube, from stage 22 HH to stage 25 HH in the chick embryo. Since its expression was not seen in the posterior half-sclerotome, further studies were not done.

3.4- Hyaluronan synthase 2 (Has2)

Hyaluronan synthase 2 (Has2) encodes an enzyme that produces hyaluronan, a glycosaminoglycan that is a key component of the extracellular matrix (ECM) (Klewer *et al*., 2006). Its expression is high in mid-gestation mouse embryos in the neural crest cell populations and endocardial cushions and it plays a role in EMT, vasculogenesis and neural crest survival (Spicer *et al*., 2002). Zebrafish *Has2* is required for multiple developmental processes, one of which is the migration of adaxial and sclerotomal cells during somite reorganization (Bakkers *et al.,* 2004). After this, *Has2*-positive cells migrate to the lateral walls of the somites, and differentiate into muscle and cartilage cells (Spicer *et al*., 2002).

Hyaluronan expression has been found around differentiating and proliferating cells in the ventrolateral part of the chick spinal cord, including early motor neurons (Mészár *et al*., 2008). The multiple expression domains of the hyaluronan synthase gene *Has2* connect it to the nervous system, however its full function is still not known. In order to investigate this, a null mutant mouse model has been created, but this is not viable (Roughley *et al*., 2011). These mice presented deformities in cartilage and in the limb joints, as these were reduced. The embryos were also smaller than usual indicating that some abnormalities might be present in the vertebral column area (Roughley *et al*., 2011). Furthermore, Hughes *et al.* (2009) detected *Has2* in the posterior half-somites in their mouse microarray screen. For this reason *Has2* was included in the present study.

Amplification of mRNA for this gene was successful and WMISH data were obtained for HH stages 16, 19, 23 and 26 (Figs. 3.4 and 3.5).

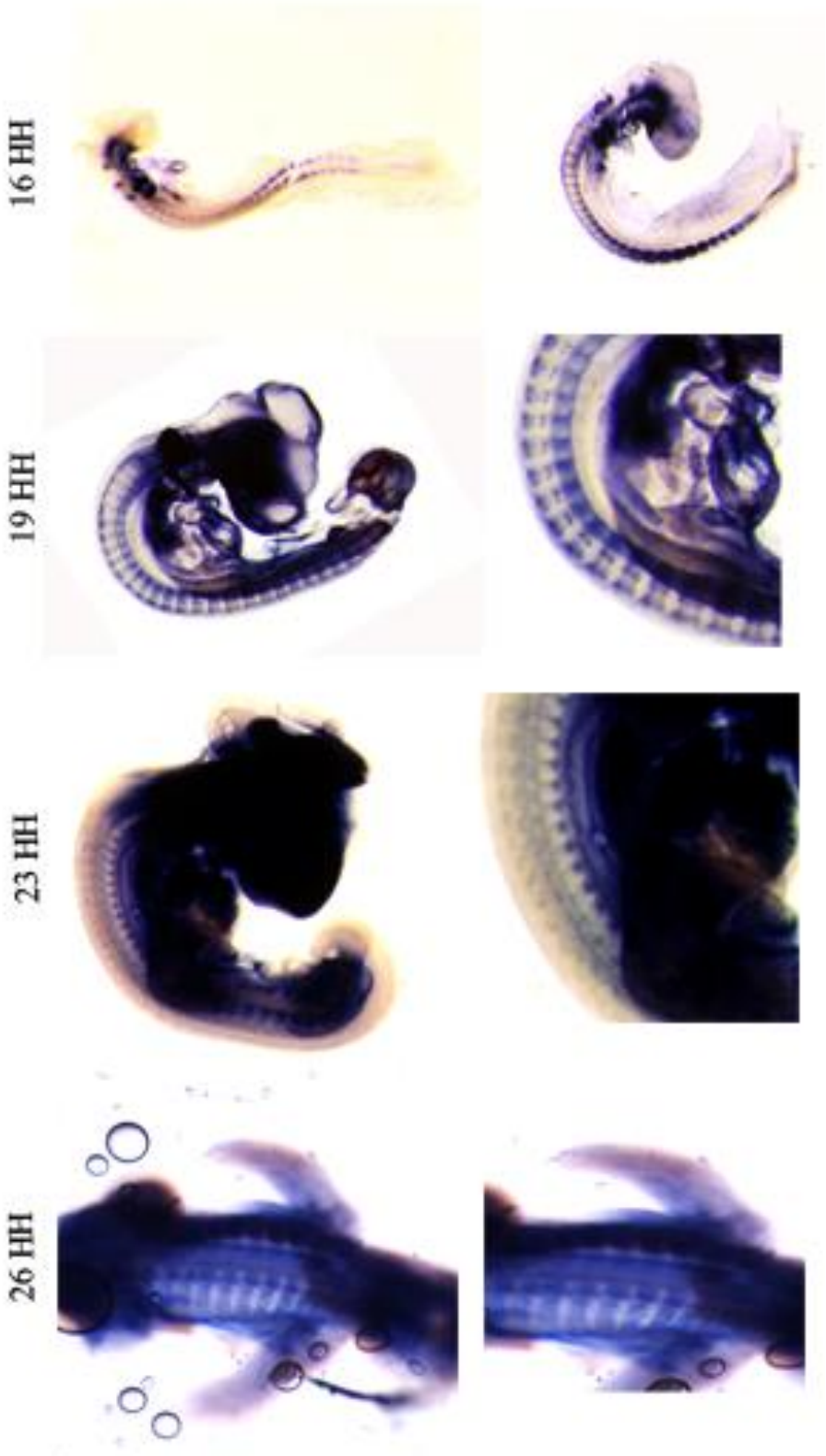

Figure 3.4- Chick embryos after WMISH for *Has2* from stage 16 HH to 26 HH. *Has 2* is expressed at stage 16 and 19 HH in the epicardium and anterior half-somite. At 23 HH, it is present in the dorsal root ganglia (DRG) and neural tube, sclerotome, limb buds, heart and mesonephros. At stage 26 HH, it is present in DRG and limb muscle.

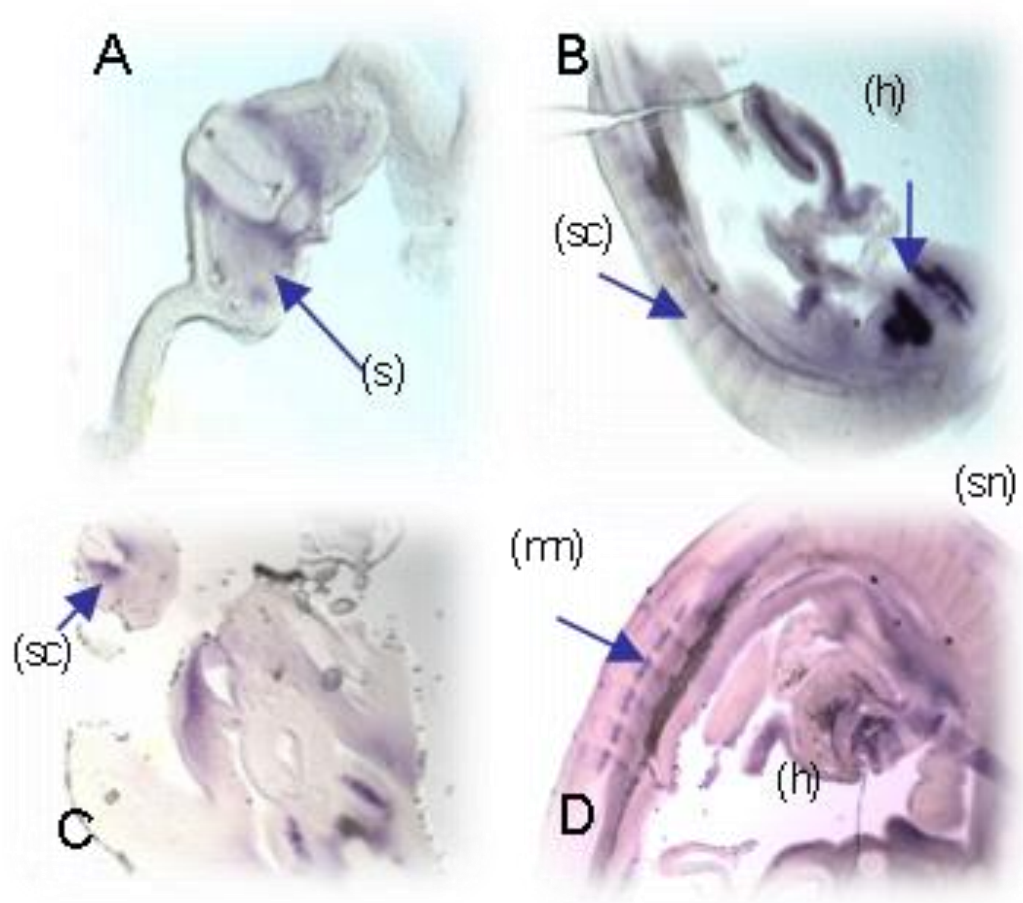

Figure 3.5- Sections of embryos after WMISH for *Has2*. (A) Transverse section of a chick embryo at stage HH 16. (B-D) different section planes of a chick embryo at stage 25 HH, Panels B and D show parasagittal sections at the level of the heart. Panel C shows a transverse section at the level of the upper limbs. (s) - somite, (sc) - sclerotome, (h) - heart, (mn) - motor neurons, (sn) -sensory neurons.

Has2 is clearly expressed in the anterior half-somite and is also highly expressed in dorsal root ganglia (Fig. 3.4 and 3.5), similar to what was described by Mészár *et al*. (2008). In the mouse microarray study by Hughes *et al*. (2009), *Has2* was reported to be expressed in the posterior half of the sclerotome, suggesting either an inter-species difference or perhaps that *Has2*-expressing cells that surround the notochord may have been included in the dissection of the posterior half sclerotome in the Hughes *et al.* (2009) study. Evidence that *Has2* should localise in the anterior sclerotome lies in the fact that the hyaluronan receptor CD44 is a well-known anterior sclerotome marker (Wheatley *et al*., 1993), and CD44 was detected by the microarray in the anterior-half of the sclerotome by Hughes *et al.* (2009) while *Has2* was in the posterior half-sclerotome,

but this might be a false positive result. The majority of HA studies have focused on limb morphogenesis. For example, *Has2* expression was found in the posterior subridge mesoderm in chicken stage 17/18 when the limb bud is being formed (Li *et al.*, 2007). However, there was also a functional study in *Xenopus* in which the loss of *XHas2* caused the disruption of somite pattern resulting in defects in muscle differentiation and the migration of hypaxial muscle cells and trunk neural crest cells (Ori *et al.*, 2006). Recently, another study in *Xenopus* described that hyaluronan is not only essential for cranial neural crest migration by promoting cell locomotion together with versican, but also to ensure neural crest survival post-migration (Casini *et al.*, 2012).

The present results show that *Has2* has a variable expression during chick development. At stage 14 HH, *Has2* has a non-segmented expression in the sclerotome but is absence in the ventral lateral sclerotome (Fig. 3.4; Fig. 3.5A,C). By stage 16 HH it becomes segmented and restricted to the anterior half of the sclerotome from the 10th somite onwards (Fig. 3.4). Fig. 3.5A shows that *Has2* has a stronger expression in the ventral sclerotome that spreads through the lateral sclerotome until the dorsal sclerotome, and then its expression is also localised in the lateral sclerotome.

By stage 17 HH, *Has2* expression becomes restricted to both motor and sensory neurons, mesonephros and heart (Fig. 3.5A,B). *Has2* might not play a role in somite patterning, but this study and previous work (Ori *et al.*, 2006) suggest that it may play a role in PNS development, being strongly expressed in the dorsal root ganglia. Due to its absence from the posterior half-sclerotome, further studies were not done.

3.5- Phosphatase and tensin homolog (Pten)

Phosphatase and tensin homolog (Pten) encodes a lipid and protein phosphatase that inhibits numerous molecules involved in cell signalling (Puig *et al.*, 2009). The Pten protein has a catalytic N-terminal phosphatase domain that acts on both protein and lipid substrates and a C-terminal C2 domain that is responsible for controlling cell migration and may have a role in axonal migration (Raftopoulou *et al.*, 2004). Elevated levels of Pten have previously been found in the peripheral projections of sectioned

DRG neurons from rat, but only small amounts were detected in DRG cultured from E18 rat embryos, instead Pten protein was highly enriched in the central domain of the growth cone where it accumulated with microtubules (Chadborn *et al.*, 2006). An interaction study of Pten with other molecules showed that Pten accumulates at the growth cone membrane during Sema3A-induced growth cone collapse (Raftopoulou *et al.*, 2004).

Pten deletion in adult retinal ganglion cells (RGCs) promotes axon regeneration after optic nerve injury, and it is likely to act upon intrinsic mechanisms other than survival to promote axon regeneration after injury (Park *et al*., 2008). These findings raise questions about the expression and possible roles of Pten in early development. As it has been shown to be involved in regeneration and growth cones, this suggests that if it is expressed in early development, Pten may be localised in the anterior half of the sclerotome. Pten is also found to be involved in bone and cartilage development: Pten deletion in osteo-chondroprogenitor cells leads to vertebrae overgrowth, mainly due to matrix deposition and accelerated differentiation (Knobbe *et al.*, 2008). These findings made it particularly appealing to establish the expression pattern of *Pten* in the developing chick embryo.

Unfortunately, WMISH results for this gene were particularly hard to obtain. Although it was possible to see some weak staining in the somites at stage 19 HH (Fig. 3.6A,C), by increasing the development time, the somite signal intensity became stronger however so did the background staining (Fig. 3.6B,D). *Pten* had a weak expression at stage 19 HH at somite boundaries and extending into the anterior half of the somite (Fig. 3.6C,D). Although a rich expression in neurons or even in the neural tube was expected, this was not observed. Even though Pten has been shown previously to couple with Sema3A signalling during growth cone collapse (Chadborn *et al.*, 2006), it does not necessary mean that Pten will have a similar gene expression to Sema3A in all situations. The weak *Pten* expression in the chick embryo suggests that it may not play an important role in axon guidance in early chick development, and definitely not in somite polarity. Therefore further analysis of this gene was not pursued.

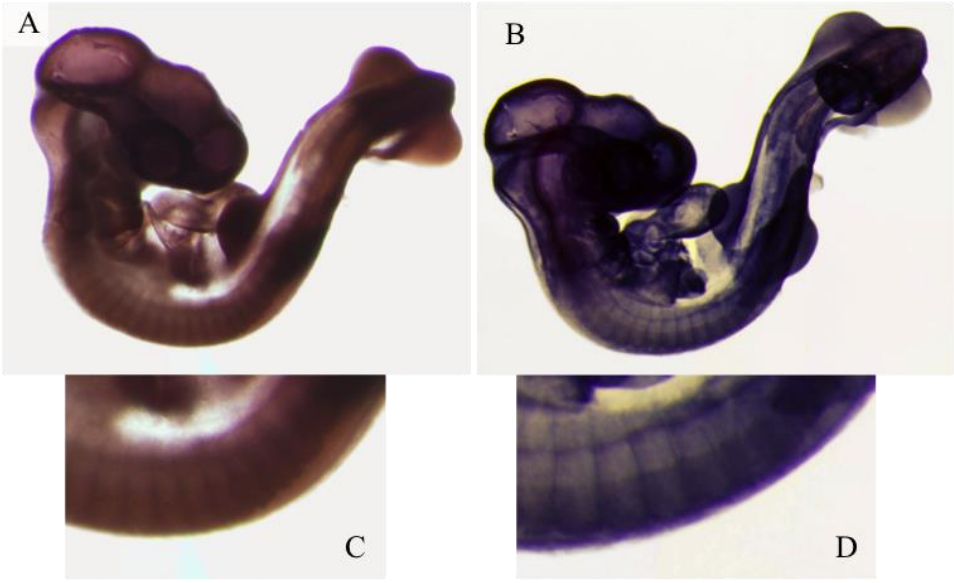

Figure 3.6- Chick embryos after WMISH for *Pten* at stage 19 HH. *Pten* is weakly expressed at somite boundaries and also in the anterior half of the somite.

3.6- Tissue Inhibitor of Metalloproteinase-3 (Timp3)

During development, a balance between synthesis and degradation of the extracellular matrix (ECM) is continuously maintained. The family of matrix metalloproteinases (MMPs) is believed to be responsible for maintaining this balance. MMPs function in the turnover of a broad spectrum of ECM proteins including collagens, laminins, fibronectin and proteoglycans (Nagase *et al.*, 1997). Their function is regulated by interaction with their natural inhibitors, the tissue inhibitors of metalloproteinases (TIMPs) (Langton *et al.*, 2000). The balance between MMPs and TIMPs plays a key role in a wide range of physiological processes in embryonic development, connective tissue remodelling, wound healing, glandular morphogenesis, and angiogenesis (Langton *et al.*, 1998). *Timp3* was discovered in chicken by Pavloff *et al.* (1992) and its role in the morphogenesis of non-neuronal tissues has since been investigated. *Timp3* expression during rat development was found in the dorsal root ganglia, ventricular zones, cartilage, epithelia of the lung, intestine and kidney, skeletal muscle, thymus and whisker vibrissae (Jaworski and Fager, 2000). *Timp3* expression

was also detected in the posterior half sclerotome by microarray and WMISH (Hughes *et al.,* 2009). This result was somehow surprising, as its expression had been found in dorsal root ganglia and therefore it would be predicted to be in the anterior and not in the posterior half-somite, so this result might be a false positive of the microarray study (Hughes *et al*., 2009). Nevertheless, I studied *Timp3* expression in the chick model.

Amplification of mRNA for this gene was successful and WMISH data were obtained for HH stages 18, 22 and 26 (Fig. 3.7). From this study, it appears that there are a number of differences in *Timp3* gene expression patterns between chicken and rodents. In rat, *Timp3* is expressed in the dorsal root ganglia, cartilage and gut (Jaworski and Fager, 2000), while in chicken, the gene is expressed in the notochord from stages 18 to 26 HH (Fig. 3.7B,C,N,O,P), consistent with a previous report of notochord expression between stages 8 and 14 HH (Cantemir *et al.,* 2004). Notochord expression starts to disappear at stage 26 HH, as its expression here becomes restricted to the embryo tail (Fig. 3.7O,P). After stage 18 HH, *Timp3* also becomes expressed in the neural tube, anterior half-sclerotome (Fig. 3.7H,I,M-O), heart (Fig. 3.7D-F,K) and limb buds (Fig. 3.7D-F,J-L), suggesting that it might have an important role in embryonic development. Brauer and Cai (2002) also detected *Timp3* expression in chick heart from stage 11-25 HH, being expressed in the myocardium, endocardium and also in the conus arteriosus, as detected in this study (Fig. 3.7K).

MMPs and TIMPs play diverse roles in the migration of the rostral migratory stream to the olfactory bulb, and in the postnatal subventricular zone (SVZ), and in glial cells to mediate the migration and to promote neurite outgrowth and growth cone extension (Jaworski and Fager, 2000: Muir *et al.*, 2002). Despite the presence of *Timp3* in the rodent CNS, it may not have the same role in chick embryos and further studies would be required to investigate this possibility. *Timp3* expression was not found in the posterior half-sclerotome in chick, instead it showed strong expression in the notochord and later in the myotome. Its restriction to the central myotome (Fig. 3.7M) suggests that *Timp3* may be involved in the orchestration of the re-segmentation process. The fact that it was not possible to localise *Timp3* expression in chicken posterior half-sclerotome despite the detection of *Timp3* in the mouse microarray study (Hughes *et al.*,

2009) and that no other studies report *Timp3* expression in mouse posterior sclerotome suggest that the result obtained by Hughes et al. (2009) might be a false positive.

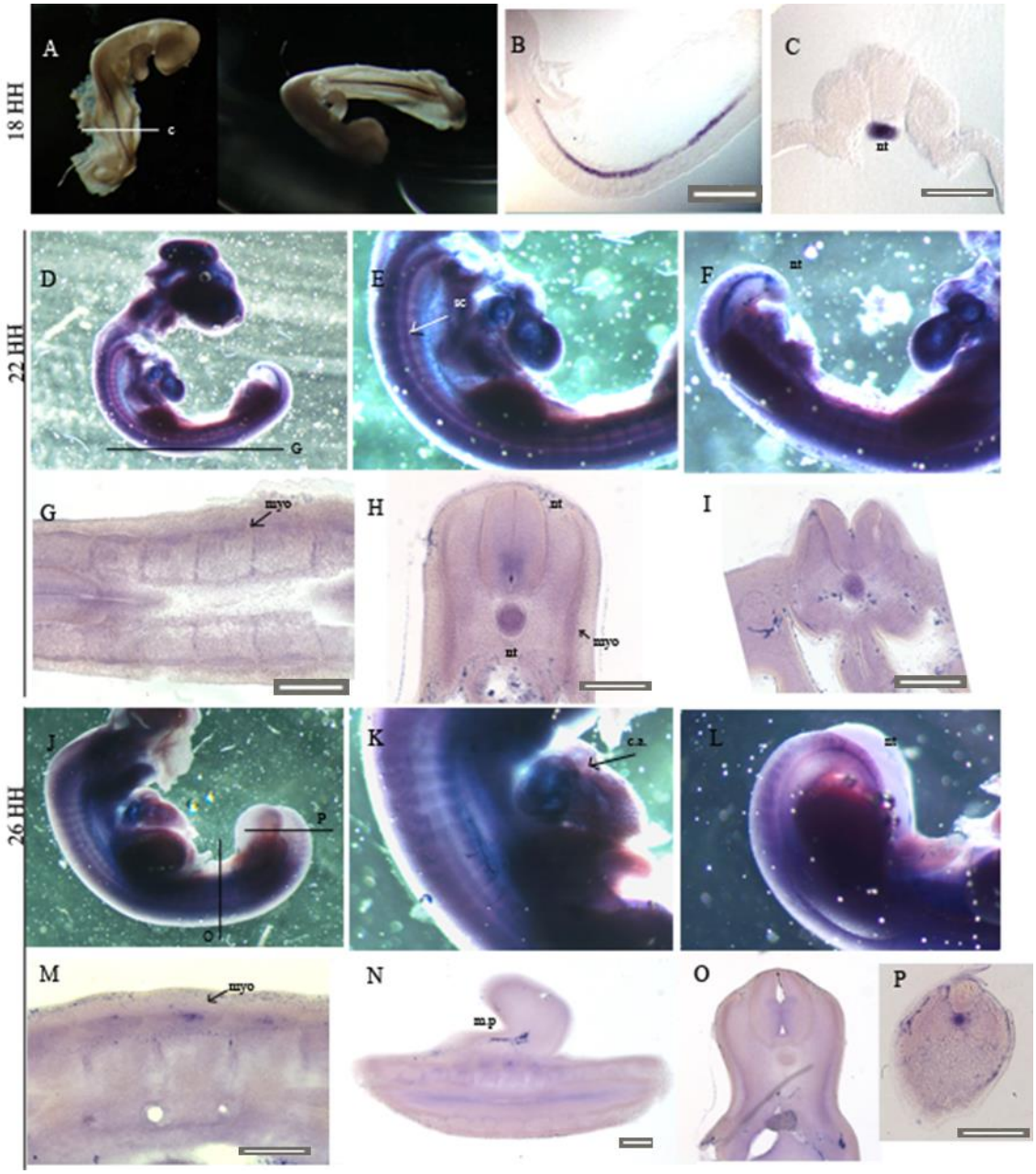

Figure 3.7- Chick embryos and embryo sections after WMISH for *Timp3*. *Timp3* is expressed in the inner sheet of the notochord at all stages examined. At stage 18 HH, *Timp3* can only be found in the notochord (B, C), while at later stages it also begins to be expressed in the limb buds and heart (D-F, J-L), the myotome (G, M-P), inner ventral neural tube (H, I, O) and faintly in the anterior sclerotome (G, I, M, N) and dorsal muscle precursors (I, N). By stage 26 HH, expression in the heart becomes restricted to the conus arteriosus (J,K). (nt)- notochord; (nt)- neural tube; (myo)- myotome; (mp)- muscle precursor; (c.a.)- conus arteriosus. Scale bar: 100 µm.

There is one study by Zeng *et al.* (1998) that connects *Timp3* expression with developing somites, bones and joints. This was detected through a β-galactosidase assay measuring lacZ expression driven by a fragment of the human *Timp3* upstream region in transgenic mice and although Zeng *et al.* (1998) did not report *Timp3* expression in somites, they showed expression in the intervertebral discs, which are formed from the notochord (McCann *et al.*, 2012) and from the anterior half-sclerotome in chick (Bruggeman *et al*., 2012), adding support to the hypothesis that the result obtained by Hughes *et al.* (2009) was a false positive. *Timp3* expression in the notochord and in the anterior half sclerotome suggests that *Timp3* might have a role in intervertebral disc formation, but further studies were not pursued.

3.7- Cystatin C (Cst3)

The carboxypeptidase inhibitor latexin was detected in the posterior half-somite in the Hughes *et al.* (2009) developing mouse microarray study. Latexin was previously used as a neuronal maker in the lateral neocortex of the developing mammalian brain (Arimatsu, 1994, Aagaard *et al.*, 2005); it plays an important role in inflammatory processes (Aagaard *et al*., 2005), pain sensitivity (Jin *et al*., 2006) and also chondrocyte differentiation (Kadouchi *et al*., 2009). The detection of latexin in the mouse posterior half-somite (Hughes *et al*., 2009) and its involvement in chondrocyte differentiation (Kadouchi *et al*., 2009) were intriguing. Although its role in vertebra formation had not been studied, it might play an important role in the fate of cells in the posterior half-somite. At the time I performed this study, there was no evidence that chicken had a latexin homologue, so I studied the expression of the cysteine proteinase inhibitor cystatin C (Cst3), which shares a high structural similarity with latexin (Liang and van Zant, 2008). (However, a chicken latexin sequence has recently become available: http://www.ncbi.nlm.nih.gov/gene/771519.)

Amplification of mRNA for this gene was successful and WMISH data were obtained for HH stages 16, 19 and 26 (Fig. 3.8). *Cst3* was found to be expressed in the notochord in the chick embryo from stage 16 HH to stage 26 HH (Fig. 3.8C,J). It has a strong expression from the presomitic mesoderm to the head.

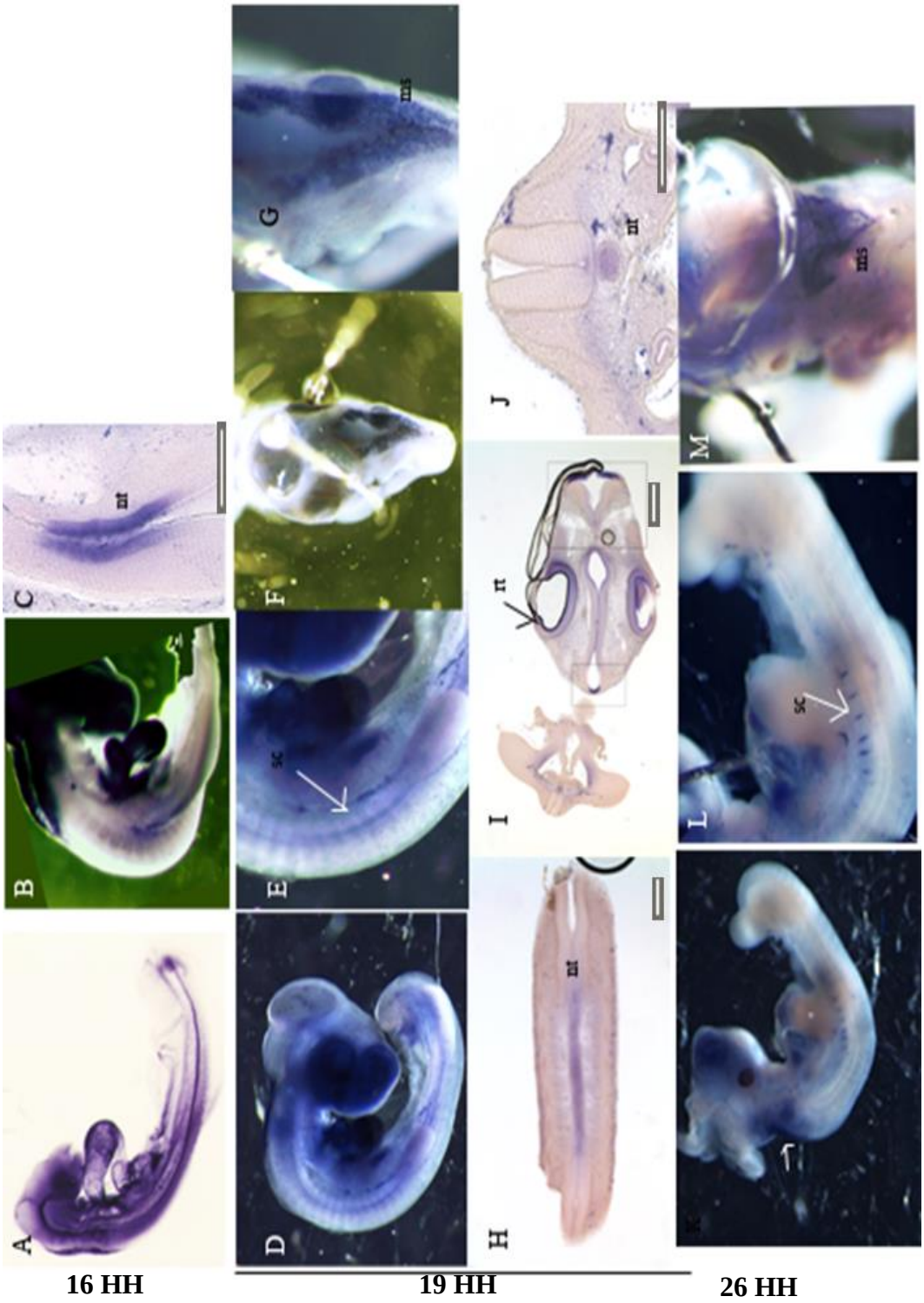

Figure 3.8- Chick embryos and embryo sections after WMISH for *Cst3* from stage 16 HH to stage 26 HH. *Cst3* is present in the inner sheet of the notochord from stage 16 HH to stage 26 HH (C, K-M). It is expressed in the mesencephalon (B, F, J), retina and lens (L), and ventral sclerotome (M white arrow in L). (rt)- retina; (sc)- sclerotome; (ms)- mesencephalon. Scale bar: 100 µm.

Contrary to the findings for mouse latexin (Hughes *et al.*, 2009), *Cst3* has strong localised expression in the mesencephalon and neural tube (Fig. 3.8G,M,H) suggesting that it may play an important role in development of the CNS. *Cst3* was detected in the ventral area of the sclerotome with a segmented pattern (Fig. 3.8E,L), suggesting that *Cst3* might be involved in the formation of the transverse process of the vertebra, but future studies would be needed to confirm this. Since the aim of this project was to study genes with potential roles in axon guidance in the somite, further studies for *Cst3* were not carried out.

3.8- Coagulation factor II (thrombin) receptor (F2r)

Coagulation factor II (thrombin) receptor (F2r), also known as PAR1 or protease-activated receptor 1, is a member of a family of G-protein-coupled receptors (GPCRs) that becomes activated after cleavage in the extracellular N-terminus (Han *et al.*, 2011; Griffin *et al.*, 2001). F2r is able to mediate the cellular responses to thrombin (Austin *et al.*, 2013). In the adult, the serine protease thrombin cleaves soluble fibrinogen to fibrin monomer, which polymerises to form fibrin matrices and is necessary to orchestrate homeostatic and inflammatory responses to tissue injury (Griffin *et al.*, 2001). *F2r* is expressed in heart, hematopoietic cells, blood vessels, brain and mesenchymal cells of E9.0- 9.5 mice (Connolly *et al*., 1996).

Despite the fact that it has been studied for wound repair, it is thought to have a role in the maintenance of the blood-brain barrier as it is expressed in brain neurons and astrocytes (Junge *et al*., 2004). The interference of F2r after cerebrovascular injury results in neurite retraction, suggesting that F2r might be responsible for the re-establishment of the connections between neurons (Suo *et al*., 2003). F2r, at first glance, does not appear a likely candidate for involvement in the polarity of somites, however considering the problems that CNS injuries represent, and the fact that *F2r* was detected in the mouse posterior half-somite microarray screen (Hughes *et al.*, 2009), raises the question of a possible role in segmentation.

Amplification of mRNA for this gene was successful and WMISH data were obtained for HH stages 16, 19 and 26 (Fig. 3.9).

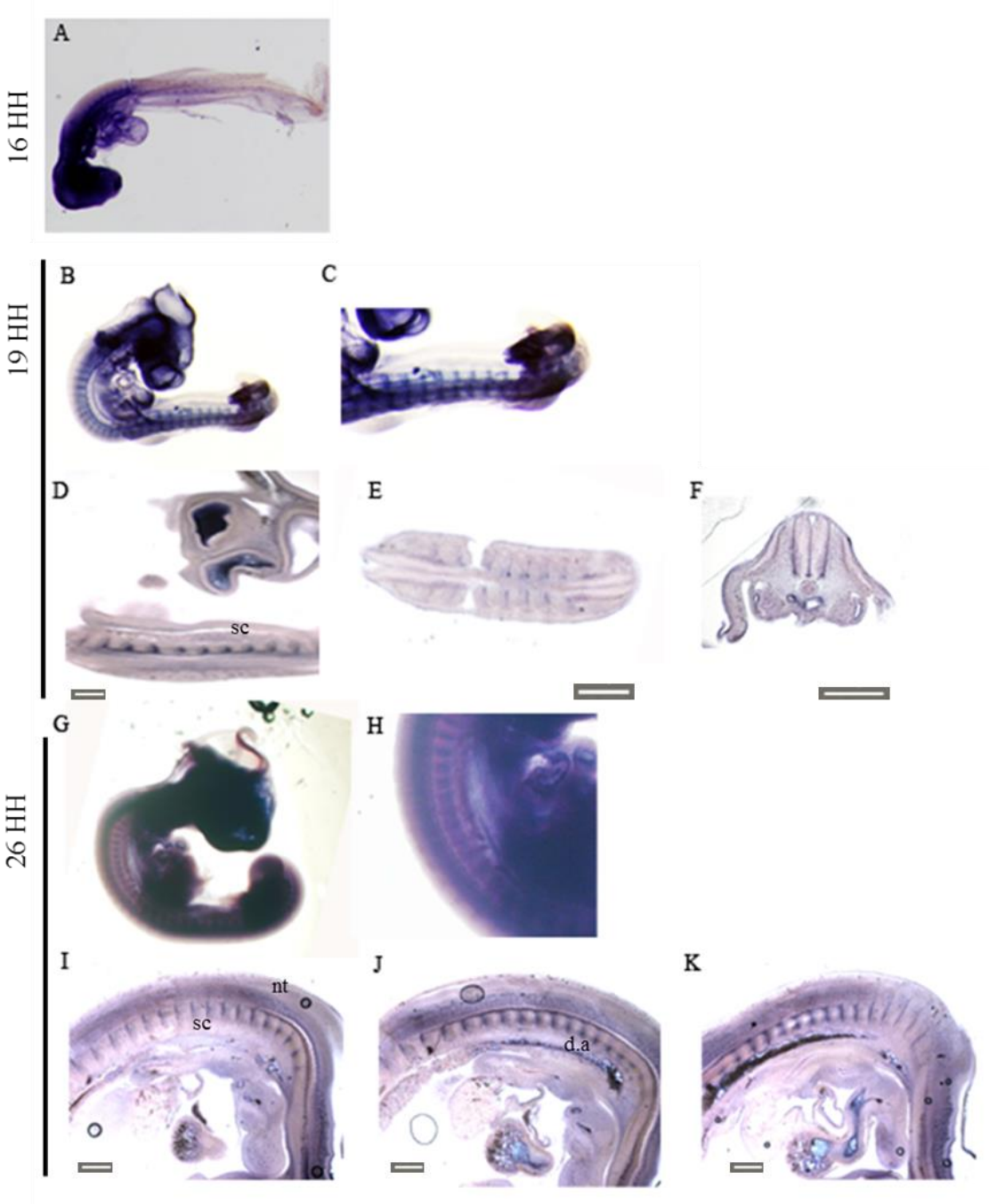

Figure 3.8- Chick embryos and embryo sections after WMISH for *F2r* from stage 16 HH to stage 26 HH. *F2r* is expressed in the ventrolateral neural tube, and in the sclerotome from stage 16 HH (A) to stage 26 HH (G). (D-E) Sections of a stage 19 HH embryo, *F2r* is present in the posterior dorsal sclerotome. (G) A stage 26 HH embryo. (H) Higher magnification view of the vagal and rostral trunk area of the embryo in G. (I-K) Serial parasagittal sections of a stage 26 HH chick embryo. *F2r* is expressed in the posterior half sclerotome and neural tube (J-K) and in the dorsal aorta (d.a). Scale bar: 100 µm.

F2r expression in chick embryos begins at approximately stage 16 HH in the somite boundaries from somite 13 forward (Fig. 3.8A). As the embryo develops (stage 19 HH), *F2r* becomes expressed from the tail to the trunk in the posterior half-somites (Fig. 3.9B-F). Despite its presence in the posterior half, it has a stronger expression in the central ventral posterior somite and inter-somitic blood vessels. Transverse sectioning revealed that *F2r* also has a strong expression near the neural tube (Fig. 3.9E,F,I-K). *F2r* is also present in forming heart within the chick embryo, being expressed in the dorsal aorta (Fig. 3.9B,H). This expression is in agreement with the already known expression of *F2r* in the endothelium of forming blood vessels (Vu *et al.*, 1991) and with the detection of *F2r* in the posterior half sclerotome of mice by Hughes *et al*. (2009). However, due to its role in the formation of blood vessels (Vu *et al.*, 1991), it is very unlikely that *F2r* is the gene responsible for axonal repulsion in the posterior sclerotome, therefore further studies were not pursued.

3.9- Ets2

Ets2 (*E26 avian leukemia oncogene 2, 3' domain*) encodes a transcription factor initially identified as a nuclear oncogene with an essential role in embryonic development (Ristevski *et al*., 2002). *Ets2* abnormalities result in craniofacial morphology in Down's syndrome (Sumarsono *et al*., 1996). *Ets2* is highly expressed in newly formed cartilage in mice (Sumarsono *et al*., 1996; Ristevski *et al*., 2002), and in osteoblasts (Raouf and Seth, 2000). In mice, *Ets2* was found to be expressed in the anterior border of the segmenting somitomere, in the anterior portion of newly formed somites, and also in the inter-somitic blood vessels (Ristevski *et al*., 2002). From these findings, its role in somite polarity was suggested; however no further studies have been done. Despite the findings of *Ets2* expression in the anterior half of the somite by Ristevski *et al*. (2002), it was detected in the posterior half-somite in the mouse microarray study by Hughes *et al*. (2009). Although the latter could therefore have been a false positive, *Ets2* expression was studied in the chick model.

Amplification of mRNA for this gene was successful and WMISH data were obtained for HH stages 16, 19, 23 and 26 (Fig. 3.10).

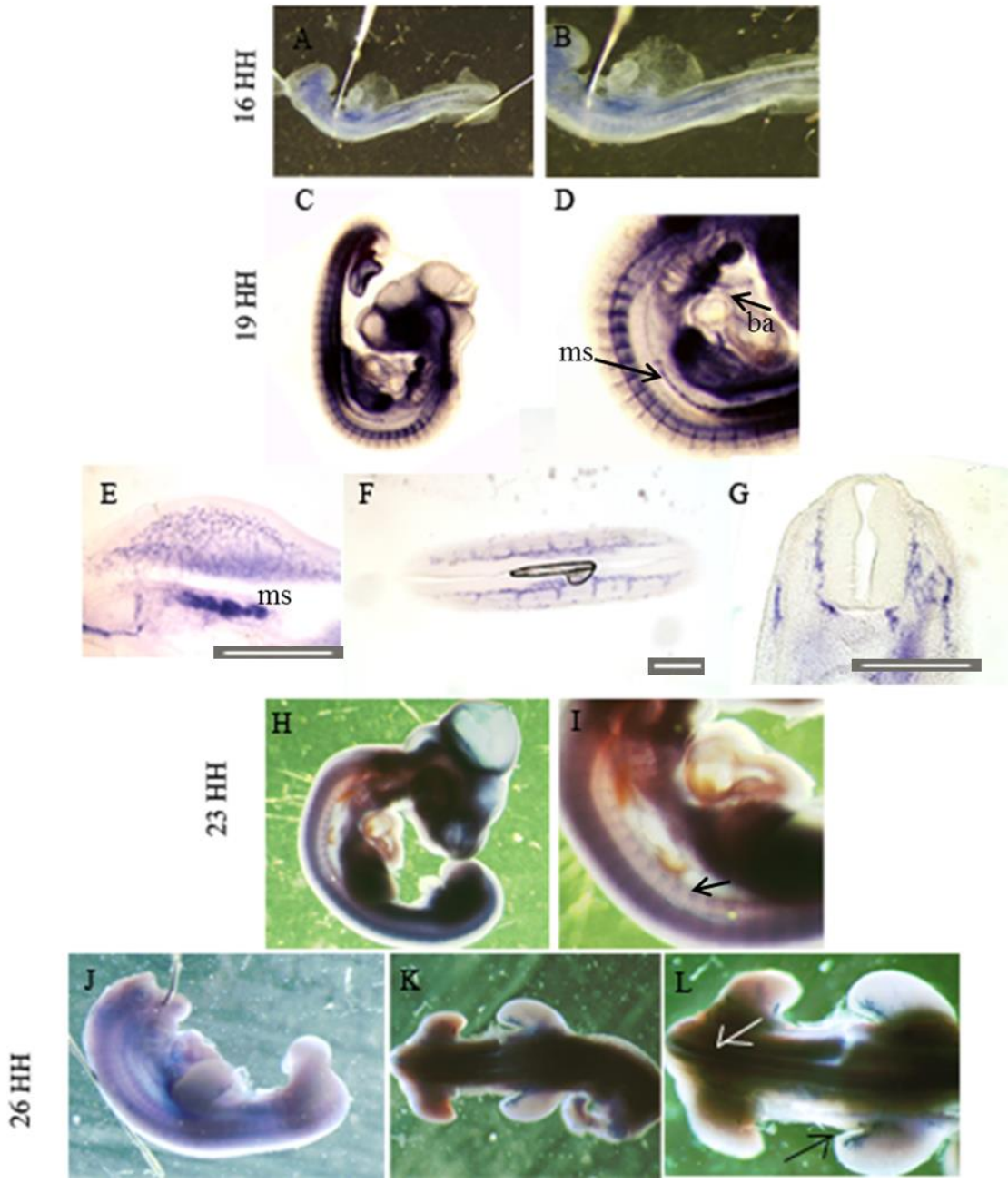

Figure 3.9- Chick embryos and embryo sections after WMISH for *Ets2* from stage 16 HH to stage 26 HH. (A,B) At stage 16 HH, *Ets2* is expressed in the inter-somitic boundaries, and in the heart. (C-G) *Ets2* expression at stage 19 HH in whole-mount (C,D) and on sections (E-G) *Ets2* is present in the limb blood vessels (C) and mesonephros (ms; D,E), inter-somitic boundaries (presumably blood vessels; C,D,F), and developing blood vessels of the sclerotome (G). (H) Embryo at stage 23 HH. (I) Higher magnification view of vagal area of embryo in H. *Ets2* is expressed in the inter-somitic boundaries (arrow) and in the limb buds. (J) Embryo at stage 26 HH. *Ets2* is expressed in the inter-somitic boundaries, dorsal neural tube (white arrow) and limb muscle (black arrow).

The findings from the present study suggest that *Ets2* has a similar gene expression pattern in chicken as reported in mouse (Ristevski *et al.,* 2002), although *Ets2* expression in the somites and around the neural tube seemed stronger in the chick than in the mouse. In chicken, *Ets2* is expressed in the developing blood vessels in both the limb (Fig. 3.10E) and sclerotome (Fig. 3.10G), suggesting that it may play a role in angiogenesis. *Ets2* expression between the somites (Fig. 3.10A,B,F,I,J) is likely in inter-somitic blood vessels, as reported by Ristevski *et al*. (2002). *Ets2* is widely expressed within the embryo, and the fact that it was detected in the posterior half-somite in the microarray screen in mouse (Hughes *et al.*, 2009) might be related to this finding. The gene expression patterns for *Ets2* suggest that it does not play a role in axon guidance in the somite and therefore further assays for this gene were not carried out.

3.10- Fibroblast Activation Protein (Fap)

Fibroblast activation protein (Fap) is a type II cell surface glycoprotein and a member of the serine prolyl oligopeptidase family (Niedermeyer *et al*., 2001). A role has been suggested for Fap in degrading the ECM or in activating growth factors at sites of tissue remodelling (Niedermayer *et al*., 2001). *Fap* is also expressed with collagen fibers, fibronectin, and collagen type I (Wang *et al.,* 2005), all important proteins for somite development and axon guidance. In mouse, *Fap* expression was found in the posterior half-somite (Hughes *et al*., 2009). Other studies have also reported *Fap* presence in embryonic mesenchyme including in the somites and primordial cartilage (Niedermeyer *et al*., 2001). For these reasons, *Fap* was included in the present study.

Amplification of mRNA for this gene was successful and WMISH data were obtained for HH stages 17, 19 and 25 (Fig. 3.11). *Fap* is expressed in the notochord from at least as early as stage 17 HH (Fig. 3.11A) to stage 25 HH (Fig. 3.7G-M). Whole-mount images from stages 25 HH suggest a segmented pattern in the notochord (Fig. 3.7H,I), although this could not be seen in coronal section (Fig. 3.11J). *Fap* expression in the notochord is interesting considering that this is a structure that undergoes numerous modifications during development (Stemple, 2005). Due to the high expression of *Fap* in the notochord it would be interesting to study whether it has

any influence on the migration and condensation of ventral sclerotome cells or in the formation of the intervertebral discs. However, because the aim of this study was to identify candidate genes involved in axon guidance in the somite, and I did not obtain any evidence to suggest an involvement of this gene in somite polarity, further studies were not done.

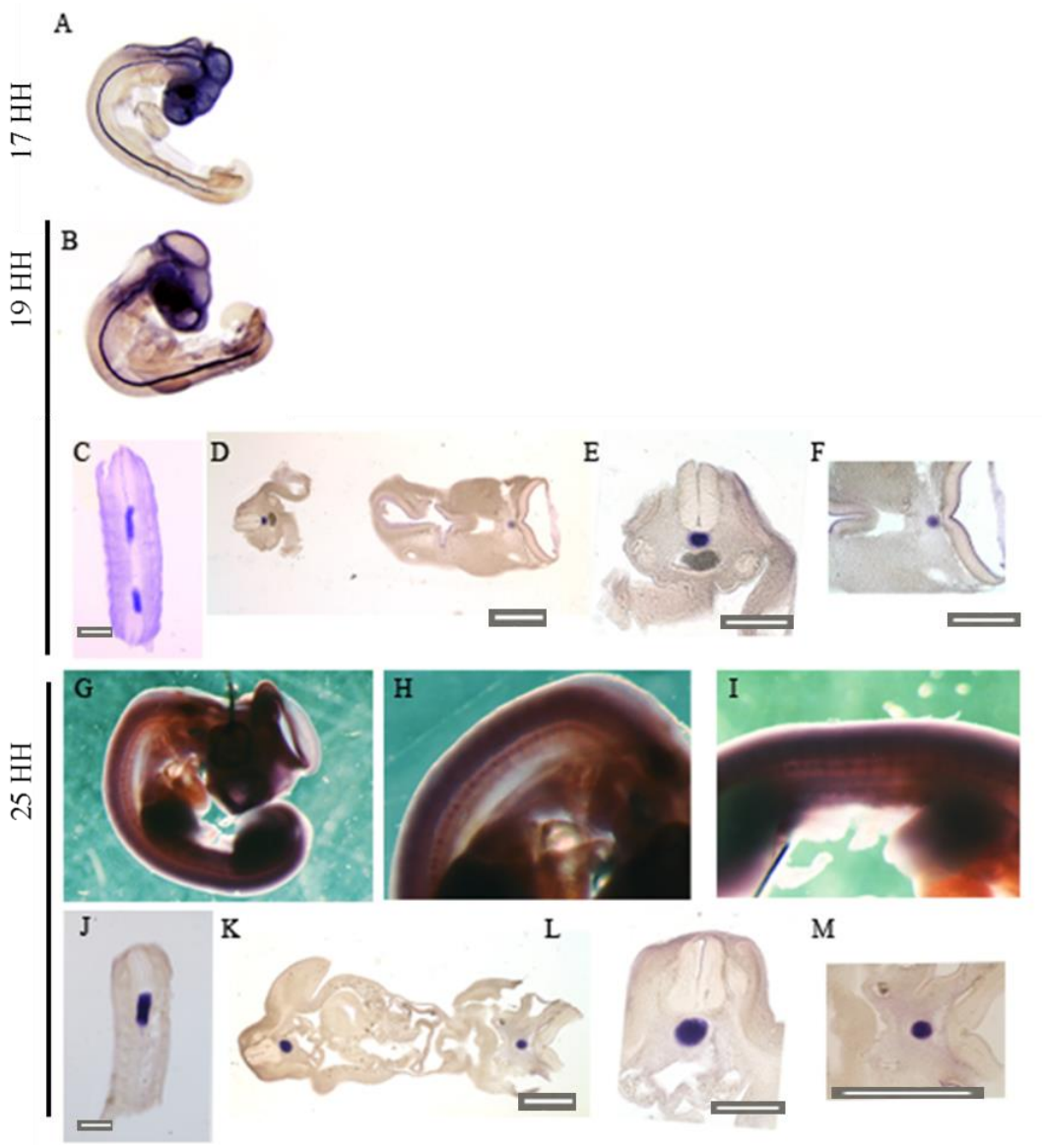

Figure 3.10- Chick embryos and embryo sections after WMISH for *Fap* from stage 17 HH to stage 25 HH. (A) Stage 17 HH. (B-F) Stage 19 HH. (G-M) Stage 25 HH. *Fap* is present in the notochord at least as early as stage 17 HH until stage 25 HH. Sections after WMISH show a very strong expression in the notochord. Whole-mount

images at higher magnification (H-I) show that *Fap* exhibits a segmented pattern within the notochord.

3.11- Insulin-like growth factor-binding protein 5 (Igfbp5)

There are six members of the insulin-like growth factor (IGF)-binding protein family: these directly bind IGF1 and IGF2, reducing the availability of IGF for receptor-binding, although this binding can also stabilize IGF, leading to a net increase in IGF signalling (Clemmens, 1998). *Igfbp5* overexpression leads to increased neonatal mortality, retarded muscle development and whole-body growth inhibition (Salih *et al.*, 2004). The two latter findings suggest that there may be an impact at the level of the somites. As gene expression studies of *Igfbp5* localisation within the vertebrae are lacking and Hughes *et al.* (2009) detected *Igfbp5* in the posterior half-somite in mice, *Igfp5* gene expression was studied in the developing chick embryo. Amplification of mRNA for this gene was successful and WMISH data were obtained for HH stages 18 and 22 (Fig. 3.12).

The pattern of *Igfbp5* expression described in this study is similar to that reported in rat by *in situ* hybridization (Green *et al.*, 1994) and immunohistochemistry (Cheng *et al.*, 1996). Expression is found in the notochord (Fig. 3.12A-D,J), regions of the central nervous system (Fig. 3.12B,H-J) including the olfactory bulb (Fig. 3.12H,I), as well as in peripheral neurons in the DRG (Fig. 3.12J). Although expression is seen in the myotome (Fig. 3.12C,D,J,K), *Igfbp5* is not expressed in the posterior half-somite in the chick embryo as detected in the mouse microarray screen (Hughes *et al.*, 2009). Detection of *Igfbp5* in the posterior half-somite in the mouse microarray screen may have been due to expression in surrounding myotome cells.

Igfpb5 expression in regions of the neural tube (Fig. 3.12B,H-J) suggests a role in the central nervous system. Indeed, a recent patent suggests that blocking Igfbp5 may help treat central nervous system cancer (Gleave *et al*. IP 20110152354).

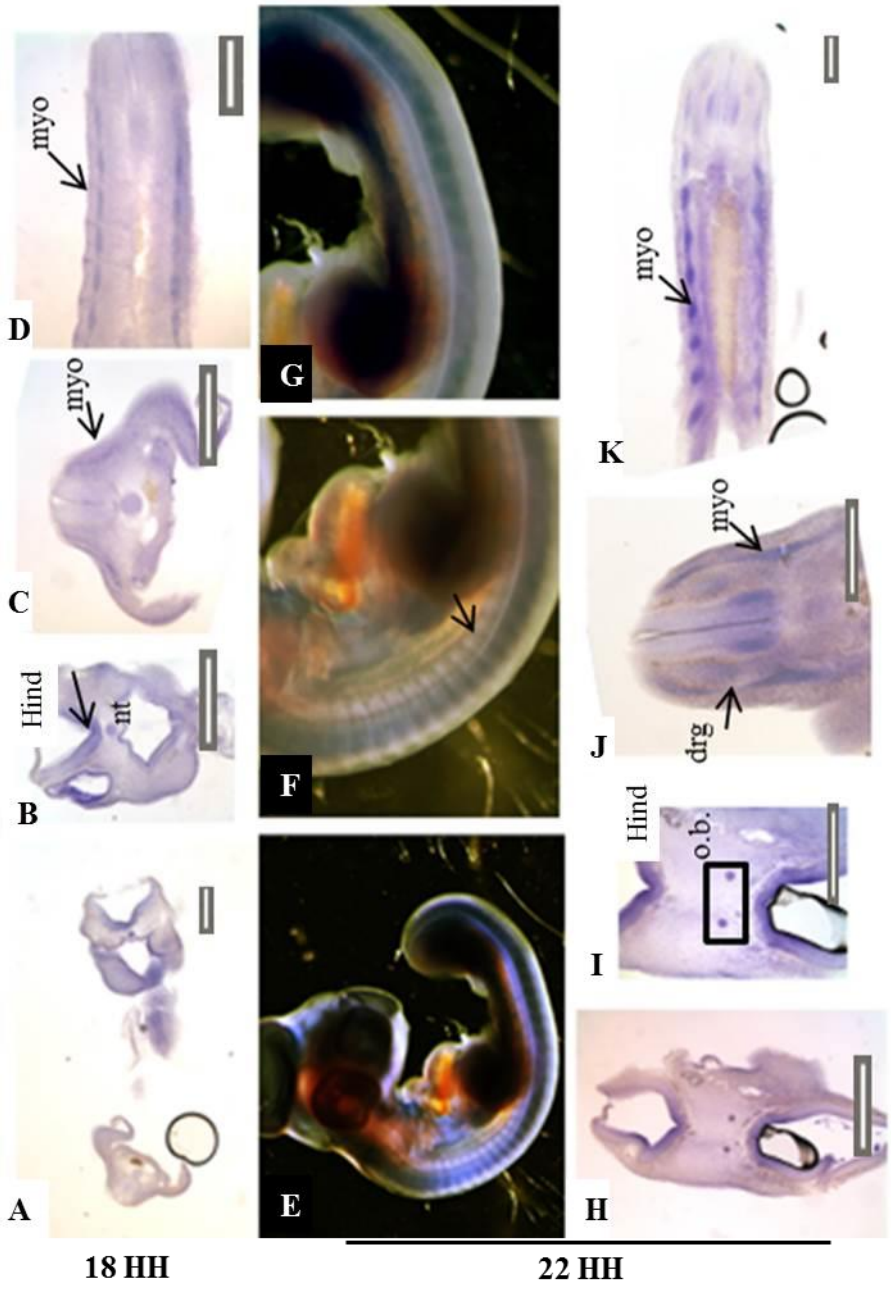

Figure 3.11- Chick embryos and embryo sections after WMISH for *Igfbp5* at stage 18 HH and 22 HH. (A-D) Stage 18 HH embryo sections after WMISH showing *Igfp5* expression in the notochord (nt), hindbrain (Hind), otic vesicle and myotome (myo). (E) Stage 22 HH embryo. (F) Higher-power view of the vagal area and rostral trunk of the embryo in E. (G) Higher-power view of the trunk, somites, limbs and mesonephros of the embryo in E. (H-K) Sections after WMISH at stage 22 HH. (H) Transverse section of the brain. (I) Higher-power view of section in H showing *Igfbp5* expression in the forebrain and putatively the edges of the paired olfactory bulbs (o.b., boxed). (J,K) Sections in the trunk region showing *Igfbp5* expression in the myotome, neural tube and dorsal root ganglia (drg). Scale bar: 100 µm.

3.12- Roundabout homolog 1 (*Drosophila*): Robo1

The Slit-Robo families are well-known axon pathfinding proteins and are considered part of one of the most important ligand-receptor connections for axon guidance (Ypsilanti *et al.*, 2010). Robo1 protein has immunoglobulin repeats and fibronectin type III repeats domains. In *Drosophila,* Robo1 prevents commissural axons from crossing the midline and also prevents re-crossing of axons by serving as a receptor for repulsive guidance molecules (Yuan *et al.*, 1999). *Robo1* is expressed in mice in the midbrain ventricular zone, distal tip of the first branchial arch, and anterior sclerotome, becoming eventually segmented into the medial and lateral anterior sclerotome (Yuan *et al.*, 1999). *Robo1* is also found in the neural tube from E10.5 in the motor columns and commissural neurons (Yuan *et al.*, 1999). Robo1 was found in the posterior somite in the mouse microarray study (Hughes *et al.*, 2009), therefore *Robo1* expression in chick was studied here. Amplification of mRNA for this gene was successful and WMISH data were obtained for HH stages 19, 22 and 26 (Fig. 3.13).

The expression of *Robo1* in chick is very similar to the expression reported in mice (Yuan *et al.*, 1999) and also previously in the chick (Jia *et al.*, 2005). From stage 19 HH to 22 HH, *Robo1* exhibited strong expression in the dorsal root ganglia (Fig. 3.13C-F) and became more restricted to the ventral lateral region of the sclerotome. *Robo1* expression was also seen in the neural tube (Fig. 3.13C-K): this expression pattern most likely represents motor columns and interneurons, as reported by Jia *et al.* (2005). These findings suggest that Robo1 may play a role in establishing neuronal connections, and that once the dorsal roots are formed, it becomes down-regulated. As *Robo1* was not detected in the posterior half sclerotome of the chick, it was not studied further.

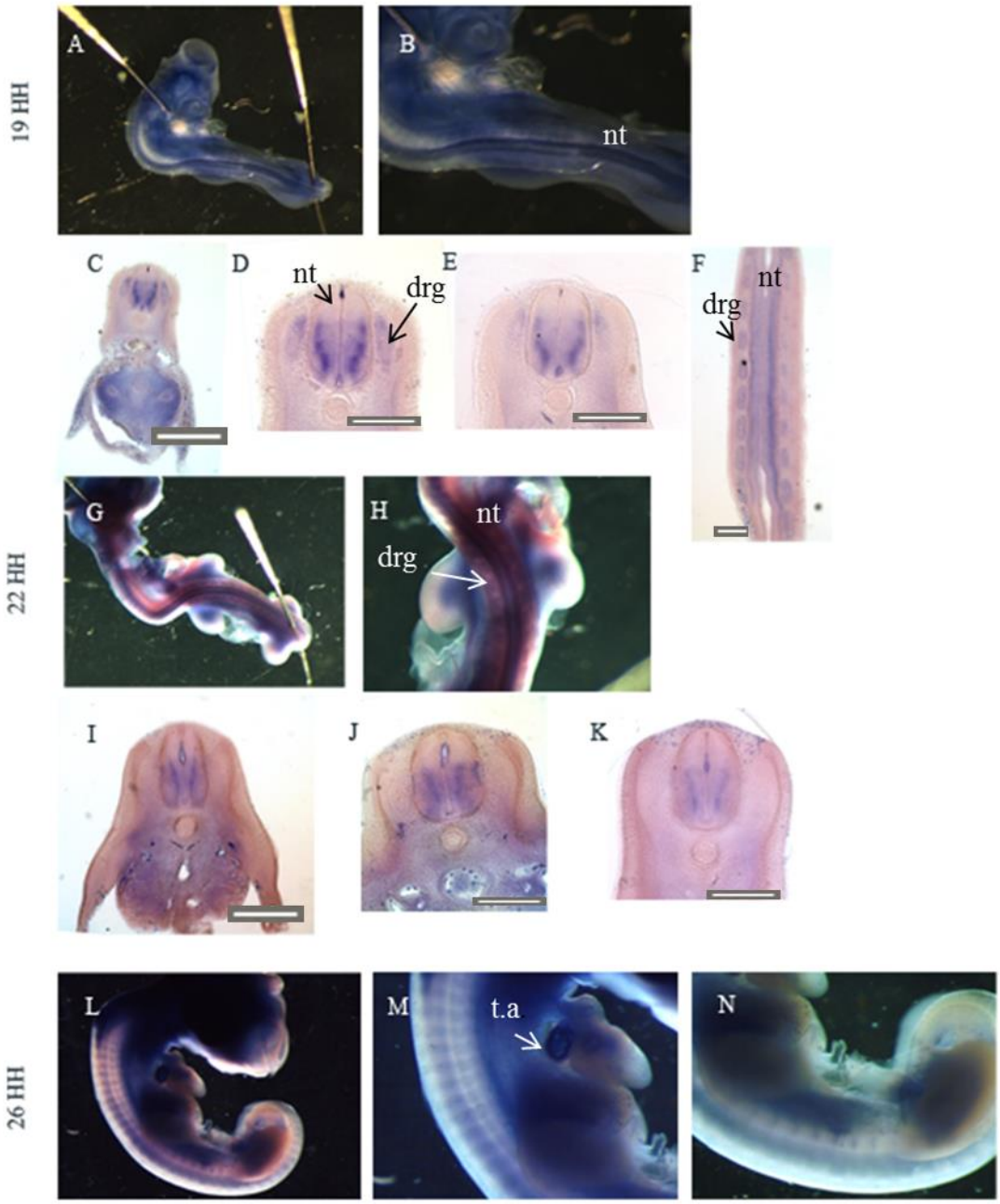

Figure 3.12- Chick embryos and embryo sections after WMISH for *Robo1*. (A) Embryo at stage 19 HH. (B) Higher-power view of the trunk of the embryo in A. (C-F) Transverse sections at stage 19 HH. *Robo1* is expressed in the neural tube and dorsal root ganglia. (G) Embryo at stage 22 HH. (H) Higher-power view of thoracic (fore-limb) area of embryo in G. *Robo1* is present in the neural tube, anterior sclerotome and wing bud. (I-K) Transverse section at stage 22 HH. *Robo1* is expressed in the neural tube and possibly neural crest cells on the roof of the neural tube. (L) Embryo at stage 26 HH. (M) Higher-power view of the vagal and thoracic area of the embryo in L. *Robo1* is present in the anterior sclerotome, wing and truncus arteriosus. (N) Stage 26 HH embryo trunk, showing *Robo1* expression in the limbs, mesonephros, neural tube, and anterior ventral and lateral sclerotome. Scale bar: 100µm.

3.13- Transforming growth factor beta receptor II (Tgfbr2)

Ligands of the transforming growth factor beta (TGFβ) superfamily act through a dual receptor system of type I (Tgfbr1) and type II (Tgfbr2) transmembrane receptor serine/threonine kinases. After TGFβ binds to type I and type II receptors, Tgfbr2 signalling is mediated by transcription factors called Smads, that regulate transcription of target genes (Wang and Serra, 2012). Tgfβs have previously been shown to be involved in skeletal development, especially in cartilage, joints, tendons development, and myogenesis (Lorda-Diez *et al*., 2010). The conditional deletion of *Tgfbr2* in presumptive skeletal tissue causes abnormalities such as failure in the dorsal closure of the neural arches (Wang and Serra, 2012), reduction or loss of the intervertebral discs, defective boundary between presumptive intervertebral discs and malformed vertebrae (Baffi *et al.,* 2006). *Tgfbr2* is also required for the development of limb bones in mice: conditional deletion of *Tgfbr2* in limb mesenchyme resulted in a decrease in chondrocyte proliferation (Seo and Serra, 2007), and in the reduction of the mesenchyme adjacent to the forming cartilage (Wang and Serra, 2012). It is clear that Tgfbr2 has an important role in skeleton formation, and since it is also expressed in mouse posterior half sclerotome (Hughes *et al*., 2009), it was important to see if *Tgfbr2* is also expressed in the posterior half sclerotome in chick.

Amplification of mRNA for *Tgfbr2* was successful and WMISH data were obtained for HH stages 16, 19 and 29 (Fig. 3.14). *Tgfbr2* was not expressed in the posterior half sclerotome at any of the studied developmental stages in chick embryo; it was however expressed in other tissues. From stage 16 HH, *Tgfbr2* is expressed in the heart and extremities of the embryo, being expressed in the anterior neural tube, then is not expressed in the lumbar area of embryo and then becomes expressed in the pre-somitic mesoderm (Fig. 3.14A,B). By stage 19 HH, *Tgfbr2* is still expressed in the heart and it becomes expressed in the entire length of the neural tube and also in the mesonephros (Fig. 3.14C-E). Transverse sections of embryos after WMISH for *Tgfbr2* showed that *Tgfbr2* is not always expressed in the neural tube as at the level of the limb (Fig. 3.14F) there was no detection in the neural tube, while in the vagal area it is expressed in the medial dorsal neural tube (Fig 3.14G). This expression is maintained at stage 29 HH (Fig. 3.14H-N). The expression of *Tgfbr2* in the neural tube suggests that this gene might have a function in the development of the CNS.

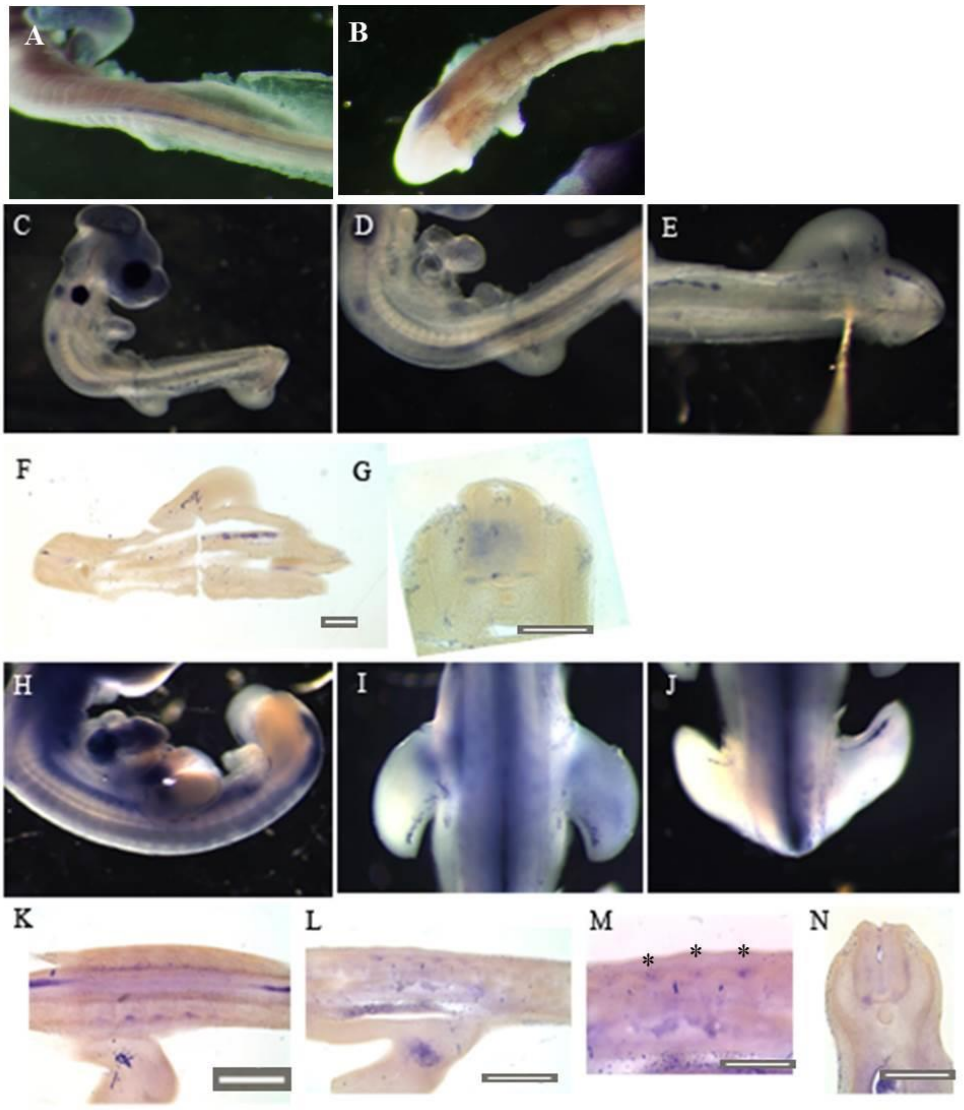

Figure 3.13- Chick embryos and embryo sections after WMISH for *Tgfbr2*. (A,B) Embryo at stage 16 HH. *Tgfbr2* is expressed in the neural tube and heart. (C) Embryo at stage 19 HH. (D) Higher magnification view of embryo in C. *Tgfbr2* is expressed in the neural tube and heart. (E) Higher magnification view of the ventral tail area of embryo in C. *Tgfbr2* is expressed in the mesonephros, limbs and neural tube. (F) Transverse section at stage 19 HH. *Tgfbr2* is expressed in the anterior wing and in the neural tube. (G) Transverse section at stage 19 HH: *Tgfbr2* is expressed in the central neural tube and ectoderm. (H) Embryo at stage 29 HH. (I) Higher magnification view of the thoracic (wing-level) area of embryo in H. *Tgfbr2* is expressed in the limb buds, primitive wing muscle and neural tube. (J) Higher magnification view of the tail and leg region of embryo in H. *Tgfbr2* is expressed in the inner limb and neural tube. (K) Longitudinal section at stage 29 HH. *Tgfbr2* is expressed in the neural tube, myotome and proximal limb. (L) Longitudinal section at stage 29 HH. *Tgfbr2* is expressed in the myotome, primitive wing muscle and mesonephros. (M) Longitudinal trunk section at stage 29 HH. *Tgfbr2* is expressed in the centre of the myotome (asterisks) and in the inter-somitic boundaries. (N) Transverse section at stage 29 HH. *Tgfbr2* is expressed in boundary cap cells and in the lateral neural tube.

Tgfbr2 is expressed in the myotome at stage 29 HH: it appears to be higher in the centre of the myotome at wing level (asterisk, Fig. 3.14M). This expression suggests that *Tgfbr2* may have a function in the resegmentation process. *Tgfbr2* is also expressed in the interior of the wings and in the joints between the wing and trunk (Fig. 3.14K,L), suggesting that *Tgfbr2* may play a role in the formation of the wing, in a similar fashion to formation of joints as previously suggested in mouse (Lorda-Diez *et al*., 2010).

Tgfbr2 gene expression patterns during development reported here suggest a potentially important role in development, and perhaps in migration events that occur during the resegmentation process. As I did not find any evidence of *Tgfbr2* being expressed in the posterior half sclerotome, further assessment of *Tgfbr2* function in chicken was not pursued.

3.14- Fibronectin leucine rich transmembrane protein 2 (Flrt2)

Flrt genes code for glycosylated membrane proteins expressed at the cell surface (Haines *et al*., 2006) with a signal peptide, 10 leucine rich repeats (LRR), type III fibronectin-domain (FNIII), transmembrane domain, and a short intracellular tail (Lacy *et al*., 1999; Karaulanov *et al.*, 2006). In mouse, *Flrt* genes are widely expressed in tissues such as kidney, skeletal muscle, lung, brain (Lacy *et al*., 1999; Haines *et al*., 2006), and cranial neural crest cells (Gong *et al*., 2009). The roles of Flrt protein domains have been studied: the LRR domain plays a role in homotypic cellular recognition (Haines *et al*., 2006) and the FNIII domain is involved in binding to Fgf receptors (Böttcher *et al*., 2004).

Different members of the *Flrt* family have distinct gene expression patterns. *Flrt1* is expressed in brain compartmental boundaries; *Flrt2* is expressed in the part of the sclerotome that will later form tendons, and *Flrt3* was found in the part of the sclerotome that will later form the ventral vertebral body (Haines *et al*., 2006). *Flrt3* was also found at the midbrain/ hindbrain boundary (Haines *et al*., 2006). Cell adhesion assays have been carried out more frequently for *Flrt3* than Flrt2. FNIII domains modulate cell adhesion and cell sorting; they are also calcium dependent and behave differently according cell type (Karaulanov *et al*., 2006). These findings are interesting

and relevant to the present study as during somitogenesis, the cells sort themselves creating a distinct barrier between the anterior and posterior halves of the somite. In addition, *Flrt3* was detected in the anterior half-somite while *Flrt2*, was detected in posterior half of the somite in the mouse microarray screen (Hughes *et al*., 2009). It is intriguing that there are two genes of the same family in two different poles of the somite, and that these proteins are able to interact with each other. Do they have repulsive properties? Or is it the interaction of these two proteins that maintains the cell barrier? Does Flrt2 have any repulsive effect on axon guidance through calcium modulation? Flrt3 has been proven to modulate neurite outgrowth (Karaulanov *et al*., 2009), and also Flrt2 and Flrt3 are repulsive guidance molecules for the netrin receptor Unc5D (Yamagishi *et al.*, 2011). However, the Yamagishi studies focused on the brain, therefore, *Flrt2* was included in the present study to explore a potential role in somite polarity.

Amplification of mRNA for this gene was successful and WMISH data were obtained for HH stages 16, 17, 19, 22 and 29 (Fig. 3.15). *Flrt2* in the chick embryo has a strong expression in the posterior half-somite (Fig. 3.15 all panels). The expression of *Flrt2* begins at around the level of somite 10 (Fig. 3.15A), while somites are still being formed. Around stage 16 HH, *Flrt2* expression is stronger in the ventral region of the somite and in the myotome, and it is also transiently expressed in the neural tube and notochord (Fig. 3.15D-F) since this expression is not visible at the level of later-formed somites. As the somites bud off and the embryo develops, at stage 17 HH *Flrt2* is strongly present in the posterior half of the somites of the 13th somite and forwards (Fig. 3.15C), in a similar fashion to the expression patterns for the PNA binding molecule (C. Casper and R. J. Keynes, personal communication). From stage 19 HH, *Flrt2* is expressed in all the posterior sclerotome and maintained until later stages (Fig. 3.15G,J), when it starts to be expressed in the neural arch and body of the vertebrae (Fig. 3.15K,L). *Flrt2* expression is also found around the neural tube and notochord, which suggests a potential role in the development of the CNS, however there is no further evidence as yet in the literature to substantiate this. As *Flrt2* expression is strong and clearly expressed in the posterior half-sclerotome, where it could be playing a role in repelling axons, the function of this gene was studied further using knock-down experiments (see Chapters 4 and 5).

Figure 3.14- (On next page) Chick embryos and embryo sections after WMISH for *Flrt2*. (A) Embryo at stage 16 HH. *Flrt2* starts to be expressed from the 10th somite forward, with stronger expression surrounding the neural tube. (B) Higher-power view of embryo in A. *Flrt2* is strongly expressed in the ventral posterior sclerotome near the neural tube. (C) Embryo at stage 17 HH. *Flrt2* is segmentally expressed in the sclerotome from the 13th somite and forwards, and is also expressed in the heart. (D) Transverse sections of an embryo at stage 16 HH. *Flrt2* is expressed in the posterior sclerotome (p), and in the myotome (black arrow). (E) Transverse section at tail level of chick embryo at stage 16 HH. *Flrt2* is expressed in the sclerotome, notochord and neural tube. (F) Transverse section at thoracic level of chick embryo at stage 16 HH. *Flrt2* is expressed in the medial ventral sclerotome. (G) Embryo at stage 19 HH. *Flrt2* is segmentally expressed in the sclerotome, in the limbs, heart and mesonephros. (H) Parasagittal section of a chick embryo at stage 19 HH. *Flrt2* is expressed in the posterior sclerotome and in the heart atrium. (I) Transverse section of a chick embryo at stage 22 HH. *Flrt2* is expressed in the medial ventral sclerotome and around the neural tube (black arrow). (J) Coronal section of a chick embryo at stage 22 HH. *Flrt2* is expressed in the posterior sclerotome (p) and in a continuous line around the neural tube. (K) Parasagittal section of chick embryo at stage 29 HH. *Flrt2* is expressed in the body of the vertebrae, in the atrium of the heart and around the notochord (n). nt. neural tube. (L) Parasagittal section of chick embryo at stage 29 HH. *Flrt2* is expressed in the vertebral body, and in the mesonephros. Scale bar: 100 µm

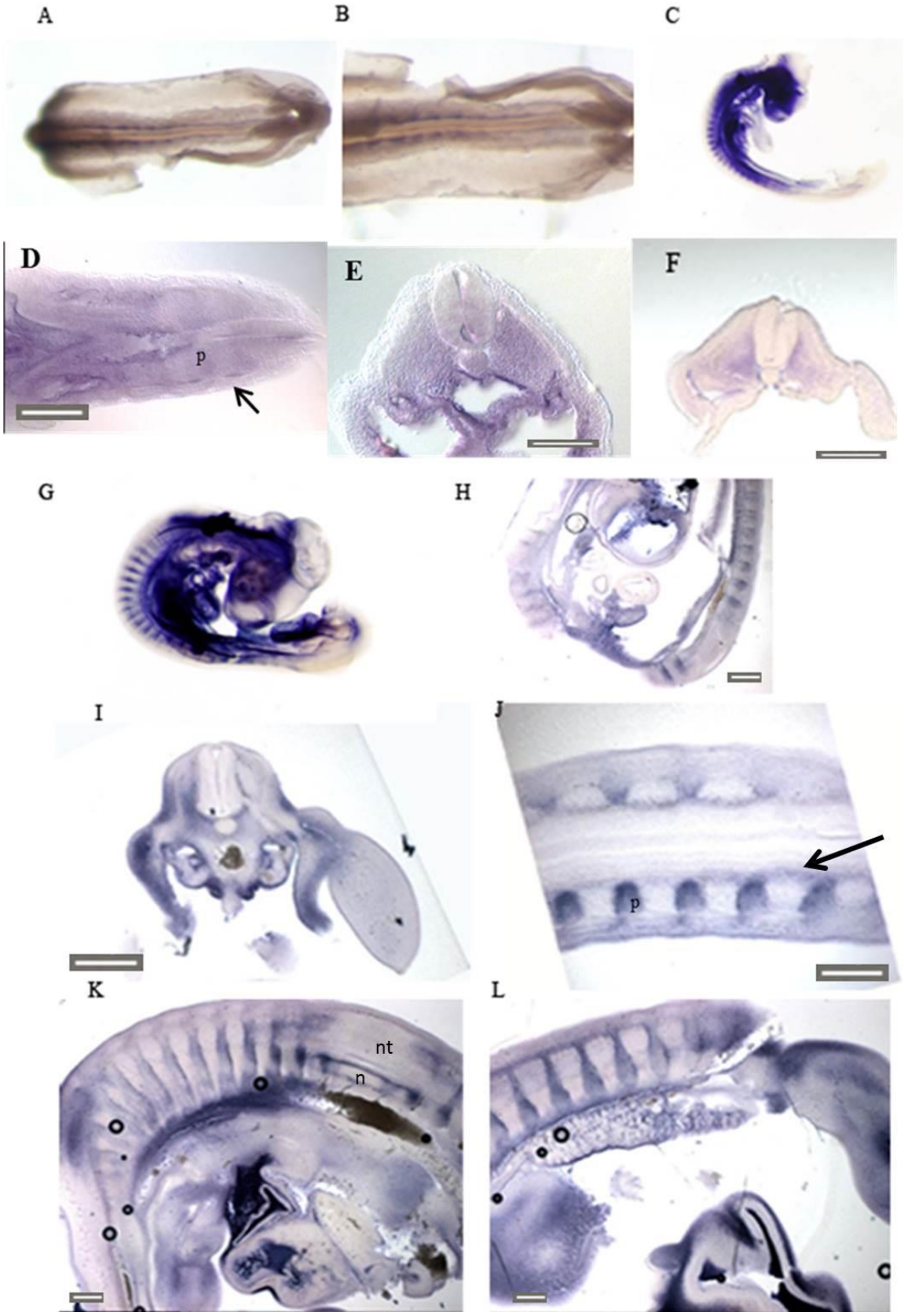

Figure 3.15- Legend on previous page.

CHAPTER 4- DEVELOPMENT OF A NEW *IN OVO* TRANSFECTION TECHNIQUE FOR TARGETING SOMITES

My aim in this part of my PhD was to knock down chicken *Flrt2* in order to test its potential role in axon guidance. *Flrt2*, which encodes a glycosylated transmembrane protein, was identified as expressed in the posterior sclerotome of mouse embryos after a differential microarray screen (Hughes et al., 2009). I confirmed that *Flrt2* is also expressed in the posterior sclerotome of chicken embryos (see section 3.15), which are more accessible for manipulation. In this chapter, I introduce different approaches to knocking down gene function in chicken embryos and report how I developed an *in ovo* transfection technique using a commercial transfection reagent, TurboFect (Thermo Scientific), as a method for introducing interference RNA (RNAi) constructs into the somites for functional knockdown. The results of knocking down *Flrt2* using this technique are described in Chapter 5.

4.1- *In vivo* transfection using electroporation

One approach to knocking down gene function in chicken embryos is to use electroporation to introduce antisense morpholino oligonucleotides or RNAi constructs. Electroporation involves the application of short electric field pulses across cells that permeabilize cell membranes by opening tiny pores in them (Haas *et al.*, 2001). During the electric pulse, charged molecules (such as plasmid DNA, double-stranded RNA or fluorescently-tagged morpholinos) are actively electrophoresed through the pores, while uncharged molecules diffuse through them passively (Haas *et al.*, 2001). The introduction of *in ovo* electroporation was a great achievement, enabling plasmid DNA and morpholinos to be introduced into cells in an accessible and cheap embryonic model system, the chicken embryo. *Flrt2* is expressed within the sclerotome (a mesenchymal derivative of the somite), and electroporation of mesenchymal cells is technically difficult and not very efficient.

Two main techniques have been developed for targeting somites by electroporation in chicken embryos. It is possible to target presumptive somites at primitive streak (gastrulation) stages, by performing the electroporation *ex ovo* in a chamber, targeting the region of epiblast that will form the somites, and using New culture to maintain the embryos until somites have formed (Voiculescu *et al.*, 2008)

(Figure 4.1). However, it is difficult to culture embryos beyond stage 12 HH in New culture (Dr. Octavian Voiculescu, personal communication).

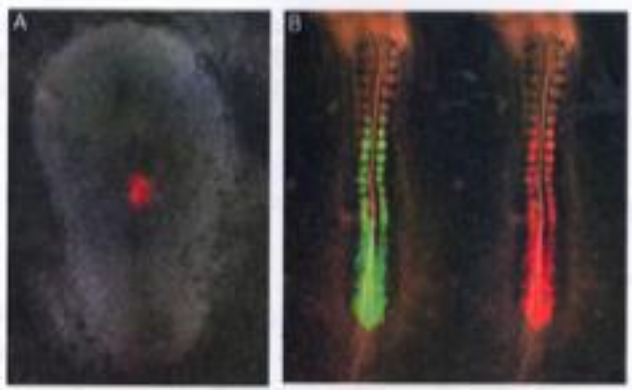

Figure 4.1- *Ex ovo* electroporation of prospective somites in a chick embryo at stage 5 HH. (A) Electroporation of epiblast in the anterior primitive streak of a stage 5 HH chicken embryo, from which segmental plate mesoderm and somites will form on both sides of the embryo. (B) Examples of labelled segmental plate mesoderm and somites 24 hours after culturing embryos targeted at stage 5 HH. Figure from Iimura and Pourquié (2008).

Professor Christophe Marcelle's lab (Australian Regeneration Medicine Institute, Monash University, Australia) has optimised the targeting of specific somite regions by *in ovo* electroporation, using a technique described by Scaal *et al.* (2004). In summary, this approach uses electrodes carefully positioned in the chick embryo to target specific regions of recently formed epithelial-stage somites, since epithelia are more efficiently electroporated than mesenchyme (Fig. 4.2). A capillary needle containing plasmid DNA is inserted at the level of the pre-somitic mesoderm and pushed anteriorly, parallel to the neural tube, up to the level of the somite IV (the fourth most recently-formed somite). The plasmid DNA is injected into the central cavity (somitocoele) of the epithelial somite, then the capillary is moved backwards to somite III where DNA is again injected, and so on until all four recently-formed somites have been filled. Electrodes are placed on either side of the embryo in order to target the medial or lateral somite (Fig. 4.2a,b), or the anterior or posterior somite (Fig. 4.2c), or above and below the embryo in order to target the dorsal or ventral somite (not shown). The negatively charged DNA moves towards the positive electrode, so the positioning of the electrodes allows specific regions to be targeted.

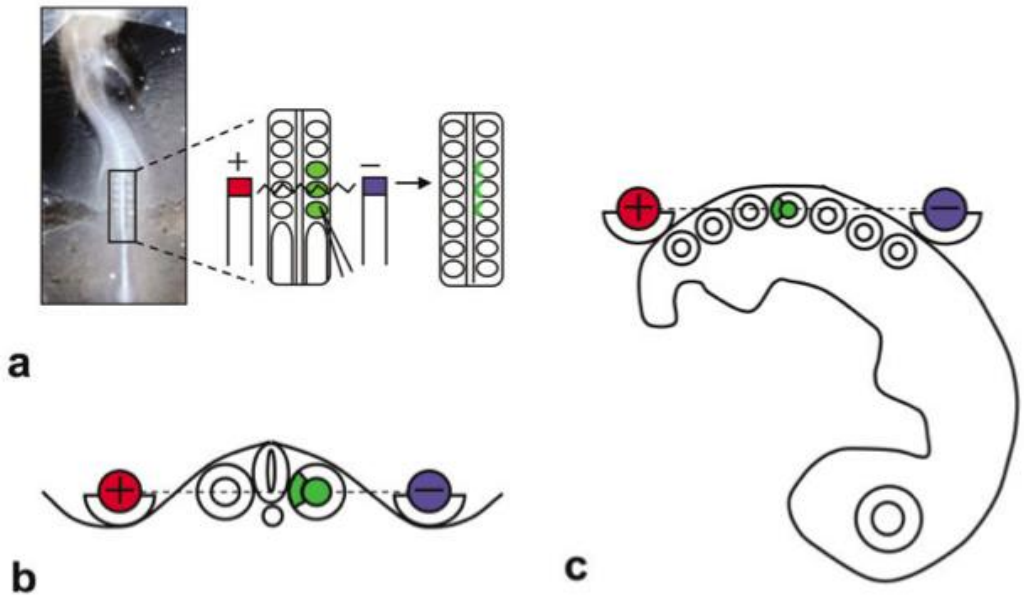

Figure 4.2- In ovo electroporation of somites using the technique of Scaal *et al.* (2004). (a) *In ovo* somite electroporation of an E2 chick embryo via injection of plasmid DNA into the centre of the epithelial somite using a finely drawn capillary tube (dorsal view). The electrodes are positioned on each side of the embryo so that the DNA (negatively charged) will enter the medial somitic cells, moving in the direction of the anode (positive electrode). (b) A transverse view of the DNA migration towards the positive electrode into medial somite cells. (c) A lateral view of an embryo in which the somite is being electroporated craniocaudally, targeting the posterior part of the somite. Figure from Scaal *et al.* (2004).

This technique was passed to Professor Philippa Francis-West's lab (Department of Craniofacial Development and Stem Cell Biology, King's College London), where Dr. Mulvaney taught me the technique. Dr. Mulvaney used an Intracel Ovodyne electroporator with a foot pedal and two separated electrodes, with a platinum wire for the positive electrode and a tungsten wire for the negative electrode, and Ringer's solution with penicillin-streptomycin. The electroporation was done by using five square-wave 70V pulses, 20 milliseconds apart. Although this was the best technique available at the time, it only has a 30% success rate, and therefore a more efficient technique was needed.

4.2- Post-transcriptional knock-down approaches

Knock-down assays allow the function of a particular gene in a system to be studied; they are more common in *in vitro* cell cultures, but *in vivo* knock-down assays enable functional studies of a particular gene in its natural cellular system. Different approaches can be adopted in order to knock-down the post-transcriptional expression of a gene. One approach is to use morpholino antisense oligonucleotides to block the translation or splicing of mRNA for the gene of interest. Morpholinos have the advantage that gene function can be restored once the morpholinos have been diluted out (Sauka-Spengler and Barembaum, 2008). They are also less toxic and more resistant, however they require a specific 30 bp stretch of nucleotides spanning the start codon which can cause off-target effects (Bill *et al.,* 2009). They can also be designed to be splice-blocking, however. If the same phenotype is obtained using either a translation-blocking morpholino or a splice-blocking morpholino against the same mRNA, this can be used as evidence of specificity.

Another approach is RNA interference (RNAi) technology, a naturally occurring process in which the presence of short double-stranded RNA results in sequence-specific post-transcriptional silencing, usually by mRNA degradation. Delivery of short interfering RNA (siRNA) in duplex form, or plasmids encoding small hairpin RNAs (shRNA) that can be cleaved inside the cell to form siRNA, results in the destruction of the mRNA of interest. There are several types of RNAi: short interfering RNA (siRNA), short hairpin RNA (shRNA), long double-stranded RNA (dsRNA) or micro-RNA (miRNA) and endoribonuclease-prepared siRNA (esiRNAs) or diced riRNAs (d-siRNAs) (Buchholz *et al.* 2006; Wang *et al.,* 2010). A short hairpin RNA (shRNA) is a DNA-based siRNA production strategy in which siRNAs are produced intracellularly from shRNA transcripts (Fig 4.3 and Fig 4.4). The plasmid or viral vector that encodes the shRNA utilizes the H1 or U6 promoter to facilitate shRNA transcription via RNA polymerase III (Fig. 4.3).

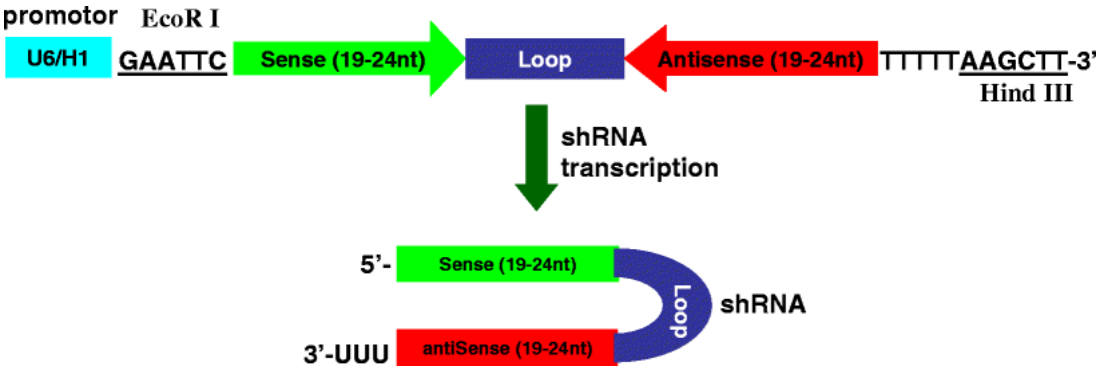

Figure 4.3- Design of DNA oligonucleotides for cloning shRNA in a vector. Once transcribed by RNA polymerase III from the U6 or H1 promoter, the result is a short hairpin of double-stranded RNA that is cleaved by the endoribonuclease Dicer into siRNA. Figure from Chen *et al.* (2008).

Gene silencing occurs post-transcriptionally in the cytoplasm and it is an ATP-dependent and translation-independent mechanism (Fig. 4.4) (Chen *et al.*, 2008). In the cytoplasm, long dsRNAs or shRNAs are cleaved by the endoribonuclease Dicer into short dsRNA duplexes or siRNA. There is an enzymatic way of doing this *in vitro* through digestion of long dsRNA with endoribonucleases by using bacterial RNAse III to convert the long dsRNA into 18-25 base-pair (bp) siRNAs, creating a heterogeneous population of siRNAs to one target mRNA (Buchholz *et al.*, 2006). The siRNAs are 9-24 bp dsRNA molecules that have a two-nucleotide 3'-overhang that allows them to be recognized by the enzymatic RNAi machinery. siRNA are loaded into the RNA-induced silencing complex (RISC) that contains Argonaute 2 (Ago-2). Ago-2 cleaves and releases one of the dsRNA strands, resulting in an activated form of RISC with a single-stranded RNA (guide siRNA) that will recognise the mRNA target through complementary base pairing. Ago-2 then cleaves the target mRNA relative to the 5' end of the siRNA antisense strand causing mRNA degradation and gene silencing (Moses *et al.*, 2010; Chen *et al.*, 2008) (Fig. 4.4).

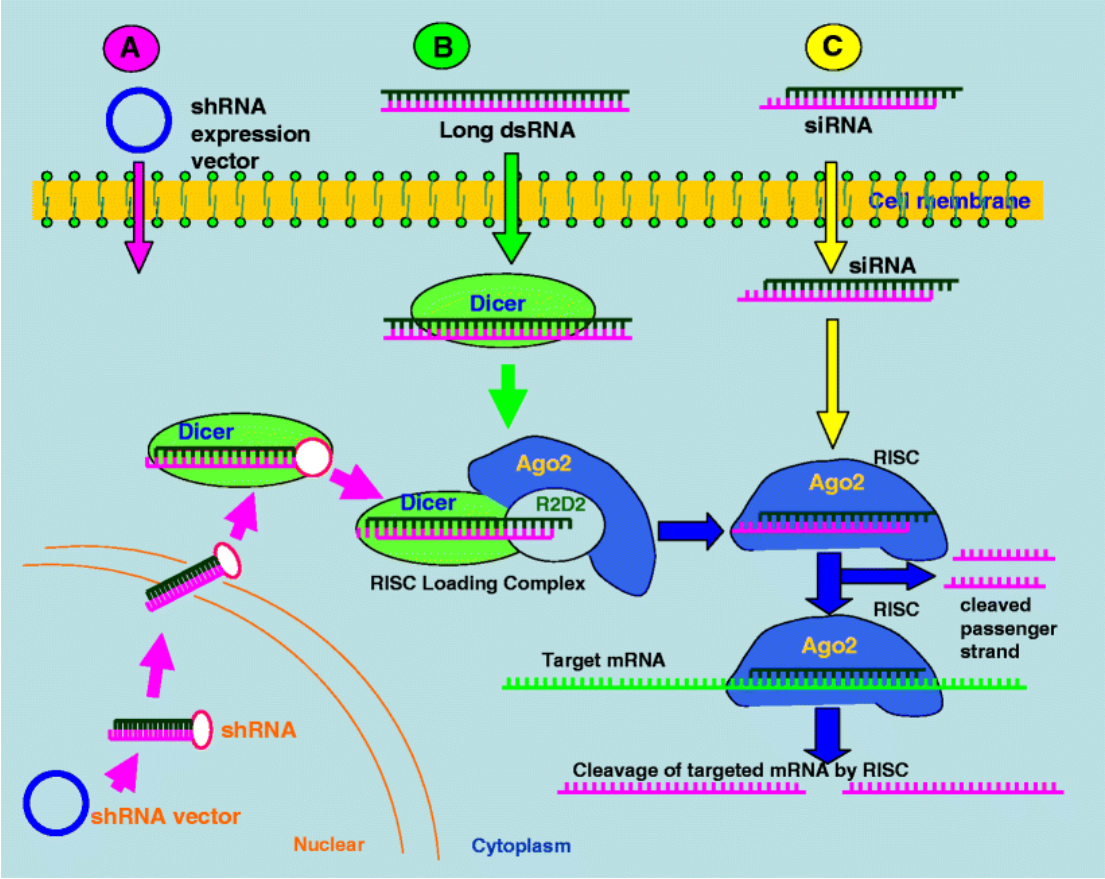

Figure 4.4- Mechanism of RNA interference (RNAi) by introducing a vector encoding shRNA (pink arrow), or by introducing long dsRNA (green arrow) or siRNA (yellow arrow). Figure from Chen *et al.* (2008).

Both of the above methods require a transfection technique such as electroporation to introduce morpholinos, shRNA-encoding plasmids, long dsRNA or siRNA into embryonic cells. The introduction of expression vectors via electroporation can often cause morphological disturbances, mis-regulation of non-targeted genes and in young embryos, cell death (Mende *et al*., 2008). For example, even when targeting a protein without endogenous cell function like GFP, the shRNA vector pRFPRNAi (Das et al., 2006), caused morphological phenotypes, mis-regulation of non-targeted genes and activation of the p53 pathway, especially when primitive streak or early-somite stage embryos were targeted (Mende *et al*., 2008). In contrast, this effect was not seen when morpholinos were introduced, suggesting that at least for young (early-somite stage and younger) embryos, the electroporation of shRNA vectors may cause non-specific phenotypes (Mende *et al*., 2008).

The genome-wide effect of electroporating the midbrain of stage 10 HH embryos with a *GFP*-containing plasmid was studied by Farley *et al.* (2011) using microarrays. Passing electric current alone, without introducing any DNA, reproducibly affected expression of less than 0.1% of genes on the array. Electric current plus GFP reproducibly affected expression of less than 0.5% of genes on the array, but did not modify any genes involved in regional identity. When the midbrain was electroporated with a plasmid encoding a known transcription factor, Dmrt5, there was a change in the expression of 309 genes in comparison to the 111 whose expression changed when *GFP* and current were applied. Overall, the authors concluded that the electroporation technique for embryos at least as old as stage 10 HH is valid for the study of gene function (Farley *et al.*, 2011), but keeping in mind that current alone affected the expression of genes that respond to oxidative stress and pH/redox changes, and genes that regulate apoptosis (Farley *et al.*, 2011). Furthermore, the three genes whose expression was affected in all experimental conditions (i.e., current alone, and current plus any plasmid) encoded a protein involved inRNA processing, metabolism and transport (Hnrnpk), a chromatin-remodelling enzyme that regulates transcription (Chd1) and a redox sensor (Txnl1) (Farley *et al.*, 2011).

Introducing siRNA duplexes has been shown to silence target genes efficiently in chick embryos, at least after early somite-stages (Rao *et al*., 2004). Rao *et al*. (2004) compared the use of long (700 bp) double-stranded RNA (dsRNA), endonuclease-digested duplexes (esiRNA) and short 21 bp RNA duplexes (siRNA). Electroporation of the same amount of construct, 200ng/µl, into the neural tube of chick embryos at stages 11-13 HH resulted in 53% knock-down efficiency for long dsRNA, 29% efficiency for esiRNA and 90% efficiency for siRNA. The siRNA also proved not to cause deregulation of house-keeping genes and did not increase cell death (Rao *et al*., 2004). In my study, I used siRNA with the same characteristics as described by Rao *et al*. (2004) to knock down *Flrt2* (Chapter 5) and a putative PNA-binding protein, P4Hb (Chapter 7), by *in ovo* transfection using a commercial transfection reagent, TurboFect *in vivo* (Thermo Scientific). This is an alternative technique to electroporation that I developed during this project.

4.2.1- siRNA design rules

Software such as RNAi Explorer (Gene Link) and Sfold (Wadsworth) was used to predict the location of binding of a siRNA to a specific sequence. However, several sequences are given and even though they recommend up to four siRNA per sequence, the same results can be obtained by using only one siRNA (Rao *et al*., 2004; Bron *et al*., 2004; Aigner, 2006). In order to select the optimal target sequence it is necessary to follow some basic rules to optimise gene knock-down. The siRNA needs to be 21 bp long and have a dinucleotide - usually two thymidines, though UU is also used - overhanging the 3' terminus. The siRNA needs to have a low CG content, and cannot have more than three nucleotides repeated in a row. It is necessary to avoid structured (e.g. helical) regions within the gene target, and to know where important protein family domains are encoded and if there are any possible variations to the Kozak consensus sequence for translation initiation (Kozak, 1984) that will still enable translation after siRNA targeting if the mRNA is not fully degraded. When a good target sequence has been selected, the Basic Local Alignment Search Tool (BLAST) from NCBI is used to compare the target sequence to the organism's genome to ensure that it is gene-specific and to avoid mis-targeting. The specific siRNA design strategy for each gene used is given in the relevant results chapter (Chapter 5 for *Flrt2*; Chapter 7 for *P4Hb*).

4.3- Developing an *in ovo* transfection technique for somites

4.3.1- TurboFect *in vivo* Transfection Reagent

TurboFect *in vivo* Transfection Reagent (from Fermentas, now Thermo Scientific; Catalog # R0541) is a commercially available non-lipid reagent based on a cationic polymer, polyalkyleneimine (U.S. patent application US20100041739A1), instead of the more traditionally used polyethylenimine (PEI). Polyalkyleneimine is a stable, low toxicity compound (currently being used in clinical trials for drug treatment; European patent application EP2359835A1). TurboFect forms a positively charged complex with DNA, facilitating delivery into cells by endocytosis (Fig. 4.5). Once the complex is inside the cell, an osmotic swelling causes endosomal rupture, releasing the DNA to the cytoplasm, from where it is translocated to the nucleus (Fig. 4.5).

TurboFect had already been tested in mice by intravenous injection (Fig. 4.6), however it had not been tested in chicken embryos. The previous mouse *in vivo* and *in vitro* tests had shown that the reagent does not cause any inflammatory response, at least during the first 24 hours post-transfection (Fig. 4.6) and that it transfects cells without any increased toxicity (Thermo Scientific). Therefore, I modified the technique until optimal delivery was achieved in chick embryos *in ovo*.

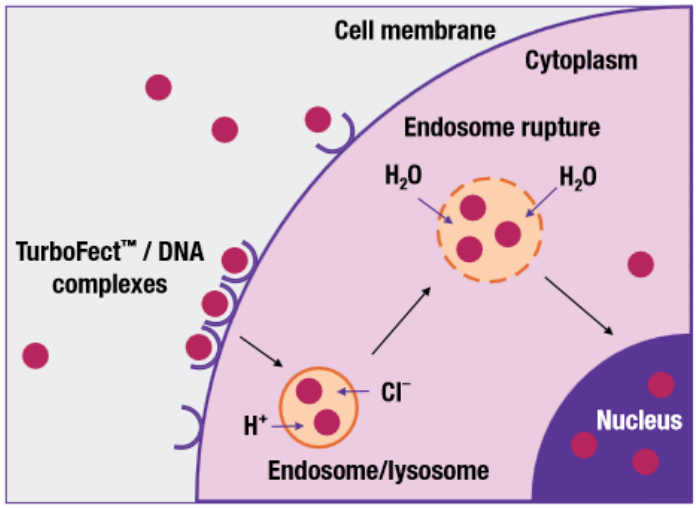

Figure 4.5- TurboFect mechanism of action. TurboFect forms small, diffusible complexes with DNA that are readily endocytosed. Once in the cytosol, rapid osmotic swelling causes endosomal rupture allowing translocation to the nucleus. Figure from TurboFect transfection reagent manual, Fermentas (now Thermo Scientific).

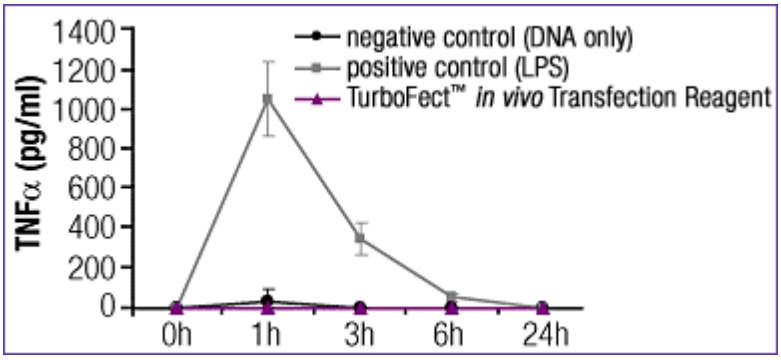

Figure 4.6- No inflammatory response for 24 hours after DNA delivery using TurboFect *in vivo* Transfection Reagent. 50 µg of plasmid DNA was administered to female BALB/c mice via intravenous injection using TurboFect *in vivo* Transfection Reagent. The inflammatory response was measured by using ELISA to determine the concentration of the proinflammatory cytokine TNFα in blood serum samples at defined time-points. (LPS- lipopolysaccharides). Figure from Thermo Scientific website (http://www.thermoscientificbio.com/transfection/turbofect-in-vivo-transfection-reagent/).

4.3.2- *In ovo* transfection of somites

Targeting the somites with a TurboFect/FITC-siRNA complex was similar to a previous method used to target somites for electroporation (Scaal *et al.*, 2004), with some modifications. The pulled glass capillary needle containing the solution was inserted at the PSM level into the most posterior (newly formed) epithelial somite of embryos at stages 9-12 HH and carefully pushed to the most anterior somite or until resistance was found from the somite using small wave movements (Fig. 4.7). When guiding the needle through the oldest somites (which will already have differentiated into dermomyotome and sclerotome), the aim was to inject ventrally and as near to the neural tube as possible. Once the most anterior somite was reached, the needle was pulled back somite by somite and the solution applied for 5-10 seconds per somite. It was possible to observe the somites filling up with solution and the tissue turned slightly white and sticky. It is important to note that using this technique, more tissues are transfected besides the somites. The approach through the PSM results in the transfection of PSM cells, leaking back sometimes to the tailbud (which generates the PSM on both sides of the embryo) so the use of the non-transfected side as a control is not suitable. Likewise, there might be some leakage of the transfection complex out of the somites towards the overlying ectoderm and adjacent neural tube.

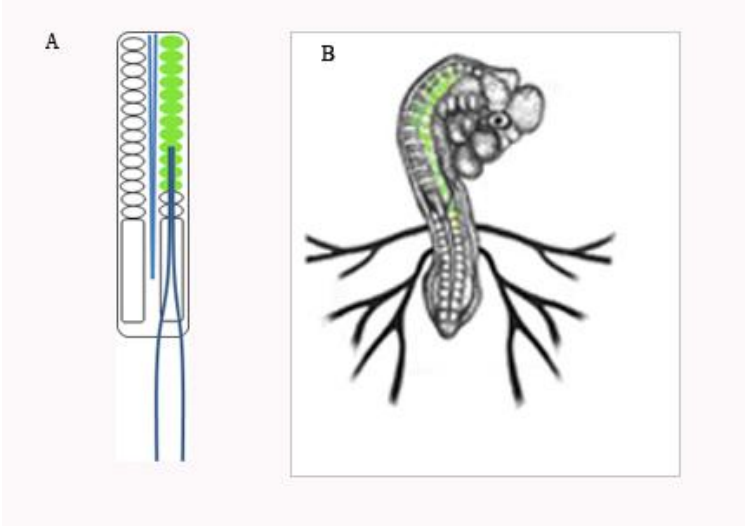

Figure 4.7- Schematic representation of sclerotome transfection *in ovo*. (A) Dorsal view of the manipulated region in a day 2 chick embryo (anterior to the top), illustrating the injection of several somites (in green) using a pulled glass capillary. The right side is the manipulated side. Schematic made by the author. (B) Representation of a transfected chick embryo HH 19 *in ovo* when observed under a fluorescent dissection scope. Schematic adapted from an image whose original source is unknown.

4.3.3- Optimizing TurboFect for *in ovo* transfection of somites with siRNA

I tested the manufacturer's protocol for use in siRNA transfection of 8 chick embryos at stage 12 HH, but did not obtain more than a few transfected cells. However, I found that increasing TurboFect to a final concentration of 20% was the best for use with siRNA in chick embryos: I then used this on 214 chick embryos: 198 were transfected with FITC-labelled scrambled siRNA, while 16 controls were subjected to the whole transfection procedure but without including siRNA in the solution. I increased the concentration of TurboFect further to 30% in 18 chick embryos at stage HH 12, but this did not result in a higher number of transfected cells within somites, and increasing the TurboFect concentration made the delivery harder by increasing precipitation within the solution.

Using TurboFect to transfect tissues, rather than electroporation (which drives charged molecules across the membrane by electrophoresis; Haas et al., 2001), means that the time that the solution remains in the tissue is vital for a good transfection. I found that the TurboFect/siRNA complex alone was lost too fast from the somite, not giving time for the siRNA/TurboFect complex to be taken inside the cells. The addition of 1% glycerol to the TurboFect and siRNA mixture improved the solution retention, however in all 31 embryos injected with this solution at stage HH 12, the somite tissue was still white even 2 days post-injection. The substitution of 10% glucose for glycerol resulted in no more than a few transfected cells in the 33 embryos injected with this solution at stage HH 12.

A commonly used cationic agent for transfection is polyethleneimine (PEI), however this has a dose-dependent toxicity (Conese *et al.*, 2009). Polyethylene glycol (PEG) has often been used with such cationic delivery agents to reduce toxicity and degradation by non-specific proteins (Kunath *et al.*, 2003; Moore *et al.*, 2009; Moore and Sakiyama-Elbert, 2012) and is known to increase the half-life of an oligonucleotide from 1.07 to 57.8 hours (Yu *et al.*, 1999). PEG has low toxicity, and is being used for drug delivery in clinical trials (Bolwell *et al.*, 2000). PEG-based vehicles were also shown to be internalized into cells non-specifically by interaction with heparan sulphate proteoglycans, either alone or in combination with integrins (Moore *et al.*, 2012). I found that adding PEG (Carbowax^{TM} 6000, Union Carbide) to a final concentration of

10% made the siRNA/TurboFect complex heavier, enabling the solution to stay inside the somites and ensure that the siRNA/TurboFect complex had time to be assimilated by the cells. (Increasing the concentration of PEG concentration to 20% in 8 chick embryos reduced the number of cells transfected to the point of almost no detection.)

I used 10% PEG for *in ovo* transfection of somites in 198 chick embryos injected at different developmental stages. The injection technique in the somite is comparable to the one used in electroporation of avian somites (Scaal *et al.*, 2004; Bron *et al.*, 2004); however, embryonic malformation and lethality were drastically reduced because electric current was not used. From 198 injected embryos only 23 died, and all the others had at least 3 transfected somites, giving a transfection success rate of 88.4%. 182 chick embryos that were transfected at stages ranging from stage HH 8 to 19 were incubated until stage HH 22-24. 16 embryos were grown until 5 days after transfection, 6 of which died on day 4. There were no visible differences between the transfected embryos and the non-transfected embryos.

Once the FITC-siRNA mixture had been injected it was possible to visualize *in ovo* the transfected area and follow it up to 72 hours after transfection. Although the signal became faint as the tissue became thicker, there was a strong signal up to 48 hours post-transfection (Fig. 4.8). Anti-FITC immunostaining on wax sections of somite-strips from embryos transfected with FITC-labelled siRNA confirmed that the combination of PEG and TurboFect delivered siRNA into the cells (Fig. 4.9).

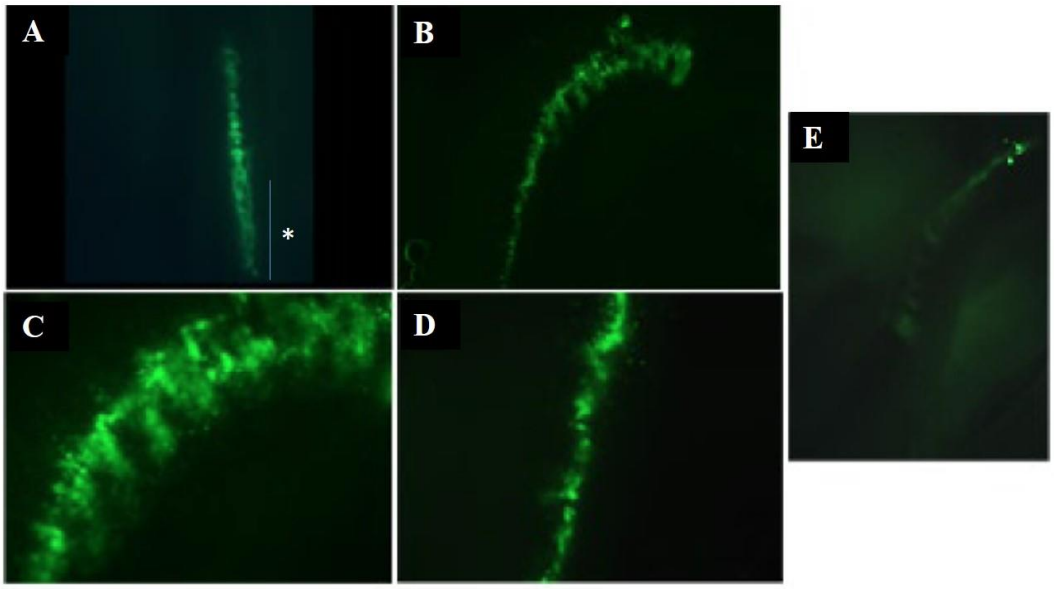

Figure 4.8- *In ovo* views of the same embryo at different time-points after transfection with FITC-labelled scrambled siRNA at HH stage 12. Anterior is up in all panels. (A) 1 hour post-transfection, it is possible to see that the PSM (asterisk) has been transfected. (B-D) Embryo at 16 hours post-transfection. (C) Higher-power view of the vagal area of the embryo in B. (D) Higher-power view of the tail of the embryo in B. (E) 72 hours post-transfection, the siRNA-FITC probe signal is weaker but still detectable.

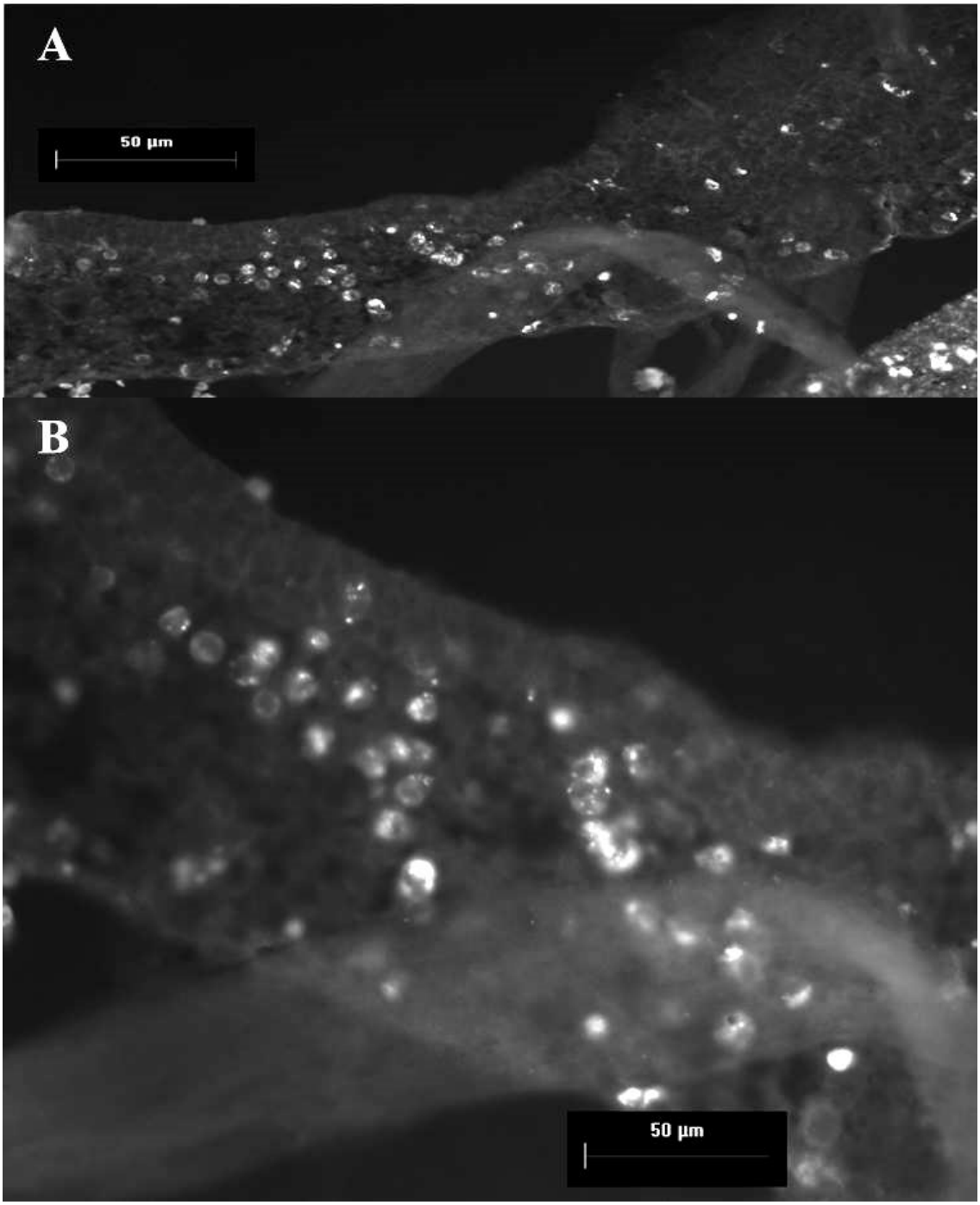

Figure 4.9- Using TurboFect and PEG delivers FITC-siRNA into cells. Somites were transfected with scrambled FITC-siRNA and the embryo fixed 48 hours post-transfection, embedded in paraffin wax and sectioned at 6µm. Alexa488-conjugated anti-FITC immunostaining labelled the transfected cells, revealing siRNA distribution within multiple cells. Panel B shows a higher magnification view of A.

4.3.4- Transfection of up to 22 somites in a single embryo

I found that there was a relationship between embryonic stage and the number of somites transfected. It was possible to transfect as many somites as the embryo had developed up to a maximum of 22 somites, even if the embryo had developed more somites than that (Table 4.1). Embryos injected between stage HH 8$^-$ to 9 (3-7 somites) had 3-5 transfected somites 48 hours post-injection. These embryos took 12 hours to recover, i.e., to start developing at the same rate as a non-transfected embryo, and had a higher probability of dying (Table 4.1). Embryos injected between stages HH 10 to 14 (10-22 somites) had 7-20 transfected somites with a visible *in ovo* signal 72 hours post-transfection. In this case, embryos only took 4-6 hours to recover and once they reached stage HH 18 they showed no differences with non-transfected embryos. At stage HH 19, it was only possible to transfect up to 22 somites, even though the embryo had 37-40 somites. The thickness of the tissue offers a higher resistance as the blood pressure tends to expel the solution faster, not allowing enough time for the solution to penetrate more cells, as a consequence, the intensity of the signal is weaker (visual observation). From stage HH 19 onward, a localized injection into the sclerotome was better (Fig 4.10): more care was necessary to avoid penetrating the endoderm, but the solution was retained inside the somite. It was also possible to transfect both somite strips of the chick embryo through the PSM, however there was a higher possibility of targeting more just somites (Fig. 4.11).

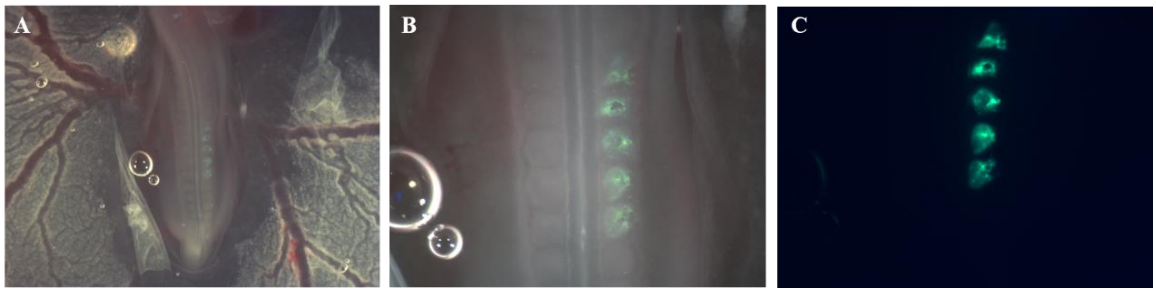

Figure 4.10- Localised transfection of chick embryo at stage HH 19. (A) Chick embryo *in ovo*, one hour post-transfection with FITC-siRNA. (B) Higher power view of transfected region of embryo in A showing overlay of GFP channel and bright field. (C) Green channel only, showing transfected somites one hour post-transfection.

Table 4.1- Breakdown of the embryonic stage at injection, number of somites at injection, number of transfected somites and survival rate of 198 embryos transfected with FITC-labelled scrambled siRNA. The number of somites transfected per HH stage correlated with the number of somites already formed at the time of injection.

*Note: 16 control embryos injected with transfection solution alone (without siRNA) were not included in this table.

Stage (HH)	Nº Somites	Nº Injected somites	Nº embryos	Nº Dead by stage HH 22	% survival
8- to 9	3-7	3-5	10	3	70.0
10	10	7	10	1	90.0
11	13	11	24	1	95.8
12	16	14	19	1	94.7
13	19	16	59*	1	98.3
14	22	20	51	0	100.0
16	26-28	22	15	0	100.0
19	37-40	5	10	0	100.0

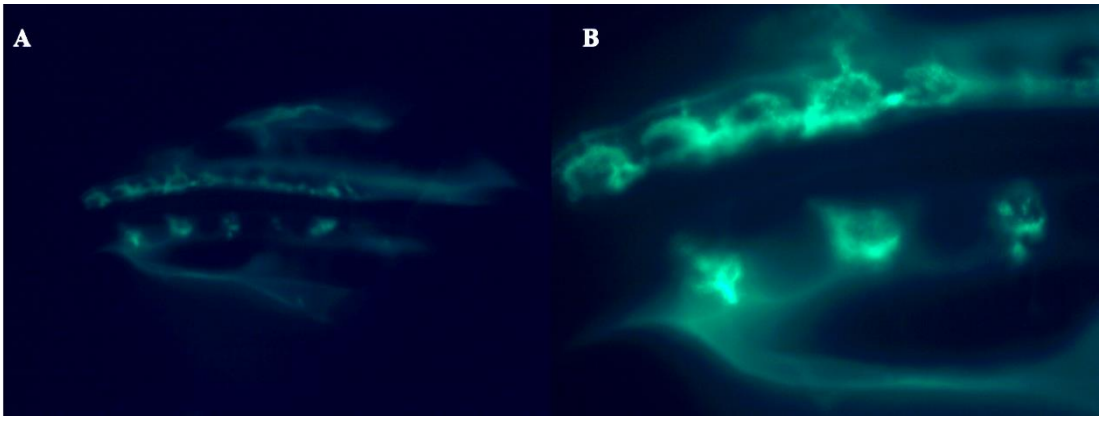

Figure 4.11- Transfection of somites on both sides of the neural tube, presumably via transfection of cells in the tailbud, which generates the PSM on both sides. (A) Low-power view of chick embryo *in ovo* at stage 16 HH with somites transfected on both sides with scrambled FITC-siRNA. (B) Higher power view of embryo in A. Somites from both sides are transfected. On one side all the somites were transfected in a row, while on the other only a few somites were transfected. Signal is also detected in the limb bud.

4.3.5- Optimizing TurboFect for *in* ovo transfection of somites with DNA

Using the same siRNA ratio to form a delivery complex with an enhanced green fluorescent protein (EGFP) expression vector (pCAβ-EGFPm5; Bron *et al*., 2007), I was able to transfect somites *in ovo* in 25 chick embryos between stages 10 and 12 HH (Fig. 4.12). The delivery of plasmid DNA into the somite required more TurboFect than for siRNA delivery, however, probably due to the plasmid size (2.5 kb) and its cell membrane internalization. By keeping the PEG concentration the same (10%) and increasing the TurboFect concentration to 40%, it was possible to transfect somites (Fig. 4.12). It was necessary to wait 6-8 hours for sufficient GFP to build up before the targeted area could be visualized. GFP-targeted cells could be followed using a UV light under a dissecting microscope for up to 72 hours after transfection.

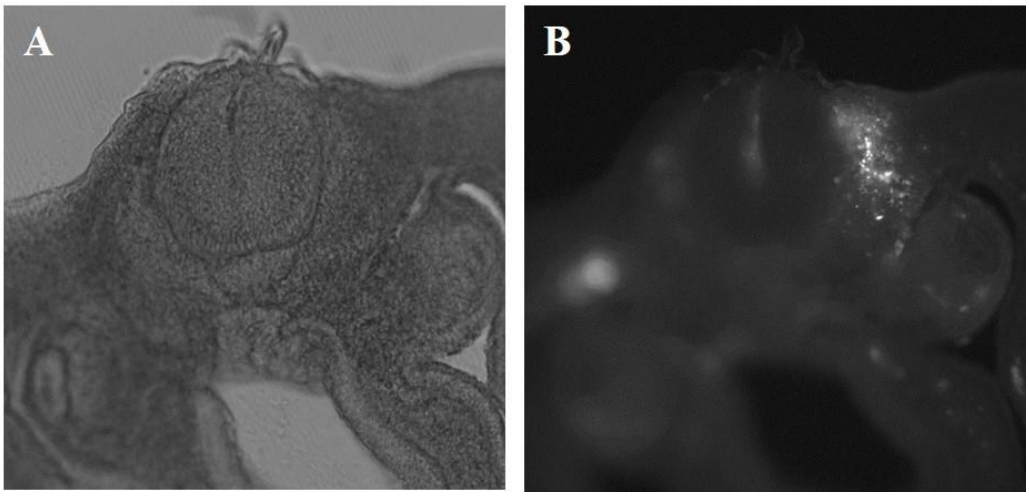

Figure 4.12- *In ovo* transfection of somites with an EGFP expression vector using TurboFect. (A) Transverse section of an embryo collected 16 hours post-transfection. (B) Same section as in A, showing GFP expression in the somite on the targeted side.

4.3.6- Transfected embryos developed normally

The transfected embryos developed normally; however some morphological changes could have been induced, so I treated 40 FITC-siRNA-transfected embryos and 6 plasmid (*GFP*)-transfected embryos with rhodamine-conjugated PNA and immuno-stained them for neurofilament (NF-M) (Fig. 4.13). No abnormalities were found on sections of the transfected embryos (Fig. 4.13A-I). Anti-caspase3 immunostaining on 5 transfected embryos did not reveal any increase in cell death (Fig. 4.13I); I assumed necrosis was not occurring since the embryo was able to develop normally.

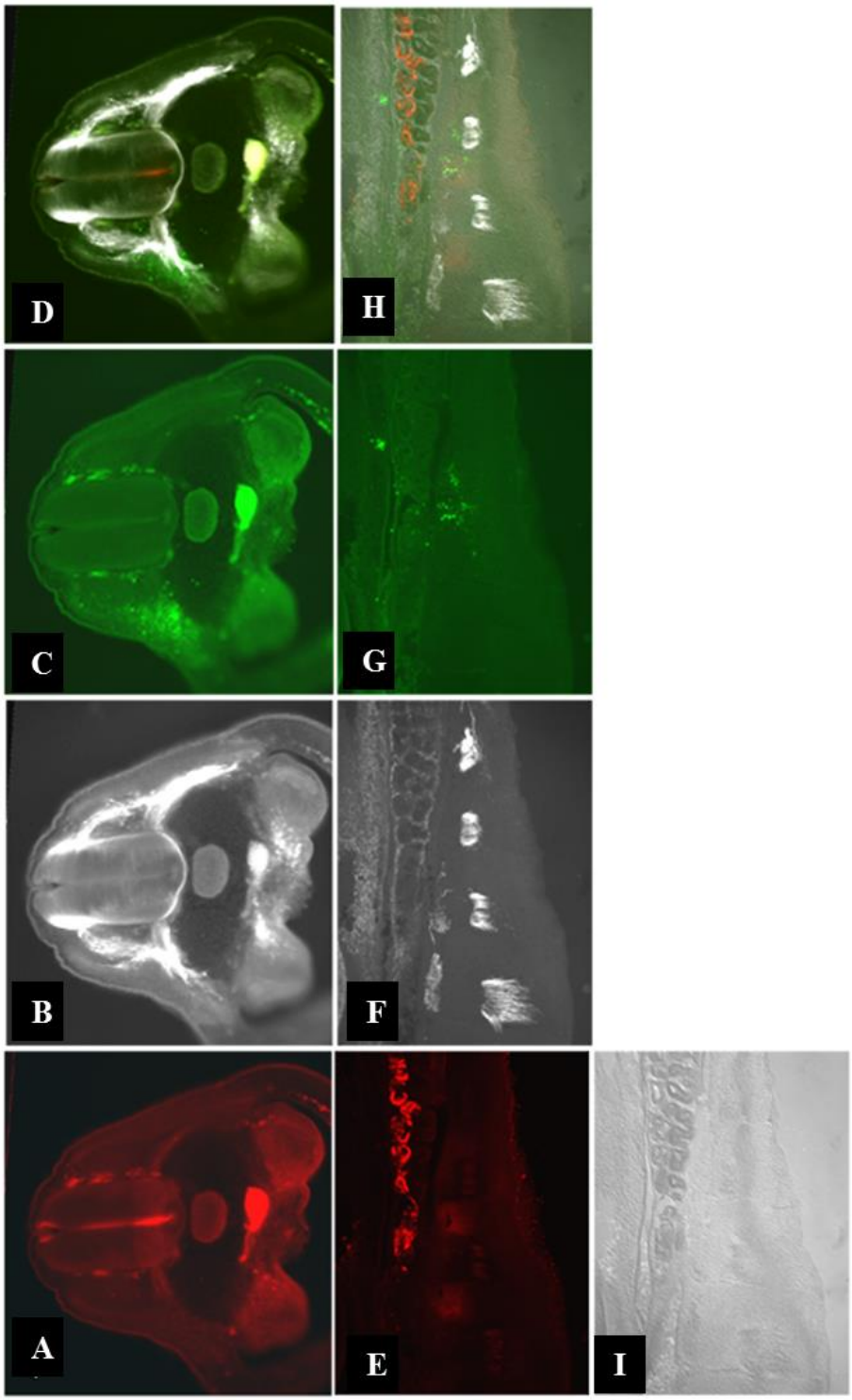

Figure 4.13- Embryos transfected with FITC-labelled scrambled siRNA develop normally. (A-D) Transverse section of a HH stage 22 chick embryo. (E-H) Longitudinal section of a HH stage 22 chick embryo. (A,E) Rhodamine-PNA labelling. (B,F) Anti-neurofilament (NF-M) immunostaining. (C,G) FITC-siRNA transfection. (D,H) Composite of the rhodamine-PNA, anti-neurofilament and siRNA transfection in the same section. (I) Caspase3 immunostaining in the same section as E-H.

4.3.7- Using TurboFect allowed the voltage to be reduced when electroporating the neural tube with DNA

For successful *in ovo* neural tube transfection with plasmid DNA at stages 9-16 HH (Fig. 4.14), it was necessary to combine TurboFect with electroporation, which opens pores in the cell membrane and electrophoreses DNA through the pores (Haas *et al.*, 2001). But still, by combining electroporation with TurboFect (using the same siRNA ratio to form the plasmid delivery complex) it was only necessary to use 5V pulses, significantly lower than the 10-30V range usually used for neural tube electroporation (e.g. Rao *et al.*, 2004; Itasaki *et al.*, 1999).

4.4- Conclusion

In ovo electroporation is a well-established method to introduce genetic material into embryonic chicken cells and tissue, and despite various limitations regarding tissue targeting and reproducibility there have been no better alternatives. I have developed a new *in ovo* transfection method that can be used to efficiently introduce siRNA or plasmids into the somites (and that can be used to transfect the neural tube in combination with electroporation pulses at reduced voltage). Employing a combination of polyethylene glycol (PEG) and a commercially available transfection reagent (TurboFect *in vivo* Transfection Reagent, Thermo Scientific), I was able to transfect somites with a success rate of 88%. Cells could be followed *in ovo* up to 72h post-transfection, and embryos survived for up to five days without any apparent morphological malformation. Further, neurofilament labelling and cell death analysis revealed no difference between transfected and control embryos.

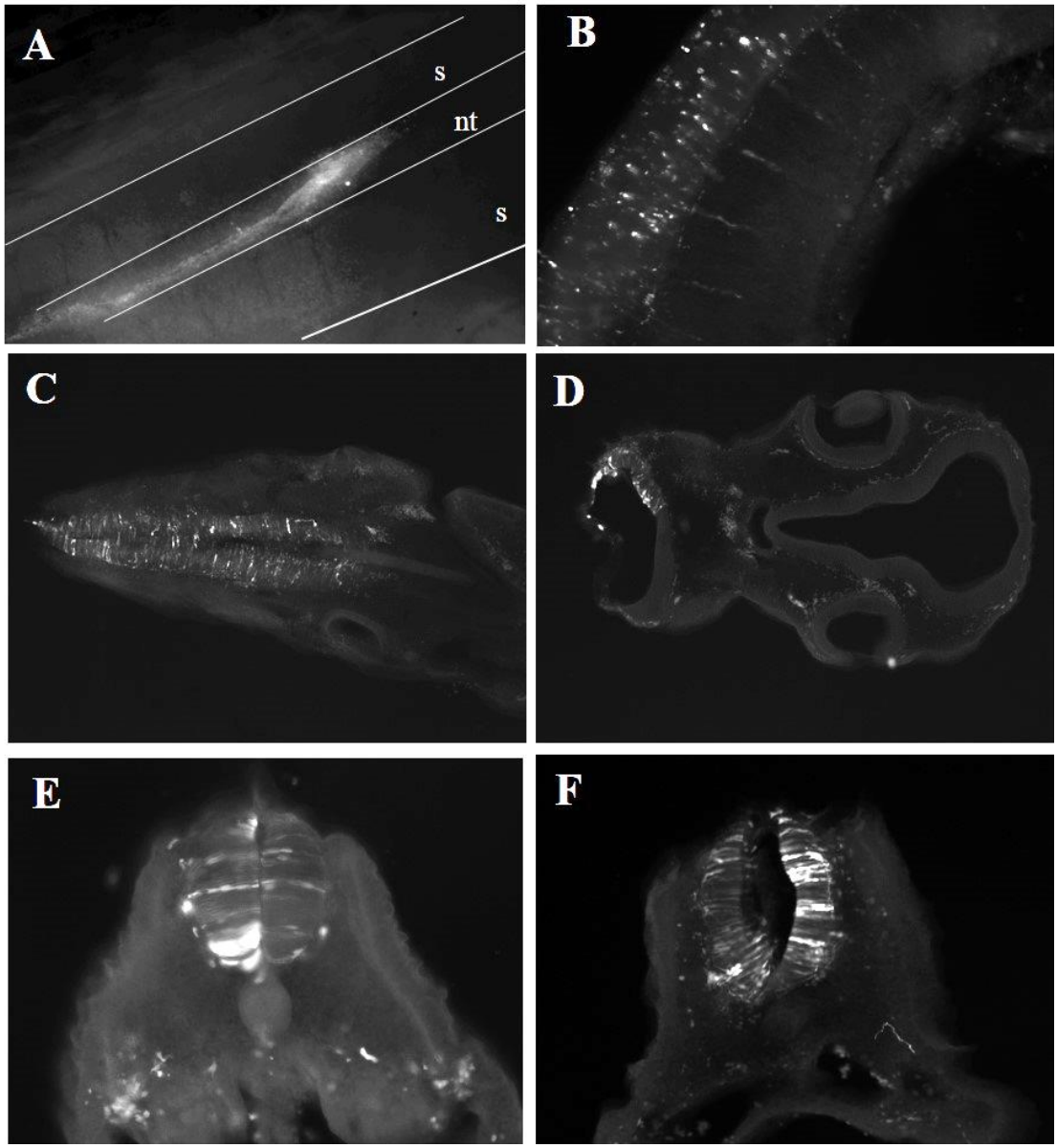

Figure 4.14- *In ovo* tranfection of neural tube with DNA by combining TurboFect with 5V electroporation pulses. (A) *In ovo* view of neural tube (nt), 12 hours after transfection with a GFP expression plasmid at stage 10 HH. s, somites. (B,C) Longitudinal sections of an embryo collected 12 hours after the neural tube was transfected at HH stage 20. GFP is visible in the dorsal neural tube. (D) Transverse section of a transfected embryo: GFP is expressed in the hindbrain. (E.F) Transverse sections through the trunk showing transfected cells in the neural tube.

CHAPTER 5- ASSESSMENT OF FLRT2 KNOCKDOWN ON EMBRYO DEVELOPMENT AND AXONAL GUIDANCE.

5.1- Introduction

The Flrt family of glycosylated membrane proteins has three members, Flrt1, Flrt2, and Flrt3, each with conserved fibronectin type III (FNIII) domains that mediate binding to the Ig-domain of FGF receptors (Karaulanov *et al*., 2006). The conserved leucine-rich repeats (LRR) and the transmembrane (TM) domains are required for cell adhesion and cell recognition (Lacy *et al*., 1999). The *Flrt* genes are expressed in many of the same tissues where FGF signalling has an important role, and can themselves be induced by FGF2 (Haines *et al*., 2006). *Flrt1* is expressed in dorsal root ganglia, trigeminal ganglia and facioacoustic ganglia, the midbrain/hindbrain and forebrain/midbrain boundaries and the eye (Haines *et al*., 2006). *Flrt3* is expressed in the hindbrain and forebrain, eye, heart epithelium and at the edges of the dermomyotome (Haines *et al*., 2006), and was shown to be necessary for cell adhesion as knockout led to embryo lethality at 10.5 dpc with defects in head fold fusion, ventral closure and endoderm migration (Maretto *et al*., 2008). *Flrt2* is expressed in the posterior half-sclerotome, cephalic mesoderm, head mesoderm and epithelia of the body wall in mouse (Haines *et al*., 2006). Flrt2 was selected for study as it was identified in the posterior half-sclerotome in the mouse microarray screen of Hughes *et al.* (2009), and shed ectodomains of Flrt2 (and Flrt3) repel Unc5D-expressing axons and neurons (Yamagishi *et al.*, 2011). Hence, Flrt2 could repel axons in the posterior half-sclerotome. As described in section 3.14, I confirmed that *Flrt2* is expressed in the posterior half-sclerotome of chicken embryos and selected this gene for functional knockdown using the transfection technique that I developed during this project, described in Chapter 4. In this chapter, I describe the effects on embryo development and axon guidance of introducing FITC-labelled siRNAs against *Flrt2* into the developing somites.

Also, as mentioned above, Flrts bind FGF receptors and their expression can be induced by FGF signalling (Haines *et al.*, 2006; Karaulanov *et al*., 2006). There are four members of the FGF receptor family: Fgfr1-4. All three Flrt proteins bind to Fgfr1 (Böttcher et al., 2004; Haines *et al*., 2006). Flrt2 (Wei *et al.*, 2011) and Flrt3 can also bind to Fgfr2 (Egea *et al*., 2008). Also, *Flrt2* knockdown *in vitro* reduces both *Fgfr2* mRNA and Fgfr2 protein expression, while Flrt2 overexpression upregulates Fgfr2 expression, suggesting a positive regulatory feedback loop (Wei *et al.*, 2011) *Fgfr1* and

Fgfr2 are expressed in the neural tube, midbrain and hindbrain and *Fgfr1* and *Fgfr3* are expressed in the somites (Walshe and Mason, 2000). Mouse *Fgfr4* is expressed mainly at later developmental stages in the liver, kidney and lung (Korhonen *et al*., 1992), while chicken *Fgfr4* (FREK) is expressed by proliferating myotome progenitor cells from stage 19 HH and plays a role in myotome proliferation and distribution (Kahane *et al.*, 2001). To test whether knocking down Flrt2 has any effect on *Flrt3* or Fgfr expression, I also used antibody staining to study the expression of *Flrt3* and Fgfr1-3 after transfecting *Flrt2* siRNA into the somites.

5.2- *Flrt2* siRNA design

Flrt2 is composed of leucine rich repeats (LRR), a type III fibronectin (FNIII) domain, a transmembrane domain, and a short intracellular tail (Lacy *et al*., 1999). The leucine rich repeats stretch from 104-198 bp and 928-1080 bp of the cDNA; and the FNIII domain from 1283-1522 bp (all identified using the conserved domains tool from NCBI (http://www.ncbi.nlm.nih.gov/cdd). Besides its Kozak consensus sequence for the initiation of translation at the 5' proximal ATG codon (Kozak, 1984), Flrt2 also has two other possible internal Kozak sequences (Kozak, 1986), one from 1034-1046 bp: TCCGAGGTATGGGC, and the other from 1065-1073 bp: GAATATGC (Kozak, 1986). So in order to knock down Flrt2 not only the conserved protein family domains, but also the internal Kozak sequences should not be available for the initiation of translation within any cleaved mRNA that escaped degradation.

The siRNA target sequences were designed following the rules described in section 4.2.1 and synthesized with the same parameters as in Rao *et al*. (2004). Using GeneLink siRNA software, a 23 bp siRNA was chosen starting at 36 bp of the *Flrt2* cDNA sequence: TCTGTTCTCATGAAATCATGGCT. Using Software for Statistical Folding of Nucleic Acids and Studies of Regulatory RNAs (Sfold; Ding and Lawrence, 2003; Ding *et al.*, 2005), a second siRNA was chosen starting from 1052 bp of the cDNA: GGGAGCTTAATATGAATATG. A scrambled siRNA sequence was synthesised from the second siRNA sequence as a negative control. The efficiency of the knockdown was assessed by *in situ* hybridization using a single-stranded antisense RNA probe designed to hybridize with *Flrt2* mRNA from 1227-1883 bp of the cDNA

sequence (Figure 4.8). The RNA probe sequence was submitted to NCBI BLAST for sequence alignment to the chicken genome and it only detected *Flrt2*.

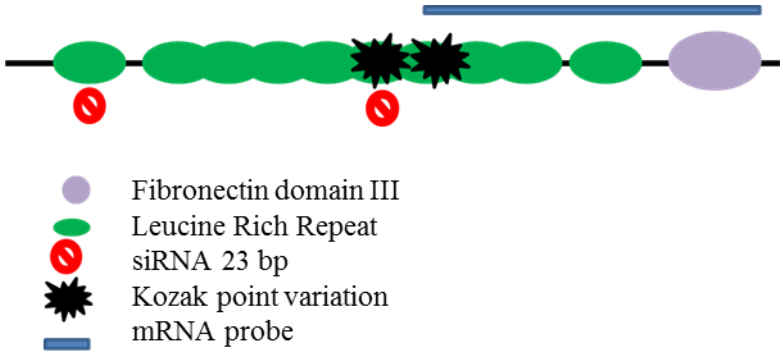

Figure 5.1- Schematic showing Flrt2 protein structure and relative position of siRNAs and antisense RNA probe. The first siRNA was strategically designed to target the translation start site, and the second siRNA to target an internal Kozak sequence, to avoid any possibility of translation from any mRNA fragments remaining after cleavage. A single-stranded antisense RNA probe was used for *in situ* hybridization to assess the impact of siRNA-mediated knockdown.

Flrt2 knockdown was done by transfecting somites on the right side of chick embryos at stages 10-14 HH (using the TurboFect-PEG complex, as described in Chapter 4) with both siRNAs simultaneously, aiming to target as many somites as possible, a maximum of 22 somites (see section 4.3.4); due to the injection method the PSM was also transfected, resulting in a higher number of transfected somites, up to 22. As a control, I used a scrambled siRNAs transfected in the same way, at the same developmental stage and aiming to target the same number of somites. As described in Chapter 4, introduction of scrambled siRNA into chick somites had no effect on development. Embryos were incubated until stage 24 HH, visualised using a dissecting microscope and any changes in phenotype recorded.

To study knockdown efficiency in whole embryos, *in situ* hybridization is normally used to assess changes in mRNA expression, while whole-mount antibody staining is used to assess effects on protein levels. As there are no commercially available antibodies that can detect Flrt2 protein in chick, the only method that could be used to assess knockdown efficiency was by *in situ* hybridization (Figure 5.2).

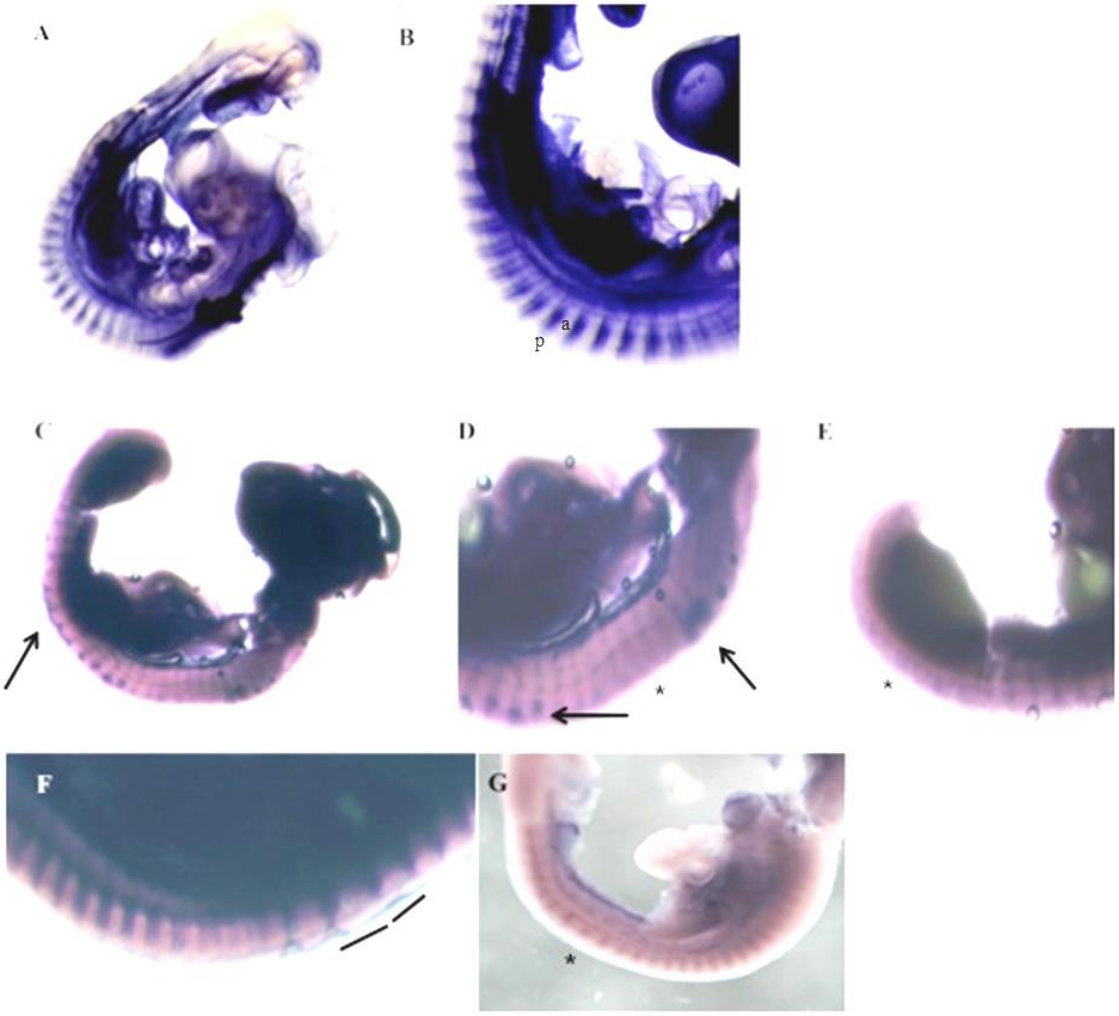

Figure 5.2- *Flrt2* expression in an uninjected embryo and in a *Flrt2* siRNA targeted embryos. Whole mount *in situ* hybridization for *Flrt2*. (A) Wild type chick embryo at stage 21 HH. (B) Higher magnification view of embryo in A: *Flrt2* is expressed in the posterior half sclerotome (p). (C) Transfected chick embryo at stage 22 HH, *Flrt2* expression is reduced in targeted somites (thoracic), while abnormal *Flrt2* expression is seen in other somites (black arrow). (D) Higher magnification view of the embryo in C., *Flrt2* expression is drastically reduced in some sclerotomes (asterisk) and abnormal in others (arrows). (E) Higher magnification view of the tail of the embryo in C, *Flrt2* is reduced in the trunk and undetectable from the leg bud down to the tail (asterisk). (F) High magnification view of a transfected chick embryo at stage 22 HH. *Flrt2* is irregularly expressed within the sclerotome. (G) A transfected chick embryo at stage 19 HH, *Flrt2* expression is weak throughout the embryo. All images show embryos positioned in the same orientation as the embryo in A.

As can be seen in Fig. 5.2, *Flrt2* expression was reduced in the targeted somites of *Flrt2* siRNA-transfected embryos (Fig. 5.2C-G) versus untransfected embryos (Fig. 5.2A-B). Out of 117 transfected embryos, *Flrt2* whole mount *in situ* hybridization was

performed on 10 chick embryos at stage 22 HH. Out of these 10 transfected embryos, seven (70%) had at least three of the targeted sclerotomes without visible *Flrt2* signal (Fig. 5.2C-G). If this was a representative proportion, then 82 of the 117 transfected embryos should have had reduced *Flrt2* expression in some of the targeted sclerotomes. At the time of injection, the embryos had between 10 and 27 somites, however, according to Fig. 5.2 it looks like more somites were affected than those that had formed at the time of injection, suggesting that somites in formation in the presomitic mesoderm (PSM) were also transfected. In this study, *in situ* hybridization followed by immunolocalisation of the labelled siRNA-FITC was not done in order to prove that the somites with *Flrt2* expression reduction were indeed transfected. It would be beneficial to confirm the presence of the FITC-labelled siRNA in the sclerotomes where *Flrt2* expression was reduced. However, there is a degree of confidence, since all the transfected embryos were observed *in ovo* under UV light using a dissecting microscope to confirm the presence of FITC-siRNA, which could be observed even 72 hours post-transfection, as described in section 4.3.3.

5.3- Phenotypic alterations in *Flrt2* siRNA-transfected embryos

Transfected embryos were observed 18 and 42 hours after transfection, and phenotypic modifications were recorded (Table 5.1). The same procedure was used for embryos transfected with scrambled siRNA and there were no obvious effects on these embryos when compared to non-transfected embryos (Fig. 5.3A; also see section 4.3.6). Phenotypic observations from the 117 *Flrt2* siRNA-transfected embryos (Table 5.1) were collected during the same time period as the observations on the 40 scrambled siRNA-transfected embryos which developed normally (Fig. 5.3A; section 4.3.6). Note that individual embryos may exhibit more than one abnormality (e.g. Fig. 5.3B).

One day after transfection of *Flrt2*-siRNA into developing chick somites it was possible to see observe some phenotypes relating to blood supply to the embryo body and the extra-embryonic blood vessels (not photographed), which appeared thin and fragile, suggesting that vasculogenesis and angiogenesis might have been affected. The vitelline arteries were abnormally displayed (compare Fig. 5.3A and B); instead of being symmetrically positioned (one on the right and one on the left), in 52% of

embryos they were asymmetrically displayed, where the right vitelline artery was connected directly to the heart (Fig 5.3B). Hence, it is possible that *Flrt2* may be required for the correct development of blood vessels.

In order to assess further the impact of *Flrt2* siRNA transfection, embryos were allowed to grow for longer, however only 5 out of 18 transfected embryos survived to E6.0 (stage 28-29 HH). The abnormalities recorded for these 5 embryos are listed in Table 5.2. As described in section 3.14, *Flrt2* is expressed at later stages of development in the neural arch and vertebral body. Alcian Blue staining for cartilage suggested that *Flrt2* siRNA transfection had an impact on vertebral body formation (Fig. 5.4), as these were abnormally bent at the tail level (Fig. 5.4), however it would be necessary to repeat this in order to confirm this as a true phenotype. The Alcian blue staining also appeared stronger than in scrambled siRNA-transfected embryos, however it is possible that this difference might be due to the difference on developmental stages between scrambled and *Flrt2* siRNA-transfected embryos. Xu *et al.* (2011) reported that reducing *Flrt2* expression results in a thicker chondrocyte matrix due to increased cell-cell interaction, visible by Alcian blue staining. However, to assess if chondrocyte matrix becomes thicker in chick embryos after *Flrt2* siRNA transfection it would be necessary to repeat the Alcian Blue staining with embryos of the same developmental stage and also with micromass culture.

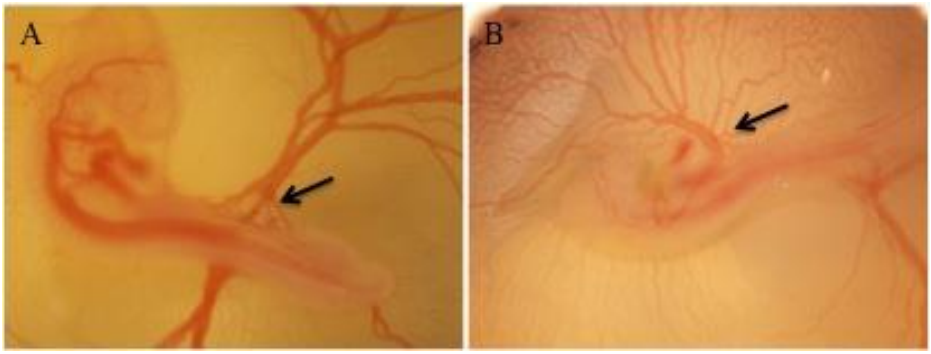

Figure 5.3- Example of a control (scrambled) siRNA-transfected embryo and a *Flrt2* siRNA-transfected embryo. Embryos photographed *in ovo* at 18 hours post-transfection, which should be stage 18 HH. (A) Scrambled siRNA-transfected chick embryo developed normally according to Hamburger and Hamilton (1951). (B) *Flrt2* siRNA-transfected chick embryo had a mislocalized vitelline artery (arrow), an apparently smaller head and a faster heart-beat.

Table 5.1- Visible changes in phenotype of 117 *Flrt2* siRNA-transfected embryos up to 42 hours post-transfection (embryos collected at stages 22 to 24 HH).

Visible phenotypic modifications	**% embryos**	**Nº embryos**
Blood supply (low irrigation, embryo colour)	44.4	52
Mislocalized vitelline artery	44.4	52
Heart formation (increased size)	51.2	60
Heart beat (increased number of beats)	44.4	52
Head formation (more rounded)	17.1	20
No. embryos that died by 18 hours post-transfection	5.9	7
No. embryos that died by 42 hours post-transfection	16.2	19

Table 5.2- Visible phenotypic alterations in five *Flrt2* siRNA-transfected embryos that survived until E6 (stage 28-29 HH).

Visible phenotypic modifications	**% embryos**	**Nº embryos**
Poor blood supply and coagulation	60	3
Head formation (more rounded)	40	2
Movement (increased)	100	5
Heart (high rhythm)	40	2
Limb formation (higher to the vertebral body)	40	2
Embryo position within the egg (not turned)	100	5
Extra-embryonic angiogenesis (coagulation)	60	3
Size (bigger)	100	5

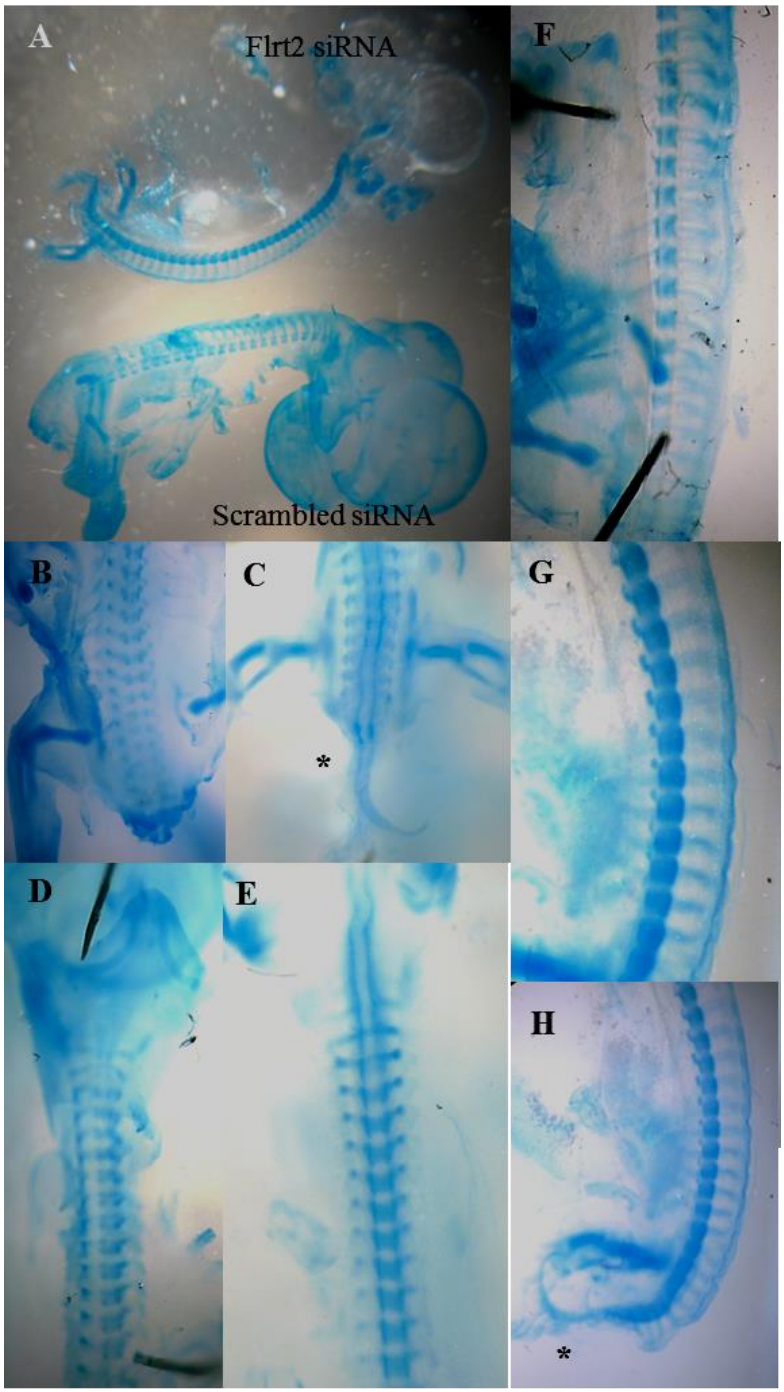

Figure 5.4- Alcian Blue staining of cartilage in a scrambled siRNA-transfected chick embryo (stage 30 HH) and a *Flrt2* siRNA-transfected embryo (stage 29 HH). (A) Low-power view of both skeletons. (B,C) Dorsal view of trunk and tail region of (B) scrambled siRNA-transfected embryo and (C) *Flrt2* siRNA-transfected embryo. The *Flrt2* siRNA-transfected embryo has a mild deformity in the tail (asterisk). (D,E) Dorsal view of cervical vertebrae of (D) scrambled siRNA-transfected embryo and (E) *Flrt2* siRNA-transfected embryo. (F) Lumbar vertebrae of scrambled siRNA-transfected embryo. (G) Lumbar vertebrae of *Flrt2* siRNA-transfected embryo. (H) Lumbar and tail vertebrae of *Flrt2* siRNA-transfected embryo. The tail vertebrae are slightly bent (asterisk).

Müller *et al*. (2011) used an *Flrt2*-null mouse mutant to show that *Flrt2* (which is expressed in cardiomyocytes and the epicardium) plays an essential role in heart morphogenesis. The *Flrt2* siRNA-transfected chick embryos also displayed heart phenotypes. Around 40% of transfected embryos had a faster heart beat than controls, while half had enlarged hearts (Table 5.2). Of the 13 out of 18 embryos that died before reaching stage 29 HH, it could be speculated that most died due to heart defects, as happens with *Flrt2*-null mice, which do not survive beyond day 12 due to cardiac insufficiency (Müller *et al.*, 2011). Hearts of transfected chick embryos appeared around 40% bigger than controls, which may be consistent with the dilated heart phenotype reported by Müller *et al*. (2011) in *Flrt2*-null mouse embryos.

Flrt2 knockdown embryos exhibited a constant modification of blood supply, through stage 22-24 HH (Table 5.1) to stage 28-29 HH (Table 5.2). Poor blood supply to the heart may also have contributed to early death, as the extra-embryonic blood vessels were much thinner than controls and embryo coloration was generally lighter (in some cases almost white). A similar phenotype was obtained after Netrin-1 overexpression in chick embryos (Bouvrée *et al*., 2008) and on Unc5B stimulation in mice (Larrivée *et al*., 2007). Of particular note is that in the mouse Flrt family, Flrt3 binds to Unc5B, while Flrt2 binds to Unc5D (Yamagishi *et al*., 2011). It has also been proposed that Flrt2/3 ectodomains can be shed to act at a distance (Yamagishi *et al*., 2011), thus knockdown of *Flrt2* may also affect Flrt3 signalling.

As can be seen in Table 5.2, *Flrt2* siRNA-transfected embryos surviving to E6.0 presented with a high number of abnormalities. The most obvious differences were that transfected embryos were around 30% larger and displayed excessive sharp rapid movements from day 4 when compared with non-transfected embryos, and abnormal blood irrigation through the body. It is possible that *Flrt2* knockdown causes blood vessels to become fragile and rupture with increase blood flow and pressure during development, leading to haemorrhage and embryo death, explaining the increase of embryo death after stage 24 HH. These embryos were terminated at stage 29 HH (E6.0) due to poor health.

5.4- Alterations in axonal migration after *Flrt2* siRNA transfection

Flrt2 was selected for knockdown because of its expression in the posterior half-sclerotome and its potential role here in axon guidance, especially given the report by Yamagashi *et al*. (2011) that *in vitro*, Flrt2 together with Flrt3 acts as a chemorepellent for Unc5D-expressing cortical neurons, resulting in growth cone collapse and modulating cortical neuron migration. My main aim in using siRNA transfection of somites to knock down Flrt2 was to investigate whether Flrt2 has a role in repelling axons from the posterior half-sclerotome. As reported in section 3.14, *Flrt2* is also expressed in the myotome, and transiently around the neural tube and notochord.

In order to assess any effect of *Flrt2* siRNA transfection on axon guidance and somite patterning, I used anti-neurofilament immunostaining to label axons, and rhodamine-conjugated PNA treatment to label the posterior sclerotome. Control scrambled FITC siRNA-chick embryos transfected at stage 9-12 HH and collected at stage 20 HH displayed no abnormalities in axonal guidance or somite patterning (Fig 5.5).

The impact of *Flrt2* siRNA transfection was assessed in the same way on chick embryos transfected at stage 9-12 HH and collected at stage 17 HH (18 hours post-transfection) (Fig. 5.6). The transfection affected a large number of somites, and the FITC-conjugated siRNA was visible on more somites than had formed at the time of transfection: 27 somites, corresponding to the vagal and thoracic area, however FITC-siRNA was present on the trunk and tail (Fig. 5.6A,B), indicating that the PSM had also been transfected.

Flrt2 siRNA-transfected embryos presented some defasciculation at stage 19 HH, with axons expanding into the posterior sclerotome (Fig 5.6C,D,F). The total number of somites did not change but they were misaligned (Fig. 5.6C,E,F) and variable in size, with very small somites next to somites of normal size (Fig 5.6E,F). The smaller somites did not present any segmentation of axons, and there was only some neurofilament staining present. The adjacent somites exhibited segmentation but there were also spots of neurofilament expression in the posterior half-sclerotome (Fig. 5.6F, arrows), which could represent mis-targeted axon bundles in cross-section and/or mis-placed neural crest-derived DRG neurons.

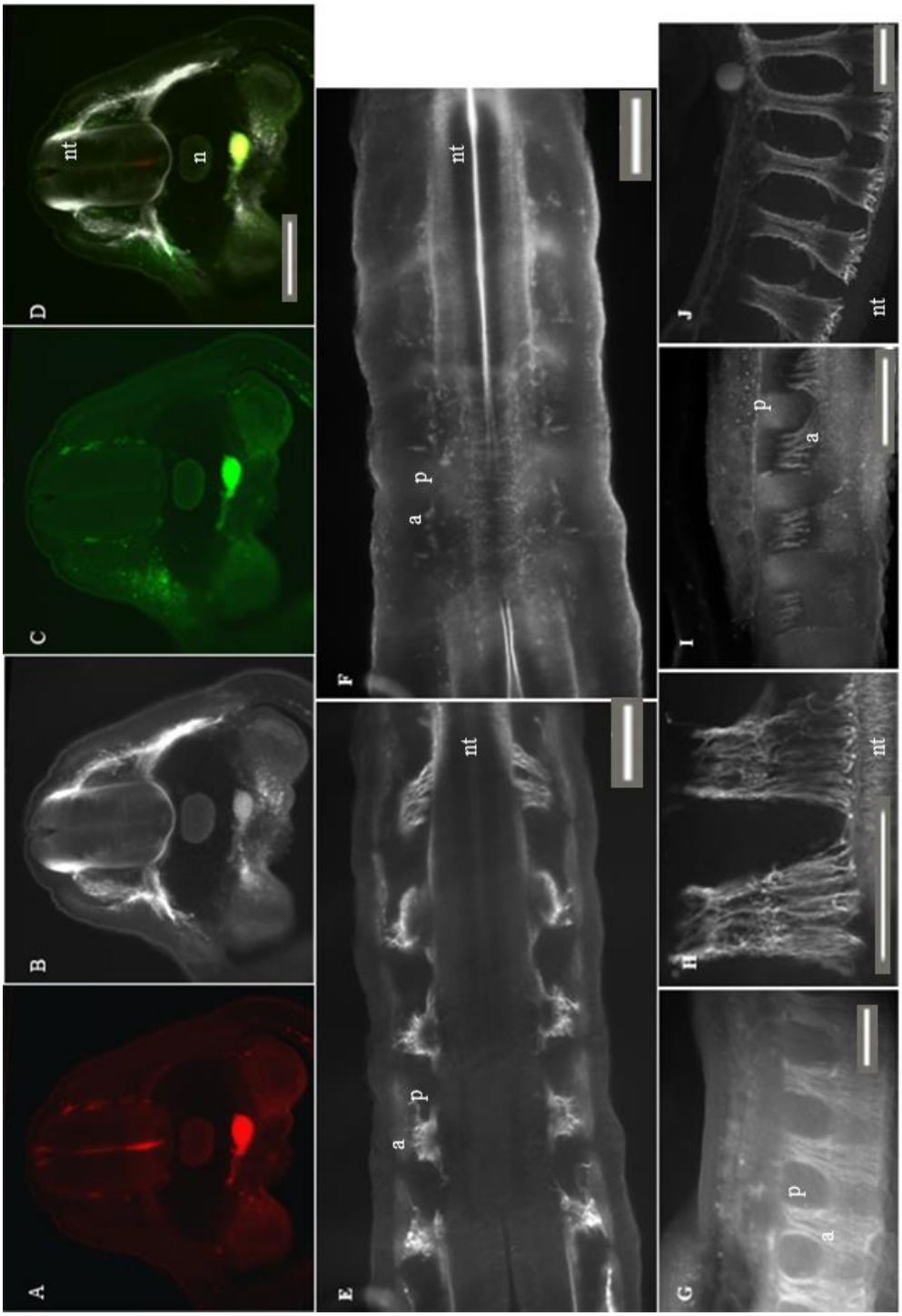

Figure 5.5- Transfection of a scrambled FITC-siRNA does not affect spinal axon patterning. Anti-neurofilament immunostaining (for axons) and rhodamine-PNA staining (for neural tube and posterior half sclerotome) of scrambled siRNA transfected chick embryos collected at stage 20 HH. (A-D) Transverse section of an anterior half-sclerotome. (A) Rhodamine-PNA staining (red). The lumen of the neural tube is PNA-positive. (B) Anti-neurofilament immunostaining for sensory and motor axons (white). (C) FITC-siRNA (green) shows transfected sclerotome is on the left side in this view. (D) Merge of panels A-C. (E-J) Longitudinal sections. (E) Anti-neurofilament immunostaining: axons display a segmented pattern, traversing the anterior half-sclerotome (a) but not the posterior half-sclerotome (p). (F) Rhodamine-PNA staining in

posterior half-sclerotomes and neural tube lumen of same section as E). (G) Anti-neurofilament immunostaining showing sensory and motor axons in the anterior sclerotome. (H) High magnification view of sensory and motor axon bundles in the anterior sclerotome. (I) Combined PNA and anti-neurofilament immunostaining: PNA is strictly in the posterior half-sclerotome while all axons are in the anterior half-sclerotome. (J) Junction of sensory and motor axons in the vagal area.

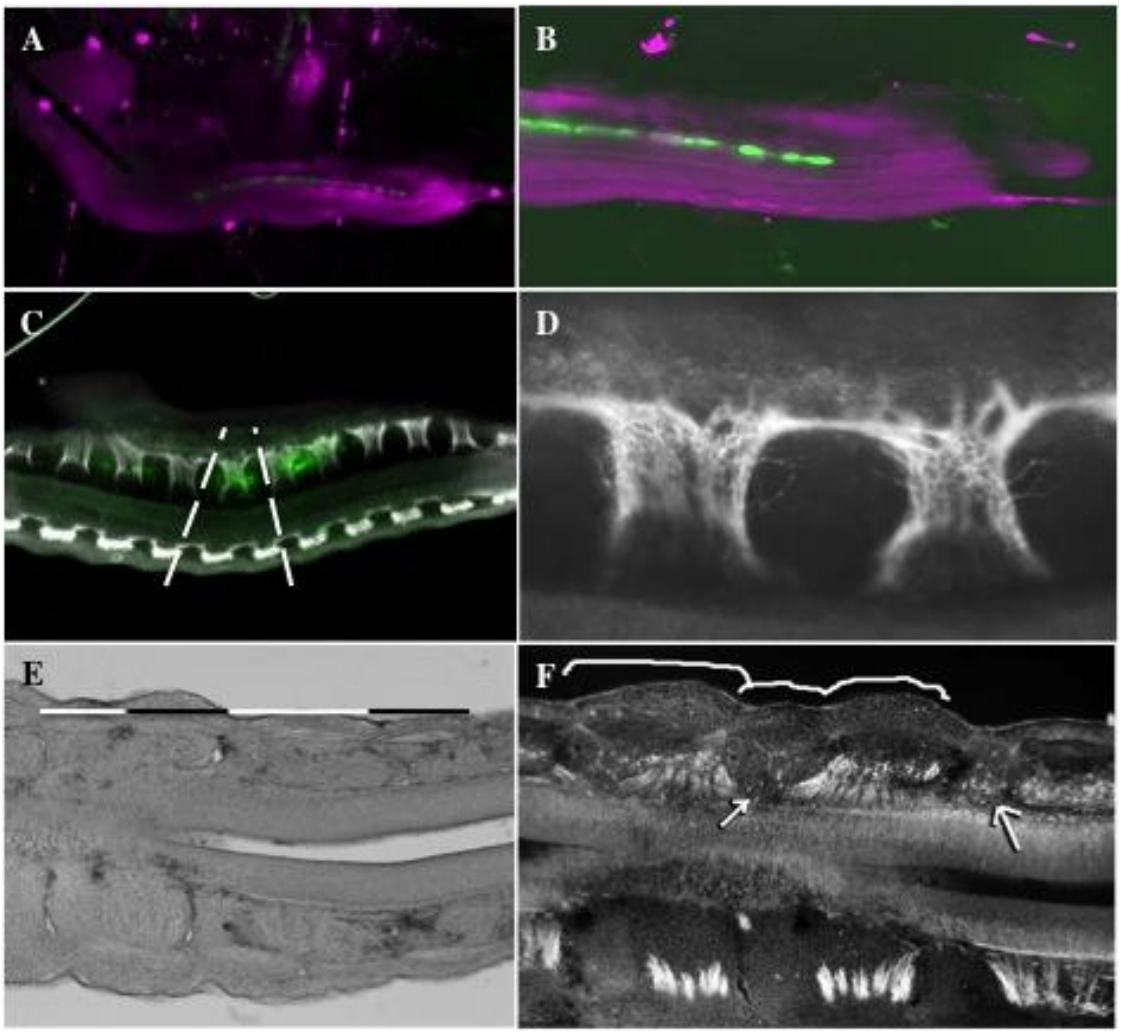

Figure 5.6- Transfection of *Flrt2* siRNA leads to defects in somitogenesis and axon patterning. (A) Chick embryo at stage 19 HH, 18 hours post-transfection: the green staining shows the FITC-siRNA transfected somites. (B) Higher magnification view of embryo in A showing that, the somites on the right side of the embryo were successfully transfected with FITC-siRNA. (C) Longitudinal section of an *Flrt2* siRNA-transfected embryo, immunostained for neurofilament. Axons still exhibit a segmented pattern; however there is a change in the somite alignment (dashed lines). (D) Higher magnification view of the misaligned region of the section in C shows that the axon bundles are defasciculated, with multiple axons sprouting from the main bundle. (E) Longitudinal section of a transfected chick embryo showing that the somites have different sizes. Limits are drawn with alternating white and black lines according to the dermomyotome. (F) Longitudinal section showing neurofilament staining in the posterior half sclerotome (arrows) and somites of different sizes (white line).

More severe phenotypes were seen in *Flrt2* siRNA-transfected chick embryos collected for analysis 41-43 hours post-transfection, at stages 22-24 HH (Fig. 5.7). Anti-neurofilament immunostaining of 21 transfected embryos showed longitudinal branches from the main axonal bundle and axons going to the posterior sclerotome (Fig. 5.7A-D), although axons still displayed segmentation. Ten of the 21 embryos also displayed axons sprouting into the dermomyotome and posterior sclerotome (Fig. 5.7E-H). An even more severe effect was seen in five of the 21 embryos (Fig. 5.8 and Fig. 5.9), in which there were multiple spots of neurofilament expression within the posterior sclerotome (which could represent cross-sections of longitudinally-projecting axon bundles in cross-section, and/or mis-placed neural crest-derived DRG neurons) and also neural tube defects (Fig. 5.9), In contrast, as described in section 4.3.6, 40 of 198 scrambled siRNA-transfected embryos at stages 19, 22 and 24 HH were immunostained for neurofilament and stained with rhodamine-conjugated PNA and that there was no obvious impact on either sclerotome segmentation or axonal guidance.

Figure 5.7- (On next page) *Flrt2* knockdown leads to abnormal axon growth into the posterior half-sclerotome and dermomyotome/myotome. Anti-neurofilament immunostaining of *Flrt2* siRNA-transfected embryos collected at stage 22 HH. (A-D) Lateral views of axons growing aberrantly in the transfected area towards the posterior half-sclerotome (arrows). (E) Transverse section showing defasciculation towards the dermomyotome, which is also abnormal (arrows). (F) Higher magnification view of E showing the sensory and motor axon junction and axons defasciculating towards the dermomyotome (arrow). (G) Longitudinal section showing that axons are present in the myotome (arrows) and in the posterior half-sclerotome. (H) Transverse section showing multiple axons migrating towards the dermomyotome. There are also multiple axons in the mid-line of the neural tube; notochord and dermomyotome morphology are also altered. (nt) neural tube. Scale bar: 100 μm.

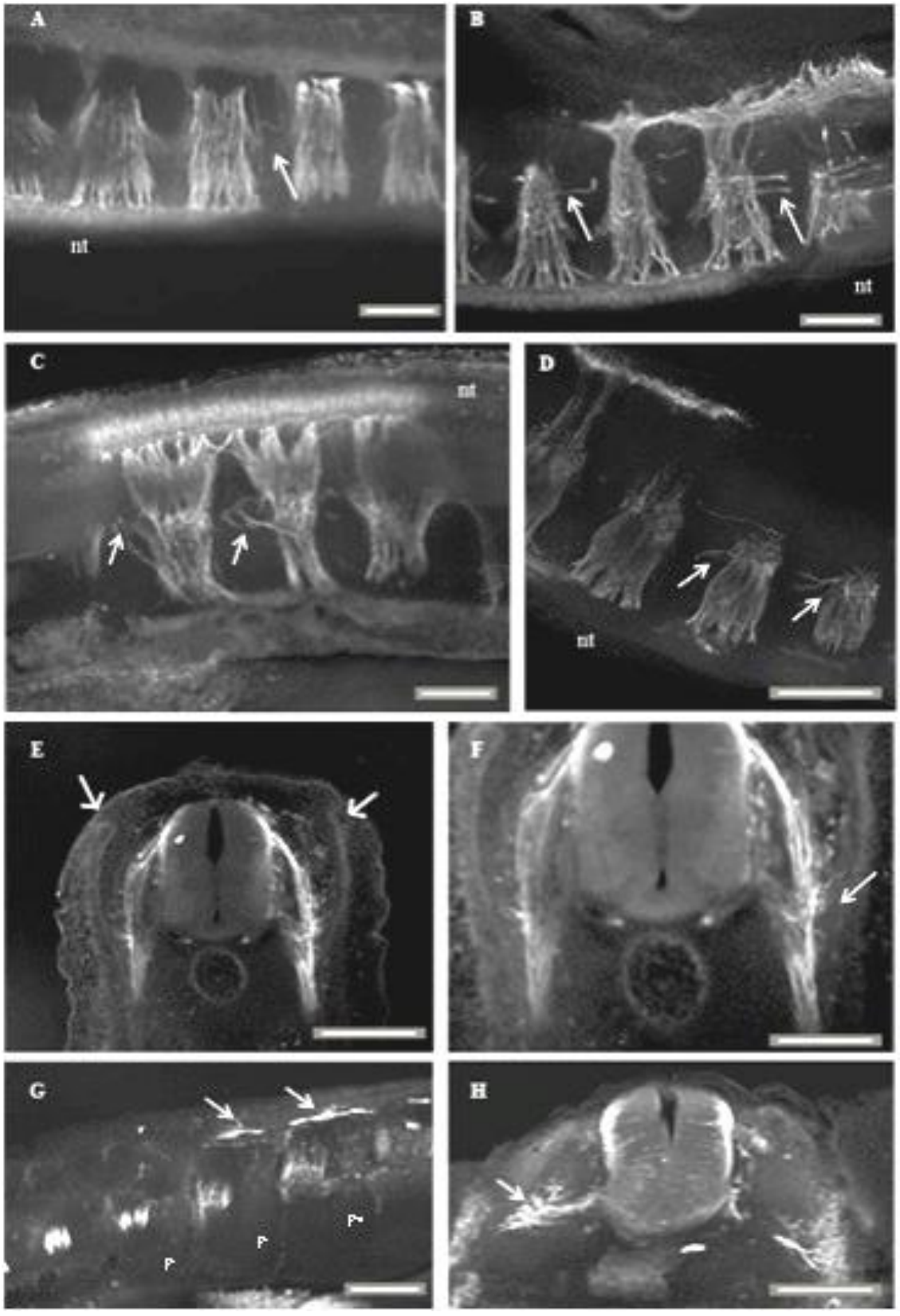

Figure 5.7- Legend on previous page.

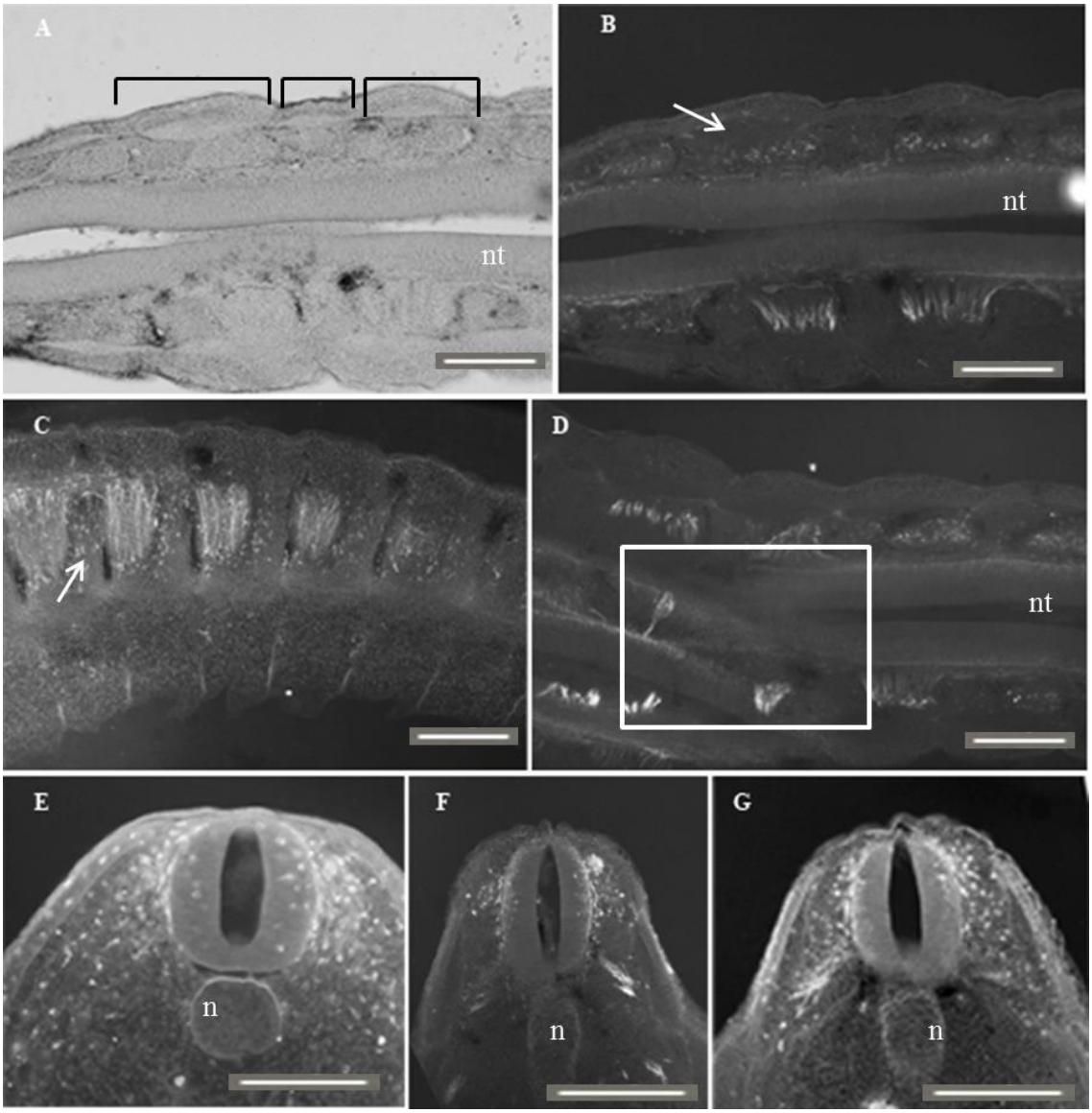

Figure 5.8- Continued abnormal axon growth and somite defects in *Flrt2* siRNA-transfected embryos collected at stage 24 HH. (A) Coronal section in bright field, showing variation in somite size. (B) The same section as in A, immunostained for neurofilament. Spots of neurofilament expression are scattered through both somite halves (arrow) while axonal segmentation is still present in the non-transfected control side. (C) Neurofilament immunostaining of a longitudinal section shows axonal bundles in the anterior half-sclerotome as normal but also spots of neurofilament scattered through the posterior sclerotome (arrow). (D) Coronal section showing abnormal neural tube morphology, with axons crossing through the lumen of the neural tube (box), and spots of neurofilament expression in the posterior half-sclerotome on both sides. (E-G) Transverse sections showing spots of neurofilament expression scattered through somite-derived tissues, and axons at all levels of the neural tube. Panel F shows some axons in the medial neural tube. The morphology of the notochord also seems disrupted in panels F and G. (n) notochord, (nt) neural tube. Scale bar: 100 µm.

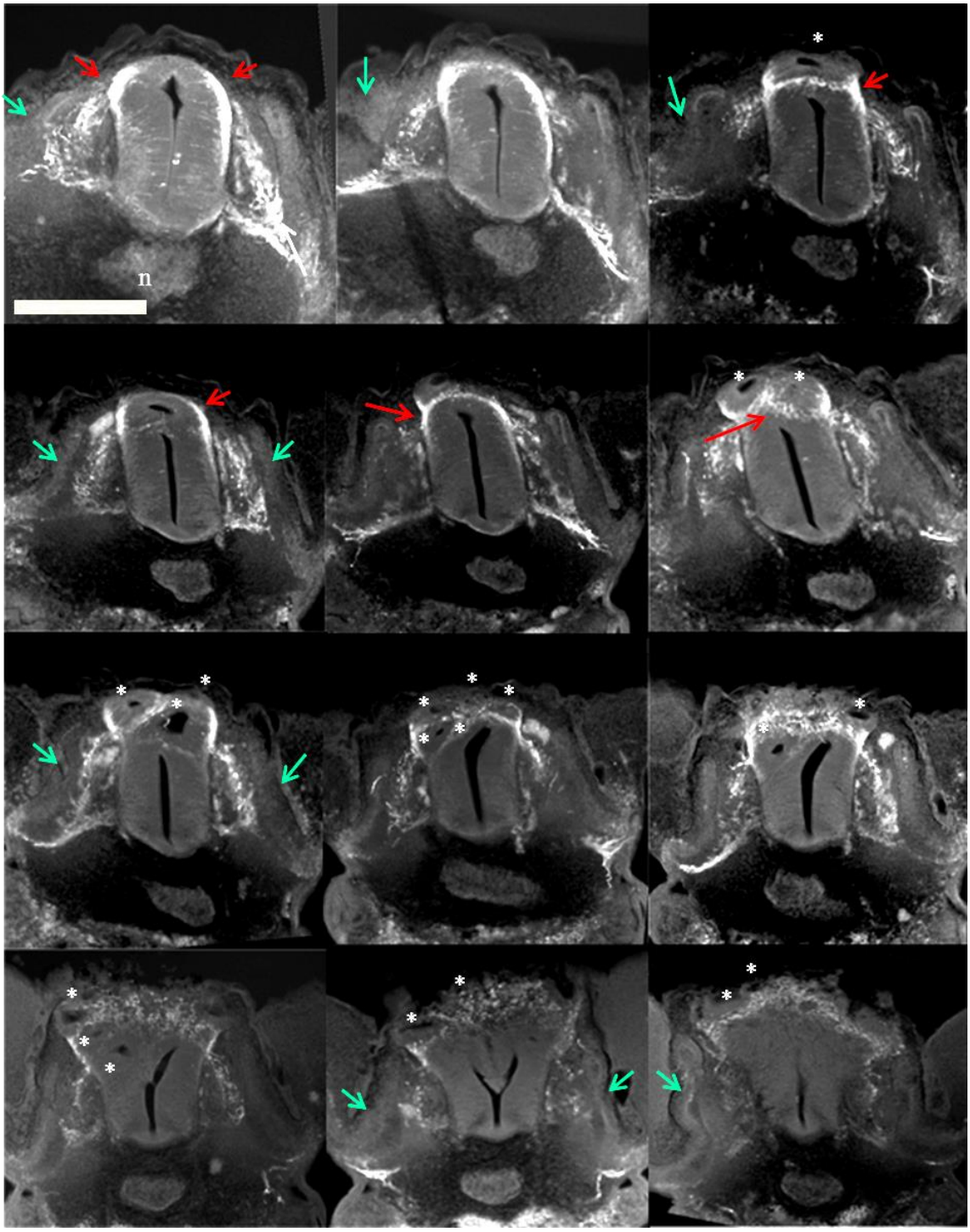

Figure 5.9- Neural tube defects in an *Flrt2* siRNA-transfected embryo collected at stage 24 HH. Serial transverse sections in a posterior-anterior sequence show axons from the dorsal neural tube (red arrows) migrating ventrally and then medially to form a physically separated neural tube with up to five lumens (*). Axons also migrate laterally, towards the deformed dermomyotome (green arrows). As the neural tube divides, forming new attached neural tubes, the notochord and dermomyotome keep changing their morphology. In the last section, the multiple neural tubes appear to erupt losing the individuated lumens. Scale bar: 100 µm.

5.5- *Flrt2* siRNA transfection has no effect on somite polarity

Somites have a distinct anteroposterior polarity and it may be that Flrt2 knockdown disturbs the establishment or maintenance of somite polarity. In order to test this, I used whole-mount *in situ* hybridization to examine the expression of *Uncx4.1*, a posterior half-sclerotome marker (Schrägle *et al*., 2004) and *Tbx18*, an anterior half-sclerotome marker (Haenig and Kispert, 2004) (also see section 3.2), in *Flrt2* siRNA-transfected chick embryos collected between stages 19 and 22 HH (Fig. 5.10). These markers were studied in four transfected chicken embryos for each probe, and in all of them there was no visible modification to their expression when compared with the same number of scrambled siRNA-transfected embryos. Although the chick embryos were not all at the same developmental stage, the polarity was constant through development. If there had been a change, it would be expected to be present at any stage post-transfection. Nevertheless, it would have been beneficial to have tested more transfected embryos for the expression of the polarity markers.

5.6- *Flrt2* siRNA transfection has little or no clear effect on FGF receptor expression

All three Flrt family members bind to Fgf receptors (Haines et al., 2006). Flrt2 interacts with Fgfr1 (Haines *et al.*, 2006) and Fgfr2 (Wei *et al.*, 2011). Furthermore, cells transfected with *Flrt2* shRNA show reduced expression of *Fgfr2* mRNA and Fgfr2 protein, while cells transfected with *Flrt2* cDNA show increased expression, suggesting that Flrt2 promotes Fgfr2 expression (Wei *et al.*, 2011). Given the decrease of *Flrt2* mRNA expression in *Flrt2* siRNA-transfected chick embryos, I investigated if there was any impact on Fgf receptor expression, by immunostaining three *Flrt2* siRNA-transfected embryos each for Fgfr1, Fgfr2 and Fgfr3, and scrambled siRNA-transfected embryos as a control. Fgfr4 expression was not studied, since there was no evidence in the literature for Flrt interaction with Fgfr4, and Fgfr4 has already been characterized as required for myotome progenitor cell proliferation and migration (Kahane *et al.*, 2001).

Fgfr1 expression did not differ much between scrambled siRNA-transfected embryos (Fig. 5.11A,B) and *Flrt2* siRNA-transfected embryos (Fig. 5.11C-E). In a scrambled siRNA-transfected embryo, Fgfr1 expression was present in the ectoderm

and posterior sclerotome (Fig. 5.11A,B). Transverse sections of Fgfr1-immunostained embryos after *Flrt2* siRNA transfection did not show a clear difference (compare Fig. 5.11B and D), however the coronal sections (Fig. 5.11A,C,E) showed Fgfr1 expression in the myotome in an *Flrt2* siRNA-transfected embryo that had abnormal axon bundles in somites on the transfected side and spots of neurofilament staining throughout the somites on the non-transfected side, as well as abnormal neural tube closure (Fig 5.11F, G). Further experiments and analysis of more embryos would be needed to verify this as a real phenotype.

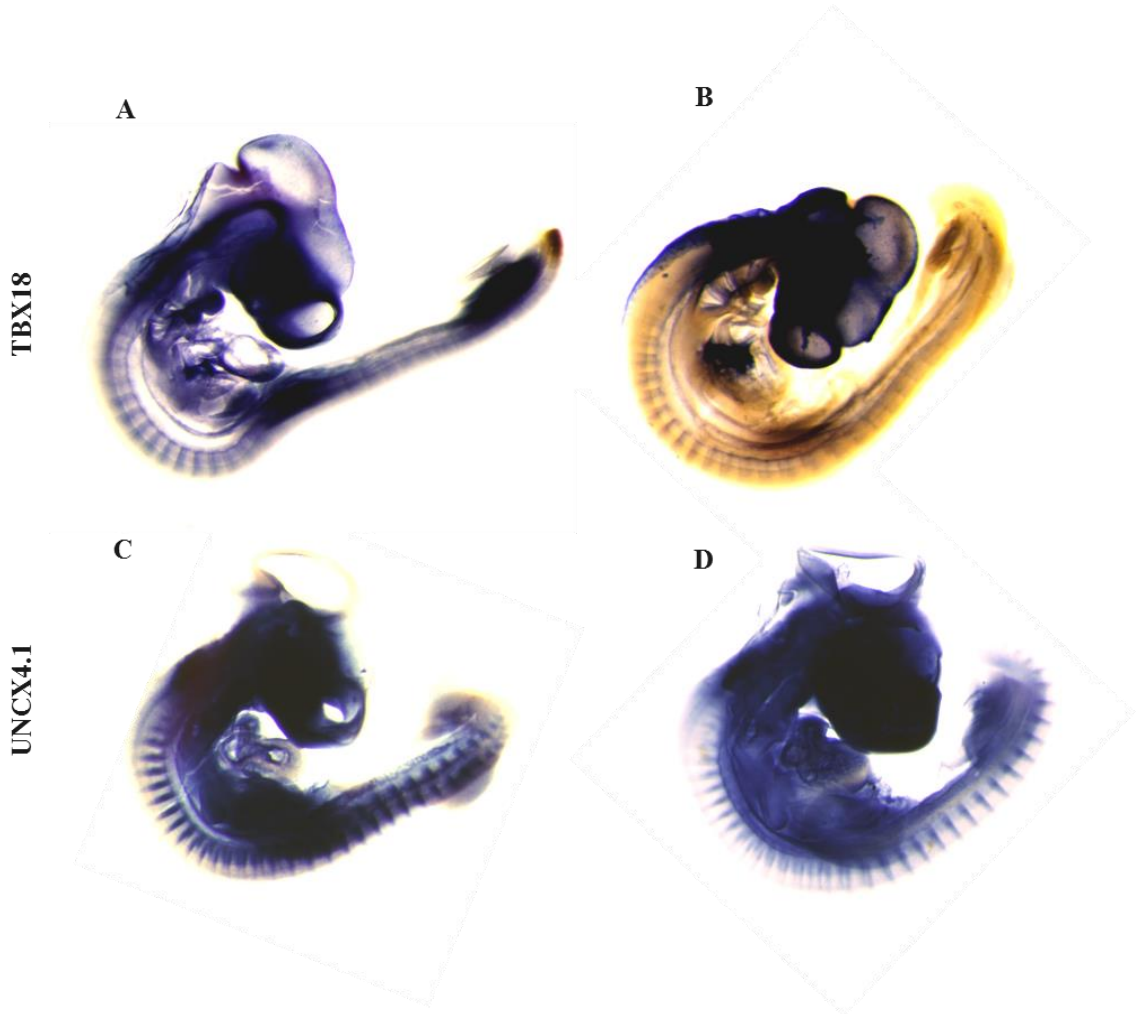

Figure 5.10- *Flrt2* knock-down does not affect somite polarity. (A)- *Tbx18* expression chick embryo stage 19 HH, *Tbx18* is expressed segmentally in the anterior half sclerotome. (B)- *Tbx18* expression on *Flrt2* knockdown chick embryo stage 18 HH, *Tbx18* is expressed remains expressed in the anterior half-sclerotome. (C)- *Uncx4.1* expression in a chick embryo stage 20 HH, *Uncx4.1* is expressed segmentally in the posterior half-sclerotome. (D)- Uncx4.1 expression in a *Flrt2* knock-down embryo stage 22 HH, *Uncx4.1* remains expressed in the posterior half-sclerotome.

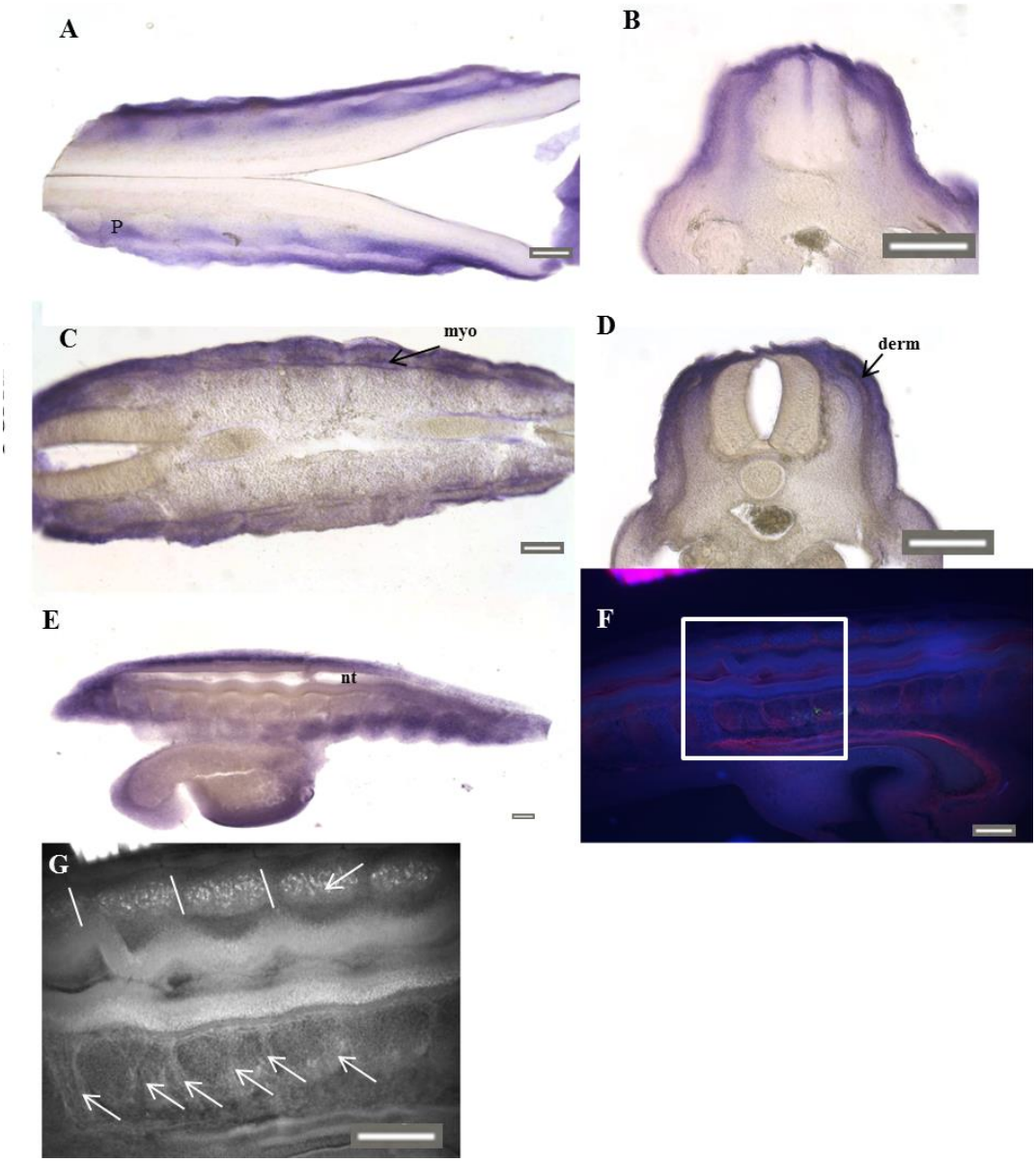

Figure 5.11- Fgfr1 expression is not significantly affected by *Flrt2* siRNA transfection. (A,B) Coronal (A) and transverse (B) sections at stage 22 HH after scrambled siRNA transfection. Fgfr1 is expressed in the ectoderm, posterior half-sclerotome (P) and dermomyotome. (C) Coronal section of an *Flrt2* siRNA-transfected embryo collected at stage 22 HH. Fgfr1 is expressed in the dermomyotome and also the myotome. (D) Transverse section of an *Flrt2* siRNA-transfected embryo collected at stage 24 HH. Fgfr1 is expressed in the ectoderm, dermomyotome (derm) and sclerotome. (E) Coronal section of an *Flrt2* siRNA-transfected embryo collected at stage 24 HH. Fgfr1 expression is reduced in several consecutive somites adjacent to an open region of neural tube (nt). (F) Rhodamine-PNA staining (red) plus anti-neurofilament (blue) and anti-FITC (green) immunostaining of embryo in E shows transfection of somites with FITC-siRNA. (G) Higher-power view of neurofilament expression in the boxed region in F. Axons are spread through several of the transfected somites (arrows) while on the opposite side there are spots of neurofilament expression throughout the somite. White lines indicate somite limits. Scale bar: 100 µm

Fgfr2 expression in *Flrt2* siRNA-transfected embryos was unchanged when compared to a scrambled siRNA-transfected embryo. In both, Fgfr2 was expressed in the ectoderm, dermomyotome and posterior half-sclerotome (compare panels A,B in Fig. 5.12 with C,D). Similarly, Fgfr3 expression did not appear to vary much: in scrambled siRNA-transfected embryos (Fig. 5.13A,B) versus *Flrt2* siRNA-transfected embryos (Fig. 5.13C,D); in both, Fgfr3 was expressed in the ectoderm, dermomyotome and sclerotome. In *Flrt2* siRNA-transfected embryos, it appeared that Fgfr3 was overexpressed (compare Fig 5.13A,B with C,D), but further assays and more embryos would have to be assessed to verify this.

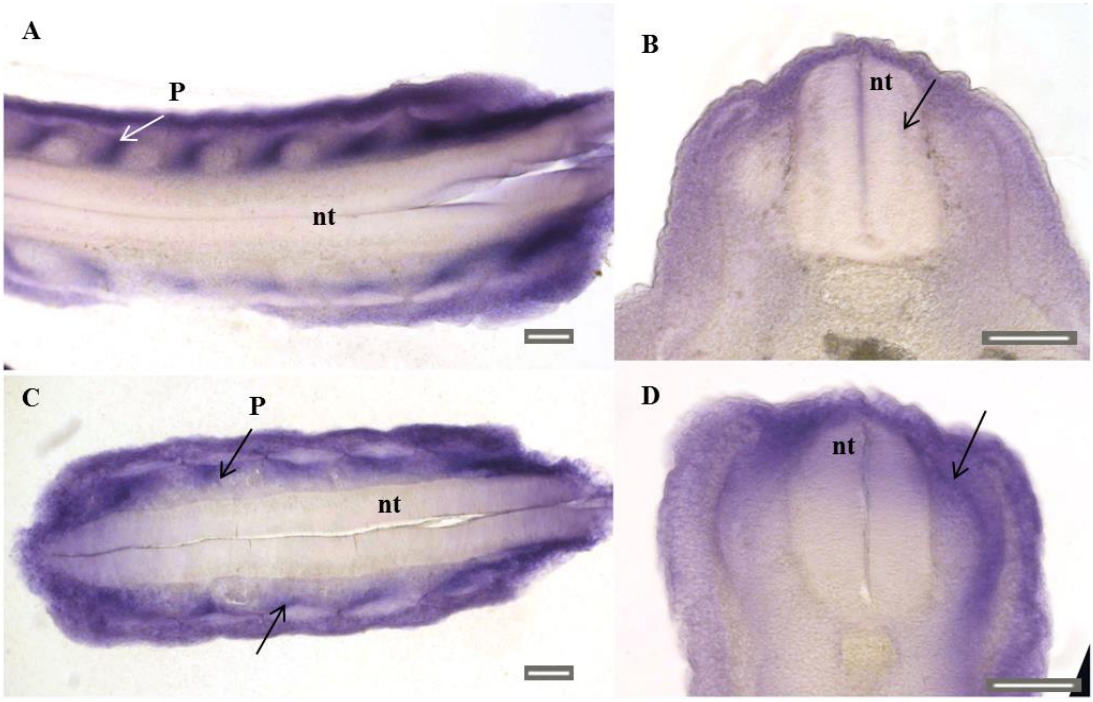

Figure 5.12- Fgfr2 expression is unaffected by *Flrt2* siRNA transfection. (A,B) Coronal (A) and transverse (B) sections at stage 24 HH after scrambled siRNA transfection. Fgfr2 is expressed in the posterior half sclerotome (P), ectoderm, dermomyotome and neural tube (nt). (C) Coronal section of an *Flrt2* siRNA-transfected embryo at stage 24 HH Fgfr2 is expressed in the posterior half-sclerotome and ectoderm. (D) Transverse section of an *Flrt2* siRNA-transfected embryo at stage 24 HH. Fgfr2 is expressed in the ectoderm, dermomyotome and sclerotome (arrow). (P)- posterior sclerotome. (nt)- neural tube. Scale bar: 100 µm.

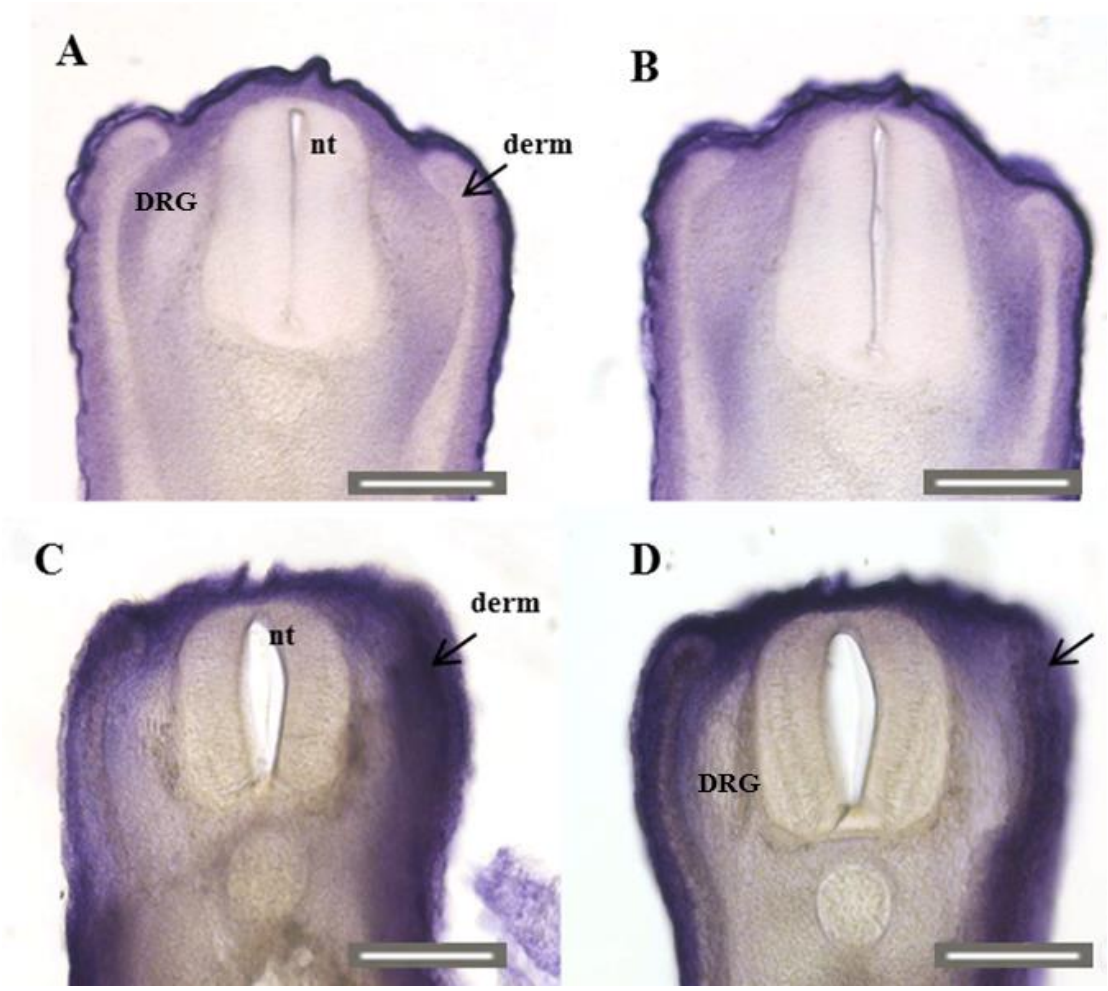

Figure 5.13- Fgfr3 expression in control and *Flrt2* siRNA-transfected embryos. (A,B) Transverse sections of a scrambled siRNA-transfected embryo at stage 24 HH. Fgfr3 is expressed in the ectoderm and sclerotome. (C) Fgfr3 expression in a *Flrt2* siRNA-transfected chick embryo at stage 24 HH. Fgfr3 is expressed in the ectoderm, dermomyotome and posterior half-sclerotome. (D) Fgfr3 expression in *Flrt2* siRNA a transfected chick embryo stage 24 HH. Fgfr3 is expressed in the ectoderm, dermomyotome and dorsal anterior half-sclerotome (identified by presence of DRG). Scale bar: 100 µm.

5.7- Transfection of *Flrt2* siRNA into somites disrupts Flrt3 expression

Flrt2 and *Flrt3* show different expression patterns in mouse somites (*Flrt2* in the posterior sclerotome and *Flrt3* in the dorsal and ventral lips of the dermomyotome; Haines *et al.*, 2006), but they are co-expressed in some regions during craniofacial development (Gong *et al.*, 2009). Furthermore, mice lacking *Flrt3* exhibited abnormalities in headfold closures and definitive endoderm migration (Maretto *et al*

2008). Given abnormal neural tube closure in *Flrt2* siRNA-transfected embryos, I investigated effects on Flrt3 expression by immunostaining 5 *Flrt2* siRNA-transfected and 3 scrambled siRNA-transfected embryos for Flrt3 (Fig. 5.14). In the control embryos, Flrt3 was expressed in the ectoderm and posterior half-sclerotome (Fig. 5.14A,B) (suggesting a difference between expression in chick and mouse; Haines *et al.*, 2006). In two out of the five *Flrt2* siRNA-transfected embryos analysed (Fig. 5.14C-I), Flrt3 expression varied along the embryo (Fig. 5.14C-E) and spots of Flrt3 expression were seen in the dermomyotome (Fig. 5.14F) and sclerotome (Fig. 5.14H). Flrt3 expression was also seen around the neural tube (Fig. 5.14H, I). Although analysis of more embryos is needed to verify this as a real phenotype, these results may suggest that Flrt2 knockdown disrupts Flrt3 expression in the somites.

5.8- Discussion

My results suggest that *Flrt2* is not involved in sclerotome segmentation in chick embryos, as there were no alterations in expression of either the anterior sclerotome marker *Tbx18* (Haenig and Kispert, 2004) or the posterior sclerotome marker *Uncx4.1* (Schrägle *et al*., 2004) after transfecting somites with *Flrt2* siRNA (which reduced *Flrt2* expression in at least some somites in 70% of targeted embryos, where *Flrt2* expression was tested; n=10). *Flrt2* siRNA transfection caused a series of morphological malformations, as well as, most importantly for this study, disturbing the normal spinal axonal pattern in the somites. In summary, *Flrt2* siRNA transfection led to the defasciculation and incorrect growth of axons into the normally repulsive posterior half sclerotome and dermomyotome. Spots of neurofilament staining were also seen in the posterior half-sclerotome after *Flrt2* siRNA transfection: these could represent aberrantly positioned axons in cross-section and/or neural crest-derived DRG neurons, which are normally confined to the anterior sclerotome. Given that shed ectodomains of Flrt2 (and Flrt3) had previously been found to repel Unc5D-expressing axons and neuronal cell bodies of cortical neurons (Yamagishi *et al*., 2011), my study suggests that Flrt2 could be involved in repelling spinal axons (and perhaps also neural crest-derived DRG neurons) from the posterior sclerotome, as discussed further below.

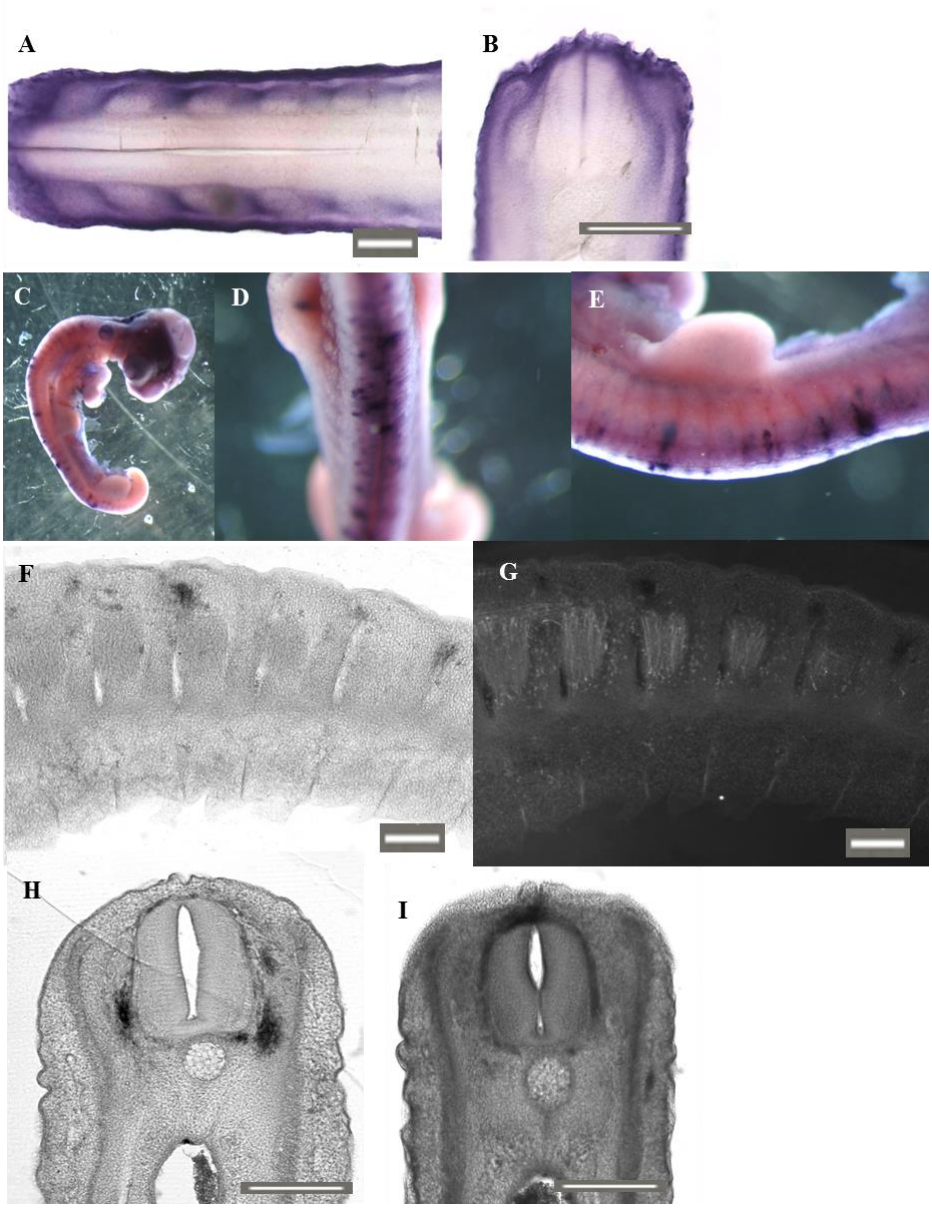

Figure 5.14- Flrt3 expression is altered by *Flrt2* siRNA transfection. (A) Flrt3 expression in a scrambled siRNA-transfected embryo at stage 22 HH. Flrt3 is expressed in the ectoderm and posterior half-sclerotome. (B) Transverse section of a scrambled siRNA-transfected embryo at stage 22 HH. Flrt3 is expressed in the ectoderm and dorsolateral sclerotome. (C) Whole-mount view of Flrt3 expression in a *Flrt2* siRNA-transfected embryo at stage 22 HH. (D) Dorsal higher magnification view of the embryo in C, showing variable Flrt3 expression between limb levels. (E) Lateral view of the embryo in C, showing the variable Flrt3 expression within the somites. (F) Section showing Flrt3 expression in a *Flrt2* siRNA-transfected embryo. Flrt3 is not expressed in all somites and appears confined between the dermomyotome and anterior half-sclerotome. (G) Neurofilament immunostaining of the section in F. Axons appear to exit segmentally through the anterior half-sclerotome normally, however, some spots of neurofilament staining are present in the posterior half-sclerotome. (H,I) Transverse sections of the embryo in C. Flrt3 is expressed in medial sclerotome around the neural tube and in cells at the top of the neural tube. Scale bar: 100 µm.

Flrt2 siRNA-transfected chick embryos presented abnormalities in spinal axon trajectories at thoracic levels, where some axons were present in the posterior half sclerotome by longitudinal sprouting as well as axonal sprouting in the junction of sensory and motor axons (Fig. 5.7). Normally spinal axons are restricted to the anterior half sclerotome through the expression of repulsive molecules from the surrounding structures, such as Sema3A that is secreted from the notochord, neural tube and dermomyotome to prevent axons from entering these medial and lateral tissues inappropriately (Anderson *et al*., 2003). Similarly, Sema3A and Sema3F together help repel spinal axons from the posterior half sclerotome (Roffers-Agarwal and Gammill, 2009). In *Flrt2* siRNA-transfected embryos, axons start to sprout into many of these tissues including the posterior half-sclerotome, myotome and neural tube (Fig. 5.7), similar to the phenotype obtained in *Sema3A* knockout mice (Anderson *et al*., 2003). These results suggest that Flrt2 could act as a chemorepellent for spinal axons, as it does for Unc5D-expressing cortical axons and neuronal cell bodies (Yamagishi *et al.*, 2011). In the embryos where such a phenotype was visible, the morphology of the dermomyotome and notochord were also modified (see later), suggesting that *Flrt2* expression might be necessary to regulate cell adhesion and tissue morphogenesis, resulting in the incorrect formation of these structures which may later result in inactivation of the expression of secreted repulsive molecules.

Another abnormality in *Flrt2* siRNA-transfected embryos was the presence of spots of neurofilament staining in the posterior sclerotome (Fig. 5.7-5.8). This staining pattern might reflect aberrantly positioned axon bundles in cross-section, or neural crest-derived DRG neurons, which are also normally confined to the anterior half-sclerotome. DRG neurons start to differentiate as early as E3 in the chick (Marusich, 1993), and the siRNA-transfected embryos were collected around stage 22-24 HH (E3.5-4). It is possible that Flrt2 repels migrating neural crest cells as well as spinal axons in chick embryos, or that it helps confine differentiated DRG neurons to the anterior sclerotome. Testing these hypotheses would require confirmation of what the spots of neurofilament staining in the posterior sclerotome represent. It would have been interesting therefore to investigate the expression of the neurogenic transcription factor genes *Neurogenin1* or *Neurogenin2* in *Flrt2* siRNA-transfected embryos, as these are expressed in and required for the differentiation of DRG neurons (Ma et al., 1999). If

they were also present in the posterior sclerotome, it would confirm that the spots of neurofilament expression indeed represent aberrantly positioned neural crest-derived DRG progenitor cells.

Another effect of *Flrt2* siRNA transfection was variation in somite size and disturbed neural tube closure (Figs. 5.6, 5.8 and 5.9). Somite size is controlled by Fgf8 signalling in the PSM (Dubrulle and Pourquié, 2004), and the results obtained in this study are similar to that obtained by grafting beads soaked in Fgf8 at the level of the neural tube, which results in a shift of somite borders and twisting of the neural tube mediated through Pax6 inactivation (Bertrand *et al*., 2000). Fgf8 suppression in the PSM also results in the shift of somite boundaries and changes in the number of cells per somite (Dubrulle *et al*., 2004). It is possible that Flrt2 acts downstream of FGF8 to control somite size in chick embryos, but further experiments would be required to test this possibility.

At stage 14 HH, *Flrt2* is weakly expressed in the notochord and neural tube with stronger expression in the myotome and posterior half-sclerotome (also see section 3.14). With further development, *Flrt2* expression becomes restricted to the posterior half sclerotome. *Flrt2* siRNA transfection of PSM cells and sclerotome in chick embryos at stages 10-13 HH resulted in an abnormal notochord, somites and neural tube morphology at vagal and thoracic levels. This corresponds to approximately eight already formed somites plus nine still to be formed from the PSM at the time of transfection. The reduction of mRNA expression in non-targeted somites suggests that transfection affected more tissues than just sclerotome. *Flrt2* would be expressed on the notochord on time of transfection, and that might have interfered with cell-cell adhesion properties and resulted in abnormal notochord morphology. Notochord rigidity maintains the embryonic alignment of axial tissues during development and embryo elongation (Cleaver and Krieg, 2001). The peri-notochordal sheath, an extracellular matrix surrounding the notochord, provides its epithelial configuration, and constrains it physically into an axially positioned rod (Carlson and Kenney, 1980). As some *Flrt2* siRNA-transfected embryos appeared to have little confinement of the notochord to an axial rod, it is possible that the integrity of the peri-notochordal sheath was lost. Such notochord abnormalities cause defects in embryo development. For example in

zebrafish, the notochord is required for the development of the heart and its vasculature (Goldstein and Fishman, 1998) and in chick it is also important for the formation of the dorsal aorta (Fouquet *et al*., 1997). It is therefore possible that the altered notochord morphology in *Flrt2* siRNA-transfected embryos might be responsible for some of abnormalities observed in body vasculature and heart formation, but further studies would be required to test this effect.

Besides its role in heart and vasculature formation, the notochord also plays an important role in patterning the ventral neural tube, including the formation of the floor plate (Stemple, 2005; Placzek *et al*., 1991; Cleaver and Krieg, 2001). Among the signals that the notochord secretes is Sonic hedgehog (shh) that together with Shh from the floorplate induces a signalling gradient to pattern the ventral neural tube. Neural tube patterning can be divided into two regulative mechanisms: dorsally the neural tube is regulated by TGF-β/BMP signalling and ventrally by Shh signalling (Muroyama *et al*., 2002). The defects shown by *Flrt2* siRNA-transfected embryos are present in the dorsal neural tube and not in the floor plate (Fig.5.9), however, suggesting that Shh signalling was not affected. The neural tube defects included in a small percentage of *Flrt2* siRNA-transfected embryos, the appearance of possessing multiple neural tubes. After immunostaining for neurofilament and sectioning, the phenotype appear to emerge from the extension of sensory axons beyond the midline, where they joined together on the roof plate forming new neural tube (Fig. 5.9). Axons are prevented from crossing the neural tube midline due to the balance kept by Slit/Robo signalling (Long *et al*., 2004). Slit genes are also expressed in the notochord and neural tube where they contribute to the repulsion of spinal motor column axons (Giovannone *et al.,* 2012; De Bellard *et al.*, 2003). It would have been interesting to study whether Flrt2 has any interaction with any Slit and Robo family members.

Flrt2 interaction with Fgf receptors in chick embryos was not very conclusive, it appears that *Flrt2* knockdown only had an apparent impact on the Fgfr1 receptor, slightly reducing its expression in the sclerotome and causing it to be expressed in the myotome (Fig. 5.11). More embryos need to be tested to confirm this as a real phenotype. The slightly increased expression of Fgfr3 might be due to over-development of the alkaline phosphatase colour reaction. Previous observations on the

interaction of Flrts with Fgf receptors are not clear: knockout studies in mice suggested that Flrts do not affect Fgf signalling (Müller *et al*., 2011), however Wei *et al.* (2011) showed that Fgfr2 expression decreases in *Flrt2* shRNA-transfected cells. In order to understand Flrt2 interaction with Fgf receptors in chick embryos, further assays would have been necessary. Flrt3 expression in *Flrt2* siRNA-transfected chick embryos was greatly reduced, leaving variable punctate spots of expression in the somites. However, this was only verified in a small percentage of the Flrt3-immunostained embryos, and it would be necessary to do do other assays like Western blots to quantify levels of Flrt3 expression in transfected embryos so that we could understand if Flrt2-Flrt3 interactions in chick embryos.

Finally, *Flrt2* siRNA transfected embryos collected at later stages showed a slight bend of the vertebral bodies at tail level, as analysed by Alcian blue staining for cartilage. Since I showed that *Flrt2* is expressed in the neural arch and vertebral body (section 3.14), this might reflect a late requirement for Flrt2 in vertebral body development. The Alcian Blue staining also seemed stronger, which is consistent with an *in vitro* study showing that reduction in *Flrt2* increases cell-cell interaction and leads to a thicker chondrocyte matrix (Wei *et al*., 2011). However, these experiments would need to be repeated and further analysis undertaken to confirm that these phenotypes were consistent and specific.

5.9- Conclusion

The results of my *Flrt2* siRNA transfection study suggest that the glycosylated transmembrane protein Flrt2 may be involved, directly or indirectly, in repelling spinal axons (and perhaps also migrating neural crest cells and/or neural crest-derived DRG neurons) from the posterior sclerotome. To confirm the specificity of these and the other phenotypes described, it would be important to try to rescue *Flrt2* expression in siRNA-transfected embryos, and/or to use mismatch siRNAs instead of scrambled siRNA as a negative control (Buehler *et al.*, 2012). It would also be of interest to transfect *Flrt2* siRNA at earlier time points (e.g. stage 3-4 HH) to determine the role of Flrt2 in early and to perform gain-of-function experiments as well by transfecting an expression vector encoding full-length Flrt2 into somites.

CHAPTER 6- EXPRESSION OF O-GLYCOSYLATION ENZYMES IN THE CHICK EMBRYO

6.1- Background

Mucin-type O-glycosylation is a common covalent modification at serine and threonine residues in eukaryote glycoproteins (Bennett *et al.*, 2012; Tran and Ten Hagen, 2013). The UDP-GalNAc:polypeptide*N*-acetylgalactosaminyltransferase (ppGalNAc-T) family of enzymes is responsible for mucin-type O-glycosylation in animals (Bennett *et al.*, 2012; Tran and Ten Hagen, 2013). Mucin-type O-glycosylation events are necessary during development (Tabak, 2010; Tran and Ten Hagen, 2013), for instance for the Notch signalling pathway during somitogenesis (Haines and Irvine, 2003), while three ppGalNAc-T family members proved to be vital for *Drosophila* viability (Tran *et al.*, 2012). Importantly for this study, there is a significant contribution of mucin-type O-glycosylation (Dr. G. Cook, personal communication) to the peanut agglutinin (PNA)-binding axonal repellent activity in posterior half-sclerotomes (Stern *et al.* 1986; Davies *et al.*, 1990). Hence, it is possible that an O-glycan-bearing glycoprotein is responsible for this activity, and that the ppGalNAc-T enzyme responsible for the biosynthesis of the O-glycan-bearing axonal repellent will also be differentially expressed in the posterior half-sclerotome. Fluorescently-labelled PNA, which specifically binds to the alpha-linked galactose on T antigen (Chacko and Appukuttan, 2001), segmentally binds to the posterior half sclerotomes of the somite (Stern *et al.*, 1986). PNA binding inhibits the activity of the axonal repellent present in the posterior sclerotome (Davies *et al.* 1990) and also allows migrating neural crest cells to enter this normally inhibitory environment (Krull *et al*. 1995). PNA binding, together with chondroitin-6-sulfate expression, labels tissues that act as barriers to axon advance in chick embryos (Oakley and Tosney, 1991). Given this, all the glycosylation events in the posterior half-sclerotome are of great interest, but they are still poorly understood.

ppGalNAc-Ts transfer an N-acetylgalactosamine (GalNAc) residue from the sugar donor, UDP-GalNAc, to serines and threonines in proteins to form the T-antigen (Thomsen-Friedenreich antigen) and initiate O-glycosylation (Young *et al*., 2003) (Fig. 6.1). Further modification of O-GalNAc glycans by O-acetylation of sialic acid and O-sulfation of galactose and N-acetylglucosamine, leads to structural heterogeneity. T antigen is recognised by PNA (Ravishankar *et al*., 1999). Large mucin glycoproteins

also share many lectin-binding domains through the presence of numerous GalNAc-linked saccharides (Raman at al., 2008).

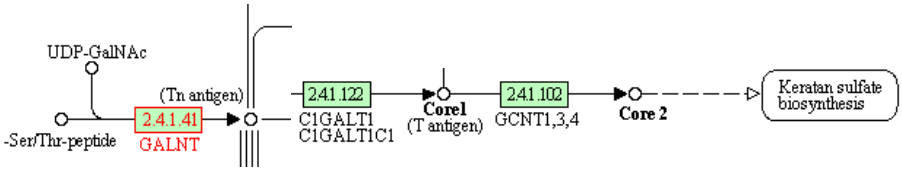

Figure 6.1- The mucin-type O-glycan biosynthesis pathway for the chicken, *Gallus gallus*. T antigen formation is highlighted. Figure obtained from the Kyoto Encyclopedia of Genes and Genomes (KEGG) database.

The 20 human *GALNT* genes can be grouped into closely related subfamilies (Fig. 6.2; Bennett *et al.*, 2012). Subfamily I members mostly have peptide substrate specificity; subfamily II members mostly have GalNAc-glycopeptide substrate specificity (Bennett *et al.*, 2012). This nomenclature (group I versus group II) does not reflect the relatedness of the different subfamily groups, however: for example, subfamily IIa (*GALN-T4/T12*) clusters with subfamily Ig (*T15*) and Ic (*T3/T6*).

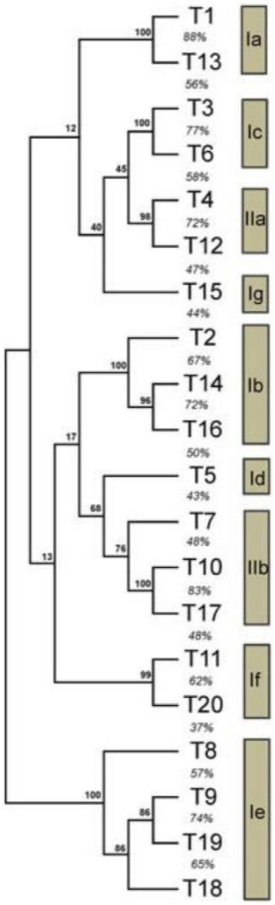

Figure 6.2- Phylogenetic tree of human *GALNT* genes. Figure from Bennett *et al.* (2012).

The ppGalNAc-T family is highly conserved throughout animal evolution (Fig. 6.3; Bennett *et al.*, 2012) but absent in bacteria, yeast and plants. The expression patterns of seven mouse *Galnt* (genes (*Galnt1-5, Galnt7* and *Galnt10*) were documented in the embryonic nervous system, neural crest and tongue (Kingsley *et al*., 2000). [Note: *Galnt10* was published in this paper as *Galnt9*, but this gene is now designated as *Galnt10* (Bennett *et al.*, 2012).] Expression data for some mouse *Galnt* genes are also available from the Eurexpress website (http://www.eurexpress.org) (Diez-Roux *et al.*, 2011). Only a single study, the differential microarray screen of Hughes *et al.* (2009), has identified a *Galnt* gene as being differentially expressed in the posterior sclerotome: *Galnt4*. However, it should be noted that this expression was not reported in the *in situ* hybridization data from Kingsley *et al.* (2000). Unfortunately, the *Galnt4* gene was lost in the chicken lineage during evolution (see Fig. 6.3; Bennett *et al*., 2012). (The *Galnt8* gene from subfamily Ie, and the *Galnt20* gene from subfamily If, were also lost in the chicken lineage, hence the existence of 17 *Galnt* genes in chicken instead of the 20 present in human; Fig. 6.3; Bennett *et al.*, 2012.) *Galnt4* is a member of subfamily IIa, which also contains *Galnt12* (Bennett *et al*., 2012). According to the phylogenetic tree in Fig. 6.2 (Bennett *et al.*, 2012), human *GALNT* subfamily IIa (*T4* and *T12*) is most related to subfamily Ig (*T15*) and then subfamily Ic (*T3* and *T6*), within a larger cluster containing subfamily Ia (*T1* and *T13*). However, this information about subfamily groupings was not available at the time the expression study was performed.

To address whether any *Galnt* genes are expressed in the posterior half-sclerotome in chick, the first aim was to identify chick *Galnt* genes for use in whole-mount *in situ* hybridization experiments (WMISH). Several *Galnt* genes are responsible for O-glycan synthesis (Kyoto Encyclopaedia of Genes and Genomes, KEGG; Kanehisa *et al.*, 2012; Kanehisa *et al.*, 2000) (Fig. 6.2). In Fig. 6.1, "2.4.1.41" corresponds to GalNAc-Ts: T14; T13; T12; T11; T10; T9; T7; T6; TL6; T5; TL4; T3; T2; TL2; T1; TL1 and Williams-Beauren syndrome chromosome region 17 (WBSCR17). Fig. 6.1 shows that mature T antigen is represented by Core 1 glycosylation, synthesised by enzyme 2.4.1.122, corresponding to Core 1 synthase, glycoprotein-N-acetylgalactosamine-3-beta-galactosyltransferase (C1GalT1), with its chaperone, C1GalT1C1.

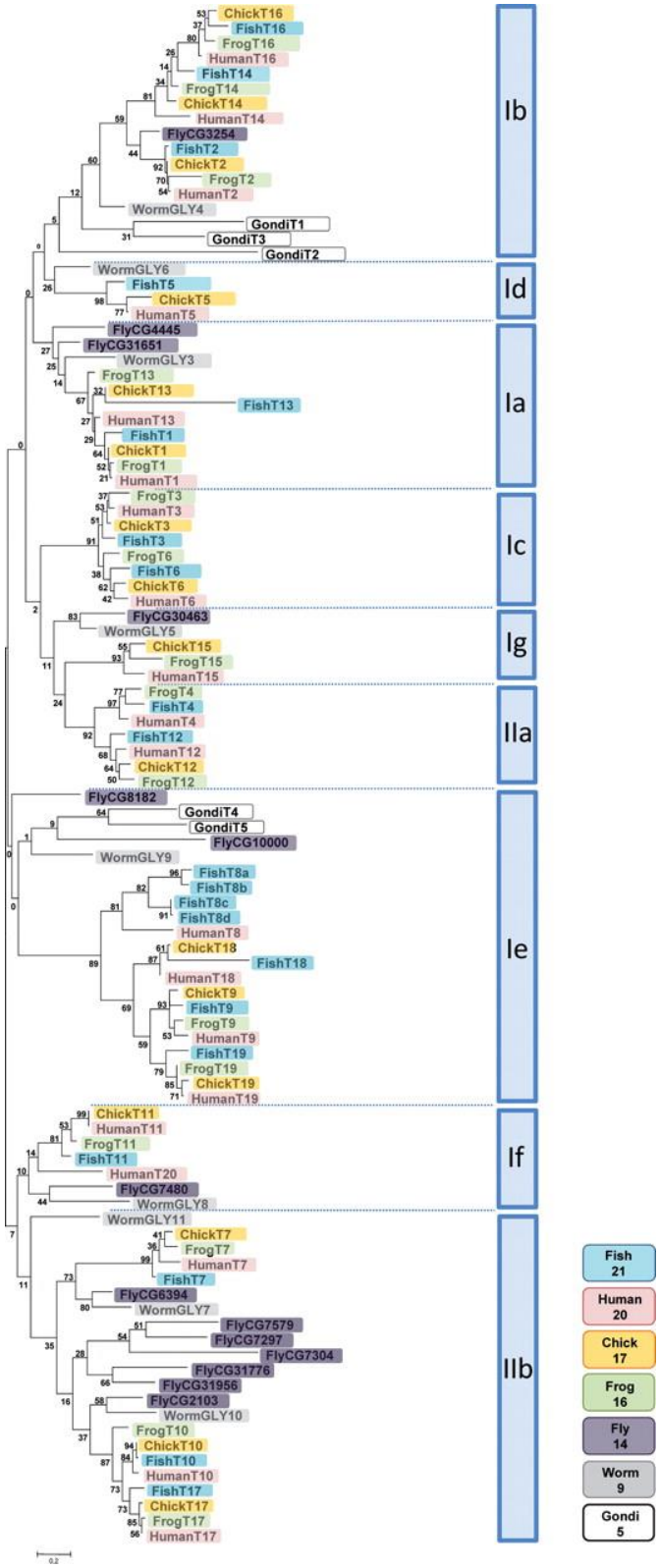

Figure 6.3- Phylogenetic tree of animal ppGalNAc-Ts. ppGalNAc-T4, encoded by *Galnt4* and reported in the posterior half-sclerotome (Hughes *et al.*, 2009) is in subfamily IIa. The number of *Galnt* genes identified in each species is indicated on the right. Figure from Bennett *et al.* (2012).

6.2- Identifying candidate chick *Galnt* genes for expression analysis

As described in the preceding section, the mouse microarray screen detected *Galnt4* as being present in the posterior half sclerotome (Hughes *et al.*, 2009). A nucleotide BLAST of mouse *Galnt4* (*T4*) to the chick database using NCBI software (http://blast.ncbi.nlm.nih.gov/Blast.cgi) did not reveal any homologous sequences, but a BLAST of the amino acid sequence revealed that several chick ppGalNAc-Ts are similar to the mouse ppGalNAc-T4 (T4) protein (Fig. 6.4). ppGalNAc-T12 showed the greatest similarity with mouse ppGalNAc-T4 (consistent with ppGalNAc-T4 and T12 forming ppGalNAc-T subfamily IIa; Figs. 6.2 and 6.3), followed by T6 then T3 (i.e., subfamily Ic), then T1 and T13 (i.e., subfamily Ia) (Fig. 6.4). These similarities are consistent with the relationships of human *GALNT* genes (Fig. 6.2; Bennett *et al*., 2012). While chick ppGalNAc-T12 showed the greatest conservation to mouse T4 (and human T4; Fig. 6.3), there was much sequence heterogeneity across the family. For this reason, the attempt was made to study the expression of as many chick ppGalNAc-T gene family members as possible.

The whole-mount *in situ* hybridization (WMISH) data for chick *Galnt* genes were generated using essentially the same protocol as described in sections 2.2 and 2.3. Primers designed for these experiments are described in Appendix B. For clarity, each gene analysed is introduced followed by a description of its expression pattern. The first gene described is the core 1 synthase gene, followed by the various *Galnt* genes in order of their similarity with mouse *Galnt4* by BLAST, keeping subfamilies together.

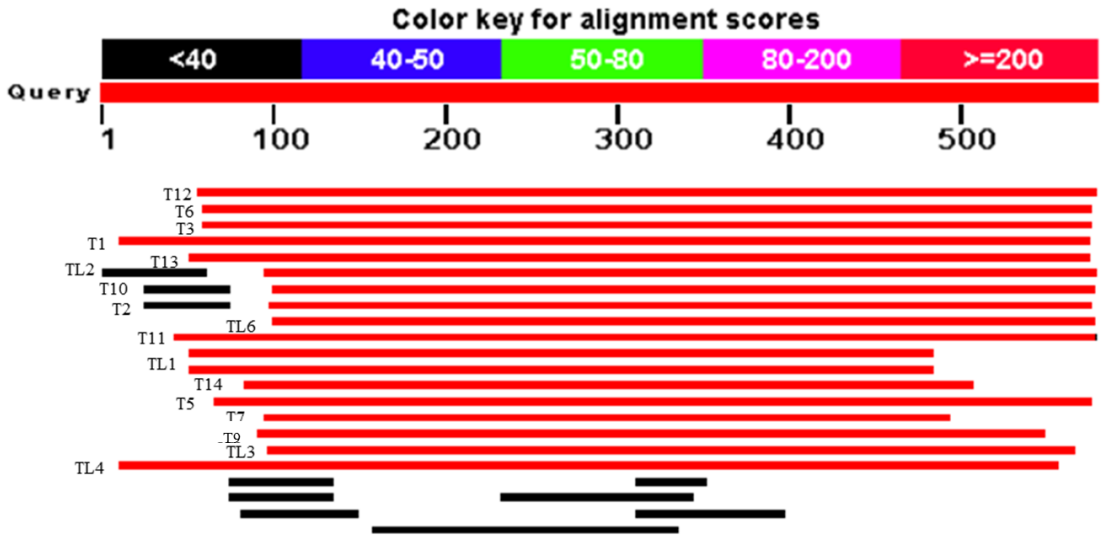

Figure 6.4- Amino acid alignment of mouse ppGalNAc-T protein T4 to the chicken (*Gallus gallus*) database. Figure generated from the NCBI website BLAST tool (http://blast.ncbi.nlm.nih.gov/Blast.cgi).

6.3- *C1GalT1*

C1GalnT1 (core 1 synthase, glycoprotein-N-acetylgalactosamine-3-beta-galactosyltransferase) is responsible for the transfer of the galactose from UDP-Gal to serine/threonines on Tn antigen to form the final T-antigen, Galβ1-3GalNAc, also called Core 1 (Tabak, 2010). In *Drosophila*, *C1GalT1* is expressed in the embryonic CNS and embryonic hemocytes, and it is of note that it shows a distinct anterior-posterior pattern of expression in imaginal discs that corresponds to the separation of the axons until stage 13 (Lin *et al*., 2008). *C1GalT1* ablation in *Drosophila* causes an elongation of ventral nerve cord and distortion of the brain hemispheres related to defects in ECM deposition by hemocytes, which is required for ventral nerve cord condensation (Lin *et al*., 2008), however there was no distortion in axon exit from the nerve cord (Yoshida *et al*., 2008), suggesting that another *Galnt* gene may be responsible for the formation of T antigen. However, there may be some role for C1GalT1 in T antigen production, perhaps with other ppGalNAc-Ts, as reduction in *C1GalT1* leads to partial loss of T antigen (Yoshida *et al*., 2008).

Fig. 6.5 shows chick *C1GalT1* expression at HH stages 17, 19 and 25. Interestingly, *C1GalT1* appears to show differential expression in anterior versus posterior half-somites. *C1GalT1* is only expressed weakly at stage 17 HH (Fig. 6.5A,B), and although somite expression was seen at stage 19 HH (Fig. 6.5C-E), restriction to the anterior half-somite was most apparent at stage 25 HH (Fig. 6.5F-H). Sections would be required to confirm the specific location of expression, i.e., sclerotome, DRG or myotome. *C1GalT1* expression in the limb buds (Fig. 6.5F-H) is probably in the pre-muscle mass, suggesting that *C1GalT1* could be involved in limb musculature formation, perhaps in cells migrating from myotome to the limbs. Since *C1GalT1* did not seem to be expressed in the posterior half sclerotome, further studies were not done.

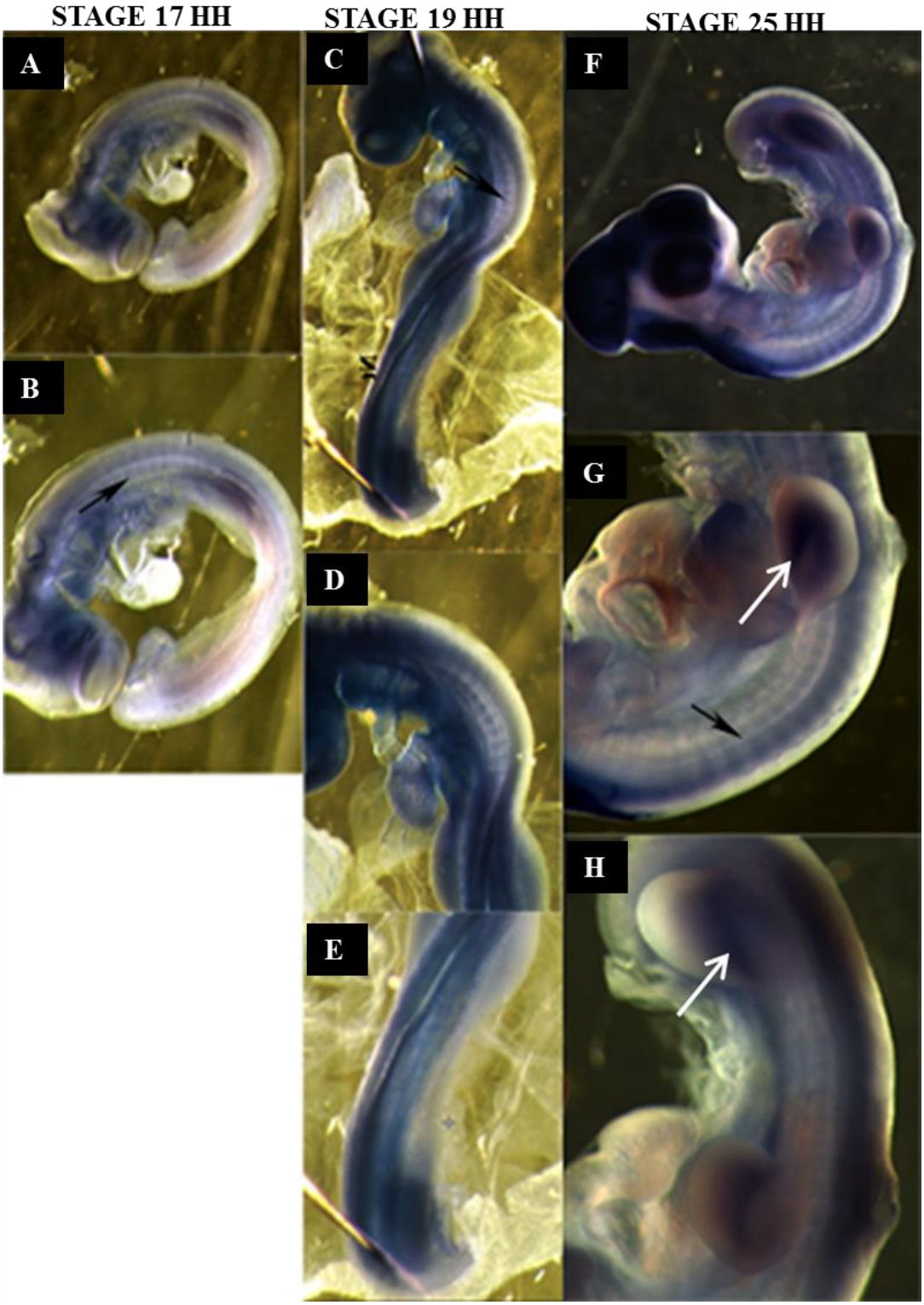

Figure 6.5- WMISH for *C1GalT1*. (A,B) Embryo at stage 17 HH. *C1GalT1* is weakly expressed on the dorsal lateral somites (arrow). (C-E) Embryo at stage 19 HH. *C1GalT1* is possibly expressed in the somites and in the neural tube. (F-H) Embryo at stage 25 HH. *C1GalT1* is expressed in the anterior half of the somites (black arrow) and in the limb buds (white arrow). Head staining was considered to be background.

6.4- *Galnt12* (subfamily IIa)

Chick ppGalNAc-T12, encoded by *Galnt12*, groups together with ppGalNAc-T4 in the IIa subfamily of ppGalNAc-Ts (Figs. 6.2 and 6.3; Bennett *et al.*, 2012). As described in section 6.2 (Fig. 6.4), my BLAST search showed that ppGalNAc-T12 is the most similar chick protein to mouse ppGalNAc-T4, whose mRNA was identified in the posterior sclerotome by Hughes *et al.* (2009) in their differential microarray screen.

Young Jr. *et al*. (2003) found using real-time PCR that *Galnt12* (*T12*) is strongly expressed in the adult mouse sublingual gland, and weakly in the colon, spleen, thymus, testis and lung. In humans it is present in brain, lung and muscle (Bennett *et al.*, 2012).

Fig. 6.6 shows the expression of *Galnt12* in chick embryos at HH stages 22 and 25. At stage 22 HH, *Galnt12* is expressed in the floor plate of the neural tube and in the notochord, although not in the perinotochordal sheath (Fig. 6.6A-D). It is also expressed in the myotome (Fig. 6.6C,D), which explains its expression in whole-mount in the anterior half of the somite at stage 25 HH (Fig. 6.6E-G). *Galnt12* is also weakly expressed in the mesonephros (Fig. 6.6H,I) and in thin stripes that could represent axons of the dorsal root ganglia or perhaps blood vessels (Fig. 6.6H,I).

The notochordal expression of *Galnt12* was interesting (although it was in the centre, rather than in the sheath; Fig. 6.6D) because PNA binds the axon-repelling peri-notochordal ECM and mesenchyme (Tosney and Oakley, 1990; Oakley and Tosney, 1991). However, it was not expressed in the posterior sclerotome so not studied further.

Figure 6.6- (On next page) Embryos and sections after WMISH for chick *Galnt12*. (A,B) Low and higher power views of embryo at stage 22 HH. *Galnt12* is expressed in the neural tube (white arrow) and heart. (C,D) Transverse sections at stage 22 HH. *Galnt12* is expressed in the myotome (black arrow), floor plate (red arrow) and notochord (green arrow). (E,F) Low and higher power views of embryo at stage 25 HH. *Galnt12* is expressed in the neural tube (white arrow), and in the anterior half of the somite (black arrow). (G) Longitudinal section of embryo at stage 25 HH. *Galnt12* is expressed in the middle of the somite (black arrow). (H,I) Low and higher power views of longitudinal section at stage 25 HH, *Galnt12* is expressed in the mesonephros (black arrow) and in stripes that could be axons or perhaps blood vessels. Scale bar: 100 μm.

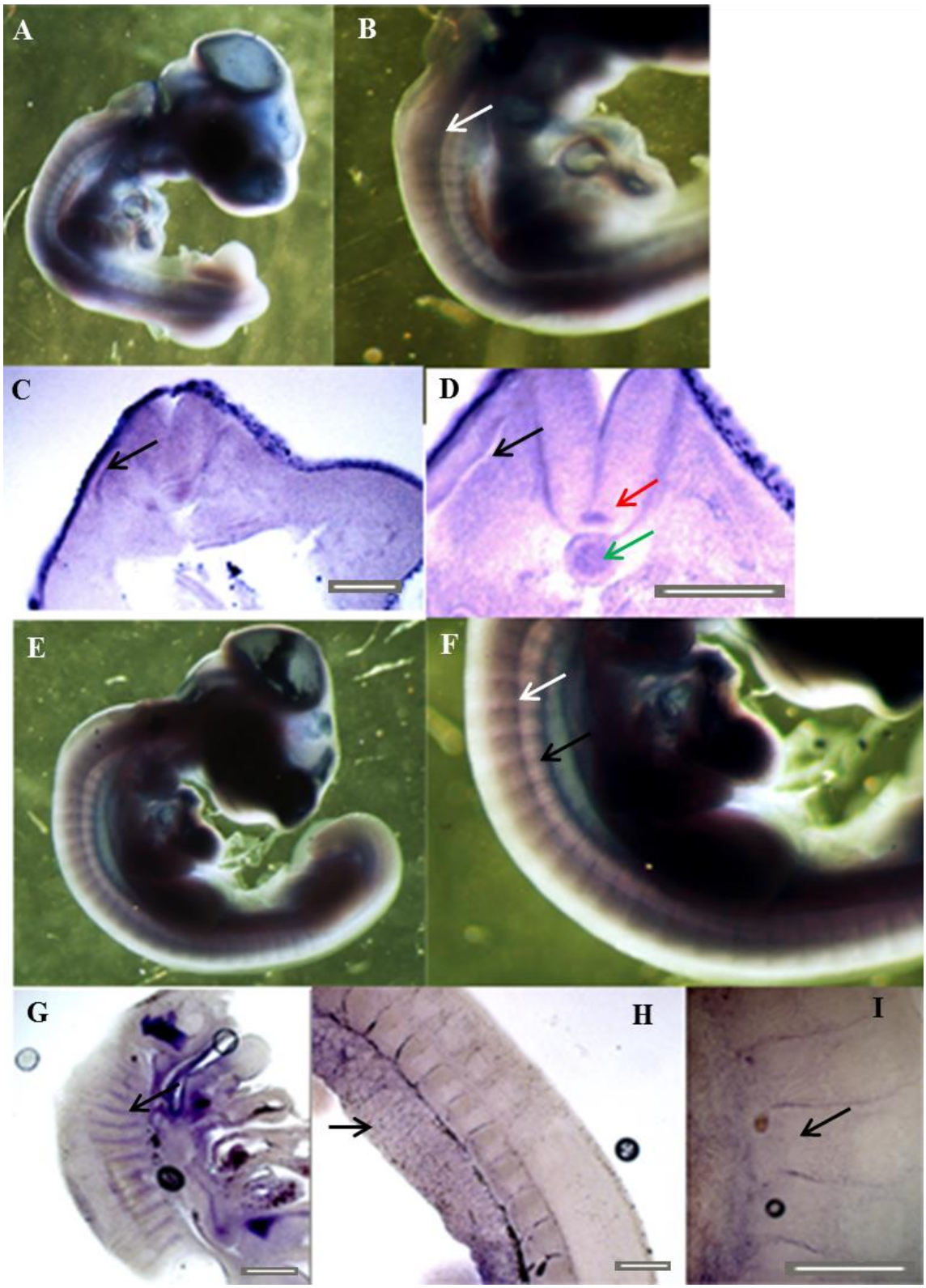

Figure 6.6- Legend on previous page.

6.5- *Galnt6* (subfamily Ic)

ppGalNAc-T6, encoded by *Galnt6*, is in the Ic subfamily, together with ppGalNAc-T3 (Fig. 6.2, 6.3; Bennett *et al.*, 2012). My BLAST search ranked ppGalNAc-T6 as the second most similar chick protein to mouse ppGalNAc-T4 (Fig. 6.4). Fig. 6.7 shows a detail from the phylogenetic tree of human *GALNT* genes (Bennett *et al.*, 2012; for the full tree, see Fig. 6.2), showing that the Ic subfamily (*GALNT6* and *GALNT3*) is sister group to subfamily IIa (*GALNT4* and *GALNT12*).

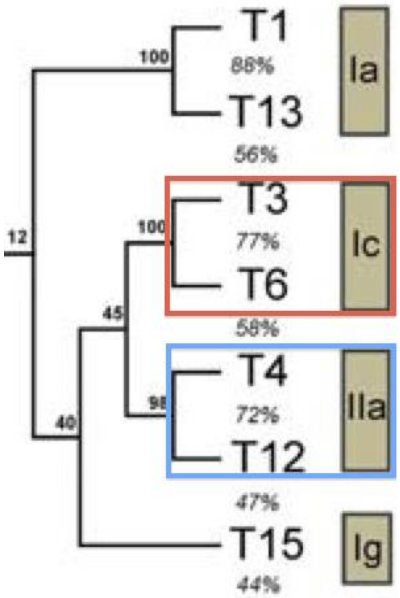

Figure 6.7- Detail from phylogenetic tree of human *GALNT* genes. *GALNT6* and GALNT3 are in subfamily Ic, the sister group to subfamily IIa, which contains *GALNT4* and *GALNT12*. The percentage values refer to the percentage amino acid identities of the catalytic domains between proteins. Figure adapted from Bennett *et al.* (2012).

Human *GALNT6* has been reported in human placenta, trachea (Bennett *et al.*, 1999), brain, cervix, kidney, lung, muscle and nerves (Bennett *et al.* 2012). Mouse *Galnt6* is not present at significant levels in adult tissues by real-time PCR (Young Jr.*et al.*, 2003). At E14.5, Eurexpress reports specific *Galnt6* expression in the sympathetic ganglia (http://www.eurexpress.org/ee/databases/assay.jsp?assayID=euxassay_009167).

Fig. 6.8 shows chick *Galnt6* expression at HH stage 25. (I was also able to detect *Galnt6* by RT-PCR at stage 22 HH.) It is expressed strongly in the limb buds, as well as in the dermomyotome and DRG, giving a segmental expression in whole-mount (Fig. 6.8A-D). Ventral somite expression in whole-mount (Fig. 6.8B) might be sympathetic ganglia, as reported at E14.5 for mouse (see above). It is also expressed in the neural tube at both brain and spinal cord levels (Fig. 6B,C,E-G). Given the absence of expression in the posterior half sclerotome, further studies were not done.

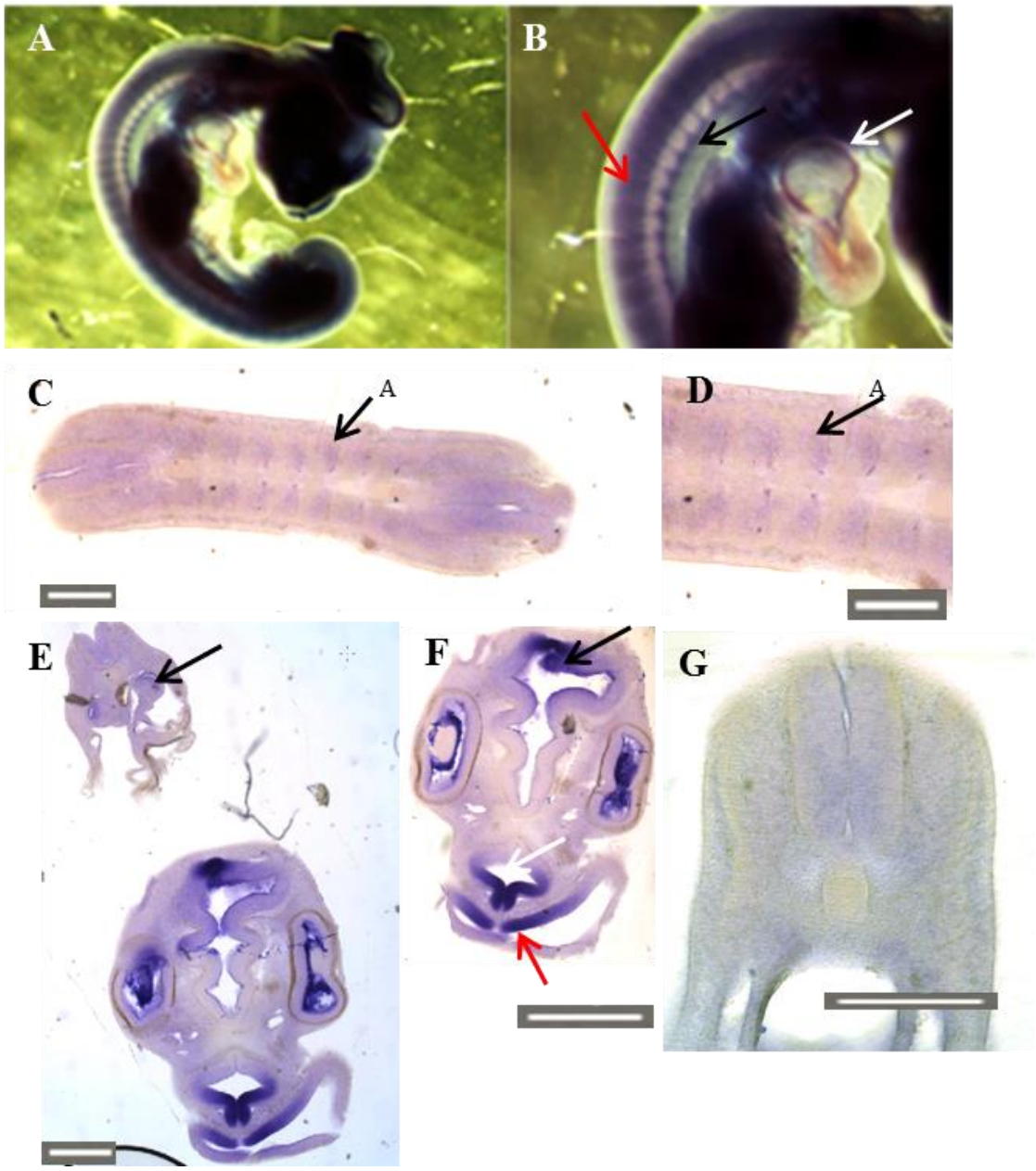

Figure 6.8- Stage 25 HH embryo and sections after WMISH for *Galnt6*. (A,B) Low and higher power views in whole-mount. *Galnt6* is expressed in the limb buds, heart atrium (white arrow), ventral somite (black arrow) and neural tube (red arrow). (C,D) Low and higher power views of longitudinal section. *Galnt6* is expressed in DRGs, dermomyotome and the neural tube. (E) Transverse section showing trunk and eye levels. *Galnt6* is expressed in the nephric duct (black arrow). (F) Higher power view of head section in E. *Galnt6* is expressed in different regions of the brain (different colour arrows). (G) Transverse section at trunk level. *Galnt6* is expressed in the neural tube and dorsal dermomyotome. Scale bar :100 µm.

6.6- *Galnt3* (subfamily Ic)

ppGalNAc-T3, encoded by *Galnt3*, is the other member of the Ic subfamily of ppGalNAc-Ts, with ppGalNAc-T6 (see Fig. 6.7; Bennett *et al.*, 2012). My BLAST search ranked ppGalNAc-T3 as the third most similar chick protein to mouse ppGalNAc-T4 (Fig. 6.4). *Galnt3* is expressed in the testis and sublingual gland, and in later pregnancy in mouse (Young Jr.*et al*., 2003; Ten Hagen *et al.*, 2003), and in human testis and pancreas (Bennett *et al.*, 1999).

Fig. 6.9 shows chick *Galnt3* expression at HH stages 19 and 26. *Galnt3* may have a function in CNS development, as it appears to be expressed in the midbrain, hindbrain and floor plate at stage 19 HH (Fig. 6.9A,B), extending further within the neural tube by stage 26 HH (Fig. 6.9C,D). Transverse sections would be necessary to confirm this, however. *Galnt3* is strongly expressed in the limb buds (Fig. 6.9A-D) and weakly expressed in the anterior half of the sclerotome (Fig. 6.9B-D), possibly myotome since it also seems to be expressed in limb musculature (Fig. 6.9D). Furthermore, *Galnt3* is expressed in the pharyngeal arches (future jaws). *Galnt3* is not expressed in the posterior half sclerotome so was not pursued further.

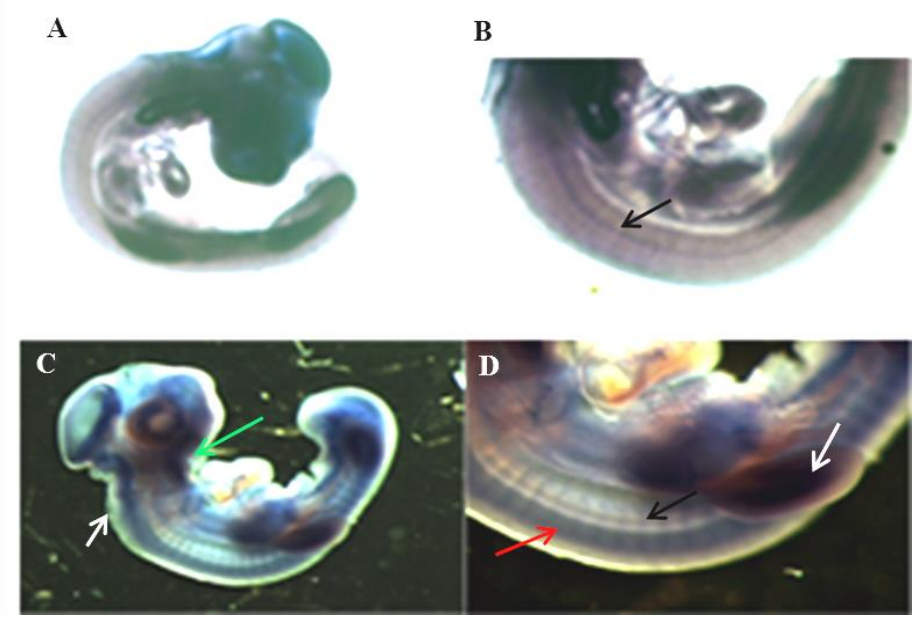

Figure 6.9- WMISH for *Galnt3*. (A,B) Low and higher power views of a stage 19 HH embryo. *Galnt3* is expressed in limb buds, brain and floor plate (arrow in B). (C,D) Low and higher power views of a stage 26 HH embryo. *Galnt3* is expressed in the midbrain, hindbrain (white arrow) and neural tube (red arrow), pharyngeal arches (green arrow), limb buds (white arrow) and anterior somite (black arrow).

6.7- *Galnt1* (subfamily Ia)

ppGalNAc-T1, encoded by *Galnt1*, is in the Ia subfamily of ppGalNAc-Ts together with ppGalNAc-T1 (Bennett *et al.*, 2012). My BLAST search ranked ppGalNAc-T1 as the fourth most similar chick protein to mouse ppGalNAc-T4 (Fig. 6.4). Fig. 6.10 shows the relationship of the human Ia subfamily to the IIa subfamily containing *GALNT4*.

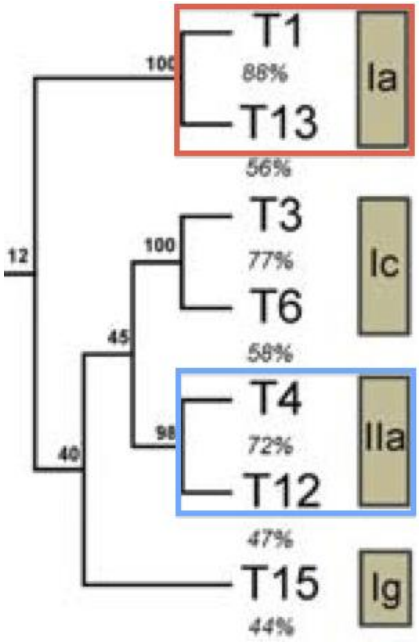

Figure 6.10- Detail from phylogenetic tree of human *GALNT* genes. *GALNT1* and *GALNT13* are in subfamily Ia, which is sister to the group that contains subfamily IIa (*GALNT4* and *GALNT12*). The percentage values refer to the percentage amino acid identities of the catalytic domains between proteins. Figure adapted from Bennett *et al.* (2012).

Human *GALNT1* (*T1*) is expressed in the liver and in the skeletal muscle, and Northern blot analysis showed that *GALNT1* is highly expressed in neurons and astrocytes (White *et al.*, 1995). ppGalNAc-T1 also has multiple structures that can recognize several T antigen subtypes (Zhang *et al.*, 2010). In mice, *Galnt1 (T1)* is highly expressed in adult lungs, spleen, testis and prostate (Young Jr. *et al.*, 2003) and is present in high quantities throughout the lifespan of the mouse (Young Jr. *et al.*, 2003). During mouse development, *Galnt1* expression was reported by *in situ* hybridization as relatively ubiquitous (Kingsley *et al.*, 2000; Ten Hagen *et al.*, 2003). It is highly expressed in the tail-forming region at E7.5, and by E12.5 also in mandibular bone-forming neural crest and brain (Ten Hagen *et al.*, 2003). The Eurexpress database (http://www.eurexpress.org/ee/databases/assay.jsp?assayID=euxassay_004959) reports

strong *Galnt1* expression at E14.5 in the jaws and teeth, clavicle, ventricular layer of the brain, thymus, liver and lung, and moderate expression in the retina, metanephros and trachea. Knocking out *Galnt1* in mice disturbed Fgf-mediated proliferation and integrin signalling, as major basement membrane components accumulated inside cells (Tian *et al.*, 2012).

Fig. 6.11 shows the expression of *Galnt1* in chick embryos at HH stages 19 and 25. At stage 19 HH, *Galnt1* was weakly expressed in the somites and limb buds (Fig. 6.11A). By stage 25 HH, *Galnt1* expression was stronger in the anterior half-sclerotome (Fig. 6.11B-E). *Galnt1* was also weakly expressed in the neural tube, but additional WMISH would have been necessary under different conditions to confirm this. The WMISH data presented in Fig 6.5 show dark staining in the head that could be background, but sections at stage 25 HH showed expression of *Galnt1* in the mandibular mesenchyme (ventral to the oral cavity) (Fig. 6.11F). This is consistent with the reported expression of mouse *Galnt1* in mandibular bone-forming neural crest (Ten Hagen *et al*., 2003). It is possible that *Galnt1* might be required for cell migration and/or formation of the mandibular bone in chick embryos, but since it was not expressed in the posterior half-sclerotome, further studies were not done.

6.8- *Galnt13* (subfamily Ia)

ppGalNAc-T13, encoded by *Galnt13*, is in the Ia subfamily with ppGalNAc-T1 (Bennett *et al.*, 2012), which was described in section 6.7 above (see Fig. 6.10 for the relationship of the Ia subfamily to the IIa subfamily containing *GALNT4*). My BLAST search ranked ppGalNAc-T13 as the fifth most similar chick protein to mouse ppGalNAc-T4 (Fig. 6.4).

Current data for *Galnt13* expression are conflicting: human *GALNT13* is found at high levels in the brain and neurons (Zhang *et al*., 2003, Bennett *et al.*, 2012), while in mouse brain only low levels are found (Young Jr. *et al*., 2003). Eurexpress (http://www.eurexpress.org/ee/databases/assay.jsp?assayID=euxassay_009032) reported no regional signal. I was able to detect *Galnt13* expression by RT-PCR at stage 22 HH, but unfortunately *in situ* hybridization did not give a specific signal.

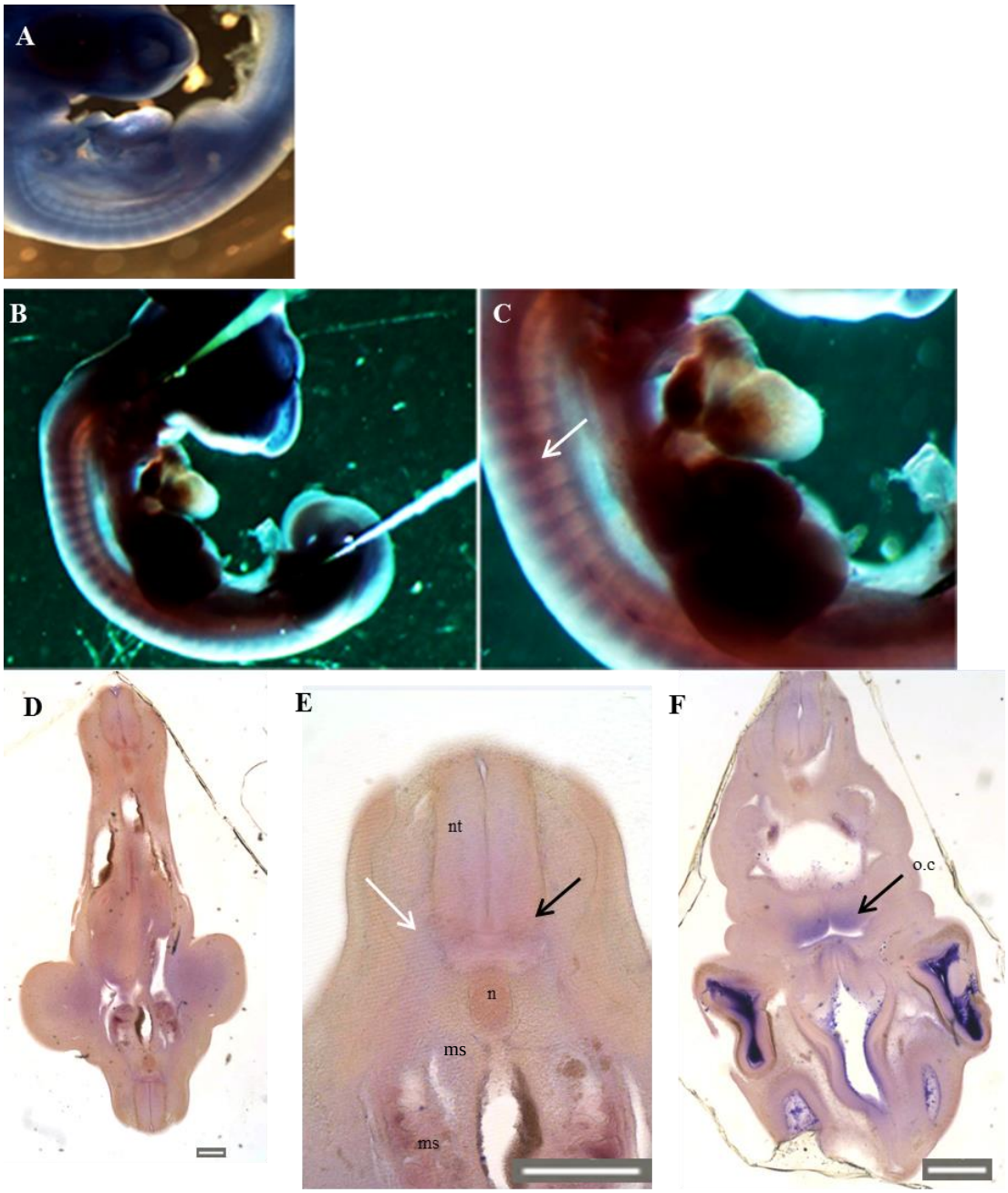

Figure 6.11- Embryos and sections after WMISH for *Galnt1*. (A) At stage 19 HH, *Galnt1* is weakly expressed in the somites and limb buds. (B) Embryo at stage 25 HH. (C) Higher power view of the vagal area of embryo in B. *Galnt1* is segmentally expressed in the anterior sclerotome (arrow) and in the limb buds. (D) Transverse section of embryo at stage 25 HH. *Galnt1* is weakly expressed in the neural tube and wing bud. (E) Transverse section of embryo at stage 25 HH. *Galnt1* is weakly expressed in the neural tube (black arrow) and in the ventral sclerotome. (F) Transverse section of embryo at stage 25 HH, *Galnt1* is expressed in the mandibular mesenchyme (arrow) below the oral cavity (o.c.) and in the diencephalon. Scale bar: 100 µm.

6.9- *Galnt15* (also known as *Galntl2*) (subfamily Ig)

ppGalNAc-T15, encoded by *Galnt15* (also known as *Galnt-like 2, Galntl2)*, forms the Ig subfamily (Bennett *et al.*, 2012). The human Ig subfamily (*GALNT15*) is sister to the group containing the Ic and IIa subfamilies, the latter containing *GALNT4* (Fig. 6.10). My BLAST search ranked ppGalNAc-T15 (TL2) as the sixth most similar chick protein to mouse ppGalNAc-T4 (Fig. 6.4). It has a unique catalytic activity when compared with other ppGalNAc-Ts, especially with ppGalNAc-T2, however, they share reaction pathways and transfer up to 7 GalNAc residues to their substrate (Muc1).

Real-time PCR showed broad expression of human *GALNT15*, with high levels in placenta, and expression in the small intestine, spleen, cerebral cortex, cerebellum, ovary and mammary gland, and in fetal brain, thyroid gland, and digestive tissues; the only place where *Galnt15* was not detected was leukocytes (Cheng *et al.*, 2004). This broad expression suggests that it is unlikely to be involved in somite polarity.

Fig. 6.12 shows *Galnt15* expression in a stage 25 HH embryo, the only stage when I could detect expression. *Galnt15* is expressed in the pharyngeal arches and the atrium and ventricle of the heart. It is weakly expressed in the limbs and in the anterior half of the somite, possibly in the DRG, but sections of the embryo would be required to confirm this. Due to its absence in the posterior half sclerotome, further studies for *Galnt15* were not pursued.

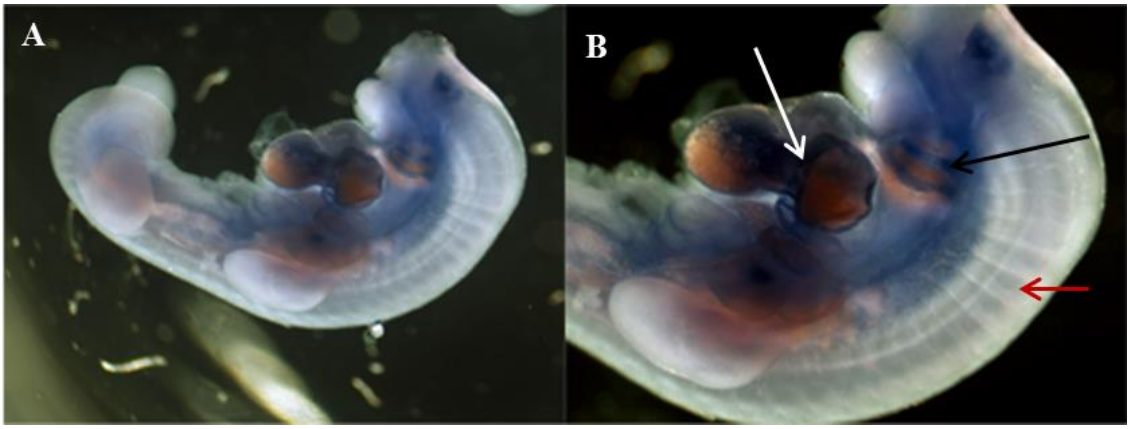

Figure 6.12- WMISH for *Galnt15* at stage 25 HH. (A) Low power view (head removed; anterior to the right). (B) Higher power view of embryo in A. *Galnt15* shows a segmented expression pattern in the anterior half of the somite (red arrow), and is also expressed in the heart (white arrow), limb buds and pharyngeal arches (black arrow).

6.10- *Galnt10* (subfamily IIb)

ppGalNAc-T10, encoded by *Galnt10*, is in the IIb subfamily with ppGalNAc-T17 and ppGalNAc-T7 (Figs. 6.2, 6.3; Bennett *et al.*, 2012). My BLAST search ranked ppGalNAc-T10 as the seventh most similar chick protein to mouse ppGalNAc-T4 (Fig. 6.4), and its sister protein ppGalNAc-T17 (also known as ppGalNAc-T-like 6, TL6), as the ninth most similar. Fig. 6.13 shows that the human IIb gene subfamily is only distantly related phylogenetically to the IIa gene subfamily containing *GALNT4*. It could be speculated that the greater sequence similarity between the proteins detected by BLAST reflects more similar catalytic domains, since the members of subfamily II mostly show GalNAc-glycopeptide substrate specificity, while the members of subfamily I mostly show peptide substrate specificity (Bennett *et al.*, 2012).

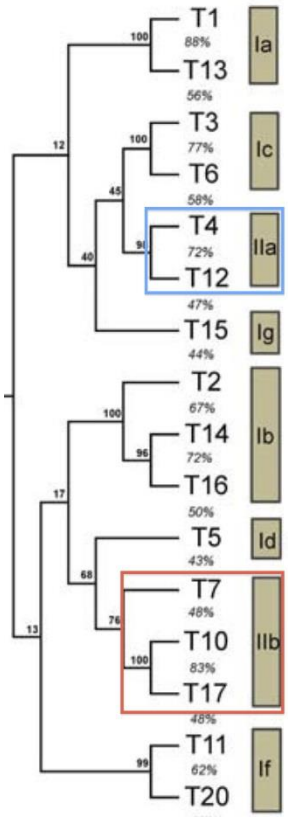

Figure 6.13- Detail from phylogenetic tree of human *GALNT* genes. *GALNT10*, its sister gene *GALNT17*, plus *GALNT7* are in subfamily IIb, which is only distantly related to subfamily IIa, containing *GALNT4* and *GALNT12*. Figure adapted from Bennett *et al.* (2012).

Mouse *Galnt10* is found in many adult tissues with greatest expression in the testis, followed by the sublingual gland, prostate, spleen and ovary (Young Jr.*et al.*, 2003). *In situ* hybridization showed *Galnt10* expression at E14.5 in cranial neural crest-derived cells that will form the mandibular bone and teeth (Kingsley *et al.*, 2000; Ten Hagen *et al*., 2003). Human *GALNT10* is also found in muscle (Bennett *et al.* 2012).

Mouse *Galnt10* was originally published as *Galnt9* (see Bennett *et al.*, 2012), so to prevent confusion, both sequences were obtained from Ensembl. In chick, *Galnt10* is on chromosome 13 and *Galnt9* on chromosome 15. Fig. 6.14 shows the expression of *Galnt10* in chick embryos at HH stages 19 and 25. *Galnt10* is strongly expressed in limb buds at both stages, with localised expression in mesenchyme (most likely future muscle) and also in the apical ectoderm ridge at the tip of the limb bud (Fig. 6.14A,B,D-F,H). *Galnt10* is also expressed in the myotome, with stronger expression in the centre of the myotome (Fig. 6.14C,D-H). and in the neural tube, with particularly strong expression in the floor plate (Fig. 6.14D,H). Pharyngeal arch expression is seen at both stages, which would be consistent with expression in cranial neural crest cells, but sectioning would be needed to confirm this. Since *Galnt10* was not expressed in the posterior half sclerotome, however, it was not studied further.

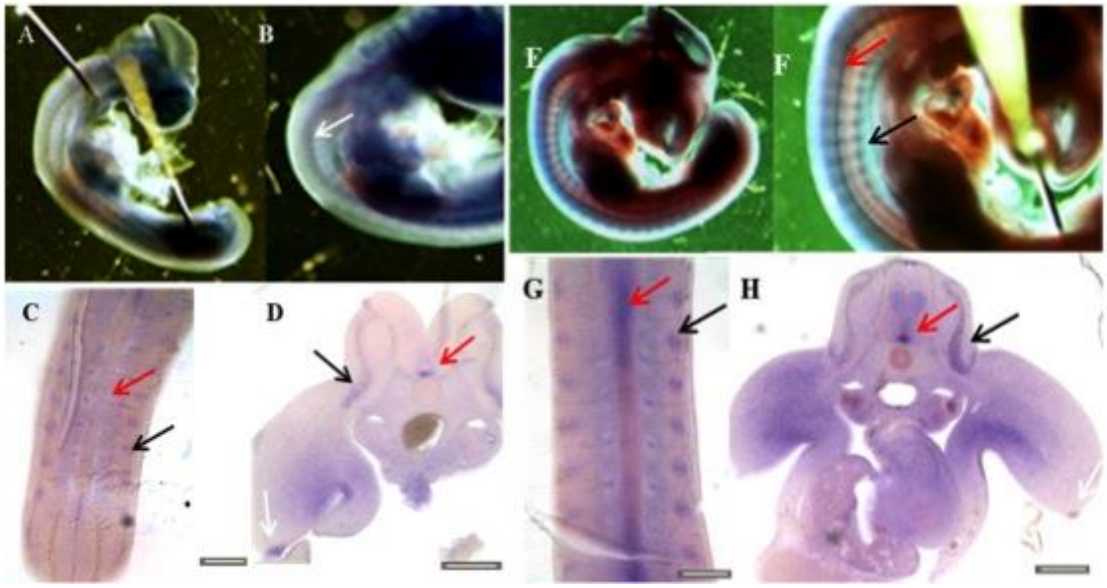

Figure 6.14- Embryos and sections after WMISH for *Galnt10*. (A,B) Low and higher power views of a stage 19 HH embryo. *Galnt10* is expressed in the limb buds and neural tube. (C) Longitudinal section at stage 19 HH. *Galnt10* is expressed in the myotome (black arrow) and neural tube (red arrow). (D) Transverse section at stage 19 HH. *Galnt10* is expressed in the myotome (black arrow), floor plate (red arrow), and at the tip of the limb (white arrow), most likely the apical ectodermal ridge. (E,F) Low and higher power views of a stage 25 HH embryo *Galnt10* is expressed in the neural tube (red arrow) and the anterior half somite (black arrow). (G) Coronal section at stage 25 HH. *Galnt10* is expressed in the myotome (black arrow), and in the neural tube (red arrow). (H) Transverse section at stage 25 HH. *Galnt10* is expressed in the myotome (black arrow) and neural tube with stronger expression in the floor plate (red arrow), in the limb muscle and in the apical ectodermal ridge at the tip of the limb (white arrow). Scale bar: 100 μm.

6.11- *Galnt7* (subfamily IIb)

ppGalNAc-T7, encoded by *Galnt7*, is in the IIb subfamily together with ppGalNAc-T10 (described in section 6.10 above) and ppGalNAc-T17 (Figs. 6.2, 6.3, 6.13; Bennett *et al.*, 2012). Although my BLAST search only ranked ppGalNAc-T7 as the fourteenth most similar chick protein to mouse ppGalNAc-T4 (Fig. 6.4), it is described here because it is in the IIb subfamily, like ppGalNAc-T10 (see Fig. 6.13).

Galnt7 is the most conserved *Galnt* gene during evolution (i.e., it has the slowest rate of nucleotide substitution) (Ten Hagen *et al.*, 2003), which is consistent with an important conserved biological function (Bennett *et al*., 2012). Human *GALNT7* is expressed in spinal cord, brain, bone, heart, kidney, trachea and digestive tract organs (Ten Hagen *et al*., 2003; Bennett *et al.*, 2012). Mouse *Galnt7* is most strongly expressed at E7.5, but is found in adult testis, ovary, prostate, and spleen (Young Jr.*et al*., 2003). Eurexpress reports strong expression of *Galnt7* at E14.5 in the stomach and rectum, and moderate expression in the midgut, adrenal gland, submandibular gland, metanephros, and in the choroid plexus and roof plate of the hindbrain and forebrain (http://www.eurexpress.org/ee/databases/assay.jsp?assayID=euxassay_005715),

Fig. 6.15 shows chick *Galnt7* expression at HH stages 17, 19 and 25. Like *Galnt10*, the other IIb subfamily member (section 6.10), *Galnt7* is expressed in limb buds, myotome, floorplate and perhaps pharyngeal arches (Fig. 6.15). The segmented expression in whole-mount is due to stronger expression in the centre of the myotome. Expression in myotome and limb buds might indicate a role in limb muscle formation. Since it is not expressed in posterior sclerotome, though, it was not studied further.

Figure 6.15- (next page) Embryos and sections after WMISH for *Galnt7*. (A,B) Low and higher power views at stage 17 HH. *Galnt10* is expressed in the neural tube (red arrow). (C,D) Low and higher power views at stage 19 HH. *Galnt7* is expressed in the limb buds, floor plate (red arrow), ventrolateral somite (black arrow) and pharyngeal arches. (E) Transverse section at stage 19 HH. *Galnt7* is expressed in the floor plate of the neural tube and perhaps generally in head mesenchyme. (F) Transverse section at stage 19 HH. *Galnt7* is expressed in the floor plate (red arrow) and in the lateral myotome (black arrow). (G, H) Low and higher power views at stage 25 HH. *Galnt7* is expressed in the floor plate (red arrow), ventrolateral somite (black arrow) and atrium. (I-K) Longitudinal sections at stage 25 HH. *Galnt7* is expressed in the medial somite (arrow, I), anterior-posterior boundary (arrow, J) and centre of the myotome (arrow, K).

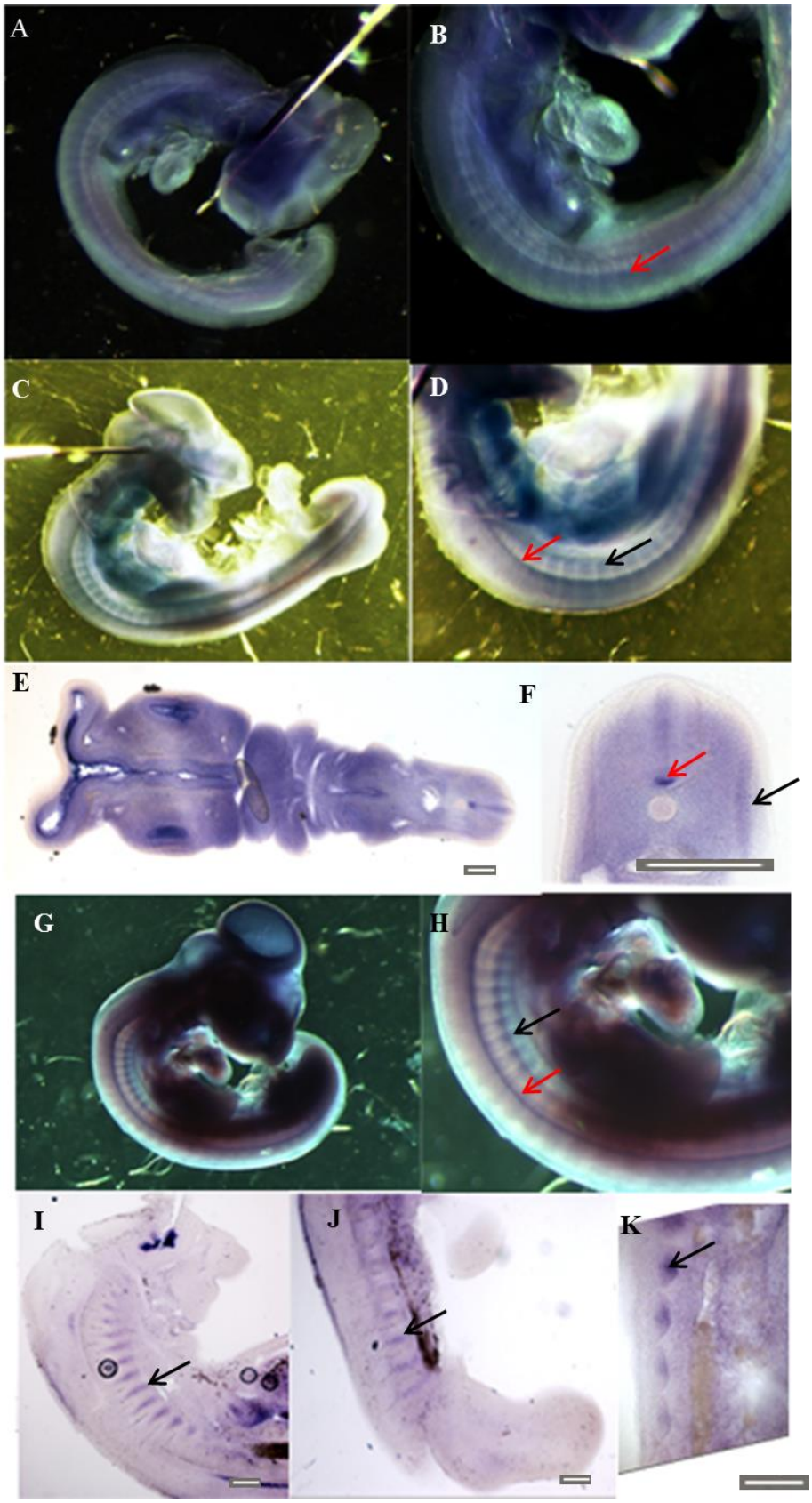

Figure 6.15- Legend on previous page.

6.12- *Galnt2* (subfamily Ib)

ppGalNAc-T2, encoded by *Galnt2*, is in the Ib subfamily (Bennett *et al.*, 2012), which also contains ppGalNAc-T16 (*Galnt16*; section 6.13) and its sister gene ppGalNAc-T14 (*Galnt14*; section 6.14) (Fig. 6.16). My BLAST search ranked ppGalNAc-T2 as the eighth most similar chick protein to mouse ppGalNAc-T4 (Fig. 6.4), although the phylogenetic tree (Fig. 6.16) suggests these are only distantly related.

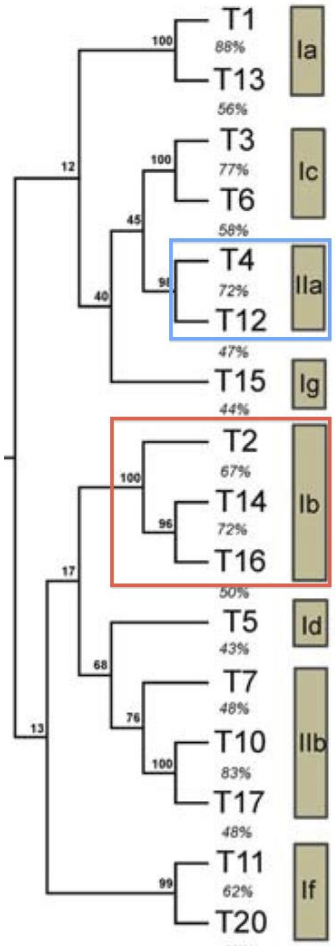

Figure 6.16- Detail from phylogenetic tree of human *GALNT* genes. *GALNT2*, plus *GALNT16* and its sister gene *GALNT14*, are in subfamily Ib, which is only distantly related to subfamily IIa, containing *GALNT4* and *GALNT12*. Figure adapted from Bennett *et al.* (2012).

Galnt2 expression is ubiquitous in the adult mouse. It is the most highly expressed *Galnt* gene in the prostate and also in the virgin mammary gland, decreasing significantly during pregnancy (Young Jr.*et al.*, 2003). During mouse development, *Galnt2* expression was reported by *in situ* hybridization as relatively ubiquitous

(Kingsley *et al*., 2000; Ten Hagen *et al*., 2003). In E12.5 mouse embryos, *Galnt2* shows strong expression in the brain; by E14.5, expression is seen in the sublingual gland, and at E16.5, expression is found in lungs, intestines, submandibular gland and in the eye (Ten Hagen *et al*., 2003). In humans, *GALNT2* is expressed in skeletal muscle and liver (White *et al.*, 1995).

Fig. 6.17 shows *Galnt2* expression in chick embryos at HH stages 19 and 25. This contrasts with what is known in mice as expression is seen at the edges of the dermomyotome and later in the myotome (Fig. 6.17C,D,K,L), suggesting ppGalNAc-T2 may be required for the cell migration that forms the myotome. *Galnt2* is also expressed in the mesonephros (Fig. 6.17J-L), neural tube (Fig. 6.17A,B,E,I) and atrium (Fig. 6.17G). *Galnt2* expression in the ventral sclerotome (Fig. 6.17E) was probably due to the symmetrical expression of *Galnt2* in 2 cell pools on the top of the dorsal aorta, most likely the mesonephros (Fig. 6.17J). Since *Galnt2* was not expressed in the posterior half-sclerotome, it was not studied further.

Figure 6.17- (On next page) Embryos and sections after WMISH for *Galnt2*. (A,B) Lower and higher magnification views of a stage 19 HH embryo. *Galnt2* is expressed in the ventral somite (arrow) and neural tube. (C,D) Lower and higher magnification views of a longitudinal section of a stage 19 HH embryo. *Galnt2* is expressed at the edges of the dermomyotome (arrow). (E) Transverse section at stage 19 HH. *Galnt2* is expressed in the dermomyotome and dorsal neural tube. (F,G) Lower and higher magnification views of a stage 25 HH embryo. *Galnt2* is expressed in the limb buds, at sclerotome boundaries (arrow) and in the atrium (arrow). (I) Longitudinal section at stage 25 HH, *Galnt2* is expressed in the middle of the somite (arrow) and in the neural tube. (J) Transverse section at stage 25 HH. *Galnt2* is expressed in the neural tube and symmetrically above the dorsal aorta (arrow), likely the mesonephros. (K,L) Lower and higher magnification views of a longitudinal section at stage 25 HH. *Galnt2* is expressed in the middle of the myotome (arrow) and in the mesonephros. Scale bar: 100 μm

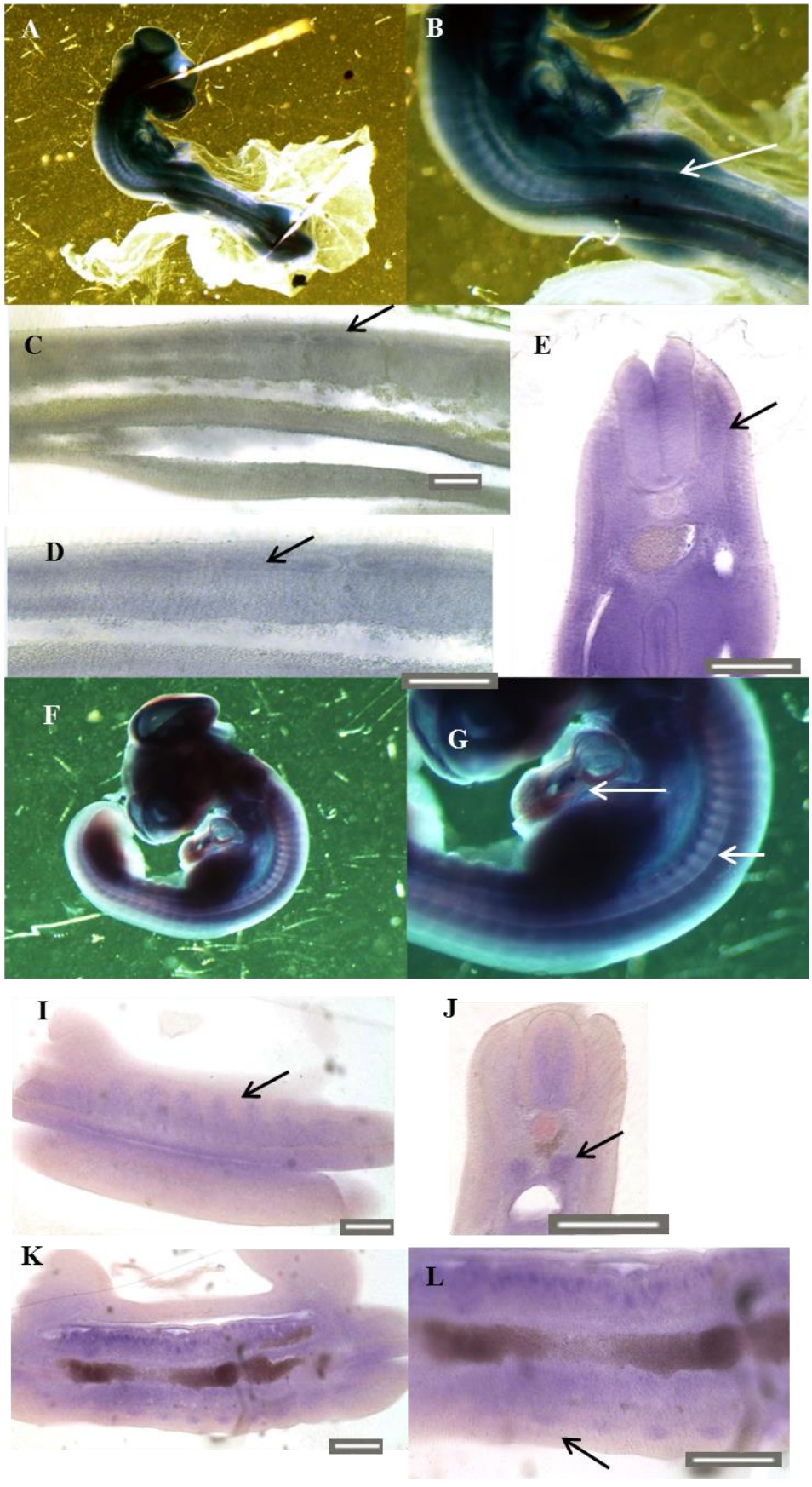

Figure 6.17- Legend on previous page.

6.13- *Galnt16* (also known as *Galnt-like1, Galntl1*) (subfamily Ib)

ppGalNAc-T16, encoded by *Galnt16* (also known as *Galnt-like1, Galntl1*), is in the Ib subfamily with its sister protein ppGalNAc-T14, described in section 6.14 below, and ppGalNAc-T2, described in section 6.12 above (Bennett *et al.*, 2012). My BLAST search ranked ppGalNAc-T16 (TL1) as the eleventh most similar chick protein to mouse ppGalNAc-T4 (Fig. 6.4), although the phylogenetic tree (Fig. 6.16) suggests these are only distantly related. (Although the If subfamily member ppGalNAc-T11 was the tenth most similar protein to mouse ppGalNAc-T4, it will be described after the other two subfamily Ib members so these can be kept together.)

Galnt16 (Galntl1) is expressed in the hypothalamus, thalamus and amygdala of the mouse brain (Nelson *et al*., 2002). In *Xenopus*, *galnt16* (*xGalntl-1*) is required for formation of the cranial neural crest, anterior notochord and spinal cord: it disrupts the common TGF-ß type II receptor activin receptor IIB, preventing it from binding to the TGF-ß type I receptor specific for activin and BMP signalling (Herr *et al*., 2008).

Fig. 6.18 shows the expression of *Galnt16* in chick embryos at HH stages 19 and 27. At stage 19 HH, *Galnt16* has a segmented expression in the anterior sclerotome, and is also expressed in the limb buds (Fig. 6.18A,B). There may also be expression in the atrium of the heart, though this could be trapping (Fig. 6.18B, white arrow). By stage 27 HH, the expression in anterior sclerotome is stronger and more defined and there also appears to be expression in the neural tube (Fig. 6.18C,D) and in the cardinal vein (Fig. 6.18D, white arrow). Sections after WMISH would have been necessary to confirm the precise location of *Galnt16* expression. The apparent expression of *Galnt16* in the atrium of the heart at stage 19 HH and in the cardinal vein at stage 27 HH might be the result of antibody entrapment, however if it is real it might be due to neural crest-derived cells, since in *Xenopus*, *galnt16 (xGalntl-1)* expression was detected in cranial neural crest cells (Herr *et al*., 2008).

Since *Galnt16* was not expressed in the posterior half-sclerotome, it was not investigated further.

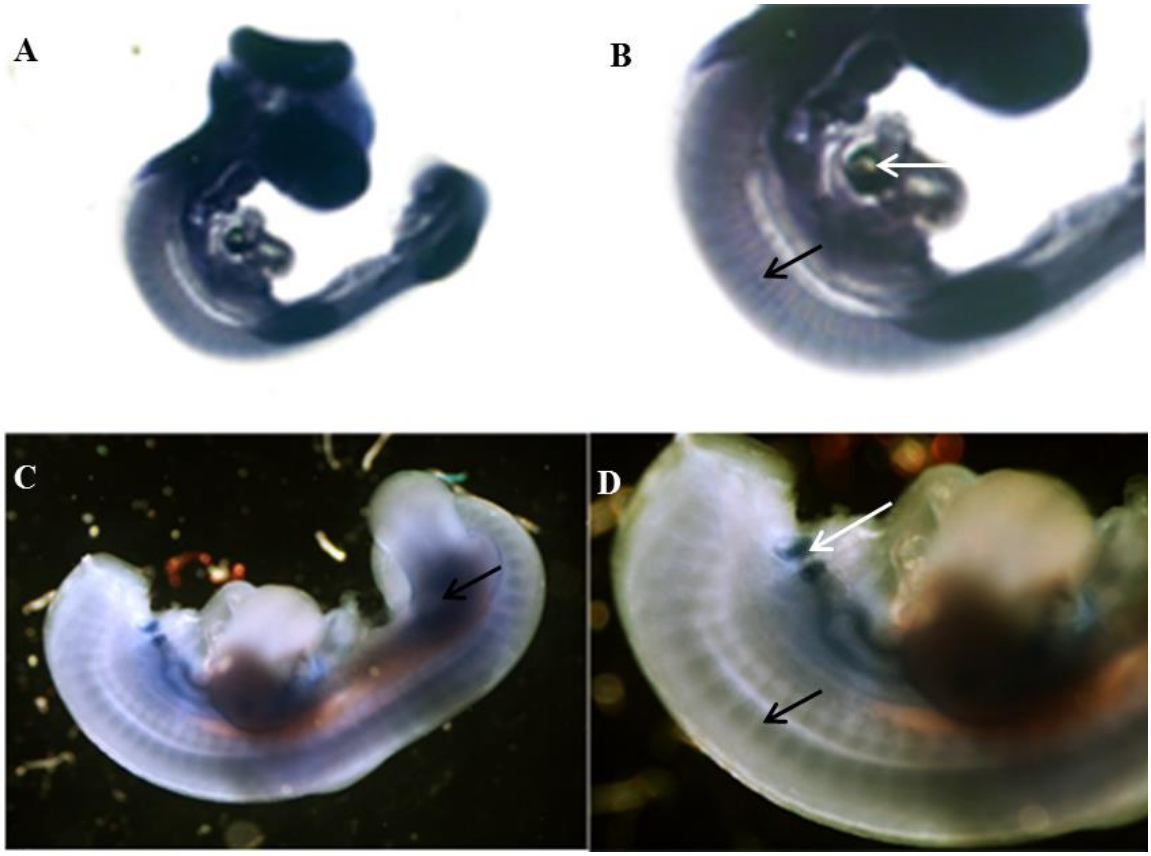

Figure 6.18- WMISH for *Galnt16 (Galntl1)*. (A,B) Low and higher power views of embryo at stage 19 HH. *Galnt16* is expressed in the anterior somite (black arrow), in the limb buds and possibly in the atrium (white arrow, although this could be trapping). (C,D) Low and higher power views of embryo at stage 27 HH. The head has been cut off; anterior is to the left. *Galnt16* is expressed in the neural tube, the proximal part of the developing limbs (black arrow in C), the anterior half sclerotome (black arrow in D), neural tube and cardinal vein (white arrow in D).

6.14- *Galnt14* (subfamily Ib)

ppGalNAc-T14, encoded by *Galnt14*, is also in the Ib subfamily with ppGalNAc-T14 (section 6.13) and ppGalNAc-T2 (section 6.12) (Bennett *et al.*, 2012). My BLAST search ranked this as the twelfth most similar chick protein to mouse ppGalNAc-T4 (Fig. 6.4), although the phylogenetic tree (Fig. 6.16) suggests these are only distantly related.

In situ hybridization in mouse at E14.5 showed *Galnt14* expression in the olfactory epithelium, retina, brain, spinal cord, cranial sensory ganglia and dorsal root ganglia (http://www.eurexpress.org/ee/databases/assay.jsp?assayID=euxassay_009033).

Galnt14 is also expressed in breast cancer, being a potential biomarker (Wu *et al*., 2010). *Galnt14* was the only gene I was unable to amplify from chick embryo RNA. Others have reported difficulty in analysing *Galnt14* expression in mouse by RT-PCR (Young Jr. *et al*., 2003).

6.15- *Galnt11* (subfamily If)

ppGalNAc-T11, encoded by *Galnt11*, is in the If subfamily with its sister protein ppGalNAc-T20 (which was lost in the chicken lineage) (Bennett *et al.*, 2012). My BLAST search ranked ppGalNAc-T11 as the tenth most similar chick protein to mouse ppGalNAc-T4 (Fig. 6.4), although the phylogenetic tree (Fig. 6.19) suggests these are only distantly related.

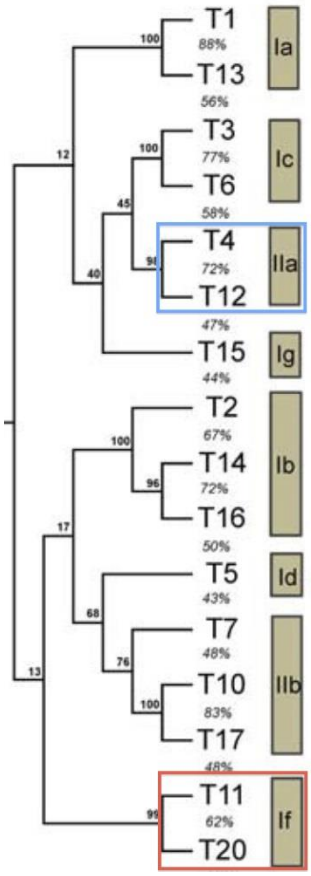

Figure 6.19- Detail from phylogenetic tree of human *GALNT* genes. *GALNT11* and its sister gene *GALNT20* form subfamily If, which is only distantly related to subfamily IIa, containing *GALNT4* and *GALNT12*. Figure adapted from Bennett *et al.* (2012).

Galnt11 is found in many tissues of adult mouse, mainly in lung but also in prostate, sublingual gland, spleen, testis and thymus, and is the most highly expressed of all *Galnt* genes in the thyroid (Young Jr.*et al*., 2003). Eurexpress (http://www.eurexpress.org/ee/databases/assay.jsp?assayID=euxassay_002021) reports no regional expression at E14.5. In humans, *GALNT11* is only expressed in kidney (Schwientek *et al*., 2002). Even though *Galnt11* cDNA was amplified by RT-PCR from a chick embryo at stage 27 HH, it was not possible to detect a clear signal by *in situ* hybridization.

6.16- *Galnt5* (subfamily Id)

ppGalNAc-T5, encoded by *Galnt5*, is the only member of the Id subfamily (Bennett *et al*., 2012). My BLAST search ranked this as the thirteenth most similar chick protein to mouse ppGalNAc-T4 (Fig. 6.4), although the phylogenetic tree (Fig. 6.20) suggests these are only distantly related.

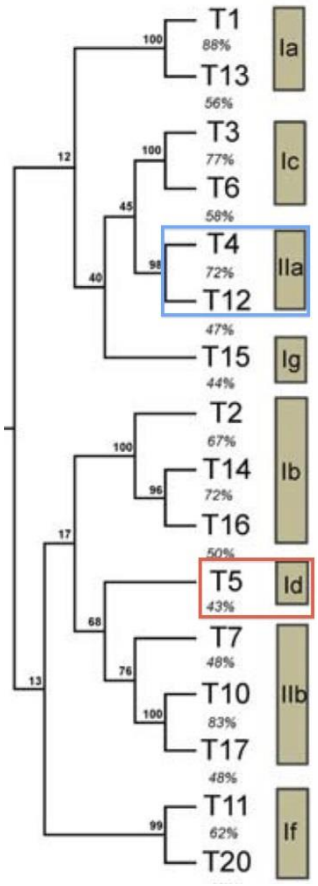

Figure 6.20- Detail from phylogenetic tree of human *GALNT* genes. *GALNT5* forms subfamily Id, which is only distantly related to subfamily IIa, containing *GALNT4* and *GALNT12*. Figure adapted from Bennett *et al.* (2012).

Galnt5 has undergone the most modifications during evolution (Ten Hagen *et al.*, 2003). In mouse embryos, *Galnt5* expression was reported by *in situ* hybridization in a subset of cells in the ventral part of the maxilla and mandible at E12.5 (Kingsley *et al.*, 2000; Ten Hagen *et al.*, 2003). At E14.5, the Eurexpress database (http://www.eurexpress.org/ee/databases/assay.jsp?assayID=euxassay_013568) shows expression in the skeleton of the maxilla and mandible, as well as in the ribs.

Fig. 6.21 shows the expression of *Galnt5* in chick embryos at HH stages 19 and 27. At stage 19 HH, *Galnt5* is expressed in the dorsal aorta, heart and limb buds (Fig. 6.21A,B). At stage 27 HH, expression in the heart might be due to entrapment, since *Galnt5* expression has never been detected in the heart (Bennett *et al.* 2012). Expression between the somites at stage 27 (Fig. 6.21C,D) could represent inter-somitic blood vessels. *Galnt5* is also expressed in the notochord and limbs.

Due to absence of expression on the posterior half sclerotome, further studies with *Galnt5* were not done.

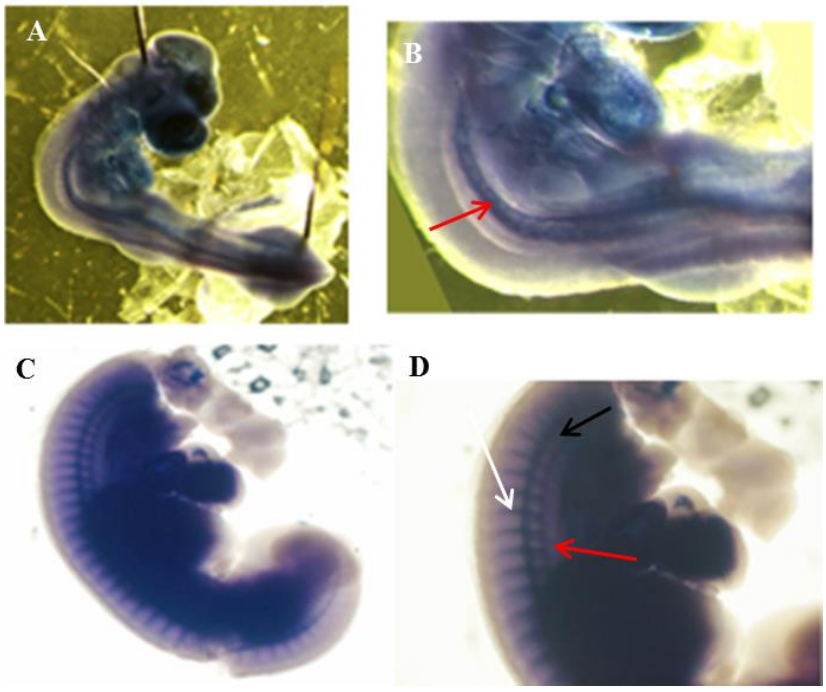

Figure 6.21- WMISH for *Galnt5*. (A,B) Low and higher power views of embryo at stage 19 HH. *Galnt5* is expressed in the dorsal aorta (red arrow), heart and limb buds. (C,D) Low and higher power views of embryo at stage 27 HH (head removed; anterior towards the top). *Galnt5* is expressed in the dorsal aorta (red arrow), between the somites (white arrow) and in the notochord (black arrow), heart and limbs.

6.17- *Galnt9* (subfamily Ie)

GALNT9, encoding ppGalNAc-T9, is in the human Ie subfamily with its sister gene *WBSCR17* (also known as *GALNT19*, *GALNT-like3*, *GALNTL3*) (section 6.18 below), *GALNT18* (also known as *GALNT-like4*, *GALNTL4*; section 6.19 below) and *GALNT8* (lost in the chicken; Bennett *et al.*, 2012) (Fig. 6.22). My BLAST search ranked ppGalNAc-T9 as the fifteenth most similar chick protein to mouse ppGalNAc-T4 (Fig. 6.4). The phylogenetic tree (Fig. 6.22) suggests these are only distantly related.

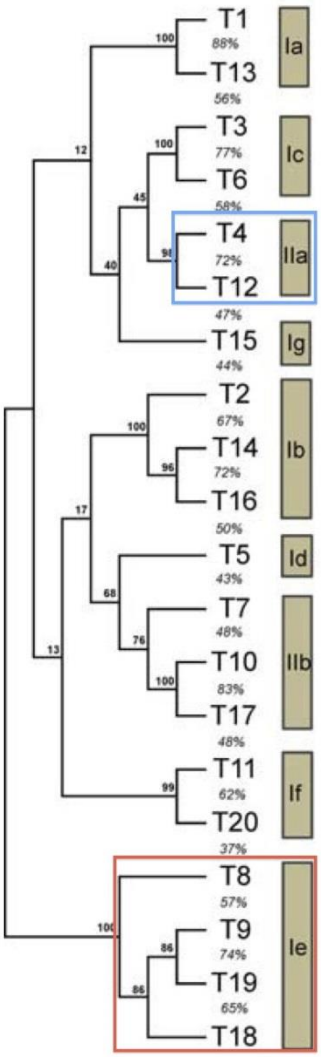

Figure 6.22- Detail from phylogenetic tree of human *GALNT* genes. *GALNT19/WBSCR17*, plus *GALNT9*, *GALNT18* and *GALNT8*, form subfamily Ie, which is only distantly related to subfamily IIa, containing *GALNT4* and *GALNT12*. Figure adapted from Bennett *et al.* (2012).

In mouse and in human, *Galnt9* is expressed in cranial sensory ganglia (Zhang *et al.*, 2002; Ten Hagen *et al.*, 2003). In mouse embryos at E14.5, the Eurexpress database (http://www.eurexpress.org/ee/databases/assay.jsp?assayID=euxassay_006920) reports

Galnt9 expression by *in situ* hybridization in brain, spinal cord, cranial sensory ganglia and dorsal root ganglia, as well as in inter-digital mesenchyme.

Fig. 6.23 shows the expression of *Galnt9* in chick embryos at stage 25 HH. *Galnt9* is expressed strongly in the neural tube and DRG (Fig. 6.23A-D), consistent with the Eurexpress report in mouse. There is also a patch of strong expression at the posterior edge of the limb bud (Fig. 6.23A,B). *Galnt9* is also expressed weakly in the myotome (Fig. 6.23C,D). Due to its absence in the posterior half sclerotome, studies of function for *Galnt9* were not done.

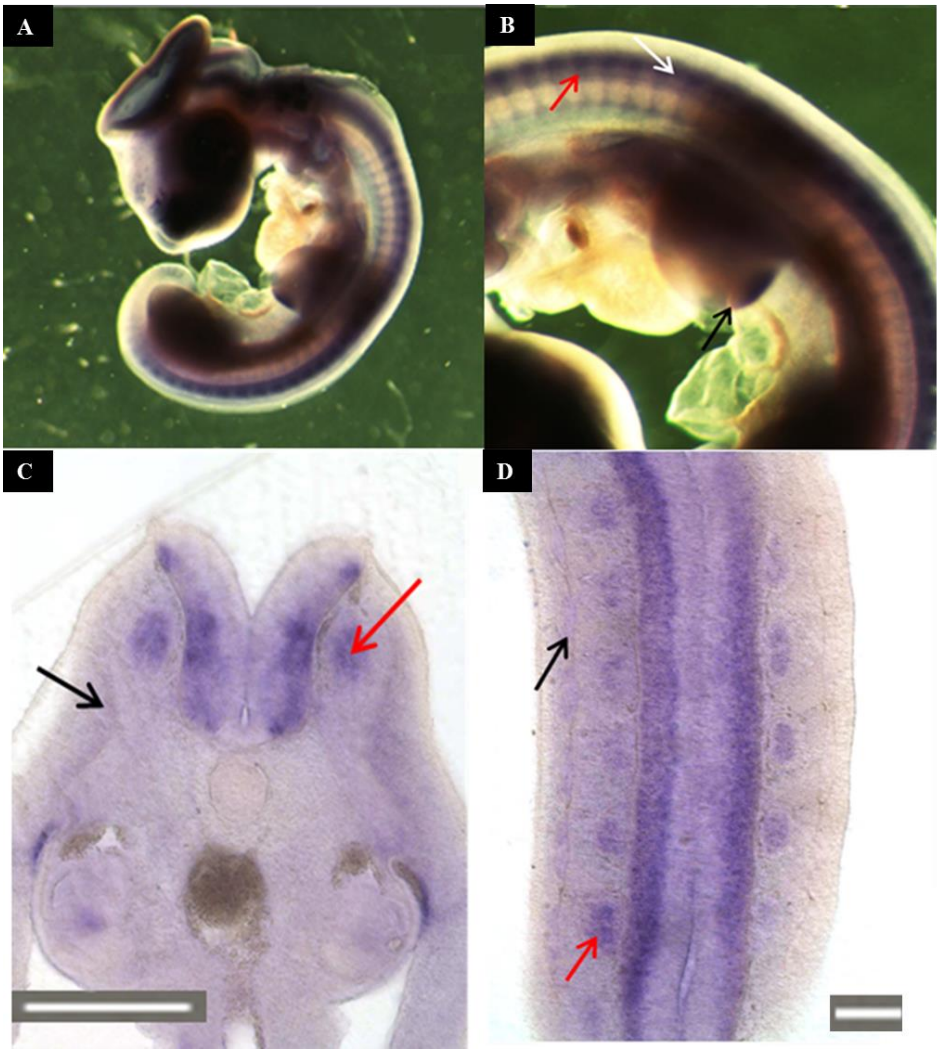

Figure 6.23- Embryos and sections after WMISH for *Galnt9* at stage 25 HH. (A,B) Lower and higher magnification views in whole-mount. *Galnt9* is strongly expressed in the posterior of the limb bud (black arrow), in the neural tube (white arrow), and in the anterior half of the somite (red arrow). (C) Transverse and (D) Coronal sections. *Galnt9* is expressed weakly in the myotome (black arrow), and strongly in the DRG (red arrow) and neural tube. Scale bar: 100 µm.

6.18- *WBSCR17* (also known as *Galnt19, Galnt-like3, Galntl3*) (subfamily Ie)

The human *Williams-Beuren syndrome chromosome region 17* gene, *WBSCR17*, is one of the nine genes whose mutation contributes to Williams-Beuren syndrome, a neurodevelopmental disorder associated with mutations on chromosome 7 (Merla *et al*., 2002). It is also known as *GALNT-like3* (*GALNTL3*) and was classified by Bennett *et al.* (2012) as ppGalNAc-T19, encoded by *GALNT19*, in the Ie subfamily with its sister gene *GALNT9* (section 6.17 above), *GALNT18* (section 6.19 below) and *GALNT8* (lost in the chicken; Bennett *et al.*, 2012) (Fig. 6.22). My BLAST search ranked WBSCR17 (ppGalNAc-T19) as the sixteenth most similar chick protein to mouse ppGalNAc-T4 (Fig. 6.4). The phylogenetic tree (Fig. 6.22) suggests these are only distantly related.

Northern blot analysis of adult mouse tissues detected *WBSCR17* in higher quantities in the brain, followed by weaker expression in the heart and kidney, with low levels in the liver, lung and spleen (Merla *et al*., 2002). At E14.5, Eurexpress (http://www.eurexpress.org/ee/databases/assay.jsp?assayID=euxassay_007480) shows strong expression in cerebral cortex, cranial sensory ganglia and DRG, and moderate expression in the rest of the brain and spinal cord, as well as axial muscle.

Fig. 6.24 shows the expression of *WBSCR17* in chick embryos at HH stages 17, 22 and 25. *WBSCR17* is strongly expressed in the brain and trunk neural tube (Fig. 6.24 all panels), consistent with the mouse expression described above. Strong expression is also seen in the limb buds (Fig. 6.24C-E,G,H) and weaker expression in the dermomyotome (Fig. 6.24F, J). Since *WBSCR17* expression is not seen in the posterior sclerotome, further studies were not done.

Figure 6.24- (On next page) Embryos and sections after WMISH for *WBSCR17*. (A,B) Low and higher power views of a stage 17 HH embryo. *WBSCR17* is expressed in the neural tube (red arrow). (C,D) Low and higher power views of a stage 22 HH embryo. *WBSCR17* is expressed in the brain, trunk neural tube (red arrow), somite (black arrow) and limb buds. (E) Transverse section at stage 22 HH. *WBSCR17* is expressed in the ventral part of the limb. (F) Higher power view of E. *WBSCR17* is expressed in the neural tube (red arrow) and dorsal dermomyotome (black arrow). (G,H) Low and higher power views of a stage 25 HH embryo. *WBSCR17* is expressed in the brain, neural tube (red arrow), ventral somite (black arrow) and limb buds. (I,J) Low and higher power views of a transverse section at stage 25 HH. *WBSCR17* is expressed in the neural tube (red arrow) and in the ventral dermomyotome (black arrow). Scale bar: 100 μm.

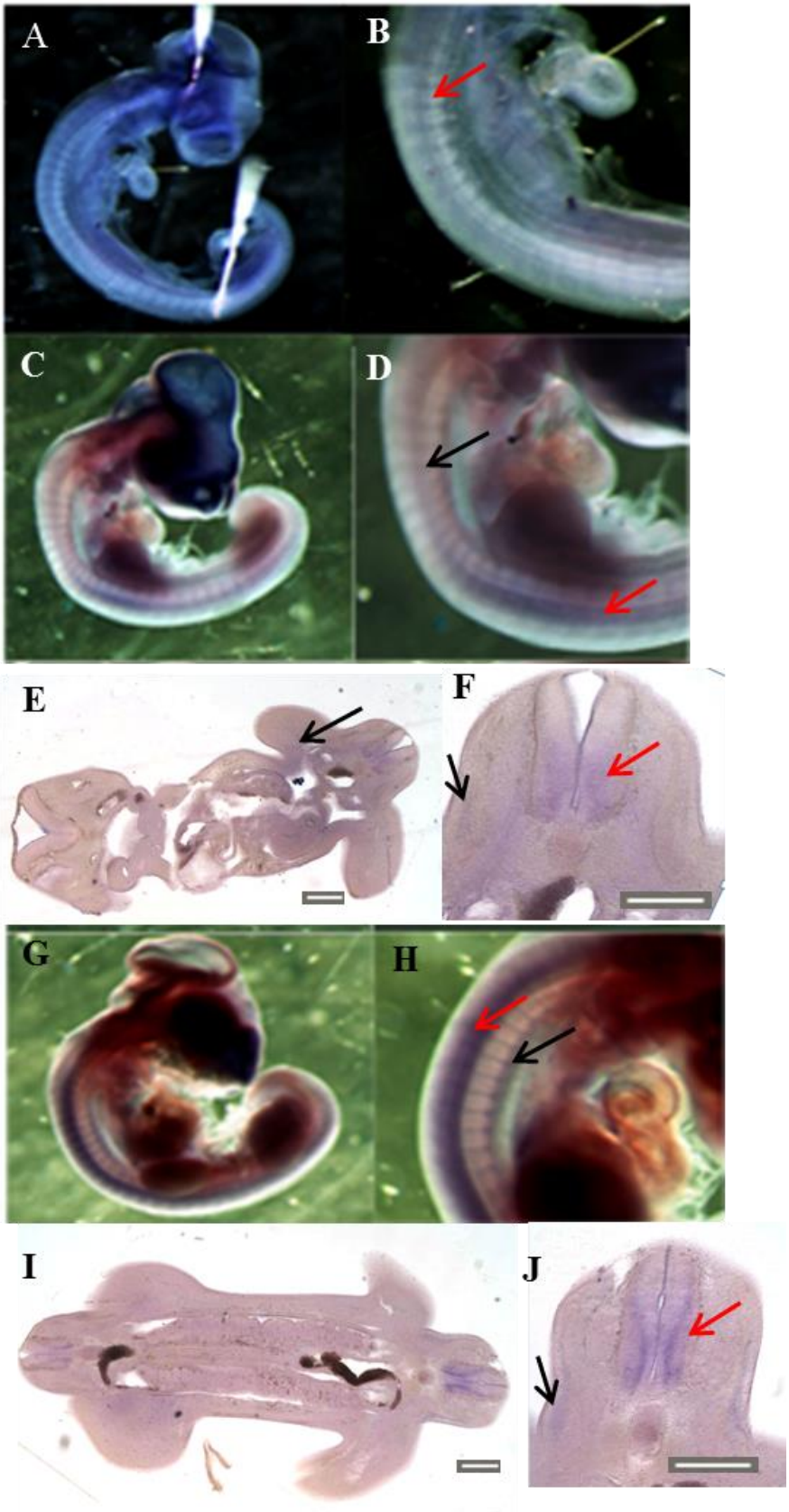

Figure 6.24- Legend on previous page.

6.19- *Galnt18* (also known as *Galnt-like 4, Galntl4*) (subfamily Ie)

Galnt18 (also known as *Galnt-like 4, Galntl4*), encoding ppGalNAc-T18 (ppGalNAc-TL4) is a member of the same Ie subfamily as *Galnt9* (section 6.17), and its sister gene *WBSCR17* (*GALNT19*) (section 6.18) (Fig. 6.22; Bennett *et al.*, 2012). My BLAST search ranked ppGalNAc-T18 (ppGalNAc-TL4) as the seventeenth most similar chick protein to mouse ppGalNAc-T4 (Fig. 6.4), and the phylogenetic tree (Fig. 6.22) suggests these are only distantly related.

Fig. 6.25 shows the expression of *Galnt18* in chick embryos at HH stages 17, 19 and 22. *Galnt18* is expressed at stage 17 HH in the notochord and in the heart (Fig. 6.24A). At stages 19 and 22 HH, segmental expression in the anterior half of the somite can be seen (Fig. 6.25B,C), which sections show to be the DRG (Fig. 6.25D-G), although expression is also present in the dermomyotome and myotome (Fig. 6.25D-G), and the lateral sclerotome (Fig. 6.25F). *Galnt18* is also expressed in the notochord (Fig. 6.25D,F,G) and the proximal part of the wing bud (Fig. 6.25F). Due to the absence of expression in the posterior half sclerotome, further studies with *Galnt18* were not done.

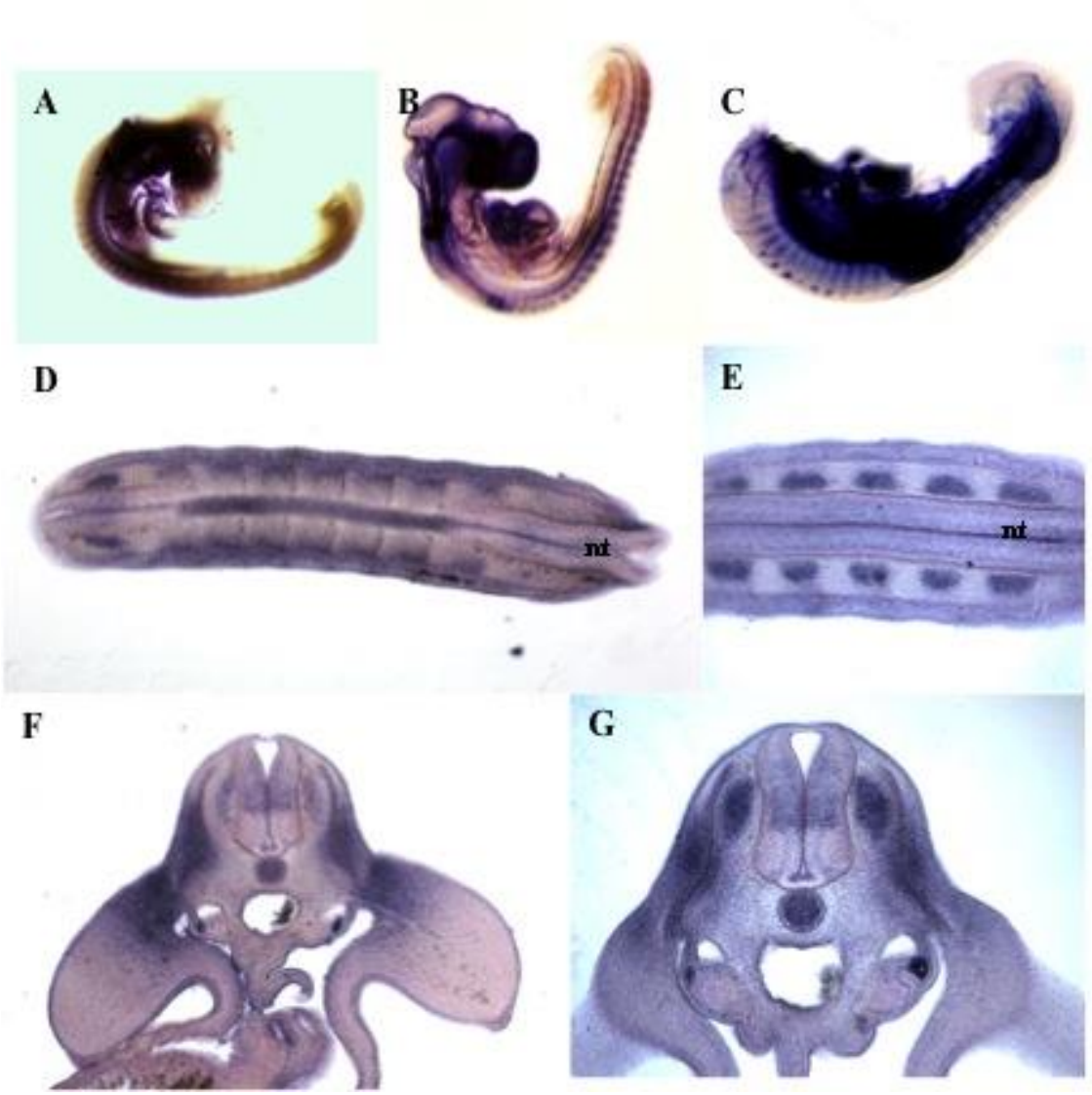

Figure 6.25- Embryos and sections after WMISH for *Galnt18*. (A) Embryo at stage 17 HH. *Galnt18* is present in the heart and somites. (B) Embryo at stage 19 HH. *Galnt18* is expressed in the anterior half somite, heart and notochord. (C) Embryo at stage HH 22 (head cut off; anterior to left). *Galnt18* is expressed in the DRG, limb buds and heart. (D) Coronal section at stage 19 HH. *Galnt18* is expressed in the DRG, neural tube (nt) and notochord. (E) Coronal section at stage 19 HH. *Galnt18* is expressed in the DRG, neural tube (nt) and myotome. (F) Transverse section at stage 22 HH. *Galnt18* is expressed in the neural tube with the exception of the ventral neural tube, and in the notochord, dermomyotome, lateral sclerotome, and proximal wing bud. (G) Transverse section at stage 22 HH. *Galnt18* is expressed in the neural tube with the exception of the ventral neural tube, and in the notochord, dermomyotome and DRG.

6.20- Conclusions

The assessment of expression patterns for the different *Galnt* genes in chick embryos did not highlight any particular enzyme that could be responsible for mucin-type O-glycosylation of the protein responsible for the axonal repellent activity localised to the posterior half sclerotome. It was not possible to detect any *Galnt* gene that showed restricted expression in the posterior half sclerotome. This may mean that an as-yet unidentified enzyme plays this role, or that some other mechanism or molecule is employed to add O-glycan groups to the repellent.

This study has generated many new embryonic expression patterns of the mucin-type O-glycosylation enzyme gene family that were not previously available in chicken or indeed other animals. Fig. 6.26 presents an overview of the expression of 15 genes in the trunk at stage 25 HH and Table 6.1 summarises the regional distribution across 8 embryonic tissues.

Most of the *Galnt* genes appear to share similar gene expression patterns (Table 6.1). These results suggest that the activity of multiple ppGalNAc-T enzymes is required for the correct formation of specific structures during development. However, these data may also indicate that there is functional redundancy.

Myotome formation requires epithelial to mesenchyme transitions for cell migration from the ventrolateral and dorsolateral dermomyotome to from the myotome (Gros *et al*., 2004). In this study, *C1T1, T1, T2, T15 (TL2*), *T7* are weakly expressed in the myotome, however *T9, T12, T10* display strong expression in the myotome and later in the limbs. It is possible that these ppGalNAc-Ts are required during myotome formation, and mesenchymal condensation during limb muscle formation.

Several *Galnt* genes are differently expressed in the neural tube. *C1T1, T1, T2, T3,* and *T5* are expressed in the mediodorsal neural tube, while *T18* (*TL4*), *T9* and *WBSCR17* are expressed in the lateroventral neural tube. There are also *Galnt* genes expressed in the floor plate of the neural tube such as *T5, T7* and *T9,* and others in the notochord. *T18* (*TL4*) is expressed only until stage 22 HH, and *T12* is expressed only in the central notochord, without being expressed in the perinotochordal sheath. Due to the

variety of expression within the neural tube and notochord it is possible that these molecules play different roles in CNS development.

These regions are known to contain molecules that coordinate migration of somites and neural crest cells, like Shh that is expressed by the notochord and the floor plate (Chan *et al.*, 2009), and even though there was no *Galnt* present in both places simultaneously, they may have different roles during the migration process. For example, Shh requires binding to proteoglycans to promote cell proliferation in the cerebellum (Chan *et al*., 2009). It is possible that *Galnt* genes such as *T5*, *T7*, *T9*, *T12* and *T18* (*TL4*) might be necessary to form the proteoglycans that regulate Shh localisation and signalling. Shh plays critical roles during embryonic development, orchestrating the patterning of the brain, spinal cord, craniofacial elements, the axial skeleton, limbs and digits (Ingham and McMahon, 2001; Dorus *et al*., 2006), and it is expressed in the notochord, floor plate and the zone of polarizing activity in the limb buds (Dorus *et al*., 2006), the same tissues where most of the detected *Galnt* genes are expressed.

Overall, the results strongly support a role for ppGalNAc-T enzymes in the development of both the central and peripheral nervous systems.

Table 6.1- Summary of sites of expression of 17 different genes encoding mucin-type O-glycosylation enzymes across 8 different tissues at stage 25 HH. Different shading indicates subfamily relationship according to Bennett *et al.* (2012). X indicates that expression was detected (DRG: dorsal root ganglia). (T19 corresponds to WBSCR17)

	C1T1	T12	T6	T3	T1	T13	T15	T10	T7	T2	T16	T14	T11	T5	T9	T19	T18
DRG		X			X					X	X						X
Neural tube	X		X							X	X				X	X	X
Notochord		X	X	X										X		X	X
Floor plate		X		X				X	X								
Myotome	X	X	X	X				X	X	X				X	X	X	X
Limbs	X		X	X			X	X		X	X			X	X	X	
Heart			X				X							X			
Mesonephros								X		X							X
Ig subfamily	IIa	Ic	Ia	Ig	IIb	Ib	If	Id	Ie								

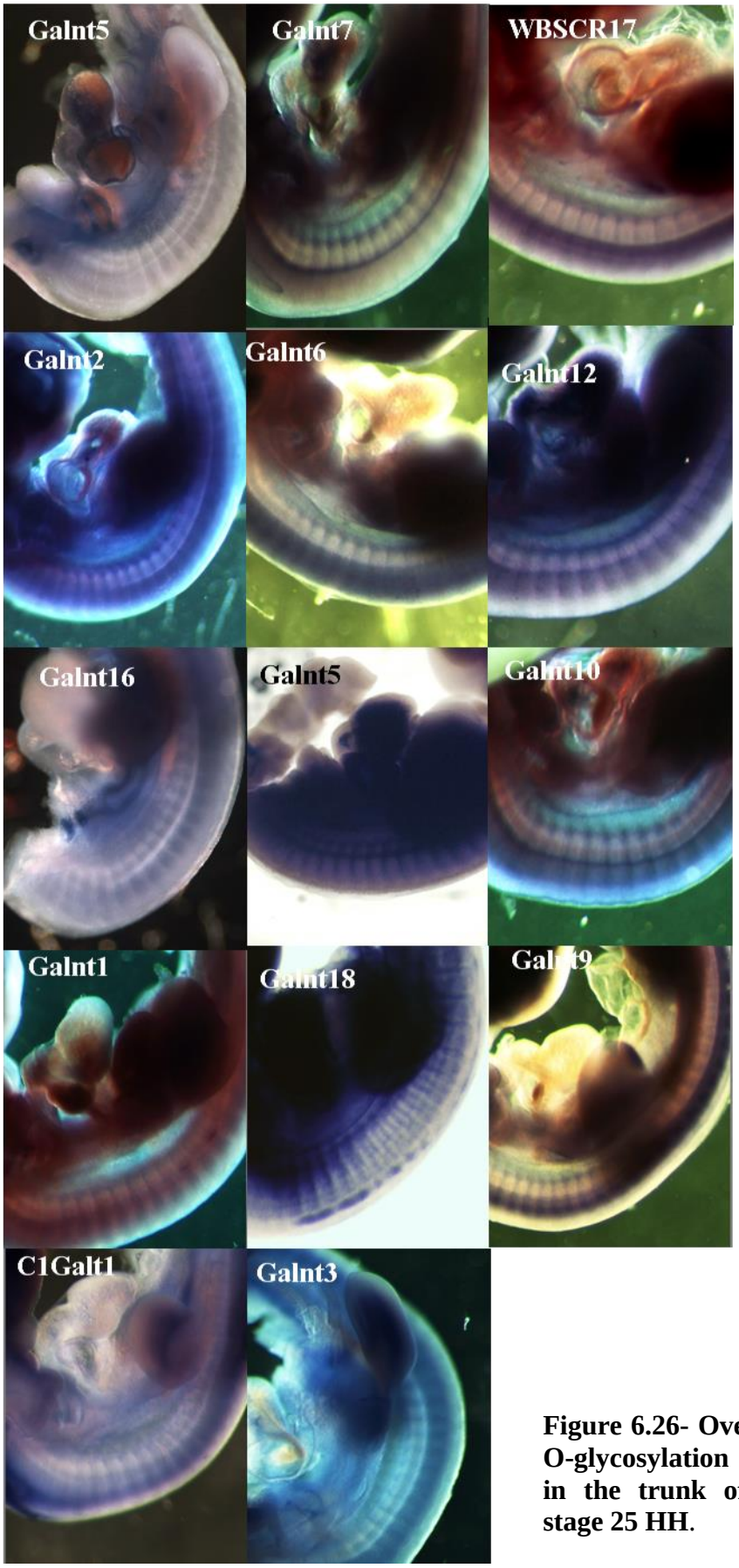

Figure 6.26- Overview of mucin-type O-glycosylation enzymes of 14 genes in the trunk of chick embryos at stage 25 HH.

CHAPTER 7- ASSESSMENT OF TWO CANDIDATE PNA-BINDING MOLECULES.

7.1- Background

The overall objective of the project was to identify genes expressed in the posterior half-sclerotome that could be responsible for somite segmentation and/or axonal guidance, and test their function. As described in sections 1.6 and 1.7, a variety of molecules present in the posterior half-sclerotome had previously been shown to be important for repelling motor axons and/or migrating neural crest cells (Fig. 7.1). For example, the double knock-out of Sema3F/Neuropilin2 and Sema3A/Neuropilin1 signalling caused sprouting of motor axons in an apparently unsegmented pattern along the spinal cord and fusion of the dorsal root ganglia (Roffers-Agarwal and Gammill, 2009) (phenotype shown in Fig. 1.25). However, motor axons were still found in fasciculated bundles in the double mutants, rather than exploring the surrounding tissues, suggesting that other key repellent molecules must be present in the sclerotome.

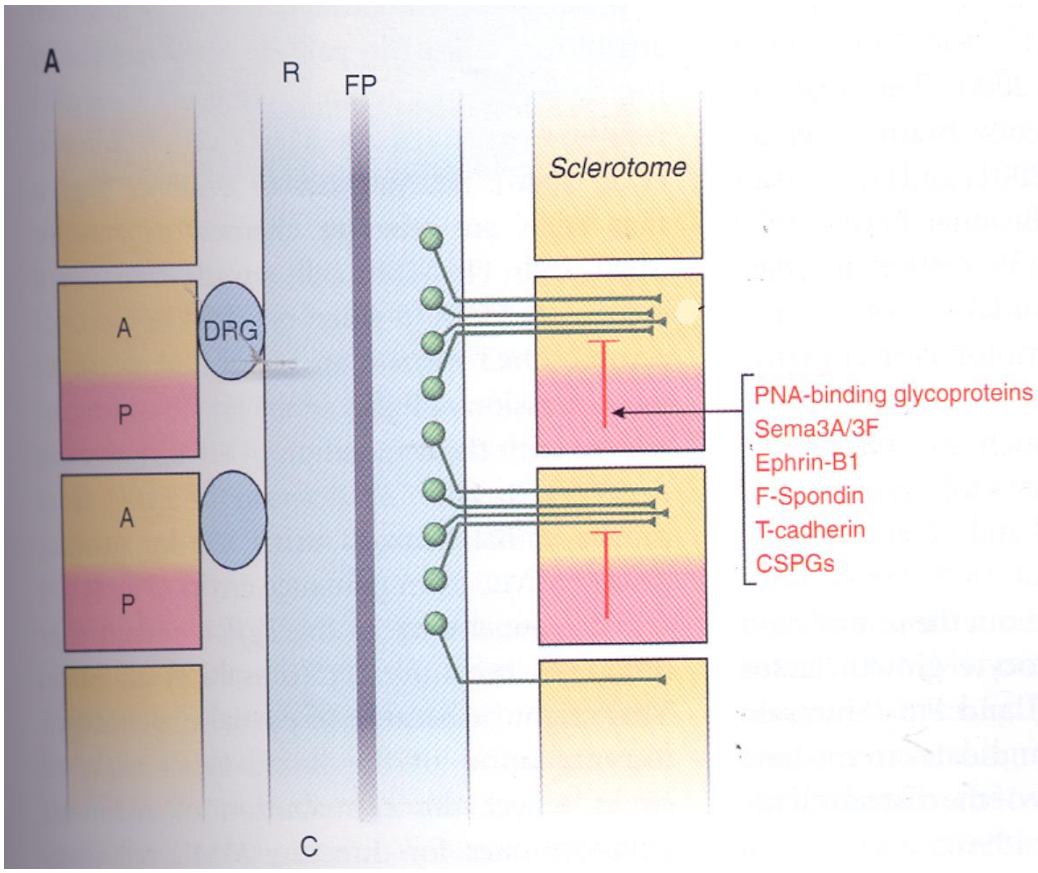

Figure 7.1- Repulsive molecules present in the posterior half sclerotome identified as being important for axonal segmentation. Figure from Bagnard (2007).

One such candidate that was identified during this project is Flrt2, a glycosylated transmembrane protein previously shown to repel axons and neurons expressing the netrin receptor Unc5D (Yamagishi *et al.*, 2011). *Flrt2* mRNA was identified in the posterior half-sclerotome in the mouse microarray screen of Hughes *et al.* (2009) and confirmed in this project to be differentially expressed in the posterior half-sclerotome of chick embryos (section 3.14). Using the *in ovo* somite transfection technique developed for this project (Chapter 4), siRNA knockdown studies suggested that Flrt2 is involved in repelling axons, and perhaps also migrating neural crest cells and/or neural crest-derived DRG neurons, from the posterior sclerotome (Chapter 5).

It has been known for more than 25 years that a PNA-binding glycoprotein is also important for this process, since PNA binds specifically to the posterior sclerotome and this allows axons to enter, suggesting that the PNA-binding glycoprotein normally repels axons from the posterior sclerotome (Stern *et al.*, 1986; Davies *et al.*, 1990; Bagnard, 2007). As described in section 1.7.1, two molecules of molecular weight 48 kDa and 55 kDa were localised by SDS-PAGE analysis of the PNA-binding glycoprotein fraction of somite extract (Davies *et al.*, 1990). However, the identity of this glycoprotein was still unknown. Studying the expression of genes encoding the ppGalNAc-T family of enzymes responsible for mucin-type O-glycosylation, which could glycosylate the PNA-binding glycoprotein, failed to identify any that were differentially expressed in the posterior sclerotome (Chapter 6). In this chapter, the results are presented of investigating two candidates for the PNA-binding protein itself: presenilin1 (section 7.1) and prolyl 4-hydroxylase, beta polypeptide (P4HB; also known as protein disulfide isomerase-associated 1, PDIA1) (section 7.2).

7.2- Presenilin1

The *Columbus* mouse mutant, which was isolated in a chemical mutagenesis screen for recessive alleles affecting spinal motor neurons (Lewcock *et al.*, 2007), showed an even more dramatic motor axon patterning phenotype than the double mutants for *Neuropilin1* and *Neuropilin2* described by Roffers-Agarwal and Gammill (2009) (shown in Fig. 1.25). In *Columbus* mutant mice, the segmentation of spinal

motor axons seemed to be lost completely (Fig. 7.2) (Lewcock *et al.*, 2007). Motor axons showed no preference for the anterior or posterior sclerotome and exhibited severe defects in ventral root formation (Lewcock *et al*., 2007; Fig. 7.2).

The *Columbus* mutation was mapped to the *Presenilin1* (*Psen1*) gene and shown to alter *Psen1* splicing, severely disrupting Psen1 protein expression (Bai *et al.*, 2011). As described in section 1.4, the multi-pass transmembrane protein Psen1 is part of the gamma-secretase complex that cleaves the Notch receptor, allowing the Notch intracellular domain (NICD) to enter the nucleus and activate transcription, and Notch signalling is critical for somite polarity.

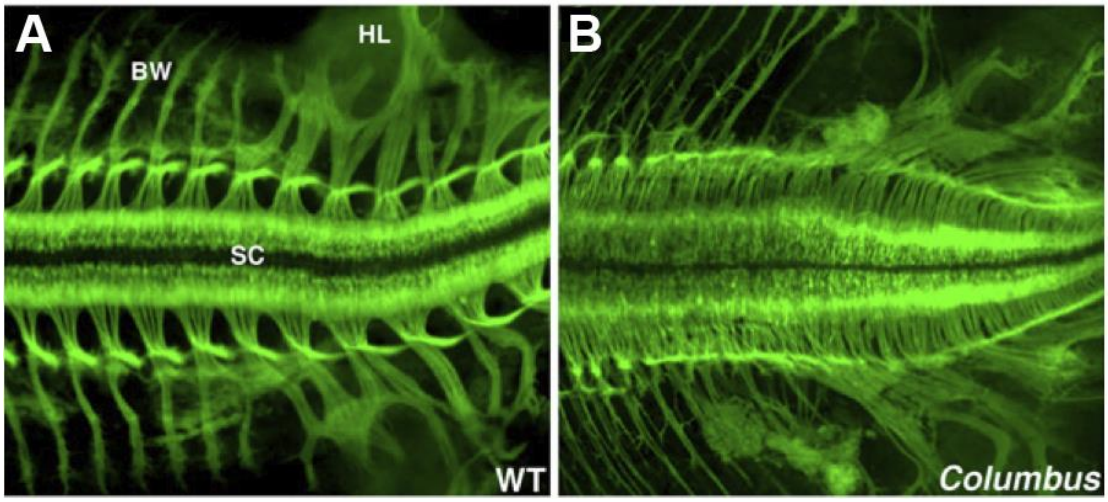

Figure 7.2- Loss of spinal motor axon patterning in *Columbus* mutant mice at E12.5. (A) Flat-mount of a wild-type embryo in which motor axons are genetically labelled with farnesylated GFP (driven by a motor neuron enhancer from the *Islet1* gene) show segmental patterning in the trunk, with discrete nerve roots. (B) Flat mount of a *Columbus* mutant (generated in the same genetic background, with motor axons genetically labelled with GFP) showing defective axon pathfinding and loss of discrete ventral motor roots. BW, body wall; HL, hindlimb; SC, spinal cord. Figure from Lewcock *et al*. (2007).

The original mouse knockouts of the *Psen1* (*PS1*) gene in 1997 reported defects in somite patterning and the axial skeleton (fused vertebrae; no axial skeleton at all caudal to the pelvis) and fused dorsal root ganglia over multiple segments, as well as CNS defects (Shen *et al.*, 1997; Wong *et al.*, 1997), indicating that *Psen1* is necessary

for anteroposterior somite patterning, even though part of the somites were still formed (Koizumi *et al*., 2001). Bai *et al.* (2011) confirmed that *Psen1* knockout led to similar motor axonal pathfinding errors as in the *Columbus* mutant, including failure to form ventral roots (and also midline crossing across the floor plate). As *Psen1* is expressed by motor neurons and interneurons in the spinal cord, as well as peripheral tissues, Bai *et al.* (2011) used a *Nestin-Cre/Psen1*$^{flox/flox}$ approach to knock *Psen1* out specifically in neural tissue. This resulted in aberrant growth of motor axons to the floorplate and midline crossing, indicating that *Psen1* mutant neurons either lost chemorepulsion from the floor plate or acquired responsiveness to a chemoattractant (Bai *et al*., 2011). However, it did not alter peripheral motor axon growth, segmentation or ventral root formation, suggesting that loss of non-neural Psen1 (presumably from the somites) was responsible for the peripheral motor axon pathfinding defects.

Despite these insights into the phenotype of the *Columbus* mutant allele of *Psen1*, somite polarity markers and the potential involvement of PNA had not yet been studied in *Psen1* mutant mice: results of these investigations are reported in this chapter. The *Psen1* hypomorphic mice used in the present study had a 500 bp insertion between exons six and seven (Rozmahel *et al*., 2002). As homozygotes, these mice produce a very small amount of mutant transcript: this is sufficient to allow normal brain development, but the defects in the axial skeleton are severe (Rozmahel *et al*., 2002). These mice were kindly provided as fixed embryos by Prof. Peter St George-Hyslop (Cambridge Institute for Medical Research).

7.2.1- Results

PNS segmentation and somite polarity were assessed at E11.0 by WMISH on *Psen1* hypomorphic and wild-type embryos for *Sox10*, encoding a Sry-related high mobility group (HMG) transcription factor expressed in migrating neural crest cells, neural crest-derived neuroglial precursors, satellite glia in ganglia and Schwann cells along nerves (Britsch *et al.*, 2001), thus allowing the identification of dorsal root ganglia and nerves, and *Uncx4.1* (*Uncx*), encoding a homeodomain transcription factor present in the posterior half-sclerotome (Schrägle *et al*., 2004).

Psen1 hypomorphs were around 30% smaller than wild type (Fig. 7.3) and appeared normally segmented, as disruption to segmentation only started caudal to the hindlimb (Figs. 7.3, 7.4, 7.5). WMISH was successful for both *Sox10* (Fig. 7.4A-H) and *Uncx4.1* (Fig. 7.4I-S). *Sox10* expression in *Psen1* hypomorphs began to differ from wild-type embryos in the lumbar area, becoming wider relative to wild-type expression, and with no visible segmentation in the tail (Fig. 7.3B,G,H). *Uncx4.1* expression was present in all the somites, and normal rostral to the hindlimb (Fig. 7.4J), however posterior to this *Uncx4.1* expression varied within the sclerotome, with expression being thinner and lost from the dorsolateral sclerotome, although it was still segmented (though thinner) within the tail (Fig. 7.4O-R). (*Uncx4.1* expression seen in the brain, neural tube and mesonephros is normal; Mansouri *et al.*, 1997.)

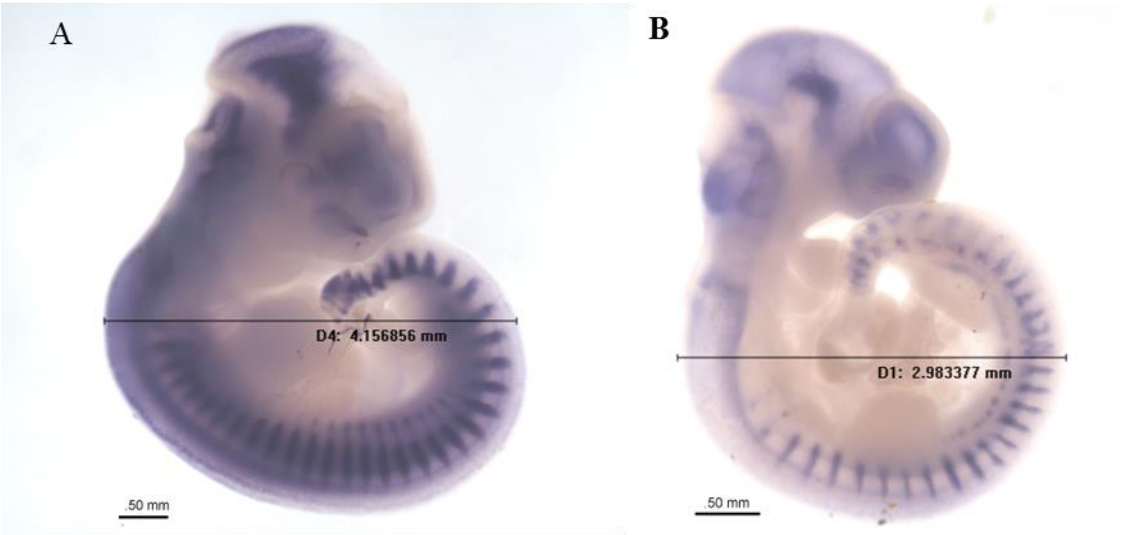

Figure 7.3- Size difference between wild type and hypomorphic *Psen1* mutant mouse embryos at E11.0 after WMISH for *Uncx4.1*. (A) Wild type mouse embryo, length along indicated line is around 4.15 mm. (B) *Psen1* hypomorphic litter mate, length along indicated line is around 3 mm.

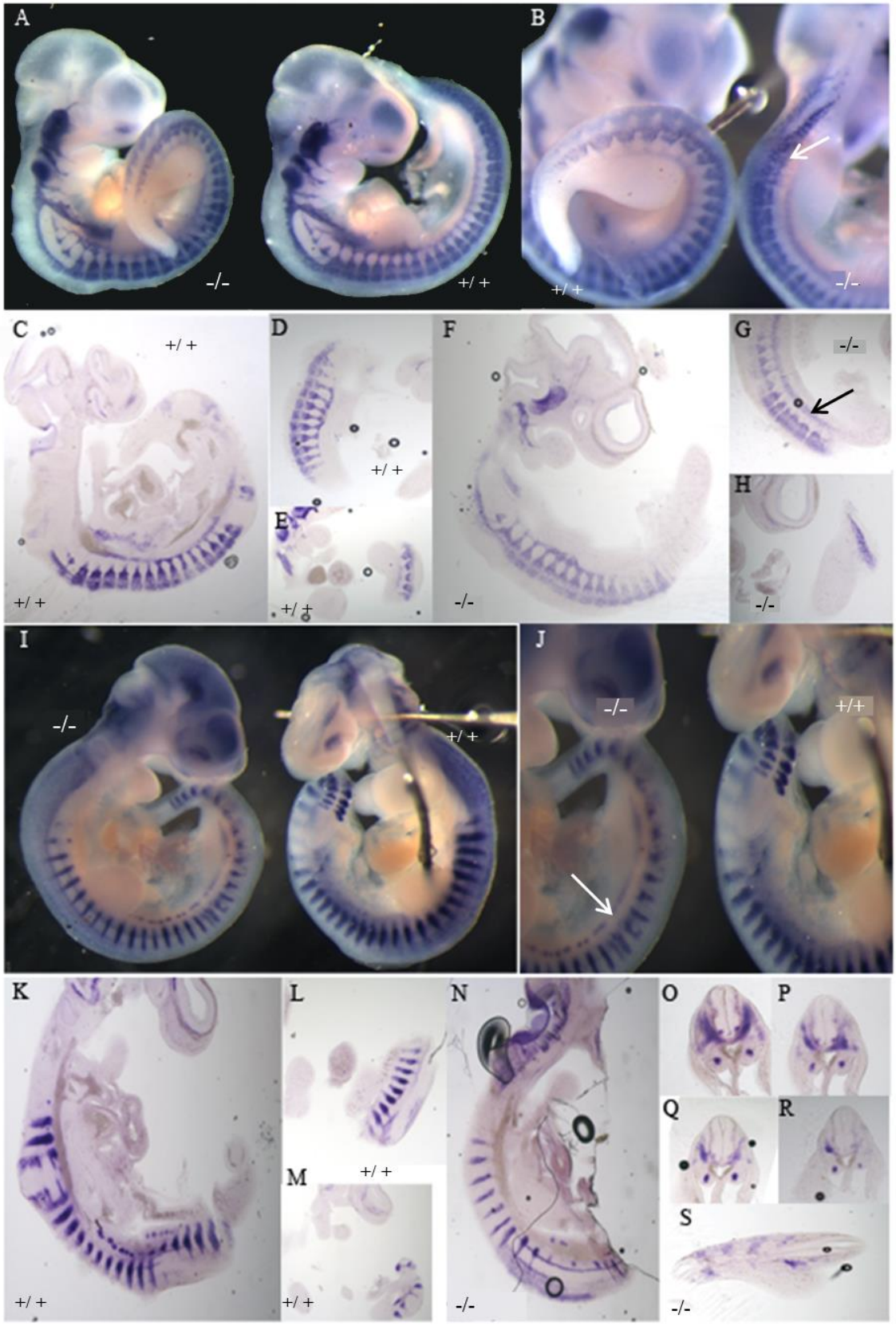

Figure 7.4- Legend on next page.

Figure 7.4- (On previous page) Mouse embryos and sections after WMISH for *Sox10* or *Uncx4.1* at E11.0. (A-H) WMISH for *Sox10*. (A) *Psen1* hypomorph (left; -/-) and wild type litter-mate (right; +/+). (B) Higher-power view of tail region. *Sox10* expression in the tail of the *Psen1* hypomorph (right; -/-) is not segmented (white arrow), unlike in the wild type embryo (left). (C-E) Parasagittal sections of a wild type embryo, showing (C) segmentation of DRG and spinal nerves; (D) axons to the limbs and (E) expression in the tail. (F-H) Parasagittal sections of *Psen1* hypomorph (-/-), showing (F) segmented pattern of DRG and spinal nerves in trunk; (G) loss of segmented pattern of DRG and spinal nerves at the level of the hind limb (arrow); (H) total loss segmentation in the tail. (I-S) WMISH for *Uncx4.1*. (I) *Uncx4.1* expression in the *Psen1* hypomorph (left; -/-) is reduced and shows variation in the expression relative to a wild type litter-mate (right; +/+). (J) Detail of the tail region of the embryos in I. *Uncx4.1* expression is reduced but still segmented in the *Psen1* hypomorph (left; -/-). (K-M) Parasagittal sections of a wild type embryo, showing *Uncx4.1* expression in posterior half-sclerotomes (K,L) near the hind limb and (M) in the tail. (N) Parasagittal section of a *Psen1* hypomorph. *Uncx4.1* expression is reduced in the sclerotome. (O-R) Transverse sections of a *Psen1* hypomorph. *Uncx4.1* expression varies through the sclerotome. (S) Coronal section of the tail of a *Psen1* hypomorph showing segmented *Uncx4.1* expression.

The complementary changes in expression of *Uncx4.1* and *Sox10* at the same location can most easily be seen in embryos side by side in the same dish (Fig. 7.5A-C). Despite the changes in *Uncx4.1* and *Sox10* expression, however, rhodamine-labelled PNA treatment showed that *Psen1* hypomorphs still display segmented PNA binding (Fig. 7.5D-F) even in the tail, where *Sox10* was most affected.

Overall, *Psen1* hypomorphic embryos at E11.0 present with defects in the sclerotome caudal to the hindlimb. Loss of *Uncx4.1* leads to loss of pedicles, transverse processes and proximal ribs (Leitges *et al.*, 2000; Mansouri *et al*., 2000). Since *Uncx4.1* expression abnormalities were seen in *Psen1* hypomorphic embryos (Fig. 7.4), Alcian blue staining for cartilage at E14.0 was used to assess any impact on axial skeleton formation (Fig. 7.6). As expected, given the severe axial skeleton deformities seen in 6-week *Psen1* hypomorphs (Rozmahel *et al.*, 2002), defects seen at E14.0 included vertebral duplications and fusions, shorter or missing pedicles, fused transverse processes and fewer ribs (11 instead of 13) (Fig. 7.6).

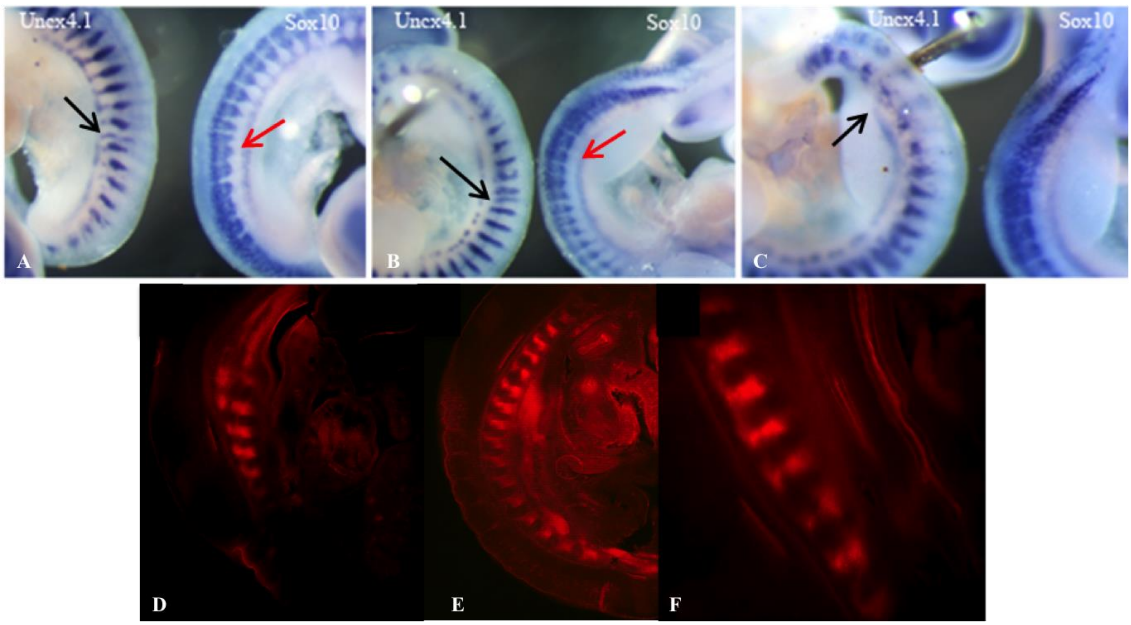

Figure 7.5- *Uncx4.1*, *Sox10* and rhodamine-labelled PNA binding in *Psen1* hypomorphs at E11.0. (A-C) WMISH for *Uncx4.1* and *Sox10* shows that *Uncx4.1* and *Sox10* expression patterns are complementary in the trunk (A), near the hind limb (B) and in the tail (C). *Uncx4.1* expression in the sclerotome becomes very thin in the sacral region (black arrow in A,B), and from that point to the end of the tail, *Sox10* expression becomes unsegmented (red arrow). In contrast, near the tail *Uncx4.1* expression

becomes normal again and continues normal to the end of the tail (arrow in C). (D-F) Rhodamine-labelled PNA binding (red) in the cervical area (D), thoracic and lumbar area (E) and sacral area (F).

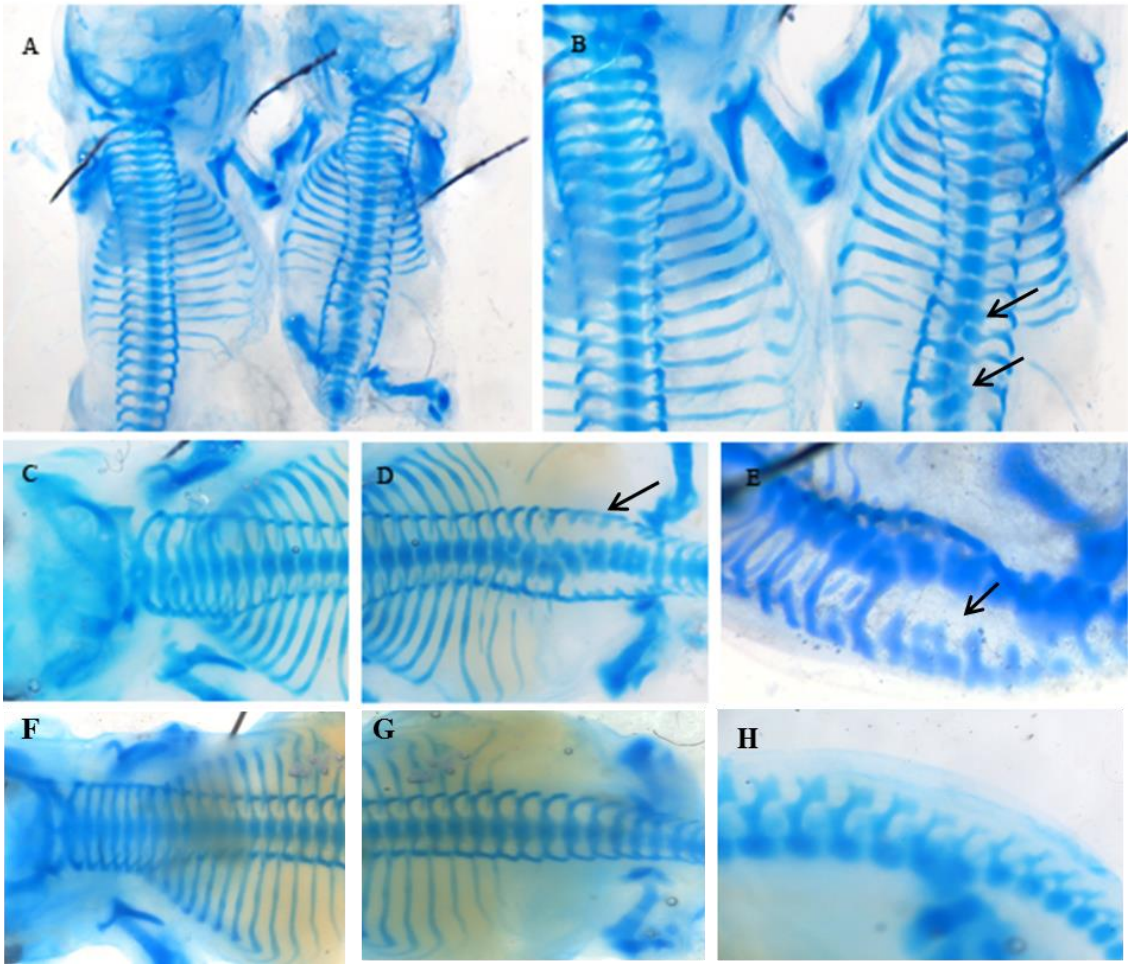

Figure 7.6- Alcian blue staining for cartilage in mouse embryos at E14.0. (A,B) Low-power and higher-power views of a wild type embryo (left) and a *Psen1* hypomorphic litter-mate (right). In the thoracic area, the *Psen1* hypomorph shows duplications and fusion of vertebrae (arrow) and fewer ribs; some ribs appear thinner. (C) Cervical region of a *Psen1* hypomorph, showing duplication of the second vertebral body (compare with F). (D) Lumbar vertebrae of a *Psen1* hypomorph (arrow) show missing pedicles and fusion of the transverse processes (compare with G). (E) Lateral view of the lumbar vertebrae in a *Psen1* hypomorph (arrow). The pedicles are shortened and the transverse process fused. (F) Cervical region of a wild type embryo. (G) Lumbar and sacral region of a wild type embryo. (H) Dorsal view of vertebral bodies and pedicles in a wild type embryo.

7.1.2- Discussion

This study was carried out to explore if *Psen1* may play a role in somite polarity and whether it could be the PNA-binding glycoprotein in the posterior sclerotome, given the striking motor axon guidance defects in mice with the *Columbus* mutation in *Psen1*, that was later shown to be phenocopied by knocking out *Psen1* (Lewcock *et al.*, 2007: Bai *et al.*, 2011). Although the PNA-binding protein was previously suggested to be 55kDa and 48kDa (Davies *et al*., 1990), and Presenilin1 is 53kDa and 20kDa (Haass and De Strooper, 1999), this does not rule out the possibility that there may be a Psen1 isoform responsible for the PNA-binding reaction. However, the *Psen1* hypomorphic mice used here, which have severe axial skeletal but not CNS phenotypes (Rozmahel *et al.*, 2002) still displayed segmental PNA-binding in the posterior sclerotome (although clearer sections of the tail would be helpful to show this more clearly). This suggests that Psen1 is not the PNA-binding glycoprotein responsible for axon repulsion in the posterior sclerotome and that this molecule still remains to be found.

In *Psen1* hypomorphic mouse embryos at E11.0, segmental expression of *Sox10* and *Uncx4.1* is still present in most of the trunk, but changes are seen in the expression of both genes beginning in the same region in the lumbar area and moving further posteriorly to the tail (Fig. 7.4 and Fig. 7.5). *Sox10* expression in the tail is continuous, with no visible segmentation, even though *Uncx4.1* expression in the tail shows a clear segmentation. Similarly, even though *Uncx4.1* expression in the rest of the embryo is thinner than in wild type embryos, it is still segmented. The neural crest/ganglion marker *Sox10* has a normal expression pattern within the embryo until the same point where *Uncx4.1* becomes thin, where *Sox10* expression becomes wider, suggesting fusion of dorsal root ganglia as previously reported for *Psen1*-deficient embryos (Shen *et al.*, 2007). Presumably the modifications in *Uncx4.1* expression could have contributed to the phenotypes observed in the axial skeleton.

The present study found that *Psen1* hypomorphic embryos are around 30% smaller than wild type embryos, perhaps due to the formation of fewer somites, later reflected by a reduction in the number of ribs present (11 instead of 13) (Fig. 7.5).

Similarly, *Psen1*-knockout mice were also smaller and had fewer ribs (Shen *et al.*, 1997).

According to Leitges *et al*. (2000), pedicles, transverse processes and proximal ribs develop from the lateral sclerotome. The *Psen1* hypomorphic mice in the present study have a similar axial skeletal phenotype at E14.0 as Leitges *et al.* (2000) described where the absence of *Uncx4.1* expression in the lateral posterior sclerotome caused modification in the formation of pedicles, transverse processes and proximal ribs and vertebral arches (Leitges *et al*., 2000). *Psen1* hypomorphic mice do not express *Uncx4.1* in the lateral sclerotome at E11.0 (Fig. 7.4O-R), and at E14.0 the embryos formed only part of the pedicles, and showed fusion of transverse processes and duplication of vertebral bodies. The alterations to the vertebral bodies, pedicles and transverse processes are only visible in the lumbar vertebrae, where *Uncx4.1* and *Sox10* expression changes were prominent. In the tail, *Sox10* expression lost its segmentation, but *Uncx4.1* was as segmented as a wild type embryo so did not have any impact on the formation of the skeleton.

It is interesting to note that the *Psen1* hypomorphs displayed the abnormal phenotype only in the lumbar vertebrae (although at 6 weeks of age, the majority of vertebrae in surviving animals were reported to be affected; Rozmahel *et al.*, 2002). However, in *Psen1* knockout animals, the axial skeleton caudal to the pelvis is completely missing and cervical, thoracic, lumbar and sacral vertebrae are fused (Shen *et al.*, 1997). Although the whole axial skeleton would need to be examined carefully in postnatal animals with the *Psen1* hypomorphic mutation to see if there are real differences with *Psen1*-null animals, is possible that the tiny amount of mutant *Psen1* mRNA produced in *Psen1* hypomorphs (Rozmahel *et al.*, 2002) partially rescues axial skeleton formation relative to *Psen1*-null animals. In *Xenopus*, morpholino-based knockdown of the Notch ligand XDelta2 showed that this is required for *Hox* gene expression during somite formation and even earlier, from gastrulation stages onward (Peres *et al.*, 2006). It would be interesting to study if there is any modification of *Hox* gene expression in *Psen1* hypomorphic and *Psen1*-null mice that could also contribute to any differences seen in the axial skeletons of these mice.

In conclusion, Psen1 is not the PNA-binding protein responsible for axonal repulsion in the posterior sclerotome; however the *Psen1* hypomorph (Rozmahel *et al.*, 2002) would be an interesting model in which to study the contribution of *Psen1* to vertebra formation.

7.3- Prolyl 4-hydroxylase, beta polypeptide (P4HB)

Davies *et al*. (1990) isolated 55 kDa and 48 kDa proteins from a detergent-soluble glycoprotein fraction that had high affinity with PNA, caused growth cone collapse and inhibited neurite extension of dorsal root ganglion neurons. It was not possible at that time to identify these proteins. More recently, a new somite extract was prepared, and proteins separated by size; the two corresponding bands (55 kDa and 48 kDa) were removed and sent for sequencing (Prof. R. J. Keynes, personal communication). After Edman degradation, the fragments were found to be chick retina-cognin (R-cognin), a cell surface form of P4HB (prolyl 4-hydroxylase, beta polypeptide), also known as protein disulfide isomerase (PDI) or PDI-associated 1 (PDIA1) (Bassuk *et al*., 1991; Phillips *et al*., 1997; Pariser *et al.*, 2000). P4HB is a protein disulfide isomerase (PDI; Fig. 7.7) found in the endoplasmic reticulum of almost all cells that catalyzes the formation and isomerisation of disulfide bonds, facilitating protein folding (Figs. 7.8 and 7.9) (Bassuk *et al*., 1991; Phillips *et al*., 1997; Andreu *et al.*, 2012). Several studies have detected PDI expression at the cell surface (Täger *et al.*, 1997; Zai *et al.*, 1999; Root *et al.*, 2004; Wan *et al.*, 2012), while Bi *et al.* (2010) showed that cell-surface P4HB binds PNA. Hence, it is indeed possible that the PNA-binding axon repellent in the posterior sclerotome is a cell surface isoform of P4HB.

The PDI protein family comprises 21 known members of foldases and chaperones (Fig. 7.7) and is necessary for the physiological function of cells (Andreu *et al.*, 2012). The accumulation of misfolded proteins generally leads to progressive decline of cell function, contributing to neurodegenerative diseases such as Alzheimer's disease, Parkinson's disease and amyotrophic lateral sclerosis (ALS), among others (Andreu *et al.*, 2012). The mechanisms by which the abnormal misfolding causes modifications in axonal transport, synapse formation, synapse maintenance and redox

balance are poorly understood, but it is known that some PDI forms have different catalytic centres with specific roles in cellular function, such as apoptosis, production of reactive oxygen species (ROS), protein aggregation, cell signalling and endoplasmic reticulum-associated degradation (Figs. 7.8 and 7.9) (Andreu *et al.*, 2012).

PDI family members are characterized by the arrangement of thioredoxin-like catalytic domains (blue domains in Fig. 7.7) and non-catalytic domains (green and purple domains in Fig. 7.7). The catalytic domains have an active-site motif (CXXC) that reacts with thiols and determines the redox potential of PDIs and their role as reductase, oxidase or isomerase. The non-catalytic domains stabilize the catalytic domain and are responsible for substrate recognition and recruitment, and have interaction sites for cofactors (Andreu *et al.*, 2012; Vinaik *et al.*, 2013).

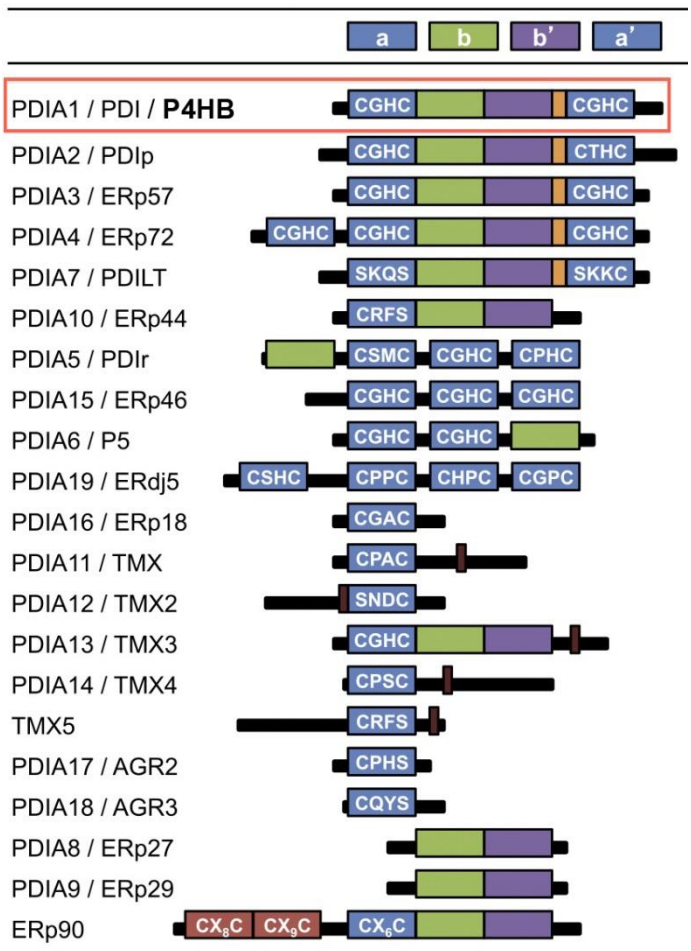

Figure 7.7- The PDI family. Catalytic domains a and a' are shown in blue; non-catalytic b and b' domains in green and purple, respectively. The cross-linker between b' and a' is in orange and transmembrane domains in dark red. P4HB, also known as

PDIA1 and PDI, is highlighted on the top row. Figure modified from Andreu *et al.* (2012).

P4HB (PDIA1, PDI) was the first PDI family member to be identified, however little is known about its function *in vivo*; in mammalian cells, P4HB is vital for oxidative protein folding (Figs. 7.8 and Fig. 7.9), and in yeast it is essential for cell survival (Andreu *et al.*, 2012). P4HB, like other PDI family members, has been linked to neurodegenerative diseases (Table 7.1). In the brain ischemia-reperfusion model, P4HB was the major protein present in the hypoxia model and its over-expression *in vivo* resulted in improved neuronal survival upon ischemia reperfusion (Andreu *et al.*, 2012). Interestingly, PNA binding is also present in specific areas in the grey matter of the brain (Prof. R. J. Keynes, personal communication): perhaps PNA is also binding to P4HB in grey matter. Here, siRNA-mediated knockdown against chick *P4HB* in somites was used to study any impact on axon targeting.

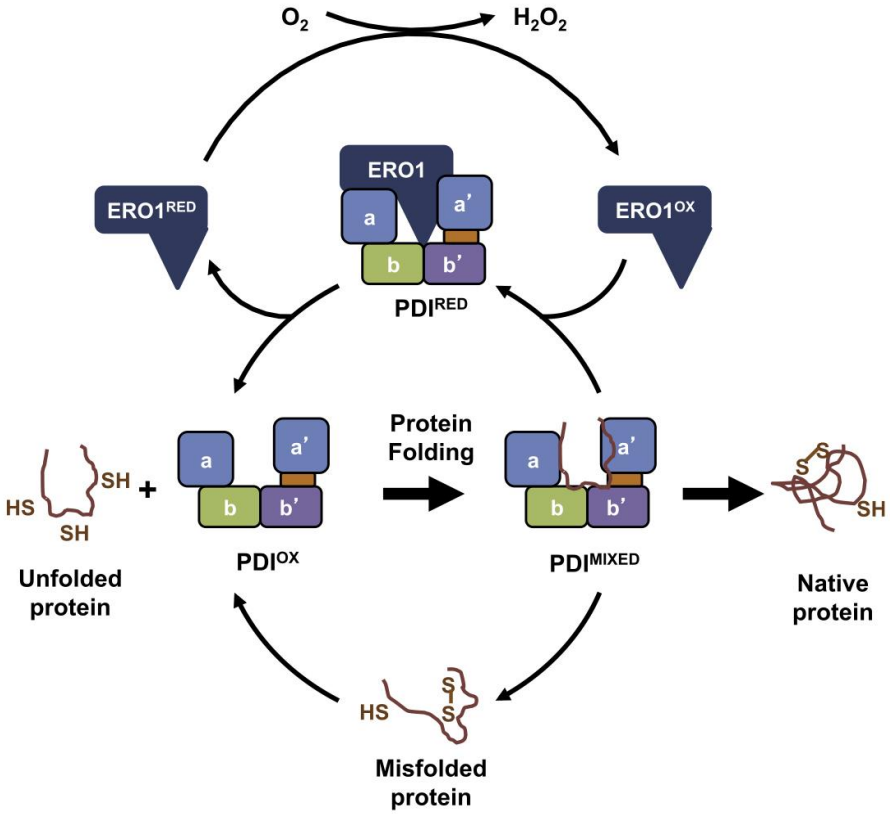

Figure 7.8- The protein folding activity of PDI and the redox relay of PDI and ERO1, resulting in the generation of H_2O_2. PDIOX: oxidized PDI; PDIRED: reduced PDI; PDIMIXED: PDI with the bound substrate; ERO1OX: oxidized ERO1; ERO1RED: reduced ERO1. PDI domains are coloured as shown in Fig. 7.7. Figure and legend from Andreu *et al.* (2012).

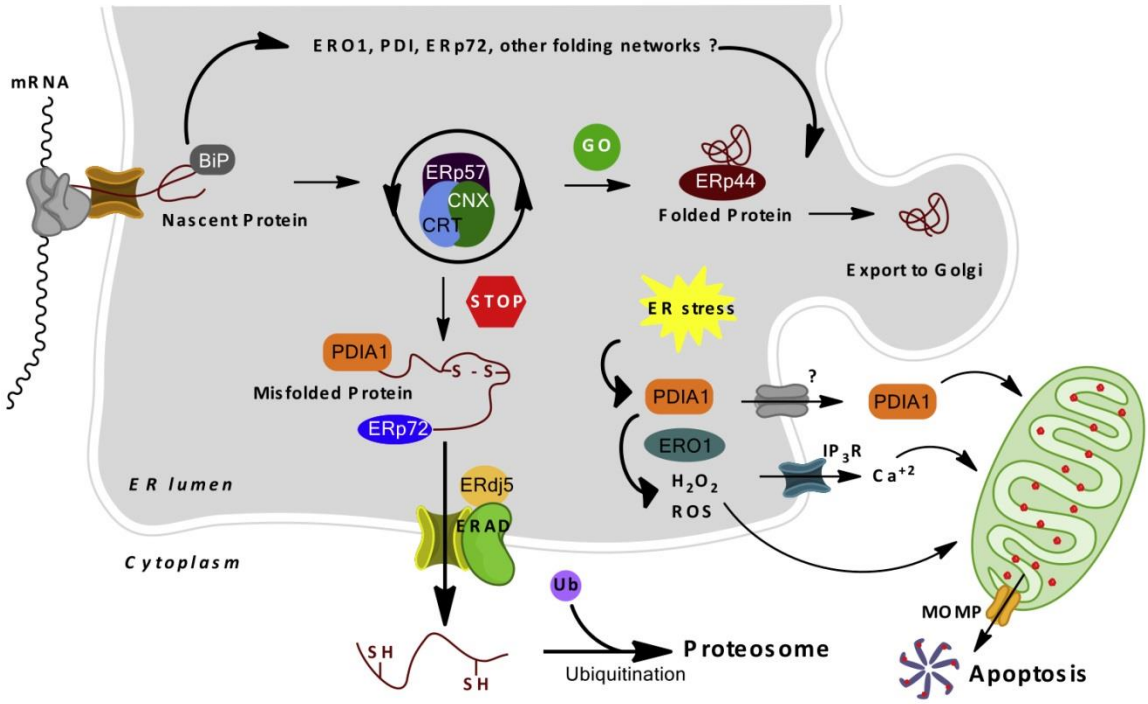

Figure 7.9- The diverse functions of PDIs, including PH4B (PDIA1), in the endoplasmic reticulum (ER). "Newly synthesized unfolded polypeptides are translocated into the ER. Folding of glycoproteins requires CNX (green) or CRT (light blue) and ERp57 (purple), the components of the CNX/CRT cycle. Non-glycosylated polypeptides may acquire a folded state by additional protein folding networks, to promote their folding, including, for example, the participation of PDIA1 or ERp72. ERp44 (dark red) retains client proteins in the ER preventing premature transport to the Golgi until the folding process is completed (GO). Then, folded proteins are exported through the secretory pathway. Misfolded proteins (STOP) may bind to PDIA1 (orange) and ERp72 (blue) and retro-translocate to the cytosol via the ERAD pathway, where ERdj5 has an important function in disrupting disulfide bonds. Under ER stress conditions, PDIA1 can be released to the cytosol through activation of BAX and BAK at the ER, targeting the mitochondria. This event triggers apoptosome assembly resulting in cell death. By modulation of the redox state of calcium channels, such as the IP3 receptor and the calcium pump SERCA, PDIs also control ER calcium release. In addition, abnormal H2O2 production by ERO1 (dark blue) could result in ROS production. These two events may also contribute to trigger mitochondrial outer membrane permeabilization and the release of cytochrome c (red circles) and the activation of the apoptosome." Note: PDIA1 is an alternative name for P4HB. Figure and legend from Andreu *et al.* (2012).

Table 7.1- Evidence linking PDI family members to neurodegenerative diseases. Note: PDIA1 is an alternative name for P4HB. ALS, amyotrophic lateral sclerosis; PD, Parkinson's disease; AD, Alzheimer's disease; PrDs, prion diseases; HD, Huntington's disease. Table from Andreu *et al.* (2012).

Disease	Effect
ALS	• PDIA1 and ERp57 are up-regulated in ALS mouse models and patients. • PDIA1 knockdown or overexpression increases or decreases mutant SOD1 aggregation, respectively. • PDIA1 inactivation by S-nitrosylated is detected in tissue from ALS mouse models and patients. • PDIA1 co-localizes with FUS and TDP-43 inclusions in ALS-derived tissue.
PD	• S-nitrosylated PDIA1 is found in the brain of PD patients. • PDIp is upregulated in the brain of PD patients, it is found in Lewy bodies, and is induced in αSynuclein transgenic mice. • PDI upregulation is observed in many toxicological models of PD.
AD	• ERp57 interacts with β-amyloid and prevents its aggregation. • PDIA1 is present in neurofibrillary tangles. • S-nitrosylated PDIA1 is detected in the brain of AD patients. • Inhibition of PDIA1 and ERp57 protects against amyloid β toxicity.
PrDs	• ERp57 is upregulated in the brain of CJD patients and in animal models of infectious prion disease. • ERp57 and PDIA1 protect cells against misfolded PrP. • PDIA1 is nitrosylated in PrD models.
HD	• Inhibition of PDIA1 or ERp57 suppresses neuronal degeneration induced by mutant Huntingtin.

7.3.1- Chicken *P4HB* siRNA design

The flurescein-labelled siRNA used to knock down cell surface P4HB (PDI) in chick was designed according to the sequence of an antisense phosphorothioate (S-oligo; nuclease-resistant oligonucleotide) successfully used to knock down cell surface P4HB (PDI) in a human erythroleukemia (HEL) cell line (Zai *et al*, 1999). These authors designed three antisense S-oligos against human *P4HB* mRNA, however only one of the three reduced the cell surface expression of P4HB significantly (by 74 ± 9.2% compared to the scrambled S-oligo control); moreover, cell viability was unaffected after transfection (Zai *et al*., 1999). The sequence for the successful oligo was 5′-GCAGCGAGACTCCGAACACGGTA-3′; this was designed to hybridize with a

sequence in the 3' UTR of the human *P4HB* mRNA. Following the rules described in section 4.2.1, an appropriate target sequence was also found in the 3' UTR of chicken *P4HB*. The sequence used to target chick *P4HB* was: 5'-TCGCCCTCACTTGTCTTTA. A FITC-labelled control scrambled siRNA with the sequence 5'-GCTCTCTCGTCTATCTACT was designed using InvivoGen Scramble siRNA software (http://www.sirnawizard.com/scrambled.php). All 21 base-pair sequences were subjected to NCBI BLAST to ensure that they would not target any other genes.

7.3.2- Testing a commercial anti-P4HB antibody and chick *P4HB* siRNA efficiency *in vitro* on human astrocytes and chick retinal cells

The first aim was to assess whether the chick *P4HB* siRNA worked to knock down P4HB. As there was no access to the P4HB-expressing HEL cell line used by Zai *et al*. (1999) in their antisense S-oligo experiments, human astrocyte cell line (Neu7) was used to transfect with a siRNA containing their antisense S-oligo sequence (see section 7.2.1). An anti-P4HB (anti-PDI) antibody (Sigma) was successfully used in live-immunostaining experiments in cultured Neu7 cells (Fig. 7.10A-F). P4HB expression was only detected in cells that appeared to be dividing and that were much smaller than other cells, whether transfected with scrambled siRNA (Fig. 7.10A,C) or untransfected (Fig. 7.10D). The knockdown of cell surface P4HB expression using *P4HB* siRNA was not very efficient as not all cells were transfected with FITC-siRNA (Fig. 7.10B,E,F). P4HB expression was still present on the cells that were not transfected and highly reduced at the surface of the *P4HB* siRNA-transfected cells, although cytoplasmic P4HB expression was still detected (Fig. 7.10E,F). However, cell adhesion and proliferation were affected, as cells kept a rounded shape and did not grow as much as non-transfected cells and were individually spread (compare Fig 7.10A and B). The anti-PH4B antibody worked well: it was possible to detect cell surface staining at higher magnification (Fig. 7.10C,F) and no staining was seen in any controls (Fig. 7.10G-I).

Combining anti-P4HB live-immunostaining with fluorescein-labelled PNA treatment showed that Neu7 cells not only expressed cell-surface P4HB, but also bound PNA at the cell surface (Fig. 7.10A), consistent with the hypothesis that P4HB could be

the PNA-binding protein in posterior sclerotome cells. The anti-P4HB antibody (which was raised against bovine P4HB), was also used successfully in live-immunostaining studies to detect P4HB on the surface of chick retinal cells (Fig. 7.11B). This was an important positive control, since chick P4HB (R-cognin; retinal-cognin), was first identified in these cells (Hausman and Moscona, 1976; Hausman and Moscona, 1979). Furthermore, transfection of these cells with FITC-labelled *P4HB* siRNA led to efficient knockdown, as no P4HB was detected 16 hours after transfection (Fig. 7.11C).

Figure 7.10- (On next page) Assessment of anti-P4HB antibody specificity and *P4HB* siRNA transfection in a human astrocyte line (Neu7). (A) P4HB expression (red) and fluorescein-labelled PNA binding (green) in a subset of Neu7 cells (DAPI-stained nuclei, blue), 16 hours after transfection with FITC-labelled scrambled siRNA. (B) P4HB expression 16 hours after transfecting cells with FITC-labelled *P4HB* siRNA. (C) Higher-power view of P4HB expression in scrambled siRNA-transfected cells. (D) Higher-power view of P4HB expression (red) and fluorescein-PNA binding (green) in untransfected cells. (E) Higher-power view of *P4HB* siRNA-transfected cells (green, FITC-siRNA) immunostained for P4HB (red). Only a subset of cells are transfected. (These cells were not treated with fluorescein-labelled PNA.) (F) Same image as in E, showing P4HB expression in greyscale. (G-H) Controls for primary antibody specificity. (G) Cells immunostained without any primary antibody (i.e., using the Alexa594-conjugated goat anti-rabbit secondary antibody alone). (H) Cells immunostained using anti-P4HB antibody that had been preadsorbed with P4HB protein. (I) Cells incubated with rabbit IgG instead anti-P4HB. Blue: DAPI (nuclei).

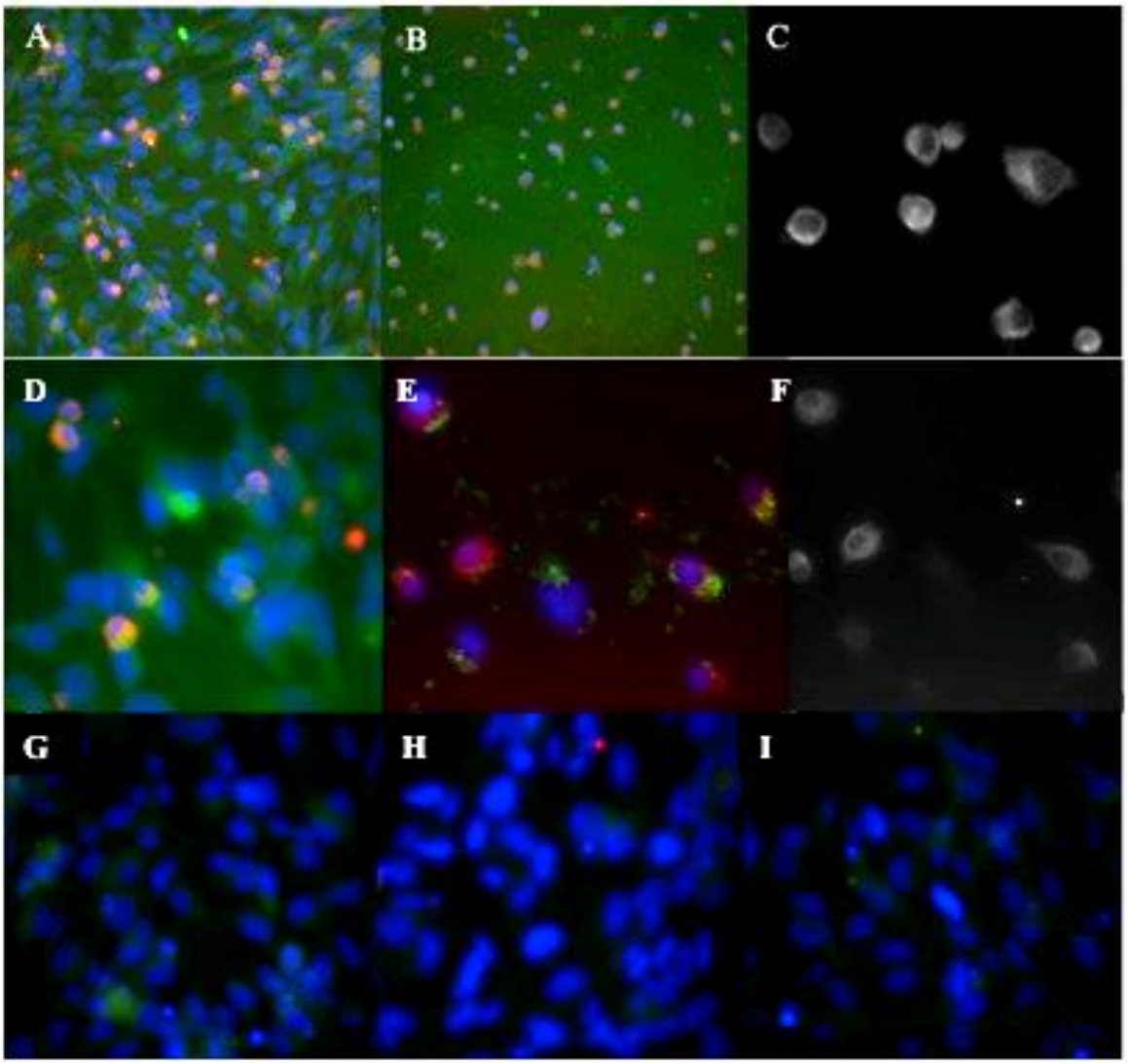

Figure 7.10- Legend on previous page.

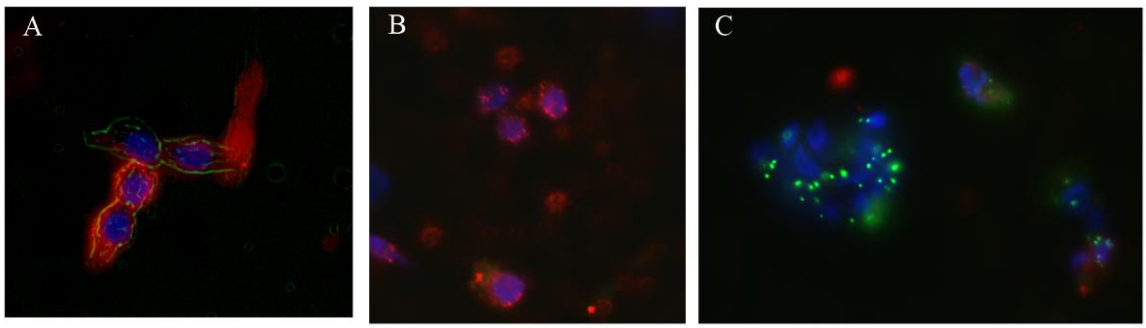

Figure 7.11- P4HB expression in Neu7 cells and chick retinal cells stage 22 HH in culture. (A) Cell surface staining of Neu7 cells (DAPI-stained nuclei, blue) for both P4HB (red) and dlurescein-labelled PNA (green). (B) Cell surface expression of P4HB (red) in chick retinal cells, showing a ring-like effect and some punctate expression. (C) Efficient suppression of P4HB expression (red) in chick retinal cells (DAPI-stained nuclei, blue) transfected with FITC-labelled *P4HB* siRNA (green).

7.3.3- Assessing P4HB expression and siRNA knockdown efficiency in dissociated sclerotome cells *in vitro*

The next step was to see if P4HB expression could be detected on posterior sclerotome cells *in vitro* by live-immunostaining, and, if so, to assess the effect on this of *P4HB* siRNA transfection. It was necessary to optimise the protocol, as it seemed very easy for posterior sclerotome cells, depending on the substrate, to differentiate into fibroblasts and lose their ability to bind PNA. Including a fragment of notochord in the culture was found to help prevent the differentiation of sclerotome cells into fibroblasts. Somite strips were explanted, dissociated mechanically with a syringe needle to avoid the loss of any cell membrane properties, and cultured for 16 hours before live-immunostaining. The dissociated somite strips included anterior half-sclerotomes, but these never expressed P4HB or bound PNA (see next section). The substrate was important, as posterior sclerotome cells kept their PNA-binding characteristics only when cultured on non-coated glass (also, using polylysine-coated slides increased antibody background). This assay was verified at least four times.

Cell-surface expression of P4HB was detected by live-immunostaining on dissociated sclerotome cells (presumably posterior; see next section) (Fig. 7.12A). When somite strips that had been transfected *in ovo* with FITC-labelled scrambled siRNA were dissociated and cultured for 16 hours, P4HB expression was still detected at the cell surface (Fig. 7.12B). However, P4HB expression was lost in sclerotome cells cultured from somite strips that had been transfected *in ovo* with FITC-labelled P4HB siRNA (Fig. 7.11C). Like *P4HB* siRNA-transfected Neu7 cells (Fig. 7.10B), *P4HB* siRNA-transfected sclerotome cells were also more spread out than scrambled siRNA-transfected sclerotome cells.

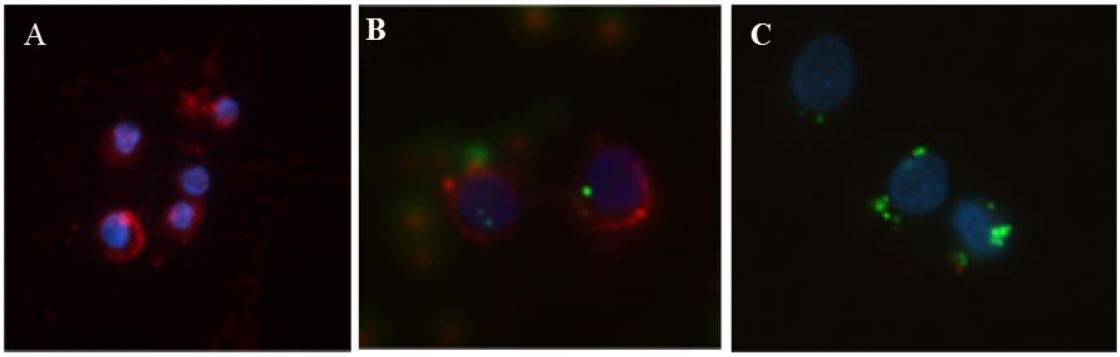

Figure 7.12- P4HB expression and siRNA_mediated knockdown in chick sclerotome cells dissociated and cultured for 16 hours after transfection *in ovo*. (A) Untransfected, dissociated chick sclerotome cells in culture (DAPI-stained nuclei, blue). P4HB (red) is expressed at the cell surface (ring-like effect) and there is punctate expression in the cytoplasm. (B) Sclerotome cells cultured after transfection *in ovo* with FITC-labelled scrambled siRNA (green). P4HB (red) is still expressed at the cell surface. (C) No P4HB expression (red) is seen in sclerotome cells cultured after transfection *in ovo* with FITC-labelled P4HB siRNA (green). Red: anti-P4HB; blue: DAPI, green: FITC-siRNA

7.3.4- P4HB expression and PNA-binding overlap in the posterior sclerotome

Since P4HB expression could be detected on the cell surface of sclerotome cells in culture, the next aim was to assess if P4HB expression was coincident with PNA binding. Somite strips were explanted from embryos, cultured intact and subjected to live immunostaining and treatment with fluorescein-labelled PNA (Fig. 7.13). P4HB expression and PNA binding were indeed coincident (Fig. 7.13A-C). At higher magnification, the staining for both P4HB and PNA also seemed to be at the cell surface. Hence, the protein originally isolated by Davies *et al*. (1990) and that according to Edman degradation corresponds to P4HB, is for the first time detected on the cell surface of posterior sclerotome cells, with the same segmented pattern as PNA.

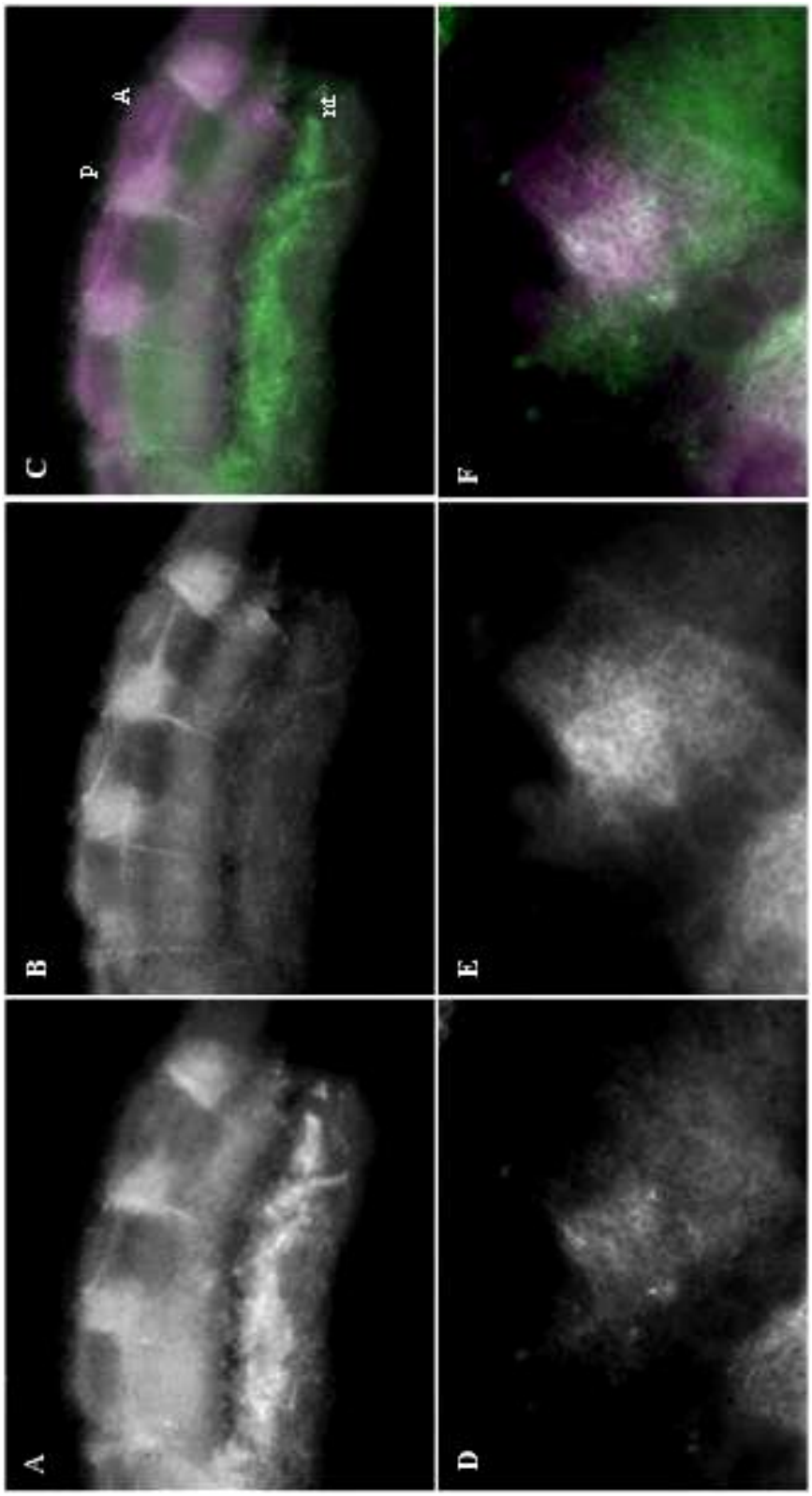

Figure 7.13- Legend on next page.

Figure 7.13- (On previous page) Live P4HB immunostaining of cultured intact somite strips treated with fluorescein-labelled PNA. (A) PNA binds the posterior sclerotome and neural tube. (B) P4HB is expressed in the posterior sclerotome. (C) Overlay of PNA (green) and P4HB (magenta) shows that both are segmented and coincident. (D) Higher magnification view suggesting cell surface binding of PNA. (E) Higher magnification view suggesting cell surface expression of P4HB. (F) Overlay of PNA-binding (green, from D) and P4HB expression (magenta, from E). PNA binding is more extensive than P4HB expression. A, anterior sclerotome; nt, neural tube; p, posterior sclerotome.

7.3.5- *P4HB* siRNA transfection into somites *in ovo* reduces the intensity and extent of PNA-binding to the posterior sclerotome

Since P4HB expression and PNA binding are both seen at the surface of posterior sclerotome cells, it is indeed possible that P4HB may be the molecule responsible for axon repulsion in the posterior sclerotome. This was tested by transfecting flurescein-labelled *P4HB* siRNA into somites *in ovo* and assessing if PNA binding to the posterior sclerotome was suppressed. *In ovo* transfection of somites was carried out in chick embryos between stages 10-14 HH and somite strips explanted and cultured intact for 16 hours before treatment with fluorescein-conjugated PNA and live immunostaining for P4HB. Three embryos were transfected with FITC-labelled *P4HB* siRNA, and two embryos with FITC-labelled scrambled siRNA. One of the lateral sides of the neural tube was kept in each somite strip for stability. Somite strips from embryos that had been transfected with scrambled siRNA showed the normal segmental pattern of PNA binding to the posterior sclerotome (and also binding to the neural tube) (Fig. 7.14A). However, PNA binding was reduced in intensity and less extensive in the posterior sclerotomes of somite strips from embryos that had been transfected with *P4HB* siRNA (Fig. 7.14B). Bright spots of staining in both anterior and posterior sclerotomes in the somite strip (Fig. 7.14C) were presumably FITC-labelled siRNA, confirming successful transfection.

Although preliminary, these siRNA transfection studies suggest not only that the *P4HB* siRNA used knocks down P4HB expression in sclerotome cells (Fig. 7.12) but also that it reduces PNA binding. These data strongly support the hypothesis that the

PNA-binding glycoprotein found by Davies *et al*. (1990) and shown to cause collapse of DRG axons *in vitro* (Davies *et al*., 1990), is indeed P4HB.

Cell surface expression of P4HB could only be detected in human Neu7 and chick posterior sclerotome cells by live immunostaining. However, it was not possible to detect P4HB expression when using whole-mount embryos, as opposed to somite strips, even by live immunostaining. Apparently, the presence of any ectoderm or endoderm inhibited the antibody from binding; only when all these tissues were removed, and sclerotome cells or somite strips were isolated, could P4HB expression be detected on the sclerotome (Figs. 7.12, 7.13 and 7.14).

Figure 7.14- (On next page) Fluorescein-conjugated PNA binding in somite strips cultured from embryos transfected *in ovo* with FITC-labelled siRNA. (A) Scrambled siRNA-transfected somite strip. Fluorescein-PNA binds in a segmented pattern to the posterior sclerotomes (and also to the lateral wall of the neural tube, retained in the somite strip for stability). (B) *P4HB* siRNA-transfected somite strip. Fluorescein-PNA binding is reduced in intensity and less extensive in the posterior sclerotome of the three somites at the left of the image (compare with the two somites on the right). (C) *P4HB* siRNA-transfected somite strip. Fluorescein-PNA binding is lower in most sclerotomes (compare with left-most sclerotome). Bright spots, presumably FITC-labelled siRNA (arrow) can be seen in some sclerotome cells (both anterior and posterior). (a) anterior sclerotome. (p)posterior sclerotome. (nt)neural tube. Scale bar: 100 µm

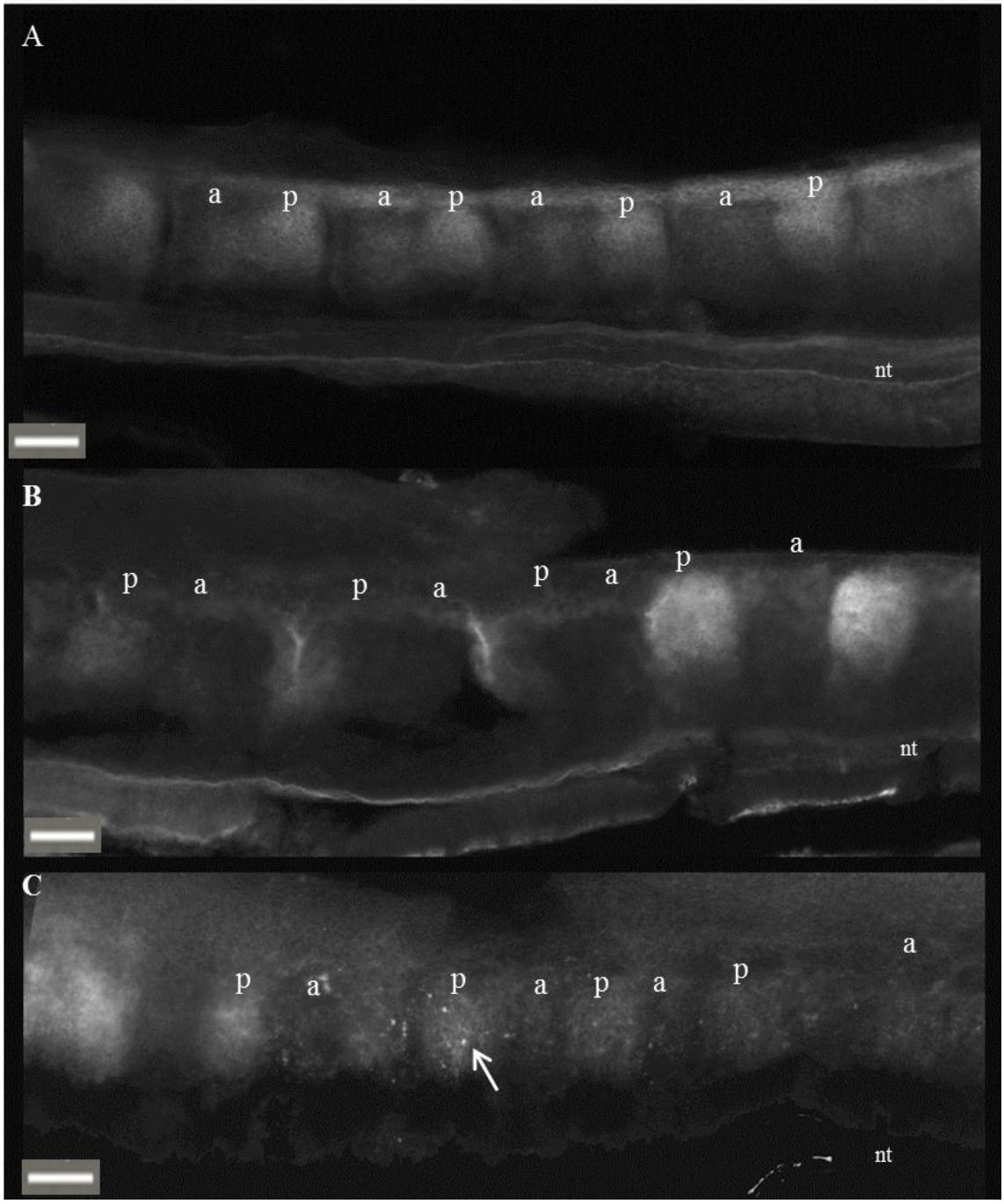

Figure 7.14- Legend on previous page.

7.3.6- *P4HB* siRNA transfection into somites *in ovo* disrupts axon segmentation

The next step was to study the impact of *P4HB* siRNA transfection on axon guidance through the somites. In total, 179 embryos were transfected *in ovo* in the somites with FITC-labelled *P4HB* siRNA and left to develop until stage 24 HH (E4.0). Table 7.2 gives a breakdown of the visible phenotypes of 149 of these embryos: these can be compared with those of the 198 embryos similarly transfected similarly with FITC-labelled scrambled siRNA, which had no obvious phenotypes (section 4.3.6) and also the 119 embryos similarly transfected with FITC-labelled *Flrt2* siRNA (Table 5.1). The "*Columbus*" phenotype in Table7.2 is so-called due to the similarity with the phenotype of the *Columbus* mutation in the *Psen1* gene (section 7.1) (Lewcock *et al*., 2007). Fig. 7.15 shows two examples of visible phenotypic alterations in *P4HB* siRNA-transfected embryos.

In order to assess any impact on axonal guidance, *P4HB* siRNA-transfected and scrambled siRNA-transfected chick embryos were immunostained for neurofilament (Fig. 7.16). Transfection of scrambled siRNA into the somites had no effect on axonal segmentation (Fig. 7.16A). In contrast, axon segmentation was lost or disrupted in discrete regions of 24 of the *P4HB* siRNA-transfected embryos (Fig. 7.16B). Axons were also seen sprouting from the bundles in the anterior half-sclerotome towards the posterior half-sclerotome, and also passing ventrally through the posterior sclerotome (Fig. 7.16C). These results suggest that knocking down cell-surface P4HB allows axons to enter the posterior sclerotome, hence that cell-surface P4HB normally repels axons from the posterior sclerotome.

Some *P4HB* siRNA-transfected transfected embryos were treated with rhodamine-conjugated PNA as well as immunostained for neurofilament (Fig. 7.17). On the transfected side (Fig. 7.17A,D), axon segmentation was disrupted (Fig. 7.17B,D) and PNA-binding reduced in the sclerotome (Fig. 7.17C,D), although the segmental pattern of both axons and PNA-binding was still seen on the untransfected side. PNA also bound the space between the ectoderm and dermomyotome very strongly, as previously reported (Oakley and Tosney, 1991). (The apparent labelling of the brightest-stained axons by PNA on the untransfected side of the embryo in this image

may be an artefact of using a biotinylated secondary antibody and Neutravidin to detect the anti-neurofilament primary antibody.)

Table 7.2- Visible phenotypic changes in 149 embryos after *in ovo* somite transfection for *P4HB* siRNA, up to 42 hours post-transfection.

Visible phenotypic alterations	**% embryos**	**No embryos**
Changes in blood supply (blood coagulation)	66.4	99
Changes in vitelline artery	22.1	33
Changes in extra-embryonic blood vessels	72.5	108
Malformed head	27.5	41
Embryo twisted	66.4	99
Indistinct somite border limits	16.8	25
Thinner lumbar region and tail	27.5	41
Abnormalities in limb formation	11.4	17
"*Columbus*" (all the above plus incomplete neural tube closure)	11.4	17
Number of embryos that died before reaching 42 hours post-transfection	72.5	108

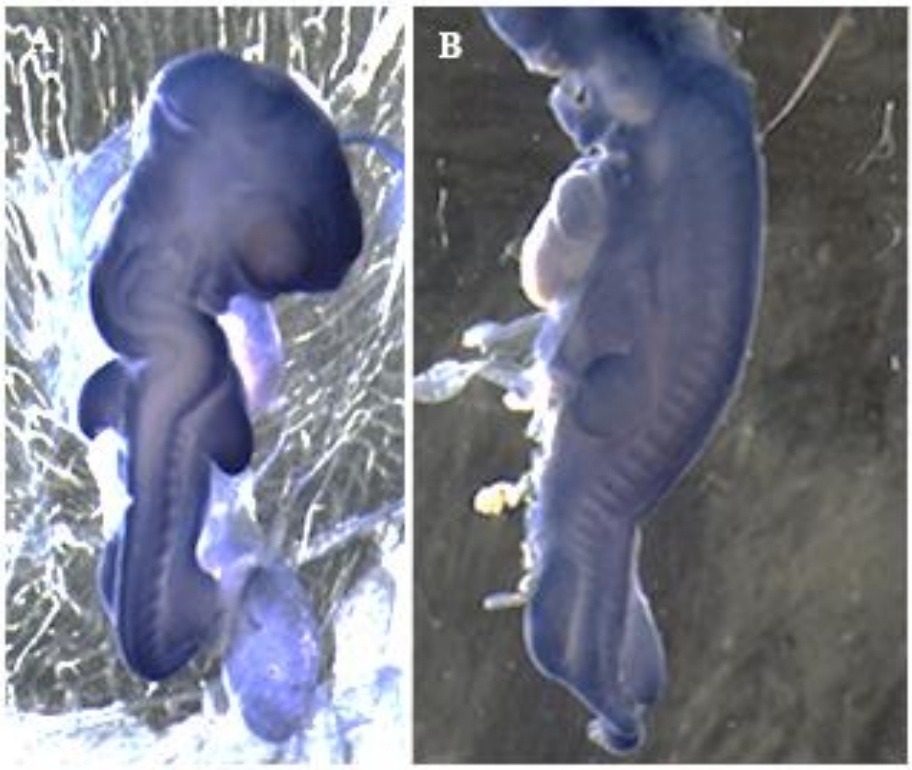

Figure 7.15- Chick embryos at stage 22 HH that had been transfected *in ovo* in the somites with *P4HB* siRNA, immunostained for neurofilament. (A) Twisting of the neural tube. (B)- Abnormal limb positioning, heart morphology and tail formation.

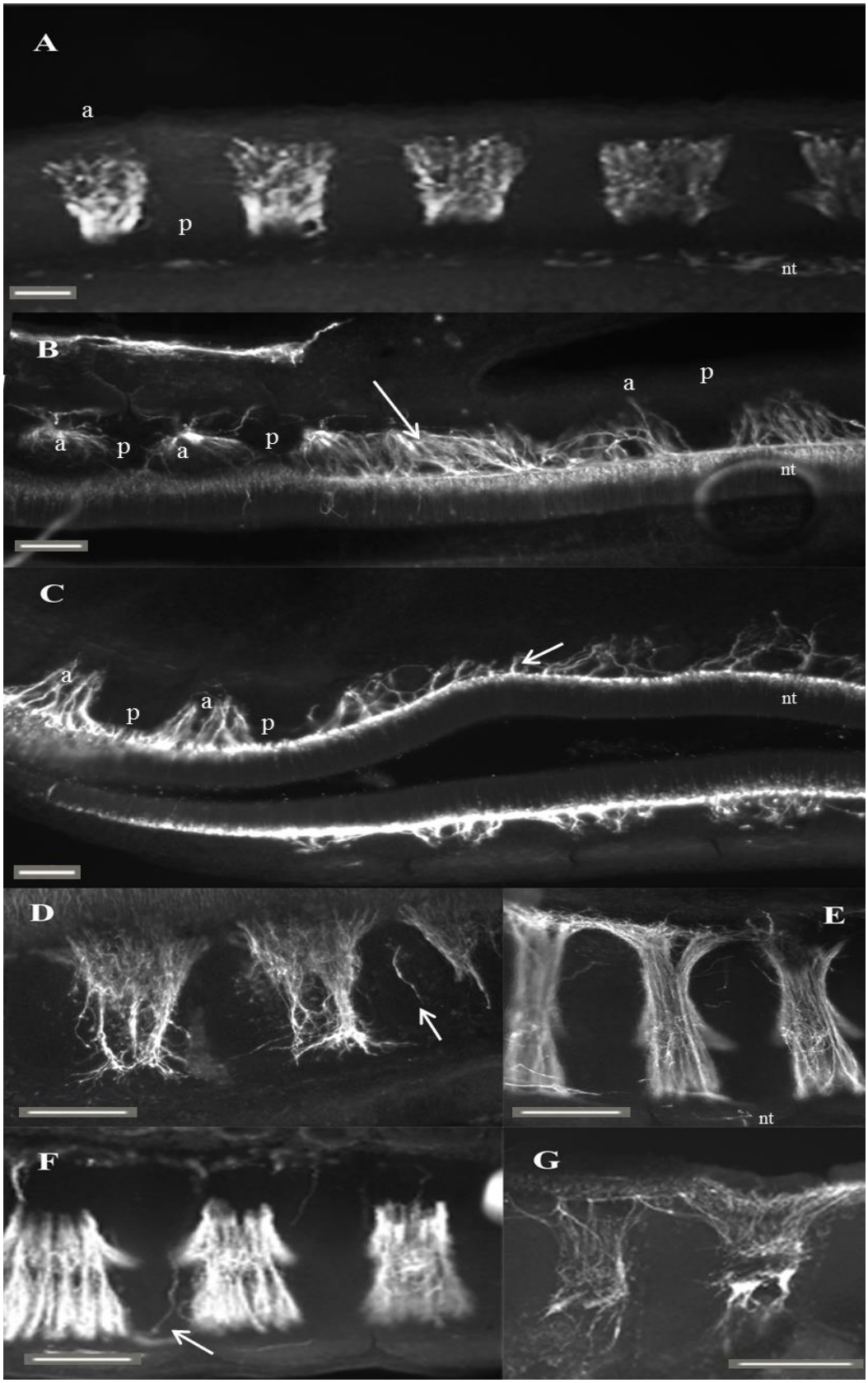

Figure 7.16- Legend on next page.

Figure 7.16- (On previous page) Neurofilament immunostaining of siRNA-transfected embryos at stage 22 HH. (A) Scrambled siRNA-transfected embryo showing motor axons crossing the anterior sclerotome. (B) *P4HB* siRNA-transfected embryo showing loss of segmentation of sensory axons (arrow). (C) *P4HB* siRNA-transfected embryo showing loss of segmentation of motor axons (arrow); axons on the non-transfected side and in nearby somites still display segmentation. (D-G) Higher-power views of *P4HB* siRNA-transfected embryos with axons in the posterior sclerotome (arrow). (a) anterior sclerotome; (p) posterior sclerotome; (nt) neural tube. Scale bar: 100 μm.

Figure 7.17- (On next page) Combined neurofilament immunostaining and rhodamine-conjugated PNA treatment of a *P4HB* siRNA-transfected embryo at stage 22 HH. (A) Green channel in grey-scale, showing FITC-labelled *P4HB* siRNA in transfected somites on the left side in the photograph. (B) Blue channel in grey-scale, showing neurofilament expression. Axons exhibit lack of segmentation on the transfected side (left), while segmentation is still present on the untransfected side (right). (C) Red channel in grey-scale, showing that rhodamine-conjugated PNA-binding is significantly reduced or absent in the sclerotome on the transfected side (left) but present on the untransfected side (right). PNA also binds the space between the ectoderm and dermomyotome, as previously reported (Oakley and Tosney, 1991). Apparent PNA binding to the most brightly stained axons on the untransfected side may be an artefact of using a biotinylated secondary antibody and Neutravidin to detect the neurofilament primary antibody. (D) Merge of green (A), blue (B) and red (C) channels, showing lack of PNA binding and axon segmentation on the transfected side. n: notochord; p: posterior half-sclerotome; a: anterior half-sclerotome.

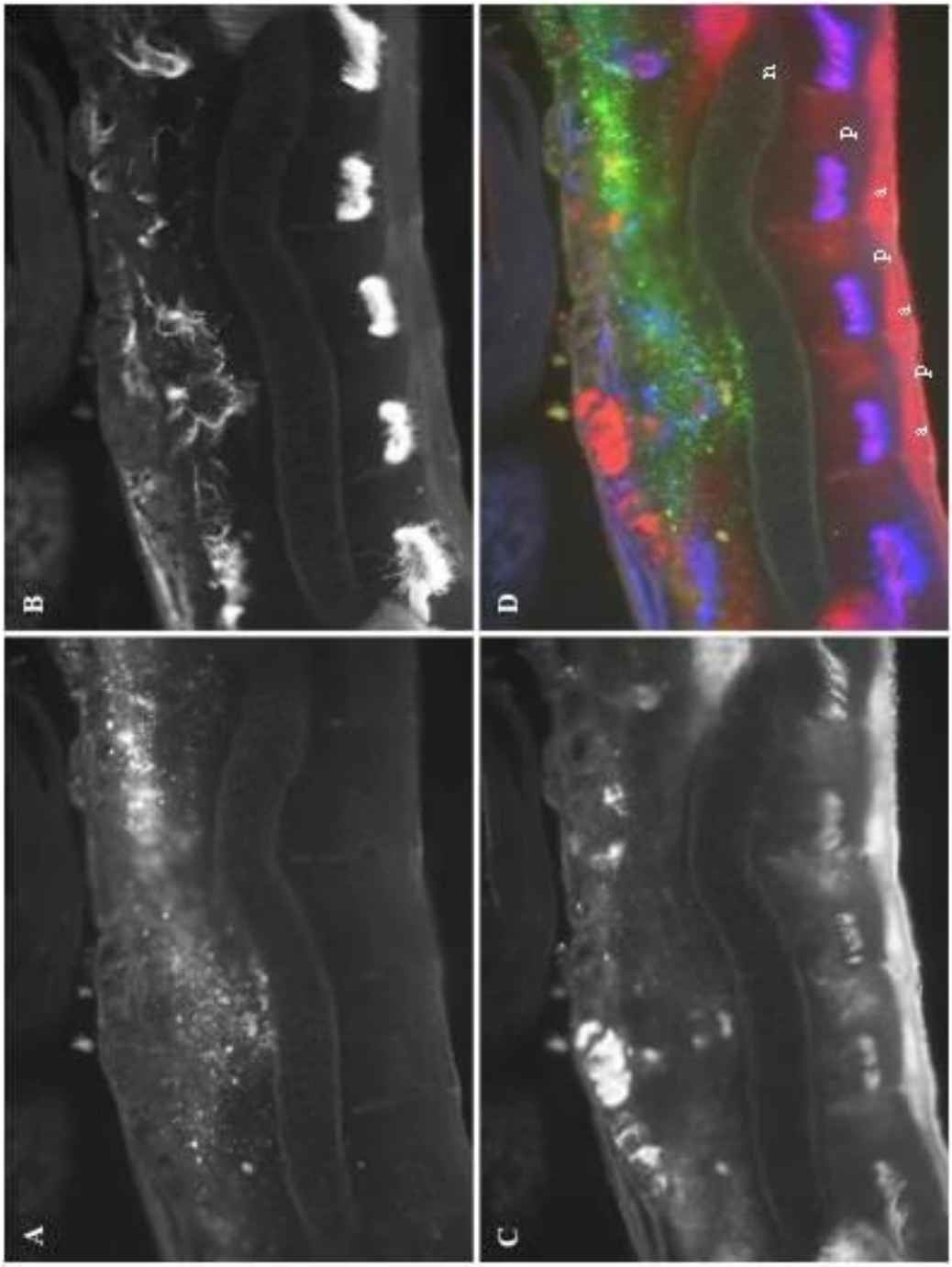

Figure 7.17- Legend on previous page.

7.3.7- P4HB siRNA transfection affects expression of posterior but not anterior sclerotome markers

The impact of *P4HB* siRNA transfection on polarity was checked using WMISH on twelve chick embryos, half of which were hybridized for the posterior half-sclerotome marker *Uncx4.1* (Schrägle *et al*., 2004) and the other half for the anterior half-sclerotome marker *Tbx18* (Haenig and Kispert, 2004). *Tbx18* hybridization did not exhibit any modification in *P4HB* siRNA-transfected embryos when compared to scrambled siRNA-transfected embryos (Fig. 7.18A-D). However, four out of six *P4HB* siRNA-transfected embryos had visible modification in *Uncx4.1* expression on both sides of the embryo (Fig. 7.18E-L).

Figure 7.18- (On next page) siRNA-transfected embryos and sections after WMISH for somite polarity markers. (A-D) WMISH for the anterior sclerotome marker *Tbx18* at stage 22 HH. (A) In a scrambled siRNA-transfected embryo, *Tbx18* is present in the anterior sclerotome. (B) In a *P4HB* siRNA-transfected embryo, *Tbx18* is present in the anterior sclerotome. (C) Parasagittal section of a scrambled siRNA-transfected embryo showing segmental *Tbx18* expression. (D) Parasagittal section of a *P4HB* siRNA-transfected embryo showing segmental *Tbx18* expression. (E,F) WMISH for the posterior sclerotome marker *Uncx4.1* at stage 22 HH. (E) Scrambled siRNA-transfected embryo (left) next to a *P4HB* siRNA-transfected embryo (right). There are gaps in *Uncx4.1* expression in the *P4HB* siRNA-transfected embryo (right). (F) Higher-power view of thoracic region of a scrambled siRNA-transfected embryo (left) next to a *P4HB* siRNA-transfected embryo (right). *Uncx4.1* expression is significantly suppressed in the *P4HB* siRNA-transfected embryo (right). (G-L) *Uncx4.1* expression at stage 19 HH. (G) Lateral view: *Uncx4.1* expression varies in the lumbar area (arrow). (H) Dorsal view: both sides display loss of segmentation and variations in *Uncx4*.1 expression. (I) Dorsal view of another embryo: both sides of the embryo have variable *Uncx4.1* expression within the somites. Some somites lack *Uncx4.1* expression (arrow). (J) Parasagittal section: some somites express *Ucx4.1* while others lack expression. (K) Parasagittal section of the tail: *Uncx4.1* is present in a row of somites. (L) Parasagittal section of the lumbar region and tail: *Uncx4.1* expression varies in each somite; in one of them, anterior and posterior segmentation is not visible (arrow). (a) anterior sclerotome; (p) posterior sclerotome; (nt) neural tube. Scale bar: 100 µm.

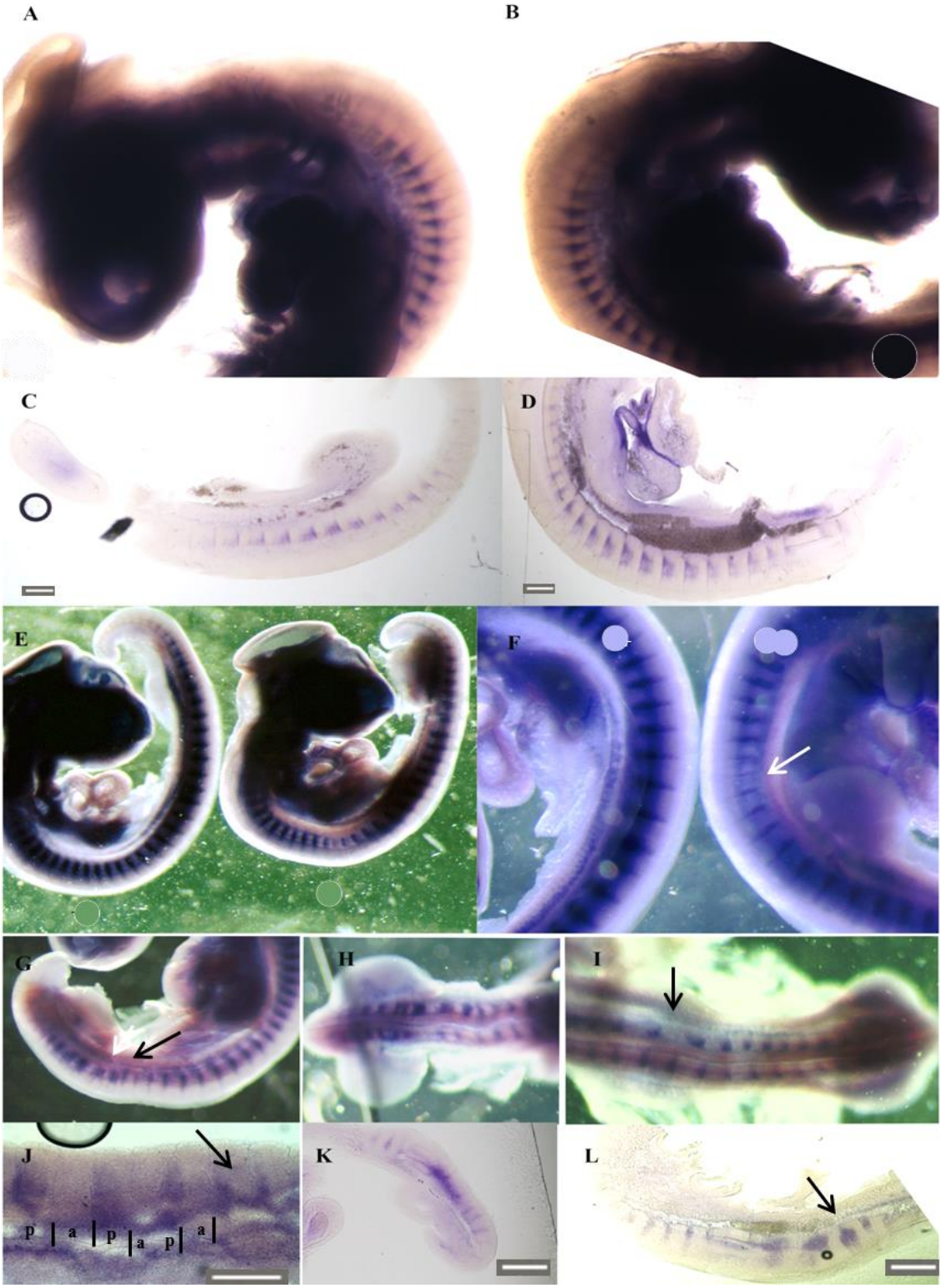

Figure 7.18- Legend on previous page.

7.3.8- Discussion and Conclusion

For over 20 years (Davies *et al*., 1990), the identity of the PNA-binding glycoprotein responsible for axon repulsion in the posterior sclerotome during development has remained a mystery. In addition, the effects of PNA on axonal guidance have been principally assessed *in vitro* on dorsal root ganglion neurons using the growth-cone collapse assay (Davies *et al*., 1990), so its proposed role *in vivo* could only be speculative. Using Edman degradation, P4HB was identified as the protein responsible for PNA-induced axonal repulsion (Prof. R. J. Keynes, personal comunication).

Previous studies had detected P4HB at the cell surface in fixed chick retinal cells (Hausman and Moscona, 1976; Hausman and Moscona, 1979) and in various mammalian cell lines (e.g. Zai *et al*., 1999; Bi *et al.*, 2011). Furthermore, Bi *et al.* (2011) showed that cell surface P4HB in a mammalian cell line binds PNA. In the present study, P4HB was detected at the surface of posterior sclerotome cells from fresh tissue. This was possible following mechanical dissociation of the cells with a needle rather than using enzymatic digestion. Membrane permeabilization reagents like Triton™ or Tween20™ were not used, and paraformaldehyde fixation was only carried out after binding of the primary antibody (i.e., live immunostaining), avoiding the destruction of binding sites for the anti-P4HB antibody. However, one of the great limitations found with this antibody was its limited permeability. The presence of ectoderm, endoderm, laminin, or collagen prevented the antibody from penetrating the embryo and reaching the sclerotome, which is why P4HB expression could not be detected on whole embryos. Western blot assays could have been done in order to study the presence of P4HB protein after *P4HB* siRNA transfection, but this would require a great number of transfected somite strips. For further work, as a complement to P4HB protein detection by immunostaining, quantitative RT-PCR should be done, to measure the level of *P4HB* mRNA relative to a housekeeping gene such as actin, in *P4HB* siRNA-transfected embryos versus scrambled siRNA-transfected embryos (or mismatch siRNA-transfected embryos; Buehler *et al.*, 2012).

Posterior sclerotome cells were maintained in an undifferentiated state by co-culturing them with notochord. Optimisation studies using poly-l-lysine and laminin

coating alone or together showed that once sclerotome cells attached to the coated surface they differentiated into fibroblasts and lost their ability to bind PNA. Therefore, sclerotome cells were grown directly on the glass surface, where PNA-binding cells formed aggregates. Cells that became separated from the aggregate did not bind PNA, suggesting that the PNA-binding molecule was only present when cells maintained physical contact. It was presumably due to this way of culturing posterior sclerotome cells that it was possible to detect P4HB expression on the cell surface.

The chick *P4HB* siRNA designed in this study significantly reduced P4HB protein expression at the cell surface. It was interesting to see that *P4HB* siRNA transfection resulted in the reduced proliferation of human Neu7 cells. Similarly, after culturing chick retinal cells transfected with *P4HB* siRNA, there were fewer cells and they were not aggregated. Indeed, cell surface P4HB, as R-cognin, was first identified as a cell aggregation factor for retinal cells (Hausman and Moscona, 1976; Hausman and Moscona, 1976; Hausman *et al.*, 1993). Knockdown of P4HB in retina resulted in a 50% reduction in cell re-aggregation (Hausman *et al*., 1993) and affected subsequent neuronal differentiation (Phillips *et al*., 1997). Similar findings emerged from the present study. After *P4HB* siRNA transfection in cultured posterior sclerotome cells, they became more widespread than scrambled siRNA-transfected cells. The posterior sclerotome is more condensed than the anterior sclerotome (Keynes and Stern, 1984; Christ *et al.*, 2004; Maroto and Whittock, 2008). It would be interesting to see if the same density changes occur in sclerotome cells *in vivo* after transfecting *P4HB* siRNA. It may be that the presence of cell surface P4HB maintains cell-cell interaction and further condensation of the posterior scleretomal cells surface by thio-disulfide exchange, as occurs in HEL cells (Zai *et al.*, 1999).

P4HB siRNA transfection also led to significant motor and sensory axon pathfinding defects, with loss of segmentation and mistargeted axons migrating within the posterior half-sclerotome as well as the anterior half-sclerotome. Presumably once cell surface P4HB has been lost, for example after siRNA-mediated knockdown, or after P4HB has been bound by PNA, the axon repulsion cue is lost, and (perhaps also aided by the sclerotome cells no longer being as tightly packed) axons are then able to pass through the entire somite.

In platelets, cell surface P4HB promotes T-cell migration and also binds with the lectin galectin-9 to regulate integrin function and alter the redox status at the plasma membrane, enhancing the susceptibility of T-cells to infection with HIV (Bi *et al.*, 2011). Cell surface P4HB also inhibits platelet aggregation in the presence of *S*-nitrosoglutathione via an integrin-disulfide-exchange route (Root *et al.*, 2004). It would be interesting to study nitrosation activity in posterior sclerotome cells after transfecting *P4HB* siRNA versus scrambled (or mismatch) siRNA.

Furthermore, following *P4HB* siRNA transfection, the barrier that normally keeps the cells of both half-sclerotomes apart became disrupted allowing a free-flow of cells and a disordered anteroposterior polarity, as demonstrated by the changes in expression of the posterior sclerotome marker *Uncx4.1* on both sides of the embryo. (The effect on both sides could be due to accidental transfection of tailbud cells, which give rise to PSM on both sides, so affecting somite development bilaterally.) These changes included expanded expression of *Uncx4.1* to the entire somite, or absence of any expression, or a "sandwich" pattern within a somite, or *Uncx4.1* expression at the anterior border of sclerotome. The next step here would be to detect *Uncx4.1* simultaneously with neurofilament immunostaining and treatment with fluorescently-conjugated PNA, in order to see how segmentation is distributed in the presence of variable *Uncx4.1* expression.

In contrast to *Uncx4.1,* expression of the anterior sclerotome marker did not appear to differ between *P4HB* siRNA-transfected and scrambled siRNA-transfected embryos. It is possible that the embryos selected for WMISH did not have enough transfected cells, or alternatively that Tbx18 acts upstream of P4HB. Davies et al. (1990) reported that the youngest somite with clear PNA-binding is ten somites anterior to the most recently formed somite, which is roughly 7 somites anterior to the oldest epithelial somite. In contrast, Oakley and Tosney (1991) reported that (using a different fixative and anti-PNA immunohistochemistry) they could detect PNA binding to posterior somite cells within the cores of recently segmented epithelial somites only two somites anterior to the PSM. In either case, if P4HB is responsible for PNA-binding activity then this is at a later stage than the establishment of *Tbx18* expression, which begins in the PSM (Bussen *et al*., 2004). Knockdown of *P4HB* would therefore not be

expected to affect *Tbx18* expression. The specification of the posterior half-somite also begins in the PSM, when the Psen1-dependent Notch cascade induces Dll1 expression. This cascade leads to the later activation of *Uncx4.1* expression in the posterior half-somite, with continued Uncx4.1 expression being maintained by auto-regulation (Bussen *et al*., 2004). It may therefore be that loss of P4HB somehow leads to mis-regulation of Dll1, leading to concomitant effects on somite polarity.

In conclusion, P4HB is a strong candidate for the molecule localised to the surface of posterior half-sclerotome cells that prevents axons from inappropriately entering this territory. Hence, after more than two decades, the key glycoprotein involved in determining spinal nerve segmentation in the vertebrate trunk may have been identified.

BIBLIOGRAPHY

Aagaard, A., Listwan, P., Cowieson, N., Huber, T., Ravasi, T., Wells, C.A., Flanagan, J.U., Kellie, S., Hume, D.A., Kobe, B., Martin, J.L. (2005) "An inflammatory role for the mammalian carboxypeptidase inhibitor latexin: relationship to cystatins and the tumor suppressor TIG1." *Structure*. 13: 309–317

Andrade, R. P., Palmeirim, I. and Bajanca, F. (2007), "Molecular Clocks Underlying Vertebrate Embryo Segmentation: A 10-Year-Old *hairy*-Go-Round." *Birth Defects Res. C Embryo Today* 81: 65-83

Andreu, C.I., Woehlbier, U., Torres, M., Hetz, C. (2012) "Protein disulfide isomerases in neurodegeneration: from disease mechanisms to biomedical applications." *FEBS Lett*. 586(18): 2826-34

Aoyama, H., Asamoto, K. (2000) "The developmental fate of the rostral/caudal half of a somite for vertebra and rib formation: experimental confirmation of the resegmentation theory using chick-quail chimeras." *Mech. Dev*. 99(1-2): 71-82

Arimatsu, Y. (1994) "Latexin: a molecular marker for regional specification in the cerebral cortex." *Neurosci. Res* 20: 131–135

Austin, K.M., Covic, L., Kuliopulos, A. (2013) "Matrix metalloproteases and PAR1 activation." *Blood*. 121(3): 431-9

Baffi, M. O., Moran, M. A., Serra, R. (2006) "Tgfbr2 regulates the maintenance of boundaries in the axial skeleton" *Dev. Biol.* 296 (2): 363–374

Bagnard, D. (2007) "*Axon Growth and Guidance" Advances in Experimental Medicine and Biology*. Volume 621. Berlin: Springer

Bai, G., Chivatakarn, O., Bonanomi, D., Lettieri, K., Franco, L., Xia, C., Stein, E., Ma, L., Lewcock, J.W., Pfaff, S.L. (2011) "Presenilin-dependent receptor processing is required for axon guidance." *Cell* 144: 106–118

Baker, R. E., Schnell, S. and Maini, P. K. (2006), "A clock and wavefront mechanism for somite formation", *Dev. Biol.* 293: 116-126

Bakkers, J., Kramer, C., Pothof, J., Quaedvlieg, N. E. M., Spaink, H. P. and Hammerschmidt, M. (2004), "Has2 is required upstream of Rac1 to govern dorsal migration of lateral cells during zebrafish gastrulation", *Development* 131: 525-537

Bassuk, J. A., Berg, R.A. (1991) "A novel 53-kDa polypeptide from chick embryo." *Jour. Biol. Chem.* 266 (35): 23732-23738

Bellairs, R., Osmond, M. (1998) "*The Atlas of Chick Development."* 1º edition, Academic Press.

Bennett, E.P., Mandel, U., Clausen, H.,Gerken, T. A., Fritz, T.A., Tabak, L.A. (2012) "Control of mucin-type O-glycosylation. A classification of the polypeptide GalNAc-transferase gene family." *Glycobiology*. 22, 736–756

Bertrand, N., Medevielle, G. and Pituello, F. (2000). "FGF signalling controls the timing of Pax6 activation in the neural tube." *Development* 127: 4837-4843

Bi, S., Hong, P.W., Lee, B., Baum, L.G. (2011) "Galectin-9 binding to cell surface protein disulfide isomerase regulates the redox environment to enhance T-cell migration and HIV entry." *Proc Natl Acad Sci USA.*10: 10650–10655

Bill, B. R., Petzold A. M., Clark K. J., Schimmenti L. A., Ekker S. C. (2009). "A primer for morpholino use in zebrafish." Zebrafish 6, 69–77

Bloechlinger, S., Karchewski, L.A., Woolf C.J. (2004) "Dynamic changes in glypican-1 expression in dorsal root ganglion neurons after peripheral and central axonal injury." *Eur. J. Neurosci*. 19: 1119–1132

Böttcher, R.T., Pollet, N., Delius, H., Niehrs, C. (2004) "The transmembrane protein XFLRT3 forms a complex with FGF receptors and promotes FGF signalling." *Nat. Cell Biol.* 6: 38–44

Bouvrée, K., Larrivée, B., Lv, X., Yuan, L., DeLafarge, B., Freitas, C., Mathivet, T., Bréant, C., Tessier-Lavigne, M., Bikfalvi, A., Eichmann, A., Pardanaud, L. (2008)

"Netrin-1 inhibits sprouting angiogenesis in developing avian embryos." *Dev. Biol.* 318(1): 172-83

Brauer, P.R., Cai, D.H. (2002) "Expression of tissue inhibitor of metalloproteinases (TIMPs) during early cardiac development." *Mech. Dev*. 113(2): 175-9

Bray, S.J. (2006) "Notch signalling: a simple pathway becomes complex." *Nat. Rev. Mol. Cell. Biol.* 7, 678-689

Britsch, S., Goerich, D.E., Riethmacher, D., Peirano, R.I., Rossner, M., Nave, K.A., Birchmeier, C., Wegner, M., (2001). "The transcription factor Sox10 is a key regulator of peripheral glial development." *Genes Dev*. 15, 66-78

Bron R., Vermeren M., Kokot N., Andrews W., Little G. E., Mitchell K. J., Cohen J. (2007). Boundary cap cells constrain spinal motor neuron somal migration at motor exit points by a semaphorin-plexin mechanism. *Neural Dev.* 2, 21

Bruggeman, B.J., Maier, J.A., Mohiuddin, Y.S., Powers, R., Lo, YT, Guimarães-Camboa, N., Evans, S.M., Harfe, B.D. (2012) "The avian intervertebral disc arises from rostral sclerotome and lacks a nucleus pulposus: Implications for evolution of the vertebrate disc". *Dev. Dyn.* 241(4): 675–683

Buehler, E., Chen, Y.C., Martin, S. (2012). "C911: A bench-level control for sequence specific siRNA off-target effects." *PLoS ONE* 7, e51942

Bussen, M., Petry, M., Schuster-Gossler, K., Leitges, M., Gossler, A., Kispert, A. (2004) "The T-box transcription factor Tbx18 maintains the separation of anterior and posterior somite compartments." *Genes Dev.* 18: 12009-1221

Cantemir, V., Cai, D. H., Reedy, M. V., Brauer, P.R. (2004) "Tissue inhibitor of metalloproteinase-2 (TIMP-2) expression during cardiac neural crest cell migration and its role in proMMP-2 activation." *Dev. Dyn.*. 231(4): 709-19

Carlson, E. C. and Kenney, M. C. (1980). "Surface ultrastructure of the isolated notochord in vitro: the effect of the perinotochord sheath." *Anat. Rec.* 197: 257-276

Casini, P., Nardi, I., Ori, M. (2012) “Hyaluronan is required for cranial neural crest cells migration and craniofacial development.” *Dev. Dyn*. 241(2): 294-302

Chacko, B.K., Appukuttan, P.S. (2001) “Peanut (*Arachis hypogaea*) lectin recognizes α-linked galactose, but not N-acetyl lactosamine in N-linked oligosaccharide terminals” *International Journal of Biological Macromolecules* 28(5): 365-371

Chadborn NH, Ahmed AI, Holt MR, Prinjha R, Dunn GA, Jones GE, Eickholt BJ. (2006) “PTEN couples Sema3A signalling to growth cone collapse.” *J. Cell Sci.* 119: 951–7

Chen, Y., Cheng, G., Mahato, R. (2008) “RNAi for Treating Hepatitis B Viral Infection.” *Pharmaceutical Research* 25: 72-86

Cheng, H. L., Sullivan, K. A., Feldman, E.L. (1996) “Immunohistochemical localization of insulin-like growth factor binding protein 5 in the developing rat nervous system.” *Brain Res. Dev. Brain Res.* 92 (2): 211-8

Christ, B., Huang, R. and Wilting, J. (2000), "The development of the avian vertebral column", *Anat. Embryol.* 202: 179-194

Christ, B., Huang, R., Scaal, M. (2004). “Formation and differentiation of the avian sclerotome.” *Anat. Embryol. (Berl.)* 208: 333-350

Christ, B., Huang, R. and Scaal, M. (2007), "Amniote Somite Derivatives", *Dev. Dyn.* 236: 2382-2396

Clay, M.R., Halloran, M. C. (2011) “Regulation of cell adhesions and motility during initiation of neural crest migration.” *Curr. Opin. Neurobiol.* 21(1): 17–22

Cleaver, O., Krieg, P.A. (2001) “Notochord patterning of the endoderm.” *Dev. Biol.* 234: 1–12

Clemmons, D.R. (1998) “Role of insulin-like growth factor binding proteins in controlling IGF actions.” *Molecular and Cellular Endocrinology* 140(1-2): 19–24

Conlon, R.A., Reaume, A.G., Rossant, J. (1995), "Notch 1 is required for the coordinate segmentation of somites." *Development* 121: 1533-1545

Connolly, A.J., Ishihara, H., Kahn, M.L., Farese Jr. R.V., Coughlin, S.R. (1996) "Role of the thrombin receptor in development and evidence for a second receptor" *Nature* 381: 516–519

Das, R.M., Van Hateren, N.J., Howell, G.R., Farrell, E.R., Bangs, F.K., Porteous, V.C., Manning, E.M., McGrew, M.J., Ohyama, K., Sacco, M.A., Halley, P.A., Sang, H.M., Storey, K.G., Placzek, M., Tickle, C., Nair, V.K., Wilson, S.A. (2006) "A robust system for RNA interference in the chicken using a modified microRNA operon." *Dev. Biol*. 294: 554–563

Davies R. J., Cook G. M. W., Stern C. D., Keynes R. J. (1990) "Isolation from chick somites of a glycoprotein fraction that causes collapse of dorsal root ganglion growth cones." *Neuron* 4: 11–20

De Bellard, M.E., Rao, Y., Bronner- Fraser, M. (2003) "Dual function of Slit2 in repulsion and enhanced migration of trunk, but not vagal, neural crest cells." *J. Cell Biol*, 162: 269–279

Diez-Roux G, Banfi S, Sultan M, Geffers L, Anand S, Rozado D, Magen A, Canidio E, Pagani M, Peluso I, Lin-Marq N, Koch M, Bilio M, Cantiello I, Verde R, De Masi C, Bianchi SA, Cicchini J, Perroud E, Mehmeti S, Dagand E, Schrinner S, Nürnberger A, Schmidt K, Metz K, Zwingmann C, Brieske N, Springer C, Hernandez AM, Herzog S, Grabbe F, Sieverding C, Fischer B, Schrader K, Brockmeyer M, Dettmer S, Helbig C, Alunni V, Battaini MA, Mura C, Henrichsen CN, Garcia-Lopez R, Echevarria D, Puelles E, Garcia-Calero E, Kruse S, Uhr M, Kauck C, Feng G, Milyaev N, Ong CK, Kumar L, Lam M, Semple CA, Gyenesei A, Mundlos S, Radelof U, Lehrach H, Sarmientos P, Reymond A, Davidson DR, Dollé P, Antonarakis SE, Yaspo ML, Martinez S, Baldock RA, Eichele G, Ballabio A. (2011) A high-resolution anatomical atlas of the transcriptome in the mouse embryo. *PLoS Biol.* 9: e1000582

Ding, Y. and Lawrence, C.E. (2003) "A statistical sampling algorithm for RNA secondary structure prediction." *Nucleic Acids Res.* 31: 7280-7301

Ding, Y., Chan, C.Y. and Lawrence, C.E. (2005) “RNA secondary structure prediction by centroids in a Boltzmann weighted ensemble.” *RNA* 11: 1157-1166

Dorus, S., Anderson, J. R., Vallender, E. J., Gilbert, S. L., Zhang, L., Chemnick, L.G., Ryder, O. A., Li, W., Lahn, B. T. (2006) “Sonic Hedgehog, a key development gene experienced intensified molecular evolution in primates.” *Hum. Mol. Genet*. 15(13): 2031-7

Dubrulle, J., Pourquié, O. (2004). “Fgf8 mRNA decay establishes a gradient that couples axial elongation to patterning in the vertebrate embryo.” *Nature* 427: 419–422

Egea, J., Erlacher, C., Montanez, E., Burtscher, I., Yamagishi, S., Hess, M., Hampel, F., Sanchez, R., Rodriguez-Manzaneque, M.T., Bösl, M.R., Fässler, R., Lickert, H., Klein, R. (2008). “Genetic ablation of FLRT3 reveals a novel morphogenetic function for the anterior visceral endoderm in suppressing mesoderm differentiation.” *Genes Dev.* 22: 3349-3362

Ferguson, T.A, Muir, D. (2000) “MMP-2 and MMP-9 increase the neurite-promoting potential of schwann cell basal laminae and are upregulated in degenerated nerve.” *Mol Cell Neurosci*. 16: 157–167

Fiúza, U.M and Martinez Arias, A. (2007) "Cell and molecular biology of Notch", *Journal of Endocrinology* 194: 459-474

Fleming, A., Keynes, R. J. and Tannahill, D. (2001) "The role of the notochord in vertebral column formation.", *J. Anat.*199: 177-180

Fouquet, B., Weinstein, B. M., Serluca, F. C. and Fishman, M. C. (1997). “Vessel patterning in the embryo of the zebrafish: guidance by notochord.” *Dev. Biol.* 183: 37-48

Giovannone, D., Reyes, M., Reyes, R., Correa, L., Martinez, D., Ra, H., Gomez, G., Kaiser, J., Ma, L., Stein, MP., De Bellard, M. E. (2012) “Slits Affect the Timely Migration of Neural Crest Cells via Robo Receptor” *Dev. Dyn.*. 241(8): 1274–1288

Goldstein, A. M. and Fishman, M. C. (1998). “Notochord regulates cardiac lineage in zebrafish embryos.” *Dev. Biol.* 201: 247-252

Gomez, C., Özbudak, E.M., Wunderlich, J., Baumann, D., Lewis, J., Pourquié, O. (2008). "Control of segment number in vertebrate embryos". *Nature* 454: 335–33

Green, B. N., Streck, R. D., Jones, S. B., Wood, T. L., Rotwein, P, Pintar, J. E. (1994) “Distinct expression patterns of insulin-like growth factor binding proteins 2 and 5 during fetal and postnatal development.” *Endocrinology* 134(2): 954-62

Gridley, T. (2006), "The Long and Short of It: Somite Formation in Mice." *Dev. Dyn.* 235: 2330-233

Griffin, C. T., Srinivasan, Y., Zheng, Y., Huang, W., Coughlin, S. R. (2001) “A Role for Thrombin Receptor Signaling in Endothelial Cells During Embryonic Development.” *Science* 293: 1666-1670

Guo, J.M., Zhang, Y., Cheng, L., Iwasaki, H., Wang, H., Kubota, T., Tachibana, K., Narimatsu, H. (2002) “Molecular cloning and characterization of a novel member of the UDP-GalNAc: polypeptide N-acetylgalactosaminyltransferase family pp-GalNAc-T12.” *FEBS Lett.* 524(1-3): 211-8

Haass, C., De Strooper, B. (1999) “The presenilins in Alzheimer's disease--proteolysis holds the key.” *Science* 286: 916-9

Haenig, B., Kispert, A. (2004) “Analysis of TBX18 expression in chick embryos.” *Dev. Genes Evol*. 214(8): 407-11

Haines, B.P., Wheldon, L.M., Summerbell, D., Heath, J.K., Rigby, P.W. (2006) “Regulated expression of FLRT genes implies a functional role in the regulation of FGF signalling during mouse development.” *Dev. Biol.* 297: 14-25

Hamburger, V., Hamilton, H.L. (1951) “A series of normal stages in the development of the chick embryo.” *J. Morphol*. 88, 49-92

Han, KS., Mannaioni, G., Hamill, C. E., Lee., J., Jungel, C. E., Lee, C. E., Traynelis, S. F. (2011) “Activation of protease activated receptor 1 increases the excitability of the dentate granule neurons of hippocampus.” *Molecular Brain* 4: 32

Hausman, R.E., Moscona, A.A. (1976) “Isolation of retina-specific cell-aggregating factor from membranes of embryonic neural retina tissue.” *Proc. Natl. Acad. Sci. U.S.A.* 73 (10): 3594-3598

Hausman, R.E., Moscona, A.A. (1979) “Immunologic detection of retina cognin on the surface of embryonic cells.” *Exp. Cell Res.* 119(2): 191-204

Hausman, R.E., Krishna Rao, A.S.M., Ren, Y., Sagar, G.D.V., Shah, B.H. (1993) “Retina Cognin, cell signalling, and neuronal differentiation in the developing retina.” *Dev. Dyn*. 196: 263-266

Herr, P., Korniychuk, G., Yamamoto, Y., Grubisic, K., Oelgeschlager, M. (2008) “Regulation of TGF-β signalling by N-acetylgalactosaminyltransferase-like 1.” *Development* 135: 1813-1822

Hughes, S. T. D., Keynes, R. J., Tannahill, D. (2009), "Extensive molecular differences between anterior- and posterior-half-sclerotomes underlie somite polarity and spinal nerve segmentation." *BMC Dev. Biol.* 9: 30

Ingham, P.W., McMahon, A.P. (2001) “Hedgehog signaling in animal development: paradigms and principles.” *Genes Dev.* 15: 3059-3087

Jaworski, D.M., Fager, N. (2000) “Regulation of tissue inhibitor of metalloproteinase-3 (Timp-3) mRNA expression during rat CNS development.” *J. Neurosci. Res*. 61: 396–408

Jia, L., Cheng, L., Raper, J. (2005) “Slit/Robo signaling is necessary to confine early neural crest cells to the ventral migratory pathway in the trunk.” *Dev. Biol*. 282: 411–421

Jiang, Y.J., Aerne, B.L., Smithers, L., Haddon, C., Ish-Horowicz, D., Lewis, J. (2000) "Notch signalling and the synchronization of the somite segmentation clock". *Nature* 408: 475–479.

Jin, M., Ishida, M., Katoh-Fukui, Y., Tsuchiya, R., Higashinakagawa, T., Ikegami, S., Arimatsu, Y. (2006) “Reduced pain sensitivity in mice lacking latexin, an inhibitor of metallocarboxypeptidases.” *Brain Res*. 1075: 117–121

Johnson, M.A., Ables, J.L., Eisch AJ. (2009) “Cell-intrinsic signals that regulate adult neurogenesis in vivo: insights from inducible approaches.” *BMB Rep.* 42(5): 245-59

Junge, C.E., Lee, C.J., Hubbard, K.B., Zhang, Z., Olson, J.J., Hepler, J.R., Brat, D.J., Traynelis, S.F. (2004). “Protease-activated receptor-1 in human brain: localization and functional expression in astrocytes.” *Experimental Neurology*, 188 (1): 94-103

Kadouchi, I., Sakamoto, K., Tangjiao, L., Murakami, T., Kobayashi, E., Hoshino, Y., Yamaguchi, A. (2009) “Latexin is involved in bone morphogenetic protein-2-induced chondrocyte differentiation.” *Biochem. Biophys. Res. Commun*. 378: 600–604

Kahane, N., Cinnamon, Y., Bachelet, I. and Kalcheim, C. (2001) “The third wave of myotome colonization by mitotically competent progenitors: regulating the balance between differentiation and proliferation during muscle development.” *Development* 128: 2187-2198

Kanehisa, M. and Goto, S. (2000) “KEGG: Kyoto Encyclopedia of Genes and Genomes.” *Nucleic Acids Res.* 28: 27-30

Kanehisa, M., Goto, S., Sato, Y., Furumichi, M., and Tanabe, M. (2012) “KEGG for integration and interpretation of large-scale molecular datasets.” *Nucleic Acids Res*. 40, D109-D114

Karaulanov, E.E., Bottcher, R.T., Niehrs, C., (2006) "A role for fibronectin-leucine rich transmembrane cell-surface proteins in homotypic cell adhesion." *EMBO Rep.* 7: 283–290

Keynes, R.J., Stern, C.D. (1986) “Somites and neural development.” In: *Somites in Developing Embryos* (R. Bellairs, D.A. Ede and J.W. Lash, eds.). London: Plenum Publishing Corp. pp 289-299

Keynes, R., Tannahill, D., Morgenstern, D.A., Johnson, A.R., Cook, G.M., Pini, A. (1997) “Surround repulsion of spinal sensory axons in higher vertebrate embryos.” *Neuron* 18(6): 889-97

Kimura, W., Yasugi, S., Stern, C. D., Fukuda, K. (2006). “Fate and plasticity of the endoderm in the early chick embryo.” *Dev. Biol.* 289, 283–295

Kingsley, P. D., Hagen, K. G. T., Maltby, K. M., Zara, J., Tabak, L. A. (2000) “Diverse spatial expression patterns of UDP-GalNAc: polypeptide N-acetylgalactosaminyl-transferase family member mRNAs during mouse development.” *Glycobiology* 10 (12): 1317-1323

Klewer, S. E., Yatskievych, T., Pogreba, K., Stevens, M. V., Antin, P. B. and Camenisch, T. D. (2006), "Has2 expression in heart forming regions is independent of BMP signaling", *Gene Expression Patterns* 6: 462-470

Knobbe C. B., Lapin V., Suzuki A., Mak T. W. (2008). “The roles of PTEN in development, physiology and tumorigenesis in mouse models: a tissue-by-tissue survey.” *Oncogene* 27, 5398–5415

Koichiro, U., Morishita, Y. and Iwasa, Y. (2009), "Traveling wave formation in vertebrate segmentation", *Journal of Theoretical Biology* 257: 385-396

Koizumi, K., Nakajima, M., Yuasa, S., Saga, Y., Sakai, T., Kuriyama, T., Shirasawa, T., Koseki, H. (2001) “The role of presenilin 1 during somite segmentation.” *Development*. 128(8): 1391-402

Kolodkin, A.L., Tessier-Lavigne, M. (2011) “Mechanisms and molecules of neuronal wiring: a primer.” *Cold Spring Harb. Perspect. Biol.* 2011 3(6) pii: a001727

Korhonen, J., Partanen, J., Alitalo, K. (1992) “Expression of FGFR-4 mRNA in developing mouse tissues.” *Int. J. Dev. Biol.* 36: 323–329

Kozak, M. (1984) “Selection of initiation sites by eucaryotic ribosomes: effect of inserting AUG triplets upstream from the coding sequence for preproinsulin.” *Nucleic Acids Res.* 12(9): 3873-93

Kozak M. (1986) “Point mutations close to the AUG initiator codon affect the efficiency of translation of rat preproinsulin in vivo.” *Nature* 308: 241-6

Krull, C.E., Collazo, A., Fraser, S.E., Bronner-Fraser, M. (1995) “Segmental migration of trunk neural crest: time-lapse analysis reveals a role for PNA-binding molecules.” *Development* 121(11): 3733-43

Kuan, C. K., Tannahill, D., Cook, C. M. W. and Keynes, R. J. (2004), "Somite polarity and segmental patterning of the peripheral nervous system", *Mech. Dev*. 121: 1055-1068

Kulesa, P.M., Fraser, S.E. (2002) “Cell dynamics during somite boundary formation revealed by time-lapse analysis.” *Science* 298: 991-5.

Lacy, S.E., Bonnemann, C.G., Buzney, E.A., Kunkel, L.M., (1999). "Identification of FLRT1, FLRT2 and FLRT3: a novel family of transmembrane leucine rich repeat proteins." *Genomics* 62: 417–426

Langton, K. P., Barker, M. D., McKie, N. (1998) “Localization of the functional domains of human tissue inhibitor of metalloproteinases-3 and the effects of a Sorsby's fundus dystrophy mutation.” *J. Biol. Chem.* 273: 16778-16781

Langton, K. P., McKie, N., Curtis, A., Goodship, J. A., Bond, P. M., Barker, M. D., Clarke, M. (2000). “A novel tissue inhibitor of metalloproteinases-3 mutation reveals a common molecular phenotype in Sorsby's fundus dystrophy.” *J. Biol. Chem.* 275: 27027-27031

Larrivée, B., Freitas, C., Trombe, M., Lv, X., Delafarge, B., Yuan, L., Bouvrée, K., Bréant, C., Del Toro, R., Brécho,t N., Germain, S., Bono, F., Dol, F., Claes, F., Fischer, C., Autiero, M., Thomas, J.L., Carmeliet, P., Tessier-Lavigne, M., Eichmann, A. (2007) “Activation of the UNC5B receptor by Netrin-1 inhibits sprouting angiogenesis.” *Genes Dev.* 21(19): 2433-47

Le Douarin, N., Kalcheim, C. (1999) “The Neural Crest.” 2nd Edition. Development and Cell Biology Series. Cambridge Universtity Press, Cambridge.

Leitges, M., Neidhardt, L., Haenig, B., Herrmann, B.G., Kispert, A. (2000) “The paired homeobox gene Uncx4.1 specifies pedicles, transverse processes and proximal ribs of the vertebral column.” *Development* 127(11): 2259-67

Lewcock, J.W., Genoud, N., Lettieri, K., Pfaff, S.L. (2007) “The ubiquitin ligase Phr1 regulates axon outgrowth through modulation of microtubule dynamics.” *Neuron* 56: 604–620

Li, Y., Toole, B.P., Dealy, C.N., Kosher, R.A. (2007) “Hyaluronan in limb morphogenesis.” *Dev. Biol.* 305: 411–420

Liang Y, Van Zant G. (2008) “Aging stem cells, latexin, and longevity.” *Exp. Cell Res.* 314(9): 1962-72

Lin YR, Reddy BV, Irvine KD. (2008) “Requirement for a core 1 galactosyltransferase in the Drosophila nervous system.” *Dev. Dyn.*. 237: 3703–3714

Long, H., Sabatier, C., Ma, L., Plump, A., Yuan, W., Ornitz, D.M., Tamada, A., Murakami, F., Goodman, C.S., Tessier-Lavigne, M. (2004) “Conserved roles for Slit and Robo proteins in midline commissural axon guidance.” *Neuron* 42(2): 213-23

Lorda-Diez, C., Montero, J. A., Garcia-Porrero, J. A., Hurle, J. M. (2010) “Tgfb22 and 3 are coexpressed with their extracellular regulator Ltbp1 in the early limb bud and modulate mesodermal outgrowth and BMP signalling in chicken embryos.” *BMC Dev. Biol.* 10: 69

Luxardi, G., Galli, A., Forlani, S., Lawson, K., Maina, F. and Dono, R. (2007) "Glypicans are differentially expressed during patterning and neurogenesis of early mouse brain", *Biochemical and Biophysical Research Communications* 352: 55-60

Ma, Q., Fode, C., Guillemot, F., Anderson, D.J. (1999) “NEUROGENIN1 and NEUROGENIN2 control two distinct waves of neurogenesis in developing dorsal root ganglia.” *Genes Dev.* 13: 1717-1728

Mansouri, A., Yokota, Y., Wehr, R., Copeland, N.G., Jenkins, N.A., Gruss, P. (1997) “Paired-related murine homeobox gene expressed in the developing sclerotome, kidney, and nervous system.” *Dev. Dyn.* 210: 53–65

Mansouri, A., Voss, A. K., Thomas, T., Yokota, Y., & Gruss, P. (2000) “Uncx4.1 is required for the formation of pedicles and proximal ribs and acts upstream of Pax9.” *Development* 127: 2251-2258.

Maretto, S., Müller, P.S., Aricescu, A.R., Cho, K.W., Bikoff, E.K., Robertson, E.J. (2008).” Ventral closure, headfold fusion and definitive endoderm migration defects in mouse embryos lacking the fibronectin leucine-rich transmembrane protein FLRT3.” *Dev. Biol*. 318: 184-193

Maroto, M., Whittock, N., (eds.) (2008) “*Somitogenesis”. Advances in Experimental Medicine and Biology,* volume 638. 1st ed. Landes Bioscence/ Springer, USA.

Maroto, M., Bone, R.A., Dale, J.K. (2012) “Somitogenesis.” *Development* 139(14): 2453-6

Marusich, M.F. (1993) “Differentiation of neurogenic precursors within the neural crest cell lineage.” *Brain Res. Bull*. 30, 257-263

McCann, M.R., Tamplin, O.J., Rossant, J., Séguin, C.A. (2012) “Tracing notochord-derived cells using a Noto-cre mouse: implications for intervertebral disc development.” *Dis. Model. Mech.* 5(1): 73-82

Merla, G, Ucla, C, Guipponi, M, Reymond, A. (2002) “Identification of additional transcripts in the Williams-Beuren syndrome critical region.” *Hum. Genet*. 110(5): 429-38

Mészár, Z., Felszeghy, S., Veress, G., Matesz, K., Székely, G, Módis L. (2008) “Hyaluronan accumulates around differentiating neurons in spinal cord of chicken embryos.” *Brain Res. Bull*. 75: 414–418

Muir, E.M., Adcock, K.H., Morgenstern, D.A., Clayton, R., von Stillfried, N., Rhodes, K., Ellis C, Fawcett JW, Rogers JH. (2002) “Matrix metalloproteases and their inhibitors are produced by overlapping populations of activated astrocytes.” *Brain Res. Mol Brain Res.* 100: 103–117

Müller, P.S., Schulz, R., Maretto, S., Costello, I., Srinivas, S., Bikoff, E., Robertson, E. (2011) “The fibronectin leucine-rich repeat transmembrane protein Flrt2 is required in the epicardium to promote heart morphogenesis.” *Development*. 138: 1297–1308

Muroyama, Y., Fujiwara, Y., Orkin, S.H, Rowitch, D.H. (2005) "Specification of astrocytes by bHLH protein SCL in a restricted region of the neural tube." *Nature* 438: 360–363

Nelson, P.A., Sutcliffe, J.G., Thomas, E.A. (2002) "A new UDP-GalNAc: polypeptide N-acetylgalactosaminyltransferase mRNA exhibits predominant expression in the hypothalamus, thalamus and amygdala of mouse forebrain." *Brain Res. Gene Expr Patterns*. 1(2): 95-9

Niedermeyer, J., Garin-Chesa, P., Kriz, M., Hilberg, F., Mueller, E., Bamberger, U., Rettig, W.J., Schnapp, A. (2001) "Expression of the fibroblast activation protein during mouse embryo development." *Int J. Dev. Biol.* 45: 445–447

Oakley, R.A., Tosney, K.W. (1991). "Peanut agglutinin and chondroitin-6-sulfate are molecular markers for tissues that act as barriers to axon advance in the avian embryo." *Dev. Biol*. 147: 187-206

Ori, M., Nardini, M., Casini, P., Perris, R., Nardi, I. (2006) "XHas2 activity is required during somitogenesis and precursor cell migration in Xenopus development." *Development* 133(4): 631-40

Palmeirim, I., Henrique, D., Ish-Horowicz, D., Pourquié, O. (1997) "Avian hairy gene expression identifies a molecular clock linked to vertebrate segmentation and somitogenesis." *Cell* 91(5): 639-48.

Pang, D., Thompson, D.N. (2011) "Embryology and bony malformations of the craniovertebral junction." *Child's Nerv. Syst.* 27(4): 523-64

Pariser, H.P., Zhang, J., Hausman, R.E., (2000). "The cell adhesion molecule retina cognin is a cell surface protein disulfide isomerase that uses disulfide exchange activity to modulate cell adhesion." *Exp. Cell Res*. 258, 42-52

Park, K.K., Liu, K., Hu, Y., Smith, P.D., Wang, C., Cai, B, Xu, B., Connolly, L., Kramvis, I., Sahin, M., He, Z. (2008) "Promoting axon regeneration in the adult CNS by modulation of the PTEN/mTOR pathway." *Science* 322: 963-966

Pavloff, N., Staskus, P.W., Kishnani, N.S., Hawkes, S.P. (1992) "A new inhibitor of metalloproteinases from chicken: ChIMP-3. A third member of the TIMP family." *J. Biol. Chem.* 267(24):17321-6

Peres, J. N., McNulty, C. L., Durston, A. J. (2006) "Interaction between X-Delta-2 and Hox genes regulates segmentation and patterning of the anteroposterior axis." *Mech. Dev*. 123(4): 321-33

Phillips, J.L., Holdengreber, V., Ben-Shaul, Y., Zhang, J., Tolan, D.R., Hausman, R.E. (1997) "Developmental localization of retina cognin synthesis by in situ hybridization." *Brain Res. Dev. Brain Res.* 104 (1-2): 143-52

Placzek, M., Yamada, T., Tessier-Lavigne, M., Jessell, T., Dodd, J. (1991). "Control of dorsoventral pattern in vertebrate neural development: induction and polarizing properties of the floor plate." *Development Suppl* 2: 105-122

Pourquié, O. (2001), "Vertebrate Somitogenesis", *Annu. Rev. Cell Dev. Biol.* 17: 311-350

Pourquié, O. (2009) "The Skeletal System." 1st ed. Cold Spring Harbor Laboratory Press, Cold Spring Harbor, New York.

Pourquié, O., Coltey, M., Bréant, C., Le Douarin, N.M. (1995) "Control of somite patterning by signals from the lateral plate." *Proc. Natl. Acad. Sci. U.S.A.* 92(8): 3219-23

Puig, I., Champeval, D., De Santa Barbara, P., Jaubert, F., Lyonnet, S., Larue, L. (2009) "Deletion of Pten in the mouse enteric nervous system induces ganglioneuromatosis and mimics intestinal pseudoobstruction*." J. Clin. Invest.* 119: 3586–3596

Raftopoulou, M., Etienne-Manneville, S., Self, A.., Nicholls, S., Hall, A. (2004). "Regulation of cell migration by the C2 domain of the tumor suppressor PTEN." *Science* 303: 1179–1181

Raman, J., Fritz, T. A., Gerken, T. A., Jamison, O., Live, D., Liu, M., Tabak, L. A.. (2008) "The catalytic and lectin domains of UDP-GalNac: Polypetide-α-

Acetylgalactosaminyltransferase function in concert to direct glycosylation site selection." *J. Biol. Chem.* 283(34): 22942-22951

Raouf, A., Seth, A. (2000) "Ets transcription factors and targets in osteogenesis." *Oncogene*. 19(55): 6455-63

Ravishankar, R., Suguna, K., Surolia, A., Vijayan, M. (1999) "StructuRes. of the complexes of peanut lectin with methyl-beta-galactose and N-acetyllactosamine and a comparative study of carbohydrate binding in Gal/GalNAc-specific legume lectins." *Acta Crystallogr. D Biol. Crystallogr.* 55(Pt 8): 1375-82

Richmond DL, Oates AC. (2012) "The segmentation clock: inherited trait or universal design principle?" *Curr. Opin. Genet. Dev*. 22(6): 600-6

Ristevski, S., Tam, P.P., Hertzog, P.J., Kola, I. (2002) "Ets2 is expressed during morphogenesis of the somite and limb in the mouse embryo." *Mech. Dev.* 116: 165–8

Ristevski, S., O'Leary, D., Thornell, A., Owen, M., Kola, I., Hertzog, P. (2004) "The ETS transcription factor GABP alpha is essential for early embryogenesis." *Mol. Cell. Biol.* 24: 5844–5849

Roffers-Agarwal,J., Gammill, L. S. (2009) "Neuropilin receptors guide distinct phases of sensory and motor neuronal segmentation." *Development*. 136(11): 1879–1888

Root, P., Sliskovic, I., Mutus, B. (2004) "Platelet cell-surface protein disulphide-isomerase mediated S-nitrosoglutathione consumption" *Biochem J.* 382(Pt 2): 575–580

Roughley, P.J., Lamplugh, L., Lee, E.R., Matsumoto, K., Yamaguchi, Y. (2011) "The role of hyaluronan produced by Has2 gene expression in development of the spine." *Spine* (Phila Pa 1976) 36(14): E914–20

Rozmahel, R., Mount, H.T., Chen, F., Nguyen, V., Huang, J., Erdebil, S., Liauw, J., Yu, G., Hasegawa, H., Gu, Y., Song, Y.Q., Schmidt, S.D., Nixon, R.A., Mathews, P.M., Bergeron, C., Fraser, P., Westaway, D., St George-Hyslop, P. (2002) "Alleles at the

Nicastrin locus modify presenilin 1-deficiency phenotype." *Proc. Natl. Acad. Sci. U.S.A.* 99: 14452–14457.

Saga, Y., Takeda, H. (2001), "The making of the somite: molecular events in vertebrate segmentation", *Nat. Rev. Genet.* 2: 835-845

Saga, Y., Hata, N., Kosebi, H., Taketo, M.M.. (1997) "Mesp2: a novel mouse gene expressed in the presegmented mesoderm and essential for segmentation initiation." *Genes & Development* 11: 1827-1839

Salih, D.A.M., Tripathi, G., Holding, C., Szestak, T.A.M., Ivelisse Gonzalez, M., Carter, E.J., Cobb, L.J., Eisemann, J.E., Pell, J.M. (2004) "Insulin-like growth factor-binding protein 5 (Igfbp5) compromises survival, growth, muscle development, and fertility in mice." *Proc Natl Acad Sci U S A.* 101(12): 4314-9

Scaal, M., Gros, J., Lesbros, C., Marcelle, C. (2004) "In ovo electroporation of avian somites." *Dev. Dyn.* 229: 643-650

Schlosser, G. (2006) "Induction and specification of cranial placodes." *Dev. Biol.* 294: 303-351

Schrägle, J., Huang, R., Christ, B., Pröls, F. (2004) "Control of the temporal and spatial Uncx4.1 expression in the paraxial mesoderm of avian embryos." *Anat. Embryol.* 208(4): 323-32

Schwientek, T., Bennett, E.P., Flores, C., Thacker, J., Hollmann, M., Reis, C.A., Behrens, J., Mandel, U., Keck, B., Schaefer, M.A., Haselmann, K., Zubarev, R., Roepstorff, P., Burchell, J.M., Taylor-Papadimitriou, J., Hollingsworth, M.A., Clausen, H.J. (2002) "Functional conservation of subfamilies of putative UDP-N-acetylgalactosamine: polypeptide N-acetylgalactosaminyltransferases in *Drosophila*, *Caenorhabditis elegans*, and mammals. One subfamily composed of l(2)35Aa is essential in *Drosophila*." *J. Biol. Chem.* 277: 22623-22638

Seo, H. S., Serra, R. (2007) "Deletion of Tgfbr2 in Prx1-cre expressing mesenchyme results in defects in development of the long bones and joints." *Dev. Biol.* 310: 304-316

Sharpe, P., Mason, I. (eds.) (2008) “Molecular Embryology Methods and Protocols” Second Edition ed, Humana Press c/o Springer Science, New York.

Shen, J., Bronson, R.T., Chen, D.F., Xia, W., Selkoe, D.J., Tonegawa, S. (1997) “Skeletal and CNS defects in Presenilin-1-deficient mice.” *Cell* 89(4): 629-39

Song, H. H., Filmus, J. (2002) “The role of glypicans in mammalian development.” *Biochim. Biophys. Acta* 1573: 241–246

Spicer, A.P., Tien, J.L., Joo, A., Bowling, R.A. Jr. (2002) “Investigation of hyaluronan function in the mouse through targeted mutagenesis.” *Glycoconj. J.* 19: 341–345

Standring, S. (2005) “Gray’s Anatomy.” 39 ed. Elsevier Ltd.

Stemple, D.L. (2005) “Structure and function of the notochord: an essential organ for chordate development.” *Development* 132(11): 2503-12

Stern, C.D. (2005) “The chick; a great model system becomes even greater.” *Dev. Cell* 8: 9-17

Stern, C.D., Keynes, R.J. (1986) “Cell lineage and the formation and maintenance of half-somites.” In: *Somites in Developing Embryos* (R. Bellairs, D.A. Ede and J.W. Lash, eds.). London: Plenum Publishing Corp. pp 147-159

Stern, C.D., Keynes, R.J. (1987) “Interactions between somite cells: the formation and maintenance of segment boundaries in the chick embryo.” *Development* 99: 261–272

Stern, C.D., Sisodiya S.M., Keynes R.J. (1986) “Interactions between neurites and somite cells: inhibition and stimulation of nerve growth in the chick embryo.” *J. Embryol. Exp. Morph.* 91: 209–226

Sumarsono, S., Wilson, T., Tymms, M., Venter, D., Corrick, C., Kola, R., Lahoud, M., Papas, T., Seth, A., Kola, I. (1996) “Down's syndrome-like skeletal abnormalities in Ets2 transgenic mice.” *Nature* 379: 534–537

Suo, Z., Wu, M., Citron, B.A., Gao, C. and Festoff, B.W. (2003) “Persistent protease-activated receptor 4 signaling mediates thrombin-induced microglial activation.” *J. Biol. Chem.* 278: 31177–31183

Tabak, L.A. (2010) “The role of mucin-type O-glycans in eukaryotic development.” *Semin. Cell Dev. Biol*. 21: 616–621

Täger, M., Kröning, H., Thiel, U., Ansorge, S. (1997) “Membrane-bound protein disulfide isomerase (PDI) is involved in regulation of surface expression of thiols and drug sensitivity of B-CLL cells” *Exp. Hematol*. 25(7): 601-7

Takahashi J, Ohbayashi A, Oginuma M, Saito D, Mochizuki A, Saga Y, Takada S. (2010) “Analysis of Ripply1/2-deficient mouse embryos reveals a mechanism underlying the rostro-caudal patterning within a somite.” *Dev. Biol.* 342(2): 134-45

Tannahill, D., Britto, J.M., Vermeren, M., Ohta, K., Cook, G.M.W., Keynes, R.J. (2000), "Orienting axon growth: spinal nerve segmentation and surround-repulsion", *Int. J. Dev. Biol.* 44: 119-127

Theveneau, E., Mayor, R. (2012) "Neural crest delamination and migration: From epithelium-to-mesenchyme transition to collective migration." *Dev. Biol.* 366: 34-54.

Tian, E., Hoffman, M.P., Ten Hagen, K.G. (2012) “O-glycosylation modulates integrin and FGF signalling by influencing the secretion of basement membrane components.” *Nat. Commun*. 3: 869

Tosney, K.W., Oakley, R.A. (1990). “The perinotochordal mesenchyme acts as a barrier to axon advance in the chick embryo: implications for a general mechanism of axonal guidance.” *Exp. Neurol.* 109(1): 75-89.

Tran, D.T., Ten Hagen, K.G. (2013). “Mucin-type O-glycosylation during development.” *J. Biol. Chem*. 288: 6921-6929

Vasiev, B., Balter, A., Chaplain, M., Glazier, J.A., Weijer, C.J. (2010) “Modeling gastrulation in the chick embryo: formation of the primitive streak.” *PLoS ONE* 5(5): e10571

Vermeren, M., Maro, G.S., Bron, R., McGonnell, I.M., Charnay, P., Topilko, P., Cohen, J. (2003) “Integrity of developing spinal motor columns is regulated by neural crest derivatives at motor exit points.” *Neuron* 37(3): 403-15

Veugelers, M., De Cat, B., Ceulemans, H., Bruystens, A. M., Coomans, C., Dürr, J., Vermeesch, J., Marynen, P., David, G. (1999) "Glypican-6, a new member of the glypican family of cell surface heparan sulfate proteoglycans." *J. Biol. Chem.* 274(38): 26968-77

Vinaik, R., Kozlov, G., Gehring. K. (2013) "Structure of the non-catalytic domain of the protein disulfide isomerase-related protein (PDIR) reveals function in protein binding." *PLoS One* 8: e62021

Vu, T.K., Hung, D.T., Wheaton, V.I., Coughlin, S.R. (1991) "Molecular cloning of a functional thrombin receptor reveals a novel proteolytic mechanism of receptor activation." *Cell* 64: 1057–1068

Walshe, J., Mason, I. (2000) "Expression of FGFR1, FGFR2 and FGFR3 during early neural development in the chick embryo." *Mech. Dev.* 90(1): 103-10

Wan, S.W., Lin, C.F., Lu, Y.T., Lei, H.Y., Anderson, R., Lin, Y.S. (2012) "Endothelial cell surface expression of protein disulfide isomerase activates β1 and β3 integrins and facilitates dengue virus infection." *J. Cell Biochem.* 113(5): 1681-91

Wang, X.M., Yu, D.M., McCaughan, G.W., Gorrell, M.D. (2005) "Fibroblast activation protein increases apoptosis, cell adhesion, and migration by the LX-2 human stellate cell line." *Hepatology.*;42: 935–945

Wang, Y., Serra, R. (2012) "PDGF mediates TGFβ-induced migration during development of the spinous process" *Dev. Biol.*, 365, (1): 110–117

Wehn, A.K., Chapman, D.L. (2010) "Tbx18 and Tbx15 null-like phenotypes in mouse embryos expressing Tbx6 in somitic and lateral plate mesoderm." *Dev. Biol.* 347: 404-13

Wei, K., Xu, Y., Tse, H., Manolson, M.F., Gong, S.G. (2011) "Mouse FLRT 2 interacts with the extracellular and intracellular regions of FGFR2."*J. Dent Res* 90: 1234-1239

Wheatley SC, Isacke CM, Crossley PH. (1993) "Restricted expression of the hyaluronan receptor, CD44, during postimplantation mouse embryogenesis suggests key roles in tissue formation and patterning." *Development.* 119: 295–306

White, T., Bennett, E.P., Takio, K., Sørensen, T., Bonding, N., and Clausen, H. (1995) "Purification and cDNA cloning of a human UDP-N-acetyl-α-D-galactosamine: polypeptide N-acetylgalactosaminyltransferase." *J. Biol. Chem.* 270, 24156–25165

Wilkinson, D.G. (1998) "*In Situ* Hybridization A Practical Approach" 2nd edition. Oxford University Press, Oxford

Wills, B.P.D., Dormans, J.P. (2006) "Nontraumatic Upper Cervical Spine Instability in Children." *J. Am. Acad. Orthop. Surg.* 14: 233-245

Wolpert, L., Jessell, T., Lawrence, P., Meyerowitz, E., Robertson, E., Smith, J. (2007) "Principles of Development." Third Edition 2007 Oxford University Press

Wong, P.C., Zheng, H., Chen, H., Becher, M.W., Sirinathsinghji, D.J.S., Trumbauer, M.E., Chen, H.Y., Price, D.L., Van der Ploeg, L.H.T., Sisodia, S.S., (1997) "Presenilin 1 is required for Notch1 and DII1 expression in the paraxial mesoderm." *Nature* 387: 288-292.

Wu, C., Guo, X., Wang, W., Shan, Y., Zhang, B., Song, W., Ma, S. (2010) "N-acetylgalactosaminyltransferase-14 as a potential biomarker for breast cancer by immunohistochemistry." *BMC Cancer* 10: 123

Yamagishi, S., Hampel, F., Hata, K., Del Toro, D., Schwark, M., Kvachnina, E., Bastmeyer, M., Yamashita, T., Tarabykin, V., Klein, R., Egea, J. (2011) "FLRT2 and FLRT3 act as repulsive guidance cues for Unc5-positive neurons." *EMBO J.* 14: 2920–2933

Ye, J., Coulouris, G., Zaretskaya, I., Cutcutache, I., Rozen, S., Madden, T. (2012) "Primer-BLAST: a tool to design target-specific primers for polymerase chain reaction." *BMC Bioinformatics* 13: 134

Yoshida, H., Fuwa, T.J., Arima, M., Hamamoto, H., Sasaki, N., Ichimiya, T., Osawa, K., Ueda, R., Nishihara, S. (2008) "Identification of the *Drosophila* core 1 beta1,3-galactosyltransferase gene that synthesizes T antigen in the embryonic central nervous system and hemocytes." *Glycobiology* 18(12): 1094-104

Young Jr., W.W., Holcomb, D.R., Ten Hagen, K.G., Tabak, L.A. (2003) "Expression of UDP-GalNac: polypeptide N-acetylgalactosaminyltransferase isoforms in murine tissues determined by real-time PCR: a new view of a large family." *Glycobiology* 13(7): 549-557.

Yuan, W., Zhou, L., Chen, J., Wu, J. Y., Rao, Y., Ornitz, D.M. (1999) "The mouse SLIT Family: secreted ligands for ROBO expressed in patterns that suggest a role in morphogenesis and axon guidance." *Dev. Biol.* 212: 290-306

Zai, A., Rudd, M.A., Scribner, A.W., Loscalzo, J. (1999) "Cell-surface protein disulfide isomerase catalyzes transnitrosation and regulates intracellular transfer of nitric oxide." *J. Clin Invest*. 103(3): 393-9

Zeng, Y., Rosborough, R..C, Li, Y., Gupta, A.R., Bennett, J. (1998) "Temporal and spatial regulation of gene expression mediated by the promoter for the human tissue inhibitor of metalloproteinases-3 (TIMP-3)-encoding gene." *Dev. Dyn.* 211: 228–237

Zhang, W., Cao, P., Chen, S., Spence, A.M., Zhu, S., Staudacher, E., Schachter, H. (2003) "Synthesis of paucimannose N-glycans by *Caenorhabditis elegans* requiRes. prior actions of UDP-N-acetyl-D-glucosamine: alpha-3-D-mannoside beta1,2-N-acetylglucosaminyltransferase I, alpha3,6-mannosidase II and a specific membrane-bound beta-N-acetylglucosaminidase." *Biochem. J*. 372; 53–64

Zhang, L., Zhang, Y., Hagen, K.G. (2008) "A mucin-type O-glycosyltransferase modulates cell adhesion during *Drosophila* development." *J. Biol. Chem.* 283: 34076-86

Zhang L., Tran D. T., Ten Hagen K. G. (2010) "An O-glycosyltransferase promotes cell adhesion during development by influencing secretion of an extracellular matrix integrin ligand." *J. Biol. Chem*. 285: 19491–19501

APPENDIX A- HAMBURGER AND HAMILTON (HH) CHICK STAGING TABLE

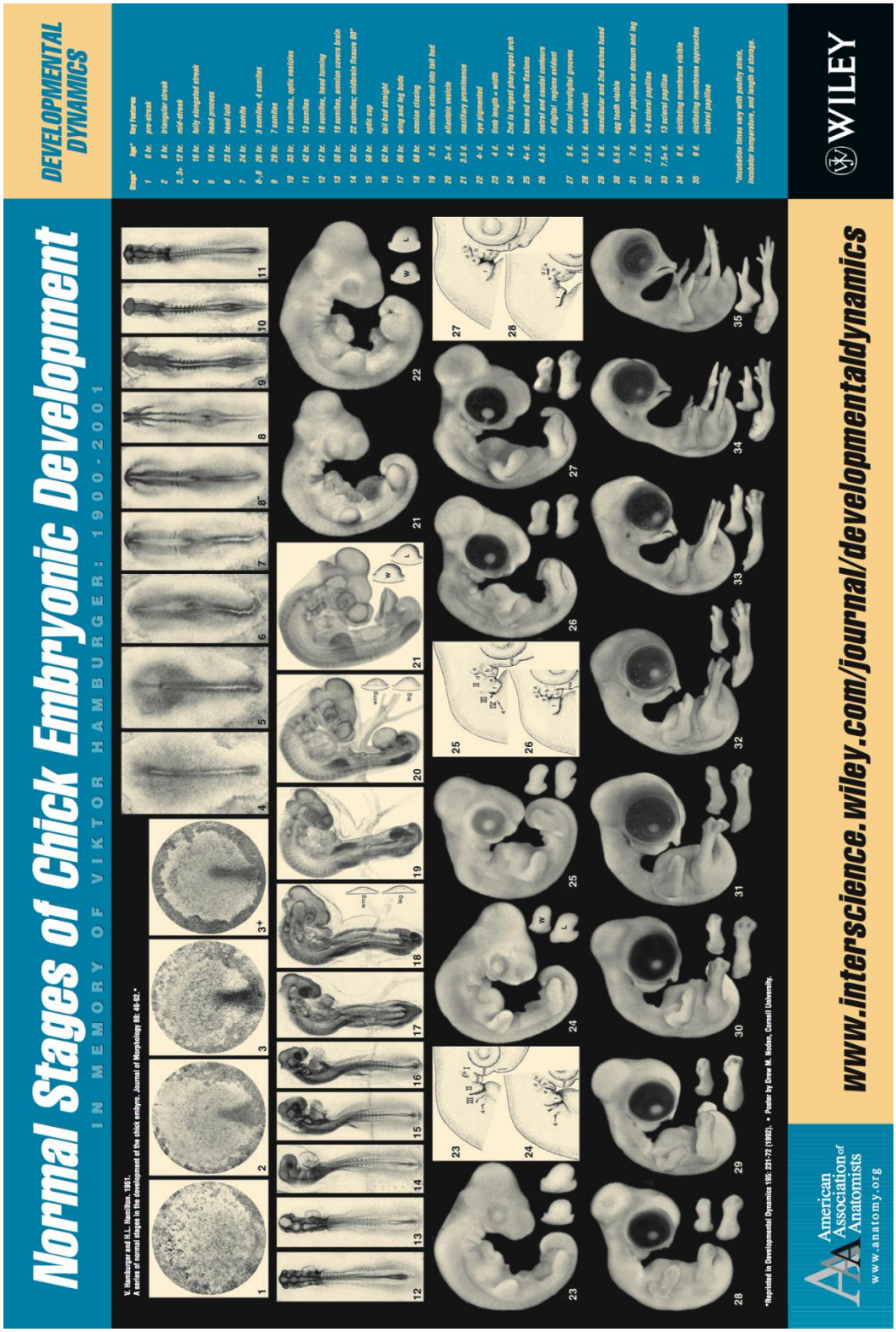

APPENDIX B- PRIMERS USED TO OBTAIN ANTISENSE RNA PROBES

IGFBP5F	ATGGCGTGCCTGCAGGTTGATG
IGFBP5R	TAATACGACTCACTATAGGGAGTCACTCCACGTTGCTGCTGTCG
GPC6-F	TCACTAGAGGGATGGGATGC
GPC6-R	TAATACGACTCACTATAGGGAGTCCTCTGCAGTAAGGGCAGT
TIMP3-F	ATGACGGCGTGGCTCGGCTTCC
TIMP3-R	TAATACGACTCACTATAGGGAGTCAGGGATCTGTGGCATTGATG
TGFBR2-F	CTGTGCCAACAACATCAACC
TGFBR2-R	TAATACGACTCACTATAGGGAGAGGGATGCTCTCGCACTTTA
UNCX4.1-F	ATCGATGGATTACTGAGCGG
UNCX4.1-R	TAATACGACTCACTATAGGGAGGTTTAAGCAAACGGACGCTG
ROBO1-F	ACAGCCCTGGCTAGCAGATA
ROBO1-R	TAATACGACTCACTATAGGGAGGTCTCCGTTCAGGTTGGTGT
CST3-F	AGCTCGGGGTTGCGTAGT
CST3-R	TAATACGACTCACTATAGGGAGTTACTGGCACTTGCTTTCCA
HAS2-F	CAGTGGACCTCTGGGAATGT
HAS2-R	TAATACGACTCACTATAGGGAGCTGCCACATTTGGTGATGAG
ETS2-F	GAACAGTGTCGGCTGGGTAT
ETS2-R	TAATACGACTCACTATAGGGAGGGCTTGTTTTTCCTCCTTCC
F2R-F	AACAACGAACAGTGTCAGCG
F2R-R	TAATACGACTCACTATAGGGAGAAAGGGATCAATGCAACAGC
TBX18-F	GTAATGCTGACTCCCCGGTA
TBX18-R	TAATACGACTCACTATAGGGAGACTGGTTTGGTTTGTGAGCC
FLRT2-F	GCCTGACAGGGAAGACAGAG
FLRT2-R	TAATACGACTCACTATAGGGAGGGCTGCAGTCTGAAATCTCC
FAP-F	GGAGGACCATGCAGTCAGAA
FAP-R	TAATACGACTCACTATAGGGAGGGCTGAAATTTGGTCCTCAA
PTEN-F	ATGATACGTGGATTTGGGGA
PTEN-R	TAATACGACTCACTATAGGGAGGCAGTTAAATTTGGCGGTGT
GalnT9-F	GCTGGGTGGAACCTGCGCTT
GalnT9-R	TAATACGACTCACTATAGGGAGTGCAGCCCGTAGGGCATTGC
GalnT6-F	CCCGGAGCAACGTGGGTTCC
GanT6-R	TAATACGACTCACTATAGGGAGTCACGGAGGTTGTGCACGGC
C1GALT1-F	CGTTTGTCCCGTGTGCCACG
C1GALT1-R	TAATACGACTCACTATAGGGAGTCCATTCCACCCGAGGCCCT
GalnT10-F	TGGTCCCTGTACCGCGAGCG
GalnT10-R	TAATACGACTCACTATAGGGAGACGTTGGCCTCGCAATGGGA
WBSCR17-F	TCGGTCATCCTGCGGTCGGT
WBSCR17-R	TAATACGACTCACTATAGGGAGCCTTCGATGCGCGCTCGGAT
GalnT11-F	CCGGTGGATCGCAGCAGTGG
GalnT11-R	TAATACGACTCACTATAGGGAGGCCATGGGCTCCCAGCACAG
GalnT15-F	CGTGCTCCCGTGTTGGGCAT

GalnT15-R	TAATACGACTCACTATAGGGAGTGCGTCTTCAGGCCGGGAGA
GalnT1-F	CCGGTCACCACGACACATGCT
GalnT1-R	TAATACGACTCACTATAGGGAGGGAAGCGGCAGCCCCCTTTA
GalnT12-F	GCCATGAGGGCTGGCTGGAAC
GalnT12-R	TAATACGACTCACTATAGGGAGCCAGGCGAGCGTGTGGGTT
GalnT14-F	GCCTGCGGAACAGACAGCGT
GalnT14-R	TAATACGACTCACTATAGGGAGTCTGCAACAGCGGGAGCAGC
GalnT2-F	TGATGCGCTCCCGGGTCAGA
GalnT2-R	TAATACGACTCACTATAGGGAGTCAGCTGACGCCCCCACGTA
GalnT17-F	AGACATCCGTCCCGGGGAGC
GalnT17-R	TAATACGACTCACTATAGGGAGTGCAGGCTGTGTGCGACTGG
GalnT7-F	ACAGCTCCGAGCCTCCTGACT
GalnT7-R	TAATACGACTCACTATAGGGAGGGTGGGCTGATGGCCACGAC
GalnT16-F	GGCTCGCTGCGGGTGACAAG
GalnT16-R	TAATACGACTCACTATAGGGAGGAGGGGTGCGGTTCAGGACG
GalnT3-F	AAGTTCAAGCGTTGCCCGCCA
GalnT3-R	TAATACGACTCACTATAGGGAGCCCGTTGCCACTGAAGCTCC
GalnT13-F	CTGCCTGCTCTGAGGGCTGTCAT
GalnT13-R	TAATACGACTCACTATAGGGAGAGCCCCGATCGCTGCTCCATA
GalnT5-F	GCACCTGGGCAGTTTGGGCA
GalnT5-R	TAATACGACTCACTATAGGGAGAGCCCACGTTGCACTCCACG